BLIND LINEAR MULTIUSER DETECTION FOR DS-CDMA WIRELESS NETWORKS

A thesis submitted for the degree of Doctor of Philosophy of The Australian National University

Peter Koon Pong Cheung

B.E. (Hon. I), University of Queensland, Australia.

Telecommunications Engineering Group
Research School of Information Sciences and Engineering
The Australian National University

January 22, 1999

To John and Anita: my parents, my inspiration.
To Ben, Eddie and David: my brothers, my protectors.

THE AUSTRALIAN
LIBRARY
NATIONAL UNIVERSITY

Declaration

The contents of this thesis are the result of original research and have not been submitted for a higher degree to any other university or institution.

Much of the work presented in this thesis has been published or will be submitted for publication as journal or conference papers. Following is a list of these papers. In some cases, the conference papers contain material overlapping with the journal papers.

Journal Papers

- P.K.P.Cheung and R.A.Kennedy, "Robust Blind Adaptive Detection for Synchronous Multiuser CDMA Systems," submitted for *IEE Proc. Commun.,* Aug. 1997.

- P.K.P.Cheung and P.B.Rapajic, "CMA-based Code Acquisition Scheme for DS-CDMA Systems," submitted for *IEEE Trans. Commun.,* (subject to revision), Oct. 1997.

- P.K.P.Cheung, P.B.Rapajic, R.A.Kennedy and I.Fijalkow, "Blind Multiuser Multiple Sensor Receiver for DS-CDMA Systems over Frequency Selective Multipath Channels," submitted for *IEEE J. Selected Areas Commun.*, Sept. 1998.

- I.Fijalkow, P.K.P.Cheung, "Blind Multiuser detection for DS-CDMA Systems over Frequency-Selective Multipath Channels using Projection-based CMA," to be submitted to *IEEE Trans. Commun.*

Conference Papers

- P.K.P.Cheung, R.A.Kennedy, "Improved Blind Adaptive Detection for Synchronous Multiuser CDMA Systems," in *Proc. IEEE Workshop on Signal Processing Adv. in Wireless Commun.,* pp.249-252, Paris, France, 16-18 Apr. 1997.

- P.K.P.Cheung and P.B.Rapajic, "Blind Adaptive Code Acquisition for Multiuser DS-CDMA Systems," in *Proc. IEEE Personal, Indoor, Mobile Radio Conf.,* pp.337-341, Helsinki, Finland, 1-4 Sept. 1997.

- P.K.P.Cheung, P.B.Rapajic and R.A.Kennedy, "Effect of new users on blind adaptive synchronous multiuser DS-CDMA detection," in *Proc. IEEE Int. Conf. on Commun.,* Atlanta, USA, 7-11 Jun. 1998.

- P.K.P.Cheung and P.B.Rapajic, "CMA-based Blind adaptive detection for Synchronous DS-CDMA systems over Frequency-selective Channels," in *Proc. IEEE Int. Symp. on Inf. Theory,* p.184, Cambridge, USA, 16-21 Aug. 1998.

Most of research presented in this thesis has been performed jointly with Dr Rodney A. Kennedy and Dr Predrag B. Rapajic. The work related to constrained CMA-based receiver in Chapter 5 was done in collaboration with Dr Inbar Fijalkow (Equipe de Traitement des Images et des Signaux (ETIS), Ecole Nationale Supérieure de l'Electronique et de ses Applications (ENSEA) - Université de Cergy-Pontoise, France). However, the majority of the work, approximately 90%, was my own.

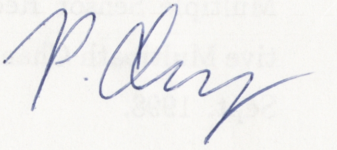

Peter Koon Pong Cheung
Australian National University
January 22, 1999

Acknowledgements

My Ph.D. would not have been possible without the support of the following people and organisations.

First and foremost, I am thankful to my family, the most caring people for supporting me for the past twenty-five years. From day one, both of my parents and all of my brothers Ben, Eddie and David have always stood by me. I would never thank my family enough for their continuous encouragement, especially during those times when I was truly down and out. Although I have been a problem child all my life, my family has always been patient and caring.

My supervisors Dr Rod Kennedy and Dr Predrag Rapajic deserve many thanks for their guidance and insight. Special thanks to Rod for his help in my enrolment and scholarship applications, overseas and interstate trips, and career advice. As for Predrag, I am particularly impressed with his own (dry) humour and drawings, during those countless visits to his office.

I would like to thank Dr Inbar Fijalkow (Universiteé de Cergy-Pontoise, France) for many useful discussion and comments regarding the CMA, during those final months of my Ph.D.

My gratitude to Dr Brian Hart and Dr Lei Wei for their tuitions on many important topics. Of course, thanks must go to both Rod and Brian for their readiness in running the *Canberra fun run* and the *City-to-Surf race.*

I thank all students in the Telecommunication Group for their friendship and a productive working environment. In particular, thanks to Deva for his presence in my regular tea breaks and his invaluable advice on life-in-general. Also, I acknowledge both past and present administrators, Keli and Maria for putting up with me and giving me all the technical assistance.

My thanks to the departmental visitor Mr Julio Castro (New Mexico State University) for proof-reading my thesis, during the final few months of my Ph.D.

For the opportunity to visit Cornell University, I thank Mr Raul Casas and Prof. Rick Johnson (also Phil Schniter for his advice). In particular, many thanks to Raul for putting me up during the visit and his helpful tuitions during the early months of my Ph.D. Also, I would like to thank Dr Miro Kraetzl and Dr Langford White for the visit to Defence Science and Technology Organization (DSTO) in Salisbury, South Australia.

A big "thank you" to all my friends in Canberra, interstate and overseas. In particular, my appreciation to Allen (thanks Allen for his 10-years long loyalty and friendship), Geoff (thanks Geoff for reading my thesis draft and his many encouragement) and Tim (thanks Tim for putting me up in Sydney) who have never lost faith in me and have never failed to show. Thanks to my friends in Ursula College who have seen my best and worst. In particular, I am deeply indebted to Mel for her continuous counsel to keep me from going insane. Also, special thanks to Luciana in Hong Kong for those never-ending well wishes and supports she gave me from her letters.

Finally, I acknowledge the generous financial support of the Australian Government for funding an Australian Postgraduate Award (APA), and the Cooperative Research Centre for Robust and Adaptive Systems (CRASys Ltd.) for the Graduate Student Assistantship.

Abstract

As business and domestic activities become globalised, wireless telecommunication must be able to provide mobile communications "anywhere" and "anytime". The Code Division Multiple Access (CDMA) technology has been proposed to implement the future wireless communication systems, mainly due to its promise of capacity improvement over the traditional multiple access schemes based on non-overlapping frequency bands or time slots. Since the same channel resource is shared by all users, signals from other users would appear as Multiple Access Interference (MAI) to the signal of interest. Unlike the conventional Matched Filter (MF) approach, multiuser detection does not treat MAI as structure-less Gaussian noise. This thesis considers the problem of "blind" adaptive linear multiuser detection for Direct Sequence (DS) - CDMA systems. The blind terminology means that the receiver has only the knowledge of the transmitted signature waveform of the desired user, and training data is not available.

For a synchronous DS-CDMA without multipath channels, two new blind detectors, one based on a constrained Minimum Output Energy (MOE) and one based on the Constant Modulus Algorithm (CMA), have been proposed as robust alternatives to the popular MOE detector. It is shown that the CMA-based detector exhibits a desirable lock convergence property which in the absence of channel noise, nulls all interferers. Unlike the CMA-based single-user channel equaliser, robust initialisation for lock convergence is possible.

In the presence of multipath under frequency selective channels, two multiple sensor based blind detectors are proposed and adapted by various CMA-based algorithms. The first detector uses a RAKE-type linear filtering to incorporate time and space diversities in a joint fashion. By combining diversity and mul-

tiuser detection, it fully exploits the benefits of multiple sensors. It highlights the limitations of using MF based beamforming in multiuser detection. The proposed second detector is based on the constrained inverse filtering approach which forces the multipath induced interference to be zero. Under some general conditions, lock convergence is always ensured for the constrained CMA in the second method, regardless of its initialisation. Also, the constrained CMA is modified to blindly acquire the timing delay of the desired user. The idea is that lock convergence should only occur for the filter associated with the correct hypothesised delay.

The final technical contribution of the thesis is a robustness investigation into various blind detectors with respect to new interferers entering the system is examined. It is shown that the robustness of the blind MOE detector is same as training-based adaptive detector based on Minimum Mean Squared Error. In the case of the CMA-based detector, its robustness is dependent on its modulus radius and existing user population.

Contents

ERRATA to PhD Thesis following examiners' Reports .....
Inside front cover

Glossary

Abbreviations

AMPS	Advanced Mobile Phone System
AWGN	Additive White Gaussian Noise
BER	Bit Error Rate
BPF	Bandpass Filter
BPSK	Binary Phase Shift Keying
CDMA	Code Division Multiple Access
CM	Constant Modulus
CMA	Constant Modulus Algorithm
conv.	convolutional
CSMA	Carrier Sense Multiple Access
CT-2	Second Generation Cordless Telecommunications
dB	decibel
DD	Decision Directed
DECT	Digital European Cordless Telecommunications
DQPSK	Differential Quadrature Phase Shift Keying
DS	Direct Sequence
EM	estimation/maxisation
ESN	Electronic Serial Number
FDD	Frequency Division Duplex
FDMA	Frequency Division Multiple Access
FH	Frequency Hopping
FIR	Finite Impulse Response

FM	Frequency Modulation
FPLMTS	Future Public Land Mobile Telecommunications Systems
GMSK	Gaussian Minimum Shift Keying
GSM	Global System for Mobile communication
HOS	Higher Order Statistics
ICI	Inter-Chip-Interference
IMT-2000	International Mobile Telecommunication
IS	Interim Standard
ISI	Inter-Symbol-Interference
ITU	International Telecommunication Union
LMS	Least Mean Squares
LOS	Line-of-Sight
LPC	Linear Predictive Code
LPF	Lowpass Filter
LTI	Linear-Time-Invariant
MA	Multiple Access
MAI	Multiple Access Interference
MBS	Mobile Broadband Systems
MC	Multi-Carrier
MF	Matched Filter
MIMO	Multiple-Input Multiple-Output
ML	Maximum Likelihood
MLSE	Maximum Likelihood Sequence Estimation
MMSE	Minimum Mean Squared Error
MOE	Minimum Output Energy
MSE	Mean Squared Error
MTSO	Mobile Telephone Switching Office
MUSIC	MUltiple SIgnal Classification
NA	North American
NBI	Narrowband Interference
NFR	Near-far ratio

NMT	Nordic Mobile Telephones
NTT	Nippon Telephone and Telegraph
PACS	Personal Access Communications System
PCS	Personal Communications Systems
PDC	Personal Digital Cellular
p.d.f.	probability density function
PHS	Personal Handyphone System
PN	Pseudo-Noise
PRMA	Packet Reservation Multiple Access
PSK	Phase Shift Keying
PSTN	Public Switching Telephone Network
QCELP	Qualcomm Code Excited Linear Predictive
RLS	Recursive Least Squares
RPE	Regular Pulse Excitation
SDMA	Space Division Multiple Access
SIR	Signal-to-Interference Ratio
SNR	Signal-to-Noise Ratio
SOS	Second Order Statistics
std.	standard
TACS	Total Access Communications System
TDD	Time Division Duplex
TDMA	Time Division Multiple Access
TH	Time Hopping
UMTS	Universal Mobile Telecommunications System
VA	Viterbi Algorithm
VSELP	Vector Sum Excited Linear Predictive
WCPN	Wireless Customer Premises Networks

Notations

$(\cdot)^T$	Matrix or vector transpose
$\lvert\cdot\rvert$	Modulus of a scalar
$\lVert\cdot\rVert$	2-norm of a vector
$rank(\cdot)$	Rank of a matrix
$*$	Convolution operator
$(\cdot)^*$	Complex conjugation
$\lfloor\cdot\rfloor$	Floor operator
$\delta(\cdot)$	Dirac delta function
$Dec(\cdot)$	Decision device operator
$sgn(\cdot)$	Signum function
$Re(\cdot)$	Real part of a complex scalar
$\mathcal{R}$	Set of real numbers
$\mathbf{I}_X$	$(X \times X)$-size identity matrix
$(\mathbf{X})_{n,m}$	The (n,m)-th component of matrix $\mathbf{X}$
$\nabla_{\mathbf{x}} Q$	Derivative of Q with respect to $\mathbf{x}$
$diag(\mathbf{X})$	Matrix extracted from $\mathbf{X}$ with the same diagonal entries, and 0 elsewhere
$\lambda_k(\mathbf{X})$	The kth eigenvalue of $\mathbf{X}$
$\mathbf{X}^\dagger$	Pseudo-inverse of $\mathbf{X}$
$trace(\mathbf{X})$	Trace of the square matrix $\mathbf{X}$
$Nullspace(\mathbf{X})$	Null-space of $\mathbf{X}$

List of Figures

List of Tables

Chapter 1

Introduction

In this introductory chapter, background material for the wireless Personal Communication Systems (PCS) is presented. For the purpose of illustration, some practical PCS standards are discussed. This is followed by an overview of this thesis and its contributions. The purpose of this chapter is to provide a concrete foundation of existing multiple acces techniques, and their implementations. In accordance with the focus of this thesis, emphasis is place on the application of the Code Division Multiple Access (CDMA) in PCS.

1.1 Background

1.1.1 Concepts of Wireless Personal Communication Systems

The purpose of Personal Communications Systems (PCS) is to provide customers with wireless access to information services [8]. It has been predicted that [9] future PCS may one day replace the wireline telephone and transform the world into a global wireless network. The ultimate goal of PCS is to achieve high-speed, high-quality and secure communication, in any place, at any time, in any form, through any medium, at minimum cost, by using hand-held terminals.

The present PCS is categorised into four separate families [8] of products and services. In the next century, it is anticipated that they will be merged as an

unified PCS. These present PCS families are:

- **Mobile Computing** — this was propelled by the popularity of portable personal computers and networking. For example, wireless local area networks provide high throughput communications (Mb/s) for slowly moving terminals in a small coverage area (tens of meters).

- **Mobile Satellite System** — this uses satellites as base stations. They provide the largest coverage (continental or global service area) but deliver the lowest bit rate services (10kb/s or less).

- **Low-Tier System** — this is designed to serve pedestrian users with low mobility, namely residential cordless phones. A common example of cordless telephone is the *telepoint* which provides an alternative to wired public telephone systems. Also, paging is an important precursor in low-tier systems and is the simplest, cheapest PCS.

- **High-Tier System** — this is designed for high mobility, vehicle-borne users with voice and data services, namely cellular networks. It has the largest commercial impact with revenues currently growing at about 40% per year [10]. In the United States, the cellular market exceeds 15% for individuals and 30% for households [8]. The popularity of cellular service is further fuelled by the continuing advances in integrated circuit technology giving low-power micro-processors that are sufficiently powerful to permit complex call control protocols.

With the explosive growth of wireless PCS in this decade, there is the need for new technology devised to meet the technical challenges. These challenges are translated into the following figures of merit [7, 8]:

- **User Subscription** — technically and economically feasible terminals (e.g., reducing its price, size and weight), lower service cost, special calling features (e.g., voice mail), near-universal geographical coverage and convenient roaming (i.e., using PCS outside one's home service area).

- **Service Quality** — near-wireline voice quality, enhanced in-building penetration, easy-to-use user interface, lower probability of call blocking, shorter setup time, ability to overcome transmission impairments (e.g., multiple fading), enhanced privacy (i.e., prevent eavesdropping), enhanced mobility, fewer dropped calls, longer talk times and lower power requirements (e.g., longer battery life).

- **Operating Company** — lower infrastructure and operating cost (e.g., fewer base stations), higher spectral efficiency (e.g., increase subscriber capacity), enhanced network security to prevent unauthorised access, early deployment and adaptability by anticipating future technology advances.

1.1.2 Basic Cellular System

Most PCSs employ some forms of cellular technology, either in cellular frequency bands or PCS bands [7, 8]. Depending on government policies, regulatory agencies in different countries have allocated limited bandwidth to PCS. Hence, advanced PCS technology must achieve high spectral efficiency. In general, there are two ways to define spectral efficiency:

1. The maximum number of channels or users that can be supported per unit service area per given bandwidth (commonly known as *channel capacity*);

2. Erlangs[1] per unit service area per given bandwidth.

For telephony, the first definition measures the maximum number of simultaneous conversations per base station per MHz, and is to be used throughout this thesis. The second measure is related to the average traffic load that a base station can handle, while meeting a specified call blocking objective.

For example, in the United States, regulators issue two cellular radio licenses in each geographical area. The resultant bandwidth allocations are 25MHz for cellular operators[2], and three 30MHz plus three 10MHz allocations for wideband

[1] Erlang is a dimensionless unit of traffic intensity, and is defined as the calling rate times the average holding time. [2] Thus, each cellular operator has 12.5MHz spectrum in each direction.

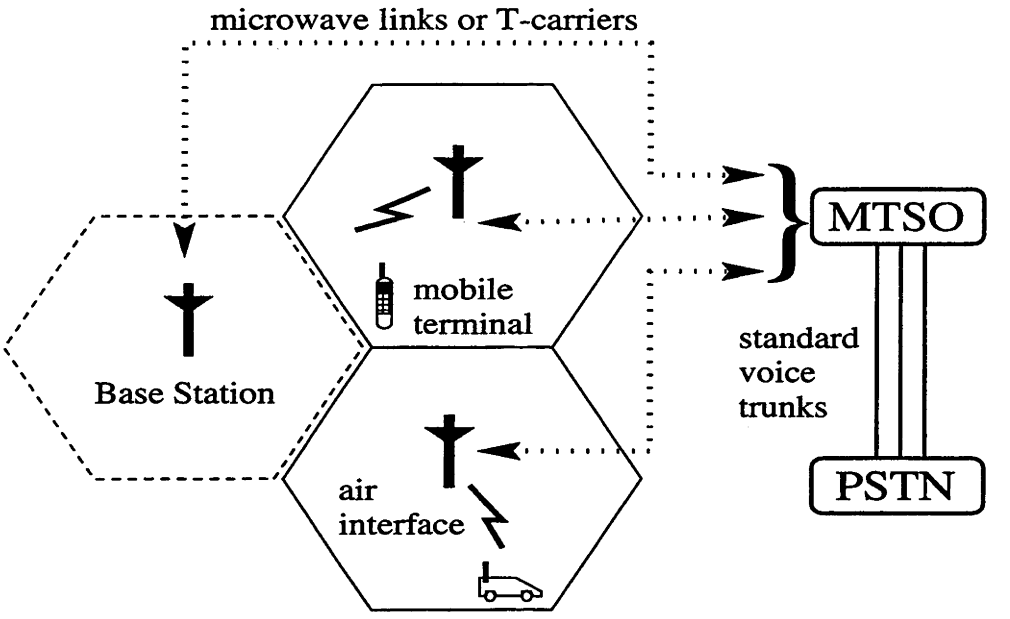

Figure 1.1: Overview of a cellular system.

PCS service. The cellular and PCS services have different frequency assignments with carrier frequencies in the vicinity of 850MHz and 1.9GHz respectively.

A basic cellular system consists of three parts: a *mobile terminal*, a *base station* and a *Mobile Telephone Switching Office (MTSO)*. As shown in Figure 1.1, the coverage area is divided into different *cells* in order to partition active mobile terminals into different subsets based on their geographical positions. Fictitious hexagonal-shaped cells are widely used in the initial planning and design of a cellular system due to their simplicity and resemblance to circular shapes. A mobile terminal can take various forms: a handheld unit, roof-mounted vehicular telephones and the recent wireless data modems in laptops. Operation within a cell is controlled by a fixed base station which provides interface between the MTSO and the mobile terminal. The MTSO serves as the central switch and controller to a group of base station, and is responsible for moving information to and from some fixed external networks. For the telephone calls, the external network is referred to as the *Public Switching Telephone Network (PSTN)*.

Over the air interface, the assigned spectrum is split into two directions of communications: the *reverse link* or *uplink* (i.e., mobile-to-base-station), and the *forward link* or *downlink* (i.e., base-station-to-mobile). For information transfer over air interface, each mobile terminal can only use one communication channel at a time. A channel can be mathematically represented by a frequency band, a time slot or a code. Between the base station and MTSO, microwave radio links or T-carriers (i.e., wired telephone lines) are used to carry both voice and data. Finally, standard voice trunks are used to connect PSTN and MTSO.

Wireless PCSs can also be classified in terms of their transmission methods as *simplex*, *half-duplex* and *full-duplex*. Simplex PCSs provide one-way communication, and the best known example is the paging system. Half-duplex and full-duplex PCSs both allow two-way communications by using the same and different radio channel respectively. Full-duplex PCSs can be supported by Frequency Divison Duplex (FDD) or Time Division Duplex (TDD), which represent by a pair of reverse and forward channels that are separated in different frequency bands or time slots respectively. Most existing PCSs are full-duplex using FDD, although new cordless telephones are using TDD.

With a call in progress, whenever the mobile terminal crosses the boundary between two cells, its communication channel is switched from one base station to another. This procedure is referred to as *handoff* or *handover* and is carried out without either interrupting the call or alerting the user. Another common scenario is *roaming* where a mobile terminal is operating outside its home service area. Since the early 1990s, the trend in cellular industries is to adopt *open* interfaces between equipments, rather than *proprietary* ones. As a result, equipment from different manufacturers can now be assembled together to facilitate mobility and roaming.

1.1.3 Multiple Access Techniques

The need for Multiple Access (MA) techniques arises whenever there is a limited communication channel resource that is accessed by more than one independent user (i.e., *multipoint-to-point communication*). In wireless PCSs, due to the

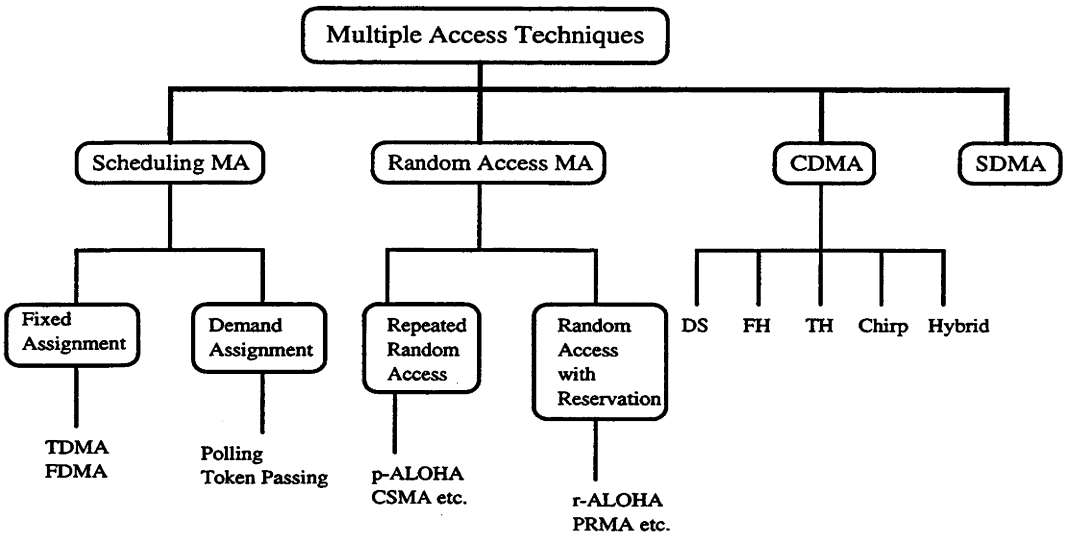

Figure 1.2: Classification of the Multiple Access techniques [1].

scarceness of channel resource (i.e., bandwidth), MA techniques are used to share the common transmission channel among all users in the system. The MA technology should be robust to channel impairments and changing conditions (e.g., traffic load is not spatially nor temporally uniform); and the receiver should be able to separate the desired signal from interfering signals.

As shown in Figure 1.2, the MA techniques can be classified into four main groups as follows [1, 11].

1. **Scheduling MA** — it avoids simultaneous access from multiple users by scheduling all transmissions. This scheduling protocol can either be implemented as a fixed assignment where the channel capacity is divided among the users in a static fashion, or as a demand assignment where the scheduled transmission takes place only if the user is active. Unlike the fixed assignment, the demand assignment does not waste channel capacity on idle users, albeit additional overhead and delay are introduced to sort out active users. Examples of demand assignment MA protocols include roll-call polling and token-passing [1].

   Traditionally radio communication systems use fixed assignment MA to di-

vide a single high-capacity MA channel into smaller orthogonal channels. This is typically done by channel partition in terms of disjoint frequency bands known as Frequency Division Multiple Access (FDMA), disjoint time slots known as Time Division Multiple Access (TDMA), or both (i.e., hybrid FDMA/TDMA). Hence, their capacities correspond to the number of channel partitions. To avoid *co-channel interference* (i.e., overlapping of different transmissions), guard times and bands are inserted between adjacent transmissions in TDMA and FDMA respectively. In cellular radio systems, to avoid co-channel interference, the concept of *frequency reuse* is used to place a minimum distance between cells using the same frequency set. A well-designed frequency reuse plan respects a compromise between high reception quality (i.e., low reuse factor) and high spectral efficiency (i.e., high reuse factor). Both TDMA and FDMA provide a simple MA solution in a steady or slowly varying traffic network. It is noted that FDMA is simpler than TDMA, since no synchronisation between users is required.

2. **Random Access MA** — it resolves the contention (or collision) that occurs when several users transmit simultaneously. The first random access system, known as ALOHA, was proposed for packet radio network in 1969 [12]. The family of ALOHA protocols assumes that there is the possibility of contention with every transmission. If the contention is detected, the user can defer its own transmission until the channel is free. Based on its access scheme, random access can be further divided into repeated random access and random access with reservation [1]. Some examples of both random access MA systems include p(ure)-ALOHA, Carrier Sense Multiple Access (CSMA), r(eservation)-ALOHA and Packet Reservation Multiple Access (PRMA). In general, random access MA is most suitable for bursty channels whereby the probability of simultaneous transmissions of more than one user occurring is sufficiently low.

3. **Code Division Multiple Access (CDMA)** — it falls between scheduling and random access MA. It allows a number users to be transmitted simultaneously without contention, but with increasing interference level as

more users are added. It was originally developed for use in military applications due to its anti-jamming property and low probability of detection. Its central concept is the usage of the spread spectrum modulation which expands the bandwidth of information-bearing signal.

In CDMA, each user is assigned a unique code such that its transmitted signal is spread into a wideband signal. At the Matched Filter based (MF) receiver (i.e., correlating the received signal with the desired user's code, as discussed in Section 2.5.3), assuming quasi-orthogonal codes, only the desired signal is "de-spread", and other signals remain wideband and appear as noise. Thus, CDMA is sometimes referred to as *spread spectrum MA*. Based on the modulation methods that generate spread spectrum signals, CDMA signals can be divided into a number of groups as follows.

- **Direct Sequence (DS)** — the information-bearing signal is directly multiplied by the spreading sequence. The usual form of modulation scheme is some form of Phase Shift Keying (e.g., Binary Phase Shift Keying (BPSK)). The one difference which sets DS-CDMA apart from all other CDMAs is the interference in the DS case is reduced by *averaging* it over a wide time interval, while interference in the others is reduced by *avoiding* it for most of the time.
- **Frequency Hopping (FH)** — the carrier frequency "hops" around pseudo-randomly according to the spreading sequence. A FH-CDMA system occupies only a fraction of spread bandwidth (i.e., hop bin) at one time, while a DS-CDMA system uses the entire spread bandwidth. Because of the difficulty of maintaining phase references as the frequency hops, non-coherent demodulations are normally used. Compared with DS-CDMA, FH-CDMA has less stringent synchronization requirement and is less sensitive to channel gain and phase fluctuations.
- **Time Hopping (TH)** — the information-bearing signal is transmitted in discontinuous, short bursts at time intervals determined by

the spreading sequence. Although its implementation is simpler than that of FD-CDMA, the required synchronization time in TH-CDMA is longer. It is noted that if all users' transmissions are synchronised, TH-CDMA is similar to a TDMA protocol.

- **Chirp Modulation** — this modulation is almost exclusively used in military radars, rather than PCSs. The radar transmits a low power signal whose frequency is varied continuously over a wide range.
- **Hybrid Modulation** — this modulation combines various CDMA signalling methods, in order to mitigate some of their disadvantages. A hybrid CDMA which has received much attention recently is the Multi-Carrier (MC)-CDMA. The MC-CDMA is a combination of CDMA and orthogonal frequency division multiplex signalling. In MC-CDMA, the information-bearing signal is spread using a given code in the frequency domain, and is potentially robust to frequency selective fading channels [1].

4. **Space Division Multiple Access (SDMA)** — it controls the radiation pattern of each user in space [13, 14]. A common application of SDMA is the use of sectorized/adaptive antennas. The direction of these antennas can be fixed or adjusted dynamically, in order to steer in the direction corresponding to the desired signal. Thus, through antenna gain, the interfering signals that lies outside the antenna's mainbeams can be attenuated. This SDMA results in spatial separation of users and is a useful method to suppress co-channel interference.

1.1.4 Application of CDMA in PCS

Although CDMA was proposed theoretically in the late 1940's, the practical application of CDMA in PCS did not occur until 1980's. There are two major incentives to its commercial applications: development of low cost digital integrated circuits and increased capacity by regulation of transmitted power from mobile terminals (i.e., *power control*). Due to its simple implementation, DS-

CDMA signal presents a popular choice for practical PCSs, and is the focus of this thesis. The system modelling for DS-CDMA is to be discussed in Section 2.3.

In comparison with the conventional TDMA and FDMA, some benefits of using CDMA in PCSs are briefly discussed as follows [1, 15, 16].

- Due to the use of orthogonal signalling in TDMA and FDMA, the given channel is partitioned into independent, single-user subchannels as disjoint time-frequency slots. Unlike TDMA and FDMA, CDMA can trade off reception quality for increased capacity. That is, the capacity of CDMA is interference-limited (i.e., *soft capacity*), while it is bandwidth-limited in TDMA and FDMA.

- The biggest benefit of CDMA is its higher spectral efficiency (i.e., capacity), as defined in Section 1.1.2, compared with TDMA and FDMA. The key to its high capacity is to use a coordinated power control scheme such that the received powers from all users are approximately equal. This usage of stringent power control is one simple method to solve the *near far problem*[3] which, in the past, has greatly reduced its capacity.

- CDMA offers protection against multipath interference and narrowband interference. As a result, the received voice quality can be dramatically improved.

- CDMA permits *soft handoff* which is characterised by transferring communication with a new base station on the same frequency assignment. Hence, the incidence of handoff failures is reduced, particularly in a multi-way simultaneous soft handoff scenario [15].

- CDMA requires lesser deployment and operating costs because fewer base stations are needed. In addition, larger cell sizes also reduce the handoff rate and significantly simplify its frequency reuse planning. Due to its inherent wideband characteristics, CDMA can be overlaid on top of existing

[3] With all mobile stations transmit constant power, the received powers in base station from nearby users may be significantly higher than those from others.

First Generation	Second Generation	Third Generation
AMPS (N.America)	GSM (Europe)	UMTS (Europe/Global)
NTT's std. (Japan)	IS-95 (N.America)	IMT-2000 (N.America/Global)
TACS (U.K.)	IS-54/136 (N.America)	MBS (Global)
NMT (Scandinavia)	PHS/PDC (Japan)	WCPNs (Global)
C-450 (Germany)	PACS (N.America)	FPLMTS (Global)
NEC's std. (Australia etc.)	DECT/CT-2 (Europe)	

Table 1.1: Some practical wireless PCS standards [1, 7].

narrowband channels, without causing significant rise in the background noise level [16].

- Apart from using directional antennas, CDMA capacity can also be increased by using variable-bit-rate speech transmission. That is, by exploiting its voice activity, a speech coder can reduce its transmission rate when a silent input is detected. This procedure can considerably reduce the average interference and battery drain from each transmitter.

1.2 Practical PCS Standards

In this section, a brief description for each of the three generations of wireless PCS standards are given. For the purpose of illustration, some practical PCS standards are summarised in Table 1.1 and four common high-tier PCS standards are summarised in Table 1.2. In Table 1.2, both the cellular and PCS frequency bands are listed in the order of reverse link followed by forward link.

1.2.1 First Generation

In 1980s, the first generation PCS was introduced in analog form. Different PCS standards were developed worldwide. All systems are mutually incompatible due to different operating frequencies and channel bandwidths. However, all analog cellular systems use frequency modulated voice transmission, and the access

	AMPS	IS-54/136	GSM	IS-95
Cellular frequency bands (MHz)	824-849 869-894	824-849 869-894	890-915 935-960	824-849 869-894
PCS frequency bands (MHz)	—	1850-1910 1930-1990	(DCS-1800) 1710-1785 1805-1885 (DCS-1900) 1850-1910 1930-1990	1850-1910 1930-1990
Carrier spacing (kHz)	30	30	200	1230
Channels per carrier	1	3	8	soft capacity
MA techniques	FDMA	TDMA/ FDMA	TDMA/ FH-FDMA	CDMA
Duplex	FDD	FDD	FDD	FDD
Spectral efficiency (channel/cell/MHz)	2.3	7.0	5.0-6.6	12.1-45.1
Modulation method	FM	$\pi/4$-DQPSK	GMSK	PSK
Frequency reuse factor	7	7	3	1
Channel rate	10 kb/s	48.6 kb/s	270.833	1.23 Mchips/s
Modulation efficiency (b/s/Hz)	0.33	1.6	1.4	1.0
Speech coding	analog FM	VSELP	RPE-LPC	QCELP
Speech rate (kb/s)	—	13	22.8	variable
Authentication	ESN	A-key	Ki-key	long code mask
Frame duration (ms)	—	40	4.6	20
Max. terminal transmitter power (W)	4	4	8	6.3
Channel coding	BCH block code	1/2 rate conv. code	1/2 rate conv. code	1/2 & 1/3 rate conv. code
Year of deployment	1983	1992	1990	1993

Table 1.2: Comparison of four common high-tier PCS standards [8].

technique used is FDMA. In particular, their network architectures and signalling systems are all similar to Advanced Mobile Phone System (AMPS). Hence, AMPS is to be used as a case study here.

AMPS has been designed to deliver basic telephony and some supplementary services (e.g., voice mail and call forwarding). Although AMPS had major success in terms of technological advances and commercial feasibility, it suffers from the following problems [8] which eventually gave rise to the second generation of PCSs.

- **Limited capacity** — capacity is traditionally increased by either cell splitting or assignment of additional spectrum allocation. However, cell splitting incurs high overhead costs as more base stations are required. Also, as in the United States in the 1980s, the Federal Communications Commission announced that no additional cellular bands would be available.

- **Roaming problems** — AMPS does not specify communications between base stations and MTSOs. Since there is no coordination between switches produced by different manufacturers, roaming became rather tedious (e.g., requires dialling of special codes). As a result, IS-41 was developed in 1991 to deliver calls and to handoff calls to roaming users.

- **Poor network security** — The AMPS authentication procedures reply on each terminal's Electronic Serial Number (ESN). Because mobile terminal transmit their ESNs through the air interface, ESN is subject to interception and fraudulent use.

1.2.2 Second Generation

In the early 1990s, the second generation PCS was deployed in digital form. The second generation systems provide digital speech and enhanced services delivered to the screens of their mobile terminals (e.g., short messages, caller identification). Compared to the first generation, they provide higher received voice quality, higher capacity, better authentication and handoff procedures. In the United States, all mobile terminals specified in Interim Standard (IS)-54/136 and IS-95

have dual-mode capability such that they are compatible with areas covered by AMPS. Except for IS-95 which is based on CDMA, TDMA is used as the MA technique. The following case study is concerned with IS-95 which is summarised as follows [17, 18].

- IS-95 is a DS-CDMA system developed by Qualcomm, Inc. and its characteristics are listed in Table 1.2.
- Compared to AMPS, IS-95 can operate with much larger co-channel interference due to the inherent interference resistance properties of CDMA. This translates to a lower Signal-to-Noise Ratio (SNR) requirement which provides a large capacity improvement [19].
- IS-95 uses a different spreading techniques for the forward and reverse links which have coherent and non-coherent demodulations respectively[4]. More details on the forward and reverse channels for IS-95 can be found in [18].
- IS-95 uses the Qualcomm Code Excited Linear Predictive (QCELP) coder for speech coding. This vocoder detects voice activity and adjusts its data rate according: 1.2 kb/s (silent period), 2.4 kb/s, 4.8 kb/s and 9.6 kb/s (full-rate).
- As discussed in Section 1.1.4, tight control of transmitted power from each user is required, in order to avoid near-far problem. IS-95 uses a combination of open-loop and fast closed-loop power control (e.g., signalling rate of 800 b/s in reverse link).
- IS-95 incorporates the same authentication procedures used in IS-54/136. In addition, IS-95 operates with a combination of private and public long code mask.
- IS-95 specifies global position system receiver to be installed in all base stations to maintain synchronism (e.g., to enable soft handoff).

[4] Since a pilot signal is not available as a coherent carrier reference, non-coherent detection is used in reverse link.

1.2.3 Third Generation

The third generation PCS will evolve from mature second generation systems and is expected to be deployed by the year 2000. Its service is predicted to penetrate up to 50% of the telecommunication services population [1]. Its goal is to provide global access with a wide range of PCS applications, in any location at any time. As discussed in Section 1.1.1, the distinctions between different existing PCSs will disappear (e.g., public or private, wired or wireless, and outdoor or indoor). For example, apart from the traditional mobile voice communication, it will use Broadband Integrated Services Digital Network to provide a diverse range of services (e.g., multimedia capabilities, Internet access, imaging and video conferencing).

About ten years ago, the International Telecommunication Union (ITU) has started to develop the third generation PCS within the framework of Future Public Land Mobile Telecommunication Systems (FPLMTS). Since the acronym FPLMTS is difficult to pronounce, the new name "International Mobile Telecommunication" (IMT-2000) has been adopted by ITU, and other names include "Universal Mobile Telecommunications System" (UMTS) within the European community. In 1992, ITU has decided to unifty both the satellite and terrestrial links in IMT-2000 with 230 MHz spectrum in the 2 GHz band [9]. Also, a flexible, variable-rate access with data rate near 2 Mb/s has been proposed for IMT-2000 systems. Currently, it appears that the MA technique for the third generation PCS will be a hybrid combination of wideband CDMA and TDMA [1].

1.3 Thesis Overview

Blind multiuser detection[5] is concerned with the scenario where no training phase is available. It is assumed that only the spreading sequence of the desired user is known. This thesis deals with various aspects of blind linear multiuser detection for DS-CDMA systems. In particular, Chapters 3 to 7 present the original contributions and serve as the main body of this thesis. The performance of blind

[5] Its detailed problem statement is to be defined in Section 2.4.

methods studied are verified by analysis and simulations. The specific content of each chapter is briefly summarised as follows.

- **Chapter 2: Overview of Multiuser Detection**

  This chapter gives a tutorial on multiuser detection in DS-CDMA system. First, the two different design concepts in CDMA are discussed. These two design classes differ by their usages of spreading codes, one uses long codes while another uses short codes. In accordance with multiuser detection which is the core subject of this thesis, short codes are to be used throughout this thesis. Second, the system model of DS-CDMA is presented in terms of its transmitter, channel and receiver. This mathematical model provides an intuitive understanding of problem setting in this thesis, and is to be further refined in each chapter. Third, background material on multiuser detection is given, including its problem statement, limitations and potential benefits.

  This introductory chapter ends with a general survey of previously proposed multiuser detection techniques for DS-CDMA systems. For each detection scheme, both its advantages and deficiencies are reviewed. To facilitate the comparisons made in the later chapters, more emphasis is placed on the topic of blind multiuser detection.

- **Chapter 3: Two Blind Linear Multiuser Detectors — Minimum Output Energy (MOE) and Constant Modulus Algorithm (CMA)**

  In Chapter 3, a popular blind method based on the Minimum Output Energy (MOE) is examined. Then, several robust alternatives to the MOE-based detector are proposed, namely the linearly constrained MOE detector and one based on the Constant Modulus Algorithm (CMA). For these two detectors, convergence analyses are presented in both the steady state and transient phases. It is shown that an important feature of this CMA approach is its lock convergence behaviour that locks onto the desired signal and nulls all interfering signals, in a noiseless situation. Finally, for a linear multiuser detector in a canonical form, the problem of signature mismatch

(i.e., imprecise knowledge of the received, desired signature waveform) is discussed .

- **Chapter 4: CMA-based RAKE-type Receiver**

  Unlike Chapter 3, Chapter 4 incorporates the usage of multiple sensors to induce spatial diversity to the receiver. Also, frequency selective multipath channels are included in the system model. Literature survey shows that the conventional blind 2-D RAKE receiver, which consists of a bank of beamformers and a temporal RAKE receiver is the first to exploit spatial diversity. However, this 2-D RAKE receiver is essentially a single user detection scheme, and is susceptible to near far effect, given non-orthogonal signature waveforms.

  To overcome the deficiencies suffered by the 2-D RAKE receiver, a CMA-based RAKE-type receiver is proposed. To exploit the temporal and spatial diversities in a joint fashion, the proposed receiver performs linear multiuser detection within a RAKE-type processing. In the same manner as in Chapter 3, its lock convergence behaviour and convergence rate are analysed, as well as the effect of channel order mismatch.

- **Chapter 5: Constrained CMA-based Receiver**

  In Chapter 5, although the problem considered is similar to that of Chapter 4, a few assumptions that were used to simplify the analysis have been removed. A constrained CMA-based blind method is proposed where by using orthogonal projection matrices, the adaptation of the CMA is now constrained in the desired subspace. In the same manner as the MOE-based receiver, the overall linear filter is decomposed into a fixed and an adaptive component. As a result, the multipath effect of the desired signal can be decoupled and removed. For its convergence analysis, all stationary points and their stabilities are derived, and the significance of the modulus radius is discussed.

  In comparison with the CMA-based RAKE-type receiver in Chapter 4, this constrained approach has less stringent lock convergence initialisation. This

is because that the constraints involved ensure that the only stable stationary point is the desired local minimum.

- **Chapter 6: Effect of Arrival of Additional Users**

  Chapter 6 studies the effect of arrival of additional users to the MOE-based and the CMA-based blind multiuser detectors. Under a synchronous and noiseless assumption without signature mismatch, the MOE- and CMA-based detectors are compared with the training-based Minimum Mean Squared Error (MMSE) detector. The perturbations caused by the birth of interferers are examined from the viewpoint of the change of respective cost functions. In terms of its robustness, the tradeoff involved in the choice of modulus modulus in the CMA is discussed.

- **Chapter 7: Constrained CMA-based Code Acquisition Scheme**

  Unlike Chapter 3 to 6, the focus of Chapter 7 is on the problem of code acquisition, or the estimation of time delay of the desired user within one chip interval. The uncertainty of the estimated delay is discretized and translated into a number of hypotheses. Using an equivalent synchronous model, the aim is to derive a blind, near far resistant acquisition scheme which selects the correct hypothesis. A literature survey has shown that the Second Order Statistics (SOS) based blind acquisition schemes are non-adaptive, as they rely on the correlation matrices of the received signal.

  Without the need to estimate its correlation matrices, a blind, near far resistant code acquisition scheme is proposed and is reminiscent of the constrained CMA-based receiver in Chapter 5. In the same manner as the MOE-based detector, hypotheses are chosen based on their respective output energies. Using appropriate linear constraints, it is shown that the lock convergence will always occur for the correct hypothesis. For all incorrect hypotheses, their filter trajectories are most likely to be trapped within some saddle points, given sufficiently small step sizes.

- **Chapter 8: Conclusions and Future Research Directions**

This final chapter contains concluding remarks and some possible directions for future work.

- **Appendix A**

  In Appendix A, the stationary points and their stabilities of the CMA-based multiuser detector are derived.

1.4 Thesis Contribution

The major contributions made in this thesis to the concept of blind multiuser detection in DS-CDMA systems are listed as follows.

- A linearly constrained MOE-based blind method is proposed. It is shown that this method is robust against finite precision errors of the original MOE method in [3]. The selection of the constraint involved, reflects a tradeoff between the Signal-to-Interference Ratio (SIR) optimisation, and robustness to the signature mismatch.

- In comparison with the popular MOE-based blind method, a CMA-based blind linear multiuser detector is proposed and is seen as a potentially more robust alternative (e.g., effect of channel noise). In the vicinity of its desired local minimum, the CMA converges twice as fast as the MOE case.

- It is shown that in the absence of channel noise, the CMA exhibits a lock convergence property which locks onto the desired signal and nulls all other interfering signals (i.e., a decorrelating property). Initialisation scheme for this lock convergence is simple and robust under practical near far conditions.

- For blind multiuser detection over frequency selective multipath channels, two novel blind methods are proposed: CMA-based RAKE-type and constrained CMA-based receiver. The first method utilises the concept of diversity and multiuser detection within a RAKE-type receiver structure. For the second method, filter adaptations are constrained to be decoupled

from the multipath effect to the desired signals. In both methods, multiple sensors are incorporated such that both time and space diversities can be jointly exploited.

- The transient performance perturbations caused by arrival of additional interferers into the system for the MOE-based, the CMA-based and the training-based MMSE detectors are examined. If the additional number of users entering the system is small enough, it is shown that both the CMA with an appropriate choice of modulus radius, and the MOE methods have similar instantaneous drops in the SIR performance to the MMSE case. Also, the robustness of the CMA with respect to adding interferers to a large user population is less than the same addition of new users to a smaller user population.

- A new blind, near far resistant code acquisition scheme is proposed and is based on a linearly constrained CMA. It is shown that its near far resistance can be further improved by appropriate scaling of the constraints involved, at the expense of slower convergence. In comparison with the conventional sliding correlator acquisition method, the proposed method gives a higher acquisition-limited capacity and higher near far resistance.

Chapter 2

Overview of Multiuser Detection

2.1 Chapter Outline

This chapter aims at giving an introductory level tutorial to multiuser detection in general, and provides a foundation for the rest of this thesis. In Section 2.2, to distinguish between the concept of multiuser detection and single user detection, two different types of CDMA system design are discussed. In Section 2.3, the system model of DS-CDMA system is presented, as well as the general assumptions made in this thesis on the signal model. In Section 2.4, introduction to the concept of multiuser detection is presented with its problem statement, limitations and potential benefits. The conventional DS-CDMA detection and blind multiuser detection are discussed as special cases of multiuser detection. Finally, in Section 2.5, a literature review on multiuser detection is given.

2.2 Two Approaches in CDMA System Design

As aforementioned in Section 1.1.3, for TDMA and FDMA systems, the term "co-channel interference" commonly refers to interference that arises from undesired transmissions. To standardize the terminology used in CDMA systems, for the rest of this thesis, the term *Multiple Access Interference* (MAI) is to be used instead which represents signal contributions from all other interferers.

As reflected in the apparent "divorce" between the IS-95 CDMA cellular standard [18] and most CDMA literature, there are fundamentally two different CDMA design approaches [20]. They differ by the type of Pseudo-Noise (PN) sequences which are used as spreading codes, and are listed as follows.

1. **Long Codes** — or *aperiodic codes*, use extremely long PN sequences whose waveform period is much larger than the symbol period.

2. **Short Codes** — or *periodic codes*, use PN sequences whose length spans only one symbol interval.

Historically, the long code design approach originated from Viterbi's interpretation [21] of the third lesson of *Shannon's Information Theory* [22]:

> "*In the presence of interference or jamming, intentional or otherwise, the communicator, through signal processing at both transmitter and receiver, can ensure that performance degradation due to the interference will be no worse than that caused by Gaussian noise at equivalent power levels.*"

That is, when its variance is constrained, the worst case MAI to any user is Additive White Gaussian Noise (AWGN) [20]. Thus, the usage of long code is fundamentally a *minimax* design solution, such that MAI appears as wideband AWGN. Using the Central Limit Theorem, it is argued that the contribution of MAI from many interferers of equal received power can be accurately approximated by a Gaussian random variable [20]. In general, the IS-95 CDMA format adopts the long code approach, and this has the following consequences.

- To alleviate the near far problem, a very accurate and fast power control is used to keep the variations of received signals to within a fraction of one dB. In addition, it is used to conserve battery energy in portable transmitters, and to alleviate the effects of fading and reduces out-of-cell interference [23].

- The only short code used for spreading is the set of 64 Walsh codes. However, the usage of Walsh codes are different in the reverse and forward channels[1].

- The two long codes used have periods of $2^{42} - 1$ and 2^{15} chips and are used for DS signal spreading and quadrature spreading (i.e., separated into I and Q channel) respectively. On the reverse link, the first long code is channel-unique, and the second one is used for signal randomization [24] to yield the desired wideband spectral characteristics (i.e., signal spectrum is uniformly distributed over the frequency).

- Essentially a *single user detection* scheme, a conventional Matched Filter (MF) which correlates the received signal with the spreading signal (its mathematical representation is presented in Section 2.5.3), is used. The MF receiver was believed to be quasi-optimal due to its Gaussian approximation. In particular, the non-coherent RAKE receivers used in base stations are implemented as a bank of delayed MFs[2].

- Overall, highly redundant error control codes are employed to mitigate the effect of MAI. On the reverse link, low rate (i.e., 1/3 rate) orthogonal convolutional codes are used to provide a robust link over fading channels with low SNR at the symbol level.

As discussed in [16, 23], there are misconceptions concerning the usage of MF and long codes. These misconceptions are addressed as follows.

- Unless the SNR is very low (e.g., less than 10dB), the Gaussian approximation is invalid, even in the ideal situation of perfect power control with moderate MAI level. Furthermore, the system parameters (e.g., number of users) encountered in practical situation render the Gaussian approximation useless.

[1] On the forward link, Walsh codes are determined by the assigned channels to preserve their orthogonalities. On the reverse link, the code is determined by the the transmitted information (i.e., at the output of encoder and interleaver). [2] The delays are in accordance with the received multipath signals, and are obtained by the front-end searcher in the receiver [17].

- The inaccuracy of the Gaussian approximation lies in the fact that only the total power of MAI is considered, but not the number of users nor the received power of an individual interferer.

- In fact, the optimality of MF is incorrect because the demodulation of desired user restricted to its MF output does not constitute a *sufficient statistics* [16]. Conversely, the structure of MAI contains valuable information for the required demodulation, but would be lost if the Gaussian approximation is used.

- The near far problem is not an inherent flaw of CDMA systems, but results from the Gaussian approximation of the MF.

- Most benefits of spread spectrum as discussed in Section 1.1.4 depend directly on the spreading gain, rather than the periodicity of the spreading code. For instance, privacy is more robust by using cryptography, rather than the long code.

The short code design approach facilitates the use of *multiuser detection* which is the main subject of this thesis. For this reason, short codes are to be used throughout this thesis. In the application of short codes, there is no fundamental reason to restrict its spreading interval to equal one symbol interval. However, it is recognized that longer spreading codes (in terms of the number of symbol intervals) would place more burden imposed on the adaptive multiuser detection strategies [23]. In [2], it is shown that if spreading codes span a number of symbol intervals (referred to as *signature overlapping*), the number of subscribers for a given spreading gain and resistance against impulse noise can be increased. In practice, the selection of spreading codes is based on two criteria: good auto-correlation and cross-correlation properties to improve synchronisation and suppression of MAI respectively [25].

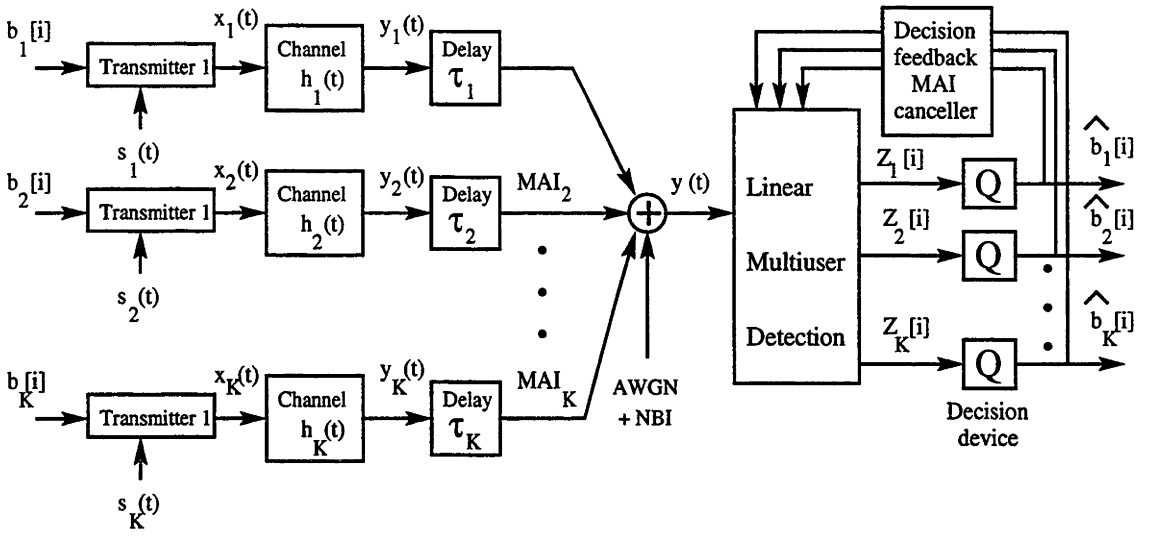

Figure 2.1: A block diagram of an asynchronous K-user DS-CDMA system with generalised multiuser detection.

2.3 System Modelling of DS-CDMA System

In this section, the system configuration is discussed and models for the transmitter, the channel and the receiver are described. In addition, the list of general assumptions regarding the signal model that are made in this thesis is given.

2.3.1 System Configuration

The most common form of CDMA, a DS-CDMA system, is considered. A block diagram of an asynchronous DS-CDMA system with multiuser detection generalised from both linear and nonlinear formats, is shown in Figure 2.1. Let the total number of users be K with the user index denoted by $k \in \{1, \ldots, K\}$. Throughout this thesis, it is assumed that user $k = 1$ corresponds to the desired user.

For the kth user, the ith transmitted symbol and its signature waveform is denoted as $b_k[i]$ and $s_k(t)$ respectively. As shown in Figure 2.1, each transmitted signal $x_k(t)$ propagates through a different channel with Finite Impulse Response

(FIR) $h_k(t)$, and output signal $y_k(t)$. To model the lack of the time alignment of the users' transmissions, symbol-epoch offsets τ_k are introduced. Hence, the total received signal $y(t)$ is modelled as the sum of the delayed contributions of $y_k(t)$ from all users. The signal model above represents an asynchronous CDMA system with different channel and delay for each user, and is typical for the reverse link. It is noted that the forward link is a special case of this model, where all users are synchronized and broadcast through the same channel (i.e., $\tau_k = \tau$ and $h_k(t) = h(t) \quad \forall k \in \{1, \ldots, K\}$), to the mobile of interest.

The total received signal $y(t)$ is subject to distortions due to AWGN, Narrowband Interference (NBI), channel impairments and MAI. Typically, AWGN consists of receiver thermal noise, while NBI may originate from intentional jamming or from the coexistance of existing narrowband channels [16]. From the viewpoint of the desired user (i.e., $k = 1$), the contribution of MAI from the kth interfering user is denoted as MAI_k, where $k \in \{2, \ldots, K\}$. The multiuser detector has been generalised[3] into two parts: a linear component and a decision feedback MAI canceller. For the kth user, the multiuser detector outputs $Z_k[i]$. By applying $Z_k[i]$ to the decision device (i.e., quantizer), its corresponding estimated symbol $\hat{b}_k[i]$ is obtained.

2.3.2 Transmitter

The DS-CDMA transmitter model is shown in Figure 2.2. The original information is first formatted in digital form as a sequence of binary data bits. Then, the data passes through an encoder which embodies several functions: source coding, encryption and channel coding. Respectively, these functions are used for data compression, induced secrecy and increased robustness against channel impairments. Next, the mapper assigns the encoded bits to specific symbols $b_k[i]$, in accordance with the given signal constellation.

As in all CDMA systems, a spread spectrum modulator is used to expand the bandwidth of information bearing signal $b_k[i]$, to that of the signature waveform

[3] It is noted that there exists various multiuser detectors, which do not fit this generalisation, as discussed in Section 2.5 (e.g., multistage detectors [26]).

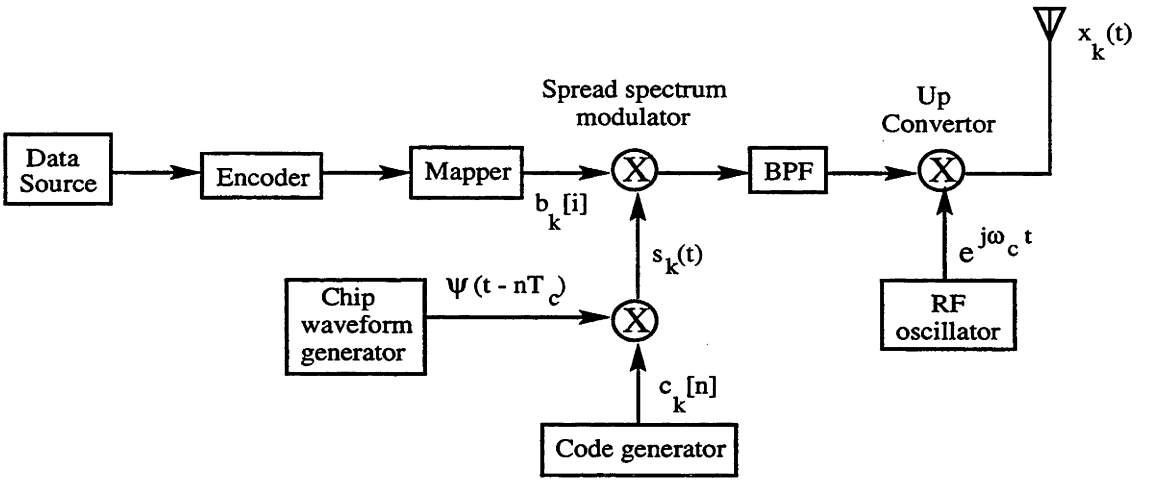

Figure 2.2: A block diagram of DS-CDMA transmitter for the kth user.

$s_k(t)$. This bandwidth expansion factor is commonly known as *spreading factor* or *processing gain*, and is defined as follows

$$N \triangleq \frac{T_b}{T_c} = \frac{W}{R_b}, \tag{2.1}$$

where T_b and T_c are the symbol and chip duration, and $R_b = 1/T_b$ and $W = 1/T_c$ are the data and chip rate, respectively. The choice of N is crucial in CDMA system design [16], since N determines its spread spectrum properties (e.g., anti-jamming). In DS-CDMA systems, the spread spectrum modulator consists of two generators, which produce a chip waveform $\psi(t)$ and PN sequence $c_k[n]$. For the kth user, the modulating carrier, the DS signature waveform with duration NT_c is obtained and is written as

$$s_k(t) = \sum_{n=1}^{N} c_k[n]\psi(t - nT_c). \tag{2.2}$$

To reduce the Inter-Symbol-Interference (ISI) at the receiver, a Bandpass Filter (BPF) (i.e., pulse shaping filter) is used to suppress the signal spectrum outside the signature bandwidth W. Before transmission, an up-converter is used to shift the baseband signal to the desired carrier frequency f_{RF}. The final

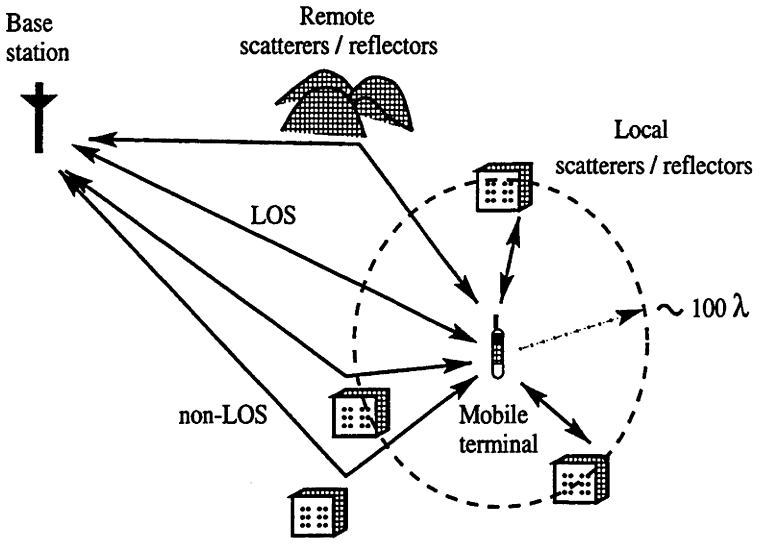

Figure 2.3: Illustration of a typical mobile radio environment.

transmitted signal from the kth user is given by

$$x_k(t) = \sum_i b_k[i] s_k(t - iT_b) e^{j[(\omega_{RF}+\omega_k)t+\varphi_k]}, \tag{2.3}$$

where $\omega_{RF} = 2\pi f_{RF}$ is the angular carrier frequency, and ω_k and φ_k are the independent, time-invariant carrier frequency and phase offset of the kth transmitter respectively.

2.3.3 Channel

As shown in Figure 2.3, propagation paths between the fixed base station and the mobile terminal can be of Line-of-Sight (LOS), or non-LOS (i.e., obstructed). Propagation models can be characterized into two classes: *small-scale* or *large-scale*. Respectively, large-scale and small-scale models focus on predicting the average received signal strength and its rapid fluctuations. The small scale model accounts for the rapid changes in signal strength over small distances, due to local scatterers or reflectors; while the large-scale model considers the case of remote objects. For instance, at 850 MHz (i.e., cellular bands), local scatterers or reflectors are located within a radius of roughly 100λ (wavelength) [27].

In terms of its underlying physics, the three basic propagation mechanisms are reflection, diffraction, and scattering. For instance, most urban environments have no LOS path, and have severe "knife-edge" diffraction loss due high-rise buildings [7]. Even when a LOS path exists, *multipath* propagations still occur due to reflections and scatterings from the ground and surrounding structures. Under the multipath conditions, multiple versions of the transmitted signal arrive at the receiver and are displaced in different time and space dimensions.

In general, the mobile radio propagation characteristics can be classified into three aspects [28] which are briefly discussed as follows.

1. **Path Loss** — the propagation path loss generally increases both with frequency and distance. For the kth user, the average received carrier power $P_k(t)$ is an exponentially decreasing function of distance between the transmitter and the receiver d_k, and is represented as follows

$$P_k \propto d_k^{-\gamma_k}, \tag{2.4}$$

where γ_k is the corresponding path loss exponent. In most outdoor environments, γ_k usually lies between 3 and 5 (typically 4), and $\gamma_k = 2$ corresponds to free space. Practical values of γ_k depend on the actual conditions (e.g., materials and structure of nearby buildings). In CDMA systems, this path loss is responsible for the near far effect, as discussed in Section 1.1.4.

2. **Multipath Fading** — the types of multipath fading can be categorized based on the following parameters:

   (a) *RMS time delay spread* T_m, and *coherence bandwidth* $(\Delta f)_c$ are used to describe the frequency selectivity (i.e., time dispersive nature) of a channel. In practice, T_m can be measured from the power delay profile, as its standard deviation. In general, T_m and $(\Delta f)_c$ are inversely proportional to one another, although their exact relationship is dependent on the actual multipath structure.

   (b) *Doppler spread* B_d, and *coherence time* $(\Delta t)_c$ are used to describe the time selectivity (i.e., time varying nature) of a channel. Analogous to

	flat or **frequency non-selective**	**frequency selective**
slow or **time non-selective**	$W \ll (\Delta f)_c$ $T_b \ll (\Delta t)_c$	$W \gg (\Delta f)_c$ $T_b \ll (\Delta t)_c$
fast or **time selective**	$W \ll (\Delta f)_c$ $T_b \gg (\Delta t)_c$	$W \gg (\Delta f)_c$ $T_b \gg (\Delta t)_c$

Table 2.1: Four types of multipath fading.

T_m and $(\Delta f)_c$, in general, B_d and $(\Delta t)_c$ are also inversely proportional to each other. In particular, B_d is related to the maximum Doppler shift f_d as follows

$$B_d = 2f_d \tag{2.5}$$

$$f_d = \frac{v \cdot f_{RF}}{c}, \tag{2.6}$$

where v is the speed of mobile terminal and c is the speed of propagation.

(c) *Angle spread* is used to describe the space selectivity of the channel. A common measure of angle spread is the range of angle of arrival at the antenna array of the receiver [28].

As shown in Table 2.1, multipath fading can be categorized in terms of their time and frequency domain properties (i.e., based on $(\Delta t)_c$ and $(\Delta f)_c$). Due to its inherent wideband characteristics (i.e., $W \gg (\Delta f)_c$), multipath fading models for CDMA systems are often frequency selective channels.

Under multipath propagation, for the kth user, the baseband complex channel FIR can be modelled as [1, 28]:

$$h_k(t,\tau) = \sum_{l=1}^{L'_k} \alpha_{k,l}(t) e^{j\phi_{k,l}(t)} \delta(\tau - \tau_{k,l}), \tag{2.7}$$

where L'_k is the total number of paths, $\delta(\cdot)$ is the Dirac delta function, and $\alpha_{k,l}$, $\phi_{k,l}$ and $\tau_{k,l}$ are the amplitude, phase and delay of the lth path,

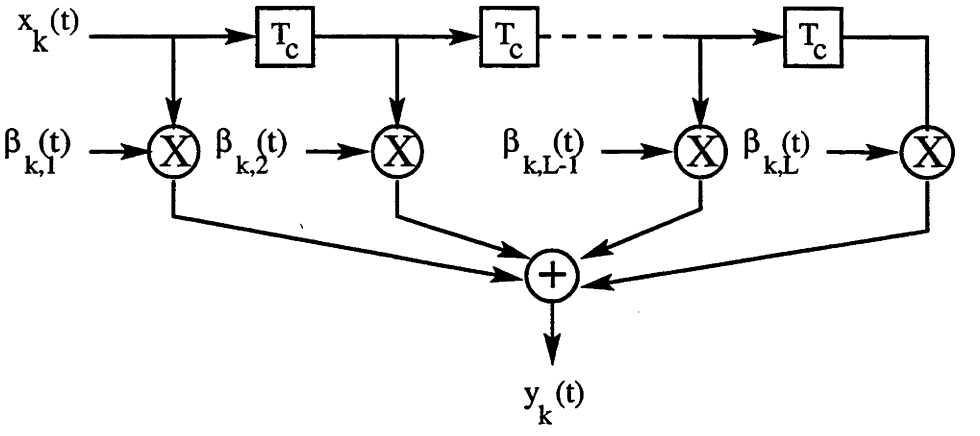

Figure 2.4: Tapped delay line model of a DS-CDMA frequency selective channel for the kth user.

respectively. Then, the maximum multipath delay spread is defined as

$$T_{k,max} = \max_{l} \tau_{k,l} - \min_{l} \tau_{k,l}. \tag{2.8}$$

For wideband signals such as CDMA, there exist a number of resolvable paths [1]. The maximum number of resolvable paths can be estimated as

$$L_k \triangleq \left\lfloor \frac{T_{k,max}}{T_c} \right\rfloor + 1, \tag{2.9}$$

where $\lfloor x \rfloor$ is the largest integer that is less than or equal to x (i.e., floor operator). That is, if two distinct physical paths are separated by at least one T_c, they can be resolved independently; otherwise, they are combined into a single path (i.e., subpath clusters). Using Turin's model [29], the channel response in (2.7) can be approximated as follows [28]

$$h_k(t,\tau) \simeq \sum_{l=1}^{L_k} \beta_{k,l}(t)\delta(\tau - \tau_{k,l}), \tag{2.10}$$

where $\beta_{k,l}(t) = \alpha_{k,l}(t)e^{j\phi_{k,l}(t)}$ are complex path gains. For frequency selective channels, (2.10) can be represented by a tapped delay line model as shown in Figure 2.4. However, it should be noted that this model is

ill-suited to *sparse* multipath channels (i.e., long delays between multipath components).

For small delay spread $T_{k,max}$, it is plausible to assume that all path gains $\beta_{k,l}(t)$ are described by the same probability density function (p.d.f.) [1]. As L becomes large, the central limit theorem can be invoked such that $\beta_{k,l}(t)$ approaches a complex Gaussian random variable. Three typical p.d.f.s associated with the distribution of $\beta_{k,l}(t)$ are described as follows [30].

(a) *Rician distribution* — includes a strong LOS component with average power $\mu^2/2$, and its path amplitude $\alpha_{k,l}$ has p.d.f.

$$f(\alpha_{k,l}) = \frac{\alpha_{k,l}}{\sigma^2} \exp\left(-\frac{\alpha_{k,l}^2 + \mu^2}{2\sigma^2}\right) I_0\left(\frac{\alpha_{k,l}\mu}{\sigma^2}\right), \quad 0 \leq \alpha_{k,l} < \infty \text{ and } \mu \geq 0; \tag{2.11}$$

where $\sigma^2 = E\{\alpha_{k,l}^2\}$ is the received power of the lth resolvable path, and $I_0(\cdot)$ is the modified Bessel function of the first kind and zero order [31].

(b) *Rayleigh distribution* — a special case of the Rician distribution, when LOS is not available. It arises when the process is zero-mean, its phase $\phi_{k,l}$ is uniformly distributed on $[0, 2\pi]$, and $\alpha_{k,l}$ has p.d.f.

$$f(\alpha_{k,l}) = \frac{\alpha_{k,l}}{\sigma^2} \exp\left(-\frac{\alpha_{k,l}^2}{2\sigma^2}\right), \quad 0 \leq \alpha_{k,l} < \infty. \tag{2.12}$$

(c) *Nakagami m-Distribution* — offers the best fit to experimental data in urban multipath channels and has p.d.f.

$$f(\alpha_{k,l}) = \frac{2}{\Gamma(m)} \left(\frac{m}{\sigma^2}\right)^m \alpha_{k,l}^{2m-1} \exp\left(-\frac{m\alpha_{k,l}^2}{\sigma^2}\right), \quad m \geq \frac{1}{2}; \tag{2.13}$$

where $m = \sigma^4 / E\{(\alpha_{k,l}^2 - \sigma^2)^2\}$ and $\Gamma(\cdot)$ is the gamma function. Analogous to Rician distribution, it is a two-parameters distribution (i.e., m and $\sigma_{k,l}^2$) with Rayleigh distribution included as a special case ($m = 1$).

3. **Shadowing** — apart from rapid signal fluctuations due to multipath fading, there are slow signal changes caused by large obstructions (e.g., buildings

or hills) along propagation paths. For the kth user, this shadowing effect on its average received power P_k is commonly modelled by a log-normal p.d.f.

$$f(P_k) = \frac{1}{\sqrt{2\pi}\sigma_k P_k} \exp\left(-\frac{\ln(P_k) - m_k}{2\sigma_k^2}\right), \tag{2.14}$$

where σ_k and m_k are the logarithmic standard deviation and mean of P_k respectively.

2.3.4 Receiver

In the case of a single sensor model (from (2.3) and (2.10)), the received signal for the kth user can be written as

$$\begin{aligned} y_k(t) &= A_k(t)\, x_k(t) * h_k(t, \tau = t) \\ &= A_k(t) \int_0^{L_k T_c} x_k(t-\tau) h_k(t,\tau) d\tau, \\ &= A_k(t) \sum_i b_k[i] f_k(t - iT_b) \cdot e^{j[(\omega_{RF}+\omega_k)t+\varphi_k]}, \end{aligned} \tag{2.15}$$

where $*$ is the convolution operator, and $A_k(t) = \sqrt{P_k(t)}$ is the received amplitude affected by the path loss in (2.4) and the shadowing effect in (2.14). In (2.15), the notation of received signature waveform is introduced and is defined as

$$\begin{aligned} f_k(t) &\triangleq s_k(t) * h_k(t, \tau = t) \\ &= \sum_{n=1}^{N} c_k[n] g_k(t - nT_c), \end{aligned} \tag{2.16}$$

where

$$g_k(t) = \int_0^{L_k T_c} \psi(t-\tau) h_k(t,\tau) d\tau, \tag{2.17}$$

is the composite FIR of the chip pulse $\psi(t)$ and the channel FIR $h_k(t, \tau)$.

From (2.15), the total received signal is represented as the sum of the delayed contributions of all users

$$\begin{aligned} y(t) &= \sum_{k=1}^{K} y_k(t - \tau_k) + n(t), \\ &= \sum_{k=1}^{K} A_k(t) \sum_i b_k[i] f_k(t - iT_b - \tau_k) \cdot e^{j[(\omega_{RF}+\omega_k)t+\varphi_k]} + n(t) \end{aligned} \tag{2.18}$$

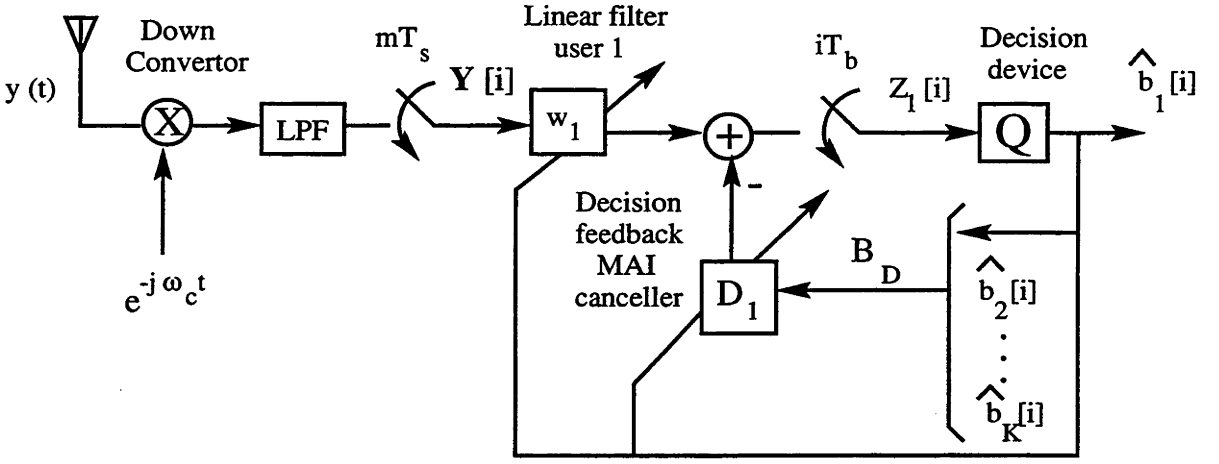

Figure 2.5: A block diagram of DS-CDMA receiver with generalised multiuser detection for user 1 [2].

where τ_k is the delay offset of the kth user and $n(t)$ is the summation of AWGN and NBI (i.e., typically modelled as correlated Gaussian noise [2]).

As shown in Figure 2.5, the received signal $y(t)$ is first downconverted to baseband and filtered by an anti-aliasing filter (i.e., Lowpass Filter (LPF)) with bandwidth B_s. To obtain the discrete-time received signal of $y(t)$ in (2.18), a chip MF is used that matches the received signal to the chip waveform $\psi(t)$. The mth sample of the ith bit of the received signal can be written as

$$y[i,m] \triangleq \frac{1}{T_s}\int_{iT_b+mT_s}^{iT_b+(m+1)T_s} y(u)\psi^*(u-t)du, \tag{2.19}$$

where T_s is the sampling interval, such that $B_s = 1/(2T_s)$. Typically, we set $T_s = T_c/p$, where p is a positive integer which is analogous to the temporal oversampling ratio in the fractionally spaced receiver structure for single user ISI channels. This fractionally chip spaced approach offers the benefit that no timing information prior to the receiver training is required [2]. If there are M received signal samples spanned by each symbol of the desired user (i.e., $b_1[i]$), it follows that both the linear FIR filter $\mathbf{w}_1$ and its received signal vector input, which is defined as

$$\mathbf{Y}[i] \triangleq (y[i,1],\ldots,y[i,M])^T, \tag{2.20}$$

are M-length column vectors.

It is assumed that the number of transmitted symbols of each user is Ω (i.e., transmission block length). For the ith symbol, it follows that [2] the *decision aided coefficients* for the kth user, $\mathbf{D}_k[i]$ and the corresponding *estimated symbol sequences* $\mathbf{B}_D[i]$ are ΩK-length column vectors, and are defined as follows.

$$\mathbf{D}_k[i] \triangleq (\mathbf{d}_{k,1}[i], \ldots, \mathbf{d}_{k,K}[i])^T, \tag{2.21}$$

$$\mathbf{B}_D[i] \triangleq (\hat{\mathbf{b}}_1[i], \ldots, \hat{\mathbf{b}}_K[i])^T, \tag{2.22}$$

where $\mathbf{d}_{k,j}[i] = (d_{k,j,1}[i], \ldots, d_{k,j,\Omega}[i])$ and $\hat{\mathbf{b}}_k[i] = (\hat{b}_k[i\Omega], \ldots, \hat{b}_k[i\Omega + \Omega - 1])$ with $k, j \in \{1, \ldots, K\}$.

Since the demodulation of users are independent from each other, the receiver is represented without loss of generality, in a decentralised form from the viewpoint of the desired user $k = 1$. Thus, both $\mathbf{D}_1$ and $\mathbf{B}_D$ form the decision feedback MAI canceller. The concept of MAI cancellation requires that some or all MAI signals are already demodulated and detected. The generalised multiuser detector output is calculated once every symbol period T_b, and is given as [2]

$$Z_1[i] = \mathbf{w}_1^T[i]\mathbf{Y}[i] - \mathbf{D}_1^T[i]\mathbf{B}_D[i], \tag{2.23}$$

where the first and second terms form the linear multiuser detection and decision feedback MAI canceller respectively. By feeding $Z_1[i]$ to a decision device, the ith estimated symbol is represented as

$$\hat{b}_1[i] = Dec(Z_1[i]), \tag{2.24}$$

where $Dec(\cdot)$ denotes the decision device operator.

2.3.5 List of General Assumptions

In this thesis, the signal models presented in Section 2.3.2 to 2.3.4 are subjected to the following assumptions.

- In all DS-CDMA systems, the chip waveforms are delayed versions of each other [16] (i.e., $\psi(t) = \psi(t - nT_c) \quad \forall n$). To ensure there is no ISI from

adjacent chip pulses, for simplicity, a rectangular pulse is used and is given by

$$\psi(t) = \begin{cases} 1, & \text{if } t \in [0, T_c) \\ 0, & \text{otherwise.} \end{cases} \tag{2.25}$$

Results presented in this thesis can be easily extended for any time-limited, Nyquist chip waveforms (e.g., raised-cosine pulse).

- Each user is assigned with a unique binary PN sequence as spreading code. To facilitate the usage of linear multiuser detection, short codes or periodic PN sequences $c_k[n]$ are used in (2.2). Furthermore, the signature waveforms $s_k(t)$ of all K users are linearly independent.

- All signature waveforms $s_k(t)$ are supported only on the time interval $[0, T]$ and are normalised to have unit energy:

$$\begin{aligned} \int_0^T s_k^2(t) = 1 \qquad & \forall k \in \{1, \ldots, K\}, \text{ or} \\ c_k[n] \in \{\pm 1/\sqrt{N}\} \qquad & \forall k \in \{1, \ldots, K\} \text{ and } \forall n \in \{1, \ldots, N\} \end{aligned} \tag{2.26}$$

- In the receiver, only linear multiuser detection or a linear FIR filter $\mathbf{w_1}$ in (2.23) is considered (i.e., no decision feedback MAI canceller or $\mathbf{B}_D[i] = \mathbf{0}$ $\forall i$ in (2.23)). This is because the blind adaptation of $\mathbf{B}_D[i]$ is still not fully understood [32], and only the training-based adaptation of $\mathbf{B}_D[i]$ is feasible [2]. Also, chip rate sampling (i.e., $T_s = T_c$) is used to obtain the received signal samples in (2.19).

- For simplicity, the DS-CDMA system uses BPSK modulation with $b_k \in \{\pm 1\}$ in (2.3) as uncoded, independent and equi-probable binary bits. It follows that the decision device operator on $b_1[i]$ in (2.24) is a signum function (i.e., $Dec(\cdot) = sgn(\cdot)$).

- Since, in general, NBI can be adequately suppressed by the subsequent despreading process in the receiver; it is sufficient to restrict $n(t)$ in (2.18) as AWGN with zero mean and power spectral density σ_n^2.

- Since short codes are used, all delay offsets are bounded within one bit duration (i.e., $\tau_k \in [0, T_b) \quad \forall k \in \{1, \ldots, K\}$ in (2.18)). These delays are defined with respect to an arbitrary origin (e.g., let one delay be zero value).

- Since coherent detection (i.e., BPSK modulation) is used, the issue of carrier synchronization[4] is not considered in this thesis. That is, there is no frequency uncertainties for frequency and phase offset parameters ω_k and φ_k in the receiver.

- All multipath channels are frequency selective, slowly fading, and have a fixed number of resolvable paths L, as defined in (2.9). Since channel parameters vary slowly in comparison with the bit duration T_b (at least during the initial adaptation stage), multipath channels can be modelled as Linear-Time-Invariant (LTI) filters with FIR

$$h_k(t, \tau) = h_k(\tau), \quad \forall t \text{ and } \forall k \in \{1, \ldots, K\}. \tag{2.27}$$

  Then, the kth channel FIR in (2.10) can be simplified to

$$h_k(\tau) = \sum_{l=1}^{L} \beta_{k,l} \delta(\tau - (l-1)T_c), \tag{2.28}$$

  where $\beta_{k,l}$ are time invariant gains, with magnitudes subject to Rayleigh distribution and uniformly distributed phases. For reasons that will be discussed in Section 2.4.2, only the reverse channel signalling is considered.

- There is no provision for power control (i.e., near far effect is considered): all users transmit the same, normalised power in (2.3), and have independent, time-invariant received amplitude A_k in (2.15).

[4] To avoid the need to maintain a permanent phase reference, differential encoding is often preferred in practical mobile radio environments. As long as the phase is stable for two consecutive bit intervals, the estimated data in (2.24) are obtained by their phase differences, i.e., $\hat{b}_1[i] = sgn\{Re(Z_1[i]Z_1^*[i-1])\}$, where $Re(\cdot)$ and $(\cdot)^*$ denote the real part and complex conjugate of a complex scalar, respectively.

2.4 Background of Multiuser Detection

In this section, background material for multiuser detection is presented. First, the problem statement of multiuser detection is defined. Second, in terms of cellular mobile communications, its potential benefits and limitations are examined. Third, the concept of blind multiuser detection which is the core subject of this thesis, is introduced.

2.4.1 Problem Statement of Multiuser Detection

As discussed in Section 2.2, the long and short codes design approaches have translated into the single user and multiuser detection schemes respectively. Unlike the single user case which treats MAI as structureless AWGN; in multiuser detection, informations from some or all users such as the signature waveforms, timings and other parameters (e.g., amplitude and phase) are jointly used to improve detection of each individual user.

The DS-CDMA system in consideration is subject to various distortions which adversely affect its detection performance. Using the assumptions listed in Section 2.3.5, these distortions can be categorized into three related interferences:

1. **MAI** — as shown in Figure 2.1, MAI contains contribution of signals from all interfering users (i.e., $y_k(t) \quad \forall k \in \{2, \ldots, K\}$ in (2.18)). Essentially, MAI is inherent to any non-orthogonal signature based CDMA systems, and constitutes the majority of the total interference. This is because, that due to the presence of asynchronism and multipath effect, the spreading codes will not be orthogonal.

2. **Inter-Chip-Interference (ICI)** — contains contribution from the desired ith bit of the desired user $k = 1$ (i.e., $b_1[i]$) due to multipath effect.

3. **ISI** — contains contribution from the adjacent bits of the desired user $k = 1$ (i.e., $b_1[i'] \quad \forall i' \neq i$) due to multipath effect and asynchronism.

The aim of various multiuser detection schemes is to obtain a more reliable symbol estimate $\hat{b}_1[i]$ in (2.24) by suppression of all three types of interference above.

2.4.2 Limitations

Before discussing the performance improvements to the conventional MF based detector, it is useful to examine factors that limit such improvement [14, 33]. There are two main limitations of multiuser detection:

1. **Inter-cell MAI** — in cellular DS-CDMA systems, signals transmitted in one cell can be viewed as MAI in neighbouring cells. The term *intra-cell MAI* is used to represent MAI from the same cell as the desired user; while *inter-cell MAI* is MAI contributed from other cells. The ratio of inter-cell MAI to intra-cell MAI is commonly referred to as the *spillover ratio*, ς. Since the capacity in terms of number of users is approximately proportional to the total MAI [19], the maximum capacity improvement factor[5] is $(1+\varsigma)/\varsigma$. In a typical cellular system, $\varsigma = 0.55$ and the capacity gain is limited to 2.8.

2. **Forward Link Capacity** — due to the size and weight restrictions for the mobile terminals, it is currently not practical to implement multiuser detection in the forward link. In addition, the reverse channel signalling is more complicated than the forward link case. In any case, the base station is required to demodulate all users in its cell, and has all system parameters available. Hence, most multiuser detectors are designed for the reverse link. However, capacity improvement of the reverse link beyond that of the forward link capacity does not increase the overall system capacity.

However, as pointed out in [23], these two limitations have been misinterpreted by the general literature. For instance, in adaptive multiuser detection [2, 34] (as discussed in Section 2.5.7), with the exception of its initialisation process, the inter-cell MAI and intra-cell MAI are both suppressed in the same fashion. Also, its implementation is particularly suitable in the mobile terminals which have tight complexity restrictions, as only the spreading code of the desired user is required to be known.

[5] Since a base station only maintains information of mobile terminals in its own cell, an ideal multiuser detection scheme should remove all intra-cell MAI, and treat inter-cell MAI as AWGN.

2.4.3 Potential Benefits

The use of multiuser detection offers the following potential benefits [14, 35]:

1. **Capacity Improvement** — despite the possible presence of "unsuppressed" inter-cell MAI, the potential capacity gain relative to the conventional MF detection is still significant, especially in the reverse link.

2. **Relaxation of Stringent Power Control Requirement** — multiuser detectors are designed to be *near far resistant* (i.e., detection performance is independent of the received amplitude of interferers), hence they sidestep the need for fast, high precision power control for the mobile transmitters. In fact, this relaxing of power control translates into a capacity benefit due to lower power consumption and processing gain requirements. However, it is noted that moderate power control is required, if synchronization is carried out using a conventional MF approach [23].

3. **Better Power/Spectrum Utilization** — especially in the case of reverse link, MAI suppression leads to a more efficient spectrum and power utilization. For instance, the same bandwidth can be used to support higher data rates, while the same transmitted power can be used to increase the coverage size.

2.4.4 Concept of Blind Multiuser Detection

Early research on the design of multiuser detectors assumed critical system parameters (e.g., the user codes, delays and received powers) to be *a priori*, such as the optimum multiuser detector in Section 2.5.4. However, detectors that require parameter estimation are generally sensitive to estimation errors [14].

In this thesis, the problem of linear multiuser detection is examined in a blind setting. That is, the adaptation of $\mathbf{w}_1$ in (2.23) is blind in the sense that neither the signature waveforms of the interfering users nor training data is required. Hence, a blind multiuser detector requires only the spreading code of the desired

user $c_1[n]$ (and possibly its timing[6] τ_1), the same knowledge as the conventional MF based detector. The objective of the blind linear multiuser detector is to emulate and converge to the MMSE adaptive linear multiuser detector in Section 2.5.7.

The motivation for the recent development of blind multiuser detection techniques are listed as follows.

- There are some drawbacks to the use of training [3]. Apart from the reduction in spectrum efficiency due to the resources spent on training, separate training for each user may not be feasible in certain situation (e.g., multipoint data networks). Also, whenever there is a significant changes in the MAI level during a deep fade or powering on of some strong interferers, retraining is required and data transmission must be interrupted accordingly.

- Blind multiuser detection allows DS-CDMA transmissions to be completely asynchronous and uncoordinated. Hence, this blind method can be used for initial adaptation and replace the training phase.

- The fact that this blind approach requires the same knowledge as the conventional MF makes it a suitable candidate for implementation in the mobile terminal [36] (as discussed in Section 2.4.2).

2.5 Literature Review of Multiuser Detection

A literature survey of multiuser detection for DS-CDMA systems can be found in many references [14, 16, 33, 35, 37]. In this section, a brief summary of multiuser detectors proposed in the past decade is presented. For convenience, a basic synchronous (i.e., $\tau_k = 0 \quad \forall k \in \{1, \ldots, K\}$ in (2.18)) DS-CDMA signal model is used to explain different multiuser detectors, and the issue of asynchronism is also discussed.

[6] The need to know the timing of the desired user can be avoided in the case of joint signal detection and parameter estimation, or using an equivalent synchronous model, as discussed in Section 2.5.2.

2.5.1 Synchronous DS-CDMA Signal Model

Unless otherwise stated, for simplicity, no multipath effect is considered in the literature survey. From (2.18), the received baseband signal for a synchronous K-users DS-CDMA system is given as

$$y(t) = \sum_{k=1}^{K} A_k \sum_{i} b_k[i] s_k(t - iT_b) + n(t), \tag{2.29}$$

where the transmitted signature $s_k(t)$ in (2.2) is the same as the received signature $f_k(t)$ in (2.16).

After chip rate sampling, the one-shot version (i.e., where each bit interval is considered independently) of the ith bit received signal vector in (2.29) can be written as a N-length vector

$$\mathbf{Y}[i] = \mathbf{SAb}[i] + \mathbf{n}[i] = (y[i,1], \ldots, y[i,N])^T, \tag{2.30}$$

where, from (2.19), the nth chip sample[7] is given by

$$y[i,n] = \frac{1}{T_c} \int_{iT_b+nT_c}^{iT_b+(n+1)T_c} y(t)dt \quad \text{where } n \in \{1, \ldots, N\}, \tag{2.31}$$

and $\mathbf{S} = (\mathbf{s}_1, \ldots, \mathbf{s}_K)$ is an $(N \times K)$ signature matrix, with the kth column denoted as $\mathbf{s}_k = (c_k[1], \ldots, c_k[N])^T$, $\mathbf{A}$ is an $(K \times K)$ diagonal matrix composed of A_k, $\mathbf{b}[i] = (b_1[i], \ldots, b_K[i])^T$ is an K-length column vector of the ith bit, and $\mathbf{n}[i]$ is an N-length vector of noise samples. Each observation interval of $\mathbf{Y}[i]$ in (2.30) corresponds to N chip samples of the ith bit, or the number samples used for each bit decision.

2.5.2 Asynchronism

Before discussing various forms of multiuser detectors, it is important to examine the case of asynchronous transmissions. An asynchronous system with K-users with each user transmitting a block of Ω bits, is equivalent to a synchronous system with ΩK fictitious users [3, 16]. Each fictitious user is viewed as each

[7] Since rectangular pulse is used for the chip waveform $\psi(t)$, the chip MF in (2.19) can be implemented as an integrate-and-dump operation in (2.31).

user's bit, $b_k[i]$ in (2.3) and is defined within the interval $[T_b, \Omega T_b]$. The following two methods describe this transformation from an asynchronous system to an equivalent synchronous case.

1. **Sliding Processing Window** — the time support of the linear FIR filter $\mathbf{w}_1$ (i.e., $[0, MT_s]$ in (2.20)) is commonly referred to as *processing window.* Increasing the processing window will improve the steady state performance of the multiuser detector, but with high complexity and slower adaptation. Rather than using the entire interval length ΩT_b, it is shown that [6] a processing window of length $2T_b$ is sufficient to encompass one complete bit of the desired transmission.

2. **Signature Partitions** — since $\tau_1 \in [0, T_b)$, a given bit of the desired user $b_1[i]$ may be overlapped with one of the two consecutive bits $b_1[i-1]$ and $b_1[i+1]$ (i.e., ISI) within an observation interval $[0, T_b]$. As a result, it can be represented as an equivalent $2K$-users synchronous system. Depending on the delays, each signature waveform is separated into its left and right partitions, as signature waveforms for two fictitious users [5, 6]. Since simple one-shot representations are used, this method has lower complexity than the sliding processing window.

2.5.3 Conventional DS-CDMA detector

For the sake of completeness, a mathematical representation of the conventional DS-CDMA detector is included here. As discussed in Section 2.2, the conventional DS-CDMA detector is a bank of MFs and is shown in Figure 2.6. After downconverting, the kth MF output can be written as

$$Z_{MF,k}[i] = \int_{iT+\tau_k}^{iT+T+\tau_k} y(t) s_k(t) dt. \tag{2.32}$$

In fact, the MF output in (2.32) is a special case of the multiuser detector in (2.23) with the kth linear FIR filter as $\mathbf{w}_k[i] = \mathbf{s}_k \ \ \forall i$. Using the synchronous signal model in (2.30), the MF outputs can be expressed in a K-length column

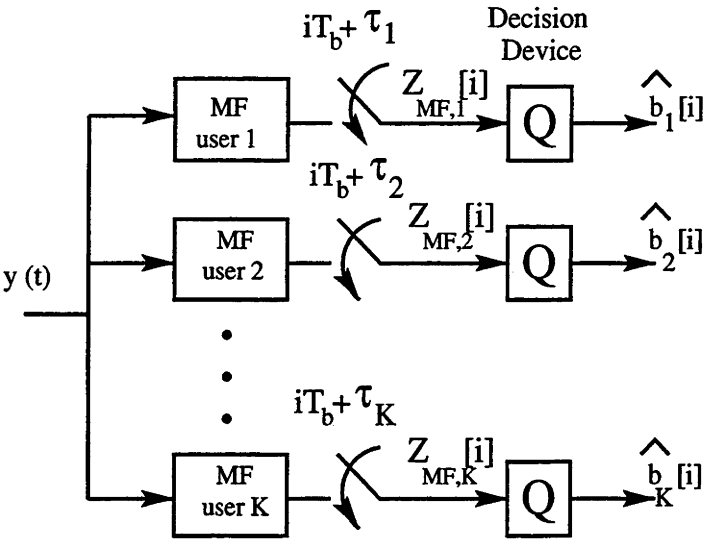

Figure 2.6: The conventional DS-CDMA detector: a bank of MFs.

vector

$$\begin{aligned}\mathbf{Z}_{MF}[i] &= (Z_{MF,1}[i], \ldots, Z_{MF,K}[i])^T \\ &= \mathbf{S}^T\mathbf{Y}[i] \\ &= \mathbf{RAb}[i] + \mathbf{n}_{MF}[i] \end{aligned} \tag{2.33}$$

where $\mathbf{R} \triangleq \mathbf{S}^T\mathbf{S}$ is the normalised[8] cross-correlation matrix, and $\mathbf{n}_{MF}[i]$ is the colored Gaussian noise vector with zero mean and covariance matrix $\sigma_n^2\mathbf{R}$.

The usage of the bank of single user MFs is optimal only in the case of a synchronous (i.e., all delays $\tau_k \quad \forall k \in \{1, \ldots, K\}$ are known) and orthogonal (i.e., no MAI or $\mathbf{R} = \mathbf{I}_K$) DS-CDMA system. In this special case, the error probability is referred to as the *single user bound*, which serves as a lower bound for any multiuser detector. For the kth user, the single user bound is given by

$$P_{k,SU}(\sigma_n) = Q\left(\frac{A_k}{\sigma_n}\right), \tag{2.34}$$

[8] Using the normalised signature waveforms in (2.26), diagonal elements of $\mathbf{R}$ are 1's, while all off-diagonal elements have magnitude less than unity.

where the Q-function is of the form

$$Q(x) = \frac{1}{\sqrt{2\pi}} \int_x^{\infty} \exp\left(\frac{-y^2}{2}\right) dy. \tag{2.35}$$

2.5.4 Optimum Multiuser Detection

The optimal multiuser detector [38] essentially uses a Maximum Likelihood Sequence Estimation (MLSE) approach. As long as all possible $\mathbf{b}[i]$ vectors are equally probable, MLSE detection is equivalent to maximize its *joint a posteriori probability*, $P(\mathbf{b}[i]|y(t))$. The aim of MLSE is to find the most likely transmitted sequence or Maximum Likelihood (ML) K-length bit vector $\hat{\mathbf{b}}_{ML} \in \{\pm 1\}^K$, which maximizes the *log-likelihood function* as follows

$$\begin{aligned} \hat{\mathbf{b}}_{ML}[i] &= \arg \min_{\mathbf{b}\in\{\pm 1\}^K} \|\mathbf{Y}[i] - \mathbf{SAb}[i]\|^2 \\ &= \arg \max_{\mathbf{b}\in\{\pm 1\}^K} \left(2\mathbf{b}^T[i]\mathbf{AZ}_{MF}[i] - \mathbf{b}^T\mathbf{ARAb}[i]\right). \end{aligned} \tag{2.36}$$

Hence, The MLSE algorithm in (2.36) requires a search over the 2^K possible bit combinations. The implementation of the optimum multiuser detector consists of a MF bank, followed by a *Viterbi algorithm* (VA) [16]. This usage of VA is analogous to the case of single user channels with $(K-1)$ memory, that are corrupted by ISI. The required VA has a computational complexity exponential in the number of users (i.e., 2^K).

As shown in [38], the MLSE algorithm in (2.36) is a NP-hard combinatorial optimization problem. That is, there exists no known algorithm that can solve (2.36) with polynominal complexity in terms of K. Hence, despite its optimal performance, this MLSE detector has prohibitive computational complexity and requires estimations of all system parameters. Nonetheless, its huge performance improvement over the conventional MF-bank motivates the search for suboptimal detectors which offer good performance (e.g., near far resistant) with low complexity.

2.5.5 Linear Multiuser Detection

These linear detectors have been developed with complexity that is linear in K. They offer high near far resistance at the expense of slight BER degradation compared to the MLSE detector in Section 2.5.4. Also, they can be implemented in a decentralised format (i.e., only the desired users are demodulated) which is particularly useful in forward links [16]. In general, linear multiuser detectors apply a linear mapping, which is represented by a $(K \times K)$ matrix $\mathbf{L}$, to the MF outputs in (2.33).

1. **Decorrelator** — similar to zero-forcing equalizer, it completely removes MAI [39] and has optimum near far resistance. In fact, the decorrelator is equivalent to a MLSE detector when the received amplitudes of all users are unknown, and has an equivalent linear mapping

$$\mathbf{L}_{DEC} = \mathbf{R}^{-1}. \tag{2.37}$$

   Hence, the decorrelator projects each MF output on the subspace which is orthogonal to one spanned by the interfering signature waveforms. Since all MAI are eliminated, its BER has a simple form [16]

$$P_{k,DEC}(\sigma_n) = Q\left(\frac{A_k}{\sigma_n\sqrt{(\mathbf{R}^{-1})_{k,k}}}\right), \tag{2.38}$$

   where $(\mathbf{R}^{-1})_{k,k}$ is the (k,k)-th component of $\mathbf{R}^{-1}$.

   The decorrelator has several drawbacks such as noise enhancement and "edge effect" [40]. In particular, its major disadvantage is the need to compute $\mathbf{R}^{-1}$ (e.g., $\mathbf{R}$ is of size $(\Omega K \times \Omega K)$ in an asynchronous system). However, a number of modified decorrelators have been proposed to improve its adaptability with complexity reduction [41, 42].

2. **MMSE** — unlike the decorrelator, the MMSE detector offers a compromise between MAI suppression and excessive noise enhancement. Its respective linear mapping is obtained by minimizing the Mean Squared Error (MSE)

between the required data and the MF outputs, and is given by

$$\begin{aligned}\mathbf{L}_{MMSE} &= \arg \min_{\mathbf{L}_{MMSE} \in \mathcal{R}^{K \times K}} E\{\|\mathbf{b}[i] - \mathbf{L}_{MMSE}\mathbf{Z}_{MF}[i]\|^2\} \\ &= \left(\mathbf{R} + \sigma_n^2 \mathbf{A}^{-2}\right)^{-1}, \end{aligned} \tag{2.39}$$

where the expectation operator $E\{\cdot\}$ denotes the ensemble average over the bit vector $\mathbf{b}[i]$. From (2.39), it can be seen that this multiuser detector is a multi-dimensional version of the MMSE linear equalizer for the single-user ISI channels [33]. As background noise disappears (i.e., $\sigma_n \rightarrow 0$), the MMSE multiuser detector converges to the decorrelator. Conversely, if MAI becomes significantly smaller compared to noise level, it converges to a conventional MF.

The major benefit of the MMSE multiuser detector is its direct implementation as a training-based adaptive detector, as discussed in Section 2.5.7. Also, unlike the decorrelator, it does not require that all signature waveforms are linearly independent of each other [23]. However, it suffers from several disadvantages such as the need to estimate the all users' received amplitudes and noise level, and some loss of near far resistance compared to the decorrelator detector [14].

3. **Lattice Structure** — involves a polynomial expansion [14] in $\mathbf{R}$ or its equivalent decomposition into a lattice structure [43, 44], to approximate the decorrelator or the MMSE detector. In the simple case of polynomial expansion, it has the linear mapping

$$\mathbf{L}_{PE} = \sum_{n=1}^{N_{PE}} w_n \mathbf{R}^n, \tag{2.40}$$

where w_n are polynomial coefficients and N_{PE} is the number of stages required to optimize some performance criteria.

This detector has a number of implementation benefits. Given sufficiently small N_{PE}, it offers lower computational complexity compared to the decorrelator and the MMSE detector (i.e., no need to calculate $\mathbf{R}$ or its inverse).

Also, the choice of N_{PE} determines the operating range of various weights w_n. This implies that not all weights are required to be updated, whenever there are changes in the system parameters. Finally, this detector permits the usage of both short and long codes.

2.5.6 Non-Linear Multiuser Detection

Most non-linear multiuser detectors use a decision-driven concept, which improves the subsequent desired user's bit estimates by subtracting a portion of MAI from the received signal $\mathbf{Y}[i]$. Since decisions made from stronger users are more reliable compared to that of the weaker users, stronger users are demodulated first. In general, these decision-driven detectors require accurate estimation of all users' received amplitudes, and may have problems of long delays and error propagation. They are suitable when each user has high SNR with high power imbalances, especially in a centralized demodulation situation (i.e., reverse link) [16].

1. **Decision Feedback** — analogous to the decision feedback equalizers used in the single user ISI channels, it uses a feedforward filter $\mathbf{w}_1$ and a feedback filter $\mathbf{D}_k$, as shown in Figure 2.5. Two popular choices for the feedforward filters are the decorrelator [45], and the MMSE detector [2, 46].

2. **Successive/Parallel MAI Cancellation** — these detectors achieve MAI cancellation using a successive/parallel approach (e.g., [24]). When there are high power differences between users, the successive method is preferred over the parallel case [47].

3. **Multi-stage** — this detector is characterized by the number of consecutive stages, which represents the number of times that users' estimates are made (e.g., [26]). To obtain more reliable decisions, the decorrelator is often used in the initial stage, instead of a conventional MF bank [33].

4. **Neural Networks** — these algorithms consist of a parallel network of interconnected nodes or *perceptrons*, and are used to solve complex problems (e.g., non-linearity, non-stationarity, and non-Gaussianity) [37]. For

example, in [48], a backpropagation neural net is used to approximate the optimal MLSE detector in Section 2.5.4.

2.5.7 Adaptive Multiuser Detection

These training-based detectors are adaptive to channel dynamics such as time varying MAI and multipath fading. They do not require knowledge of spreading codes of any user, although the convergence rate is faster if spreading code of the desired user is used as the filter initialisation.

1. **MMSE** — this detector computes the linear filter $\mathbf{w}_1$ and the decision aided coefficients $\mathbf{D}_1$ adaptively based on minimizing the MSE cost

$$\begin{aligned} J_{MSE}(\mathbf{w}_1) &= E\{|e[i]|^2\} \\ &= E\{|Z_1[i] - \hat{b}_1[i]|^2\}, \end{aligned} \tag{2.41}$$

where $Z_1[i]$ is the filter output given in (2.23), and $\hat{b}_1[i]$ is the bit estimate obtained from the training sequence, or by decision-directed mode.

For linear multiuser detection without a decision feedback MAI canceller, it can be shown that [2, 34] the optimum MMSE solution of (2.41) is given by

$$\mathbf{w}_{1,MMSE} = \mathbf{R}_{\mathbf{yy}}^{-1}\mathbf{p}_1, \tag{2.42}$$

where $\mathbf{R}_{\mathbf{yy}} \triangleq E\{\mathbf{Y}[i]\mathbf{Y}^T[i]\}$, and $\mathbf{p}_1 = E\{\hat{b}_1[i]\mathbf{Y}[i]\}$ is the *windowed signature* for data $\hat{b}_1[i]$. For adaptive implementation, the corresponding stochastic gradient or *Least Mean Squares* (LMS) algorithm is given by

$$\mathbf{w}_1[i+1] = \mathbf{w}_1[i] - \mu e[i]\mathbf{Y}[i], \tag{2.43}$$

where μ is the step size. Because of the convexity of (2.41), the LMS adaptation in (2.43) ensures an unique local minimum. To increase the convergence speed of LMS algorithm, faster implementations can be used such as *Recursive Least Squares* (RLS) algorithm [34], lattice structure and some orthogonal transformation pre-processings [49], at the expense of higher

complexity. The adaptive MMSE detector is able to track the time varying channel dynamics, as long as their parameter variations are slower compared to the convergence speed of the adaptation.

A typical operation would be to have the initial adaptation based on training, and then to switch to Decision Directed (DD) mode during the actual data transmission. For example, the DD-LMS algorithm is identical to the MMSE-LMS algorithm in (2.43), except with the prediction error $e[i]$ replaces by $Z_1[i] - sgn(Z_1[i])$.

As discussed in [23], the dimensionality of the adaptive vector $\mathbf{w}_1$ is equal to the spreading gain N, or its small multiples (i.e., independent of K). This supports the claim in Section 2.4.2 that the adaptive receiver does not differentiate an interferer based on its inter-cell or intra-cell origins, but only on its received SNR. In the presence of asynchronism and the multipath effect, the observation interval of $\mathbf{p}_1$ is increased to a truncated window that spans more than one bit period [16].

2. **Cyclostationarity Algorithms** — many signals such as CDMA exhibit cyclostationarity properties, which have periodic correlation statistics. In particular, spectral diversity is easily exploited when short codes are used for DS-CDMA systems (i.e., signal spreading is performed on symbol-by-symbol basis) [37]. In the same manner as the fractionally spaced equalizers, spectral diversity can be exploited by time dependent adaptive filters to suppress MAI (e.g., [50]).

3. **Complexity Reduction Schemes** — several methods have been proposed to reduce the complexity and output noise of the linear MMSE detector. These complexity reduction schemes are particularly useful when N is large, and the received energy per chip is low. Examples include the cyclically shifted filter bank [34], and the symmetric dimension reduction scheme [51].

4. **Minimum BER** — a low complexity adaptive multiuser detector algorithm which minimizes BER directly, has been proposed [52]. Depending on the level of MAI, it can outperform the linear MMSE detector. However,

it suffers from slow convergence at high SNR, since the detector is updated only when an error is made (i.e., DD mode).

5. **Hybrids** — there are other hybrid forms of adaptive multiuser detectors which are variations of the aforementioned linear/nonlinear detectors. Specifically, there has been work done on the joint adaptive multiuser detection and timing acquisition (e.g., [53, 54]).

2.5.8 Blind Multiuser Detection

As discussed in Section 2.4.4, blind multiuser detectors have been developed to replace the cumbersome training phase in adaptive multiuser detectors. A comprehensive list of blind multiuser detectors recently proposed in the literature is given below. In particular, the first three blind methods are to be further discussed and examined in details in the subsequent chapters, and their performance are used as benchmarks where necessary.

1. **Minimum Output Energy (MOE)** — this linear blind method was originally proposed in [3], and is based on a Minimum Output Energy (MOE) criterion with cost function

$$J_{MOE}(\mathbf{w}_1) = E\left\{|Z_1[i]|^2\right\}. \tag{2.44}$$

The linear filter $\mathbf{w}_1$ is orthogonally decomposed into a fixed MF and an adaptive component, as explained in Section 3.3. This blind method offers the advantages of low computational complexity, its adaptability to converge to the MMSE adaptive detector and its global convergence behavior due to the convexity of the MOE cost function in (2.44).

Various forms of modified blind MOE detectors have also been proposed and are listed as follows.

(a) *RLS-based MOE* — RLS-implementation with systolic arrays [55] can be used to achieve fast convergence. Typically, a Ricatti equation is used to update the matrix stepsize iteratively.

(b) *Linearly constrained MOE* — instead of using two orthogonal filters as in [3], Frost's constraint projection is used [56, 57]. Also, linear constraints are imposed to combat multipath effect [58, 59].

(c) *Joint timing acquisition and demodulation* — the desired user's time delay τ_1 can be jointly estimated by selecting the largest MOE cost in (2.44), from a range of delay hypotheses [6]. Also, the MOE detector is modified in [60] to increase its robustness to asynchronous MAI and carrier phase offset.

2. **Constant Modulus Algorithm (CMA)** — the usage of CMA in linear blind multiuser detection is motivated by its applications in blind equalization in single user ISI channels [61, 62] and blind beamforming in array processing [63]. Its underlying concept is to exploit the Constant Modulus (CM) property of the desired signal [27, 56]. The cost function based on the CM criterion is designed to penalise envelope variations, and is given by

$$J_{CM}(\mathbf{w}_1) = E\left\{(|Z_1[i]|^2 - \xi)^2\right\}, \tag{2.45}$$

where the modulus radius ξ is a positive constant, without loss of generality. The standard adaptive implementation using a steepest gradient descent strategy is known as the CMA, as explained in Section 3.4.3. The CM criterion has been chosen because of its reported robustness properties, faster local convergence rate, and since it has less computational complexity than the subspace-based methods [4, 64]. However, due to the multi-modal nature of its cost surface, the analysis of CMA convergence behavior (e.g., the ill-convergence problem [65]) and initialisation is more difficult than with uni-modal case such as the MOE multiuser detector.

As a large part of this thesis is dedicated to the application of CMA in linear blind multiuser detection, it is useful to know various forms of modified CMA that have been proposed in the literature. These modified CMAs are summarized as follows.

(a) *RLS-based or normalized CMA* — rapid convergence using least squares approach (i.e., independent of step size μ) [66, 67].

(b) *Dithered signed error CMA* — reduced-complexity CMA with robustness properties of CMA retained [68].

(c) *Multi-modulus algorithm* — instead of reducing the deviation from the CM, it is used to fit the filtered output to a square. This method yields correct phase rotation (modulo $\pi/2$) and has reduced complexity [69].

(d) *Multi-stage CM-array* — for each stage, one signal component is captured by CMA, and is then removed by a LMS-like adaptive canceller [63].

(e) *Linearly constrained CMA and anchored CMA* — ensures convergence to the desired user (i.e., desired local minimum) [70–72].

(f) *SOS-based constrained CMA* and *subtraction-based CMA* — modified CMAs that avoid convergence to the same user source [73–76].

(g) *DD-CM array* — hybrid algorithms between CM and DD types with improved convergence speed and avoidance of ill-convergence [67, 77].

(h) *Analytical CMA* — uses a generalized eigenvalue formulation which can estimate the number of CM signals, and reject non-CM signals [78].

(i) *decision feedback CMA* — for some channel classes, it is found [32] that decision feedback CMA (i.e., adaptation of $\mathbf{D}_1$ in (2.23)) would converge, where decision feedback DD would not.

3. **Subspace-based** — this method is motivated by the class of blind multipath channel identification and equalisation schemes that exploits the cyclostationarity of over-sampled signals in single user ISI channels (e.g., [79]). This class of blind method is characterized by its reliance on the estimated, time varying SOS of the received signal (i.e., $\mathbf{R}_{\mathbf{yy}}$ in (2.42)).

   In particular, a popular implementation is the subspace-based matrix pencil method [80] proposed in [81] that exploits the orthogonality between the signal and noise subspaces. In DS-CDMA systems, the applications of this subspace-based SOS method are listed as follows.

(a) *Linear multiuser detection* — based on the eigen-decomposition of $\mathbf{R_{yy}}$, signal and noise subspaces correspond to the K largest eigenvalues and remaining $(N-K)$ eigenvalues of $\mathbf{R_{yy}}$ respectively [82]. Furthermore, it can be shown that both the decorrelator and the MMSE detector in Section 2.5.5 are special cases of this subspace-based linear detector.

(b) *Combined spatial-temporal diversities* — using multiple sensors (i.e., antennas), space-time processing in a 2-D RAKE receiver structure can significantly enhance the detection performance [28, 83].

(c) *Channel estimation* — the channel estimates are derived by projecting the desired user's signature waveform $s_1(t)$ onto the estimated noise subspace [84–86]. Specifically, the desired user's time delay τ_1 can be estimated through the well-known MUltiple SIgnal Classification (MUSIC) algorithm.

(d) *Pre-coding* — to facilitate the equalization task, specific coding and interleaving are used at the transmitter to induce cyclostationarity [87]. This is done at the expense of additional transmitter complexity and some decoding delays.

To improve its tracking capability with reduced complexity, various signal subspace tracking algorithms have been developed which are robust to multipath fading (e.g., [82]).

Unfortunately, the subspace-based approach suffers from the lack of robustness (e.g., channel model mismatch [88]). Also, analogous to the re-training scenarios of a MMSE detector, re-estimations of SOS are required whenever there are significant changes in the system parameters. Apart from the usage of SOS, it is noted that Higher Order Statistics (HOS) can also be used for multiuser detections [89, 90]. But for these HOS-based methods, adaptive implementations are difficult, due to its prohibitive complexity, slower convergence compared to SOS-based methods, and existence of undesired local minima.

4. **Hidden Markov Models Approach** — by modelling the received signal $\mathbf{Y}[i]$ using the Hidden Markov Model, training sequences can be replaced by estimates of the transmitted data based on the *Baum & Welch Re-estimation* procedure (e.g., [91]). In the same manner as the nonlinear multiuser detectors in Section 2.5.6, this method extracts users' contributions sequentially according to decreasing received power order. Hence, it is also sensitive to users' received power estimates, and may have problems of long delay and error propagation.

5. **Finite Alphabet** — similar to the CM criterion, this is another property-restoral approach to exploit the temporal structure of all digitally modulated schemes. This method utilizes the fact that the information bearing bits $\mathbf{b}[i]$ in (2.30) are from a pre-assigned, discrete, finite alphabet. Given sufficient data samples, either by using multiple antennas [92] or over-sampling [93], a low complexity, iterative least squares algorithm is developed that projects the output symbols onto the the closest alphabet.

6. **Blind MLSE** — a blind, self-tuning MLSE detector has been proposed in [94] and requires no prior knowledge of received amplitudes and signature cross-correlation. Also, an approximate maximum likelihood estimator is proposed in [86] that uses the separation of variables technique. However, its resulting cost function is highly nonlinear with many local minima, and hence requires correct initialisation.

7. **Minimum BER** — this is the blind version [36] of the adaptive minimum BER detector in Section 2.5.7. In the same manner as the blind MOE-based detector, an orthogonal, auxiliary vector component has been added to the conventional MF vector. Following the MMSE concept, this approach aims to achieve a compromise between the MAI and channel noise suppression. It has a low complexity implementation (similar to MOE), since the filters are parameterized based on only one single scalar parameter (i.e., SIR in (3.58)), and require no matrix inversion.

8. **Minimum Entropy** — it follows from the MF approach that as K becomes

large, the MAI contribution tends towards Gaussianity. This motivates a class of blind estimation methods known as *minimum entropy* methods, as first described in [95]. Its underlying principle is to maximize the distance between Gaussian and the distribution of the filter output $Z_1[i]$. Conversely, since each user source is a non-Gaussian process, the distance between distributions of $b_1[i]$ and $Z_1[i]$ is minimized.

Based on HOS, one simple measure of this distance from Gaussianity is *kurtosis*, and is defined for $Z_1[i]$ as

$$\kappa(Z_1[i]) \triangleq \frac{E\{|Z_1[i]|^4\}}{E\{|Z_1[i]|^2\}^2}. \tag{2.46}$$

Some typical values for the kurtosis of the transmitted signals are: 1 for any CM source, $1.32 - 1.40$ for 16-QAM to 1024-QAM, and 3 for a Gaussian source [64]. In [96, 97], an aggregate cost function of the window average estimate of $\kappa(Z_1[i])$ in (2.46) and the CM criterion in (2.45) is used.

2.6 Chapter Summary

This chapter gives a tutorial on multiuser detection for the DS-CDMA system. The different usage of short and long spreading codes is explained. The system model is developed and relevant assumptions to be used in this thesis are listed. An extensive literature review of multiuser detection is presented, with emphasis placed on linear blind multiuser detection.

Chapter 3

Two Blind Linear Multiuser Detectors — Minimum Output Energy (MOE) and Constant Modulus Algorithm (CMA)

3.1 Chapter Outline

A review of the popular MOE-based blind detector in [3] has revealed several weaknesses. In order to alleviate these weaknesses, two new blind linear multiuser detectors have been proposed, namely the linearly constrained MOE and the CMA approach. The objective of this chapter is to examine and compare these two blind linear multiuser detectors via simulations and analysis. Also, in the case of signature mismatch where there are modelling errors in the received signature of the desired user, the effect of the constraint constant in the constrained MOE detector is examined.

The rest of this chapter is organised as follows. In Section 3.2, the system model used in this chapter is defined. In Section 3.3, a canonical representation of linear multiuser detectors is presented, and the MOE detector is reviewed. In Section 3.4, the proposed constrained MOE and the CMA multiuser detectors

are presented. In Section 3.5 and 3.6, the steady state and transient behaviours of these two detectors are examined respectively. In Section 3.7, the robustness of the constrained MOE detector against the signature mismatch problem is expressed in terms of the constraint constant. In Section 3.8, simulation results are presented to compare the constrained MOE and CMA detectors with the conventional MF and decorrelator. Finally, Section 3.9 contains the chapter's conclusions.

3.2 System Modelling

For simplicity, throughout this chapter (except Section 3.7), no multipath effect is considered, and the synchronous received signal model $\mathbf{Y}[i]$ in (2.30) is used. From (2.23), linear multiuser detection yields the ith bit estimate of the desired user $k = 1$ as

$$\hat{b}_1[i] = sgn(Z_1[i]) = sgn(\mathbf{w}_1^T[i]\mathbf{Y}[i]). \tag{3.1}$$

Recall from Section 2.4.4, the problem of linear blind multiuser detection is to determine a suitable FIR filter $\mathbf{w}_1$ of length N to suppress MAI, where only the desired user's spreading code $\mathbf{s}_1$ is known.

3.3 Review of MOE Detector

In this section, the MOE-based linear blind multiuser detector in [3] is reviewed. Before the derivation of the MOE method, it is useful to present a canonical representation for any linear multiuser detectors, as the sum of two orthogonal components. Then, the gradient descent adaptation of the MOE detector is derived, and its benefits and potential deficiencies are discussed.

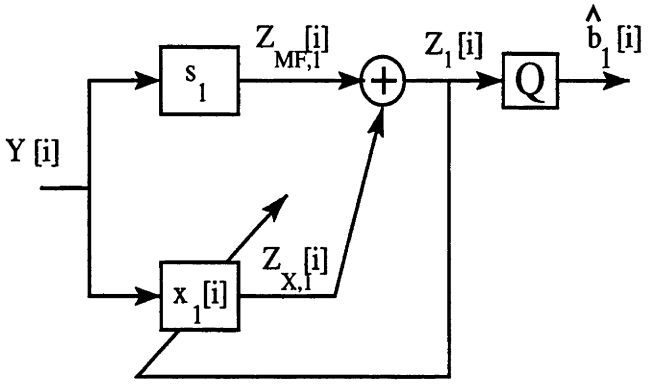

Figure 3.1: The canonical representation of a linear multiuser detector [3]

3.3.1 Canonical Representation of Linear Multiuser Detectors

As shown in Figure 3.1, a *canonical form* [3, 16] for any linear multiuser detectors $\mathbf{w}_1[i]$ is represented as

$$\mathbf{w}_1[i] = \mathbf{s}_1 + \mathbf{x}_1[i], \tag{3.2}$$

where

$$\mathbf{x}_1^T[i]\mathbf{s}_1 = 0 \quad \forall i. \tag{3.3}$$

Hence, any adaptive linear multiuser detector can be expressed as two orthogonal component: a fixed MF $\mathbf{s}_1$ and an adaptive component $\mathbf{x}_1[i]$. Then, the filter output can be expressed as

$$Z_1[i] = Z_{MF,1}[i] + Z_{X,1}[i], \tag{3.4}$$

where $Z_{MF,1}[i] = \mathbf{Y}^T[i]\mathbf{s}_1$ is the MF output and $Z_{X,1}[i] \triangleq \mathbf{Y}^T[i]\mathbf{x}_1[i]$ is the adaptive filter output. In accordance with the normalised signature assumption in Section 2.3.5, $\mathbf{w}_1$ in (3.2) and (3.3) satisfies the following condition

$$\mathbf{w}_1^T[i]\mathbf{s}_1 = \|\mathbf{s}_1\|^2 = 1 \quad \forall i. \tag{3.5}$$

3.3.2 MOE Detector

It follows from (3.3) that the required adaptation for $\mathbf{x}_1[i]$ is constrained along the subspace orthogonal to $\mathbf{s}_1$. Using the canonical filter representation in (3.2), the MOE cost in (2.44) can be written as

$$\begin{aligned} J_{MOE}(\mathbf{x}_1) &= E\left\{\left(\mathbf{w}_1^T[i]\mathbf{Y}[i]\right)^2\right\} \\ &= E\left\{\left(\mathbf{x}_1^T[i]\mathbf{Y}[i]\right)^2 + \left(\mathbf{s}_1^T\mathbf{Y}[i]\right)^2\right\}. \end{aligned} \tag{3.6}$$

In [3], the stochastic gradient adaptation of the MOE cost in (3.6) uses a gradient projection implementation. That is, in order to adapt $\mathbf{x}_1[i]$, the unconstrained gradient of the MOE cost is projected on the subspace orthogonal to $\mathbf{s}_1$. The resultant, stochastic gradient adaptation of the MOE detector is given as

$$\begin{aligned} \mathbf{x}_1[i+1] &= \mathbf{x}_1[i] - \mu\frac{1}{2}\nabla_{\mathbf{x}_1[i]}J_{MOE}(\mathbf{x}_1) \\ &= \mathbf{x}_1[i] - \mu Z_1[i](\mathbf{Y}[i] - Z_{MF,1}[i]\mathbf{s}_1), \end{aligned} \tag{3.7}$$

where μ is the step size and $\nabla_{\mathbf{x}_1[i]}J_{MOE}(\mathbf{x}_1)$ denotes the derivative of $J_{MOE}(\mathbf{x}_1)$ with respect to $\mathbf{x}_1[i]$. The component $(\mathbf{Y}[i] - Z_{MF,1}[i]\mathbf{s}_1)$ within the adaptation term in (3.7) is the component of $\mathbf{Y}[i]$ orthogonal to $\mathbf{s}_1$.

In the same manner as the training-based adaptive MMSE detector in (2.43), the MOE detector in (3.7) is updated at the bit rate (i.e., $1/T_b$). In this blind scenario, a typical initialisation of the MOE detector is the MF setting

$$\mathbf{w}_1[0] = \mathbf{s}_1; \quad \text{or} \quad \mathbf{x}_1[0] = \mathbf{0}. \tag{3.8}$$

Hence, the implementation of the MOE detector is equivalent to augment an adaptive filter $\mathbf{x}_1[i]$ to the conventional MF. Various modified MOE detectors have also been proposed, and are listed in Section 2.5.8.

3.3.3 Benefits of MOE Detector

The benefits of the MOE-based linear blind multiuser detectors are stated as follows.

- Due to its LMS-like adaptation, the MOE algorithm in (3.7) has low computational complexity.
- Since the MOE cost function in (2.44) is strictly convex (i.e., quadratic cost), its adaptation in (3.7) is globally convergent and avoids any ill-convergence problems. That is, it converges to the desired minimum, regardless of its initialisation.
- Using the canonical representation in (3.2), the MSE cost[1] in (2.41) can be written as [3]

$$\begin{aligned} J_{MSE}(\mathbf{w}_1) &= E\{\left(A_1 b_1 - \mathbf{Y}^T[i]\mathbf{w}_1[i]\right)^2\} \\ &= A_1^2 + J_{MOE}(\mathbf{w}_1) - 2A_1^2\mathbf{w}_1^T[i]\mathbf{s}_1 \\ &= J_{MOE}(\mathbf{w}_1) - A_1^2. \end{aligned} \tag{3.9}$$

  In deriving (3.9), the received signal model of the DS-CDMA system in (2.30) have not been used, and the only assumption used is that the desired bit $b_1[i]$ is uncorrelated with the MAI. Since the MOE cost is related to the MSE cost by a constant, the MOE detector converges to the linear MMSE detector in (2.42) which can be written as

$$\mathbf{w}_{1,MMSE} = \mathbf{R}_{\mathbf{yy}}^{-1} E\{\hat{b}_1[i]\mathbf{Y}[i]\} = A_1\mathbf{R}_{\mathbf{yy}}^{-1}\mathbf{s}_1, \tag{3.10}$$

  where $\mathbf{R}_{\mathbf{yy}} \triangleq E\left\{\mathbf{Y}[i]\mathbf{Y}^T[i]\right\}$. From (3.9), since minimising MOE also minimising MSE, the near far resistance of the converged MOE solution approaches that of the MMSE detector [16].

3.3.4 Weaknesses of MOE Detector

Despite its simple implementation and convergence to the MMSE detector, the MOE detector exhibits the following weaknesses.

- All linear multiuser detectors in (3.1) fail to generate reliable data estimates when the received signal vector $\mathbf{Y}[i]$ becomes near orthogonal to the linear

[1] Using training-based adaptation, it is assumed that the bit estimate $\hat{b}_1[i]$ in (2.41) is replaced by $A_1 b_1$.

filter $\mathbf{w}_1[i]$. This implies that the filter output $Z_1[i]$ approaches zero, and therefore noise will more likely cause errors. Using the orthogonal filter decomposition in (3.2), this failure mechanism arises if $Z_{MF,1}[i] \simeq -Z_{X,1}[i]$, or when both $Z_{MF,1}[i]$ and $Z_{X,1}[i]$ are close to zero. It is suggested that there may arise some pathological cases where $Z_{MF,1}[i]$ gives correct decision, and the addition of $Z_{X,1}[i]$ may cause errors.

- The energy of the linear filter is given by

$$\|\mathbf{w}_1[i]\|^2 = \|\mathbf{s}_1\|^2 + \|\mathbf{x}_1[i]\|^2 = 1 + \chi[i], \tag{3.11}$$

where $\chi[i] \triangleq \|\mathbf{x}_1[i]\|^2$ is referred to as the *surplus energy*. Thus, the MOE detector always gives noise enhancement (i.e., $\|\mathbf{w}_1[i]\|^2 > 1$), unless the surplus energy vanishes completely as in the MF case. It is noted that this noise enhancement usually does not cause significant performance degradation, since the MAI is typically the dominant component compared to the AWGN.

- In the presence of multipath induced ICI and ISI, signature mismatch problem occurs when the desired user's received signature waveform $f_1(t)$ in (2.16) can no longer be modelled by its transmitted counterpart $s_1(t)$ in (2.2). In [3], the MOE detector is made robust to this signature mismatch problem, by constraining the surplus energy, as discussed in Section 3.7.1. However, this surplus energy constraint is empirically based, and assumes that the signature modelling error is sufficiently small.

- It is well-known that the gradient projection algorithm in (3.7) is susceptible to the *finite precision effect* [57, 98]. It is because that this incorrectly assumes that the constraint in (3.5) is satisfied along the entire filter trajectory. Then, the small deviations from the constraint can lead to accumulating errors which may cause signal cancellation. Thus, practical implementation of the MOE detector [3] requires to occasionally update $\mathbf{x}_1[i]$ by its orthogonal projection

$$\mathbf{x}_1[i] - \left(\mathbf{x}_1^T[i]\mathbf{s}_1\right)\mathbf{s}_1. \tag{3.12}$$

3.4 Robust Alternative to MOE

In this section, in order to alleviate the weaknesses of the MOE detector in (3.7), several robust alternatives are proposed. First, to guide the later development of an improved blind algorithm, a non-blind, non-adaptive constrained MOE detector is presented. Second, a blind, adaptive version of this constrained MOE detector is proposed, when only the code of the desired user is known. Third, a CMA-based linear blind multiuser detector is proposed.

3.4.1 Non-Blind Constrained MOE

To avoid the pathological case where $Z_{MF,1}[i] \simeq -Z_{X,1}[i]$, the MOE detector is modified without the usage of the orthogonal filter decomposition in (3.2). The constrained MOE-based optimisation is re-formulated as follows [56, 57]

$$\min_{\mathbf{w}_1} \mathbf{w}_1^T \mathbf{R}_{yy} \mathbf{w}_1 \quad \text{subject to} \quad \mathbf{S}^T \mathbf{w}_1[i] = \mathbf{F} \ \ \forall i, \tag{3.13}$$

where

$$\mathbf{F} = (a\ 0\ 0 \ldots 0)^T, \tag{3.14}$$

is a K-length column vector with $\mathbf{w}_1^T[i]\mathbf{s}_1 = a \quad \forall i$, as the *constraint constant* (e.g., (3.5) represents a special case of $a = 1$), and $\mathbf{S}$ is the signature matrix defined in (2.30). In order to implement the set of K linear constraints in (3.13), the knowledge of signatures of all users are required.

The closed form, optimal solution[2] to (3.13) can be obtained via Lagrange multipliers [98], and is given by

$$\mathbf{w}_{1,opt} = \mathbf{R}_{yy}^{-1}\mathbf{S}\left[\mathbf{S}^T\mathbf{R}_{yy}^{-1}\mathbf{S}\right]^{-1}\mathbf{F}. \tag{3.15}$$

It can be shown [16] that the non-adaptive decorrelator in (2.37) is a special case of (3.15), and is given by

$$\mathbf{w}_{1,DEC} = a\sum_{k=1}^{K}\left(\mathbf{R}^{-1}\right)_{1,k}\mathbf{s}_k = \mathbf{S}\mathbf{R}^{-1}\mathbf{F}. \tag{3.16}$$

[2] For $\left[\mathbf{S}^T\mathbf{R}_{yy}^{-1}\mathbf{S}\right]^{-1}$ to exist in (3.15), it is generally assumed that $\mathbf{R}_{yy}$ is positive definite, and $\mathbf{S}$ has full column rank K.

3.4.2 Blindly Constrained MOE

In blind multiuser detection where the signatures of interfering users are unknown, only a constraint related to the desired user can be implemented. Thus, the aim is to derive an adaptive version of (3.15) using a single constraint $\mathbf{w}_1^T[i]\mathbf{s}_1 = a \quad \forall i$ in (3.14).

It is well-known [99] that the convexity of a cost function is retained, if linear constraints are imposed. Using Frost's constraint projection [98], a constrained gradient descent MOE algorithm[3] is given by

$$\mathbf{w}_1[i+1] = \mathbf{P}_{\mathbf{s}_1}^{\perp}\left(\mathbf{w}_1 - \mu Z_1[i]\mathbf{Y}[i]\right) + a \cdot \mathbf{s}_1, \tag{3.17}$$

where

$$\mathbf{P}_{\mathbf{s}_1}^{\perp} \triangleq \mathbf{I}_N - \mathbf{s}_1\left(\mathbf{s}_1^T\mathbf{s}_1\right)^{-1}\mathbf{s}_1^T = \mathbf{I}_N - \mathbf{s}_1\mathbf{s}_1^T \tag{3.18}$$

is a projection operator which projects any vector into the subspace orthogonal to $\mathbf{s}_1$. Its initialisation is given by

$$\mathbf{w}_1[0] = a \cdot \mathbf{s}_1. \tag{3.19}$$

In fact, (3.17) can be decomposed as two separate adaptation steps:

$$\mathbf{w}_1[i+1] = \mathbf{w}_1[i] - \mu Z_1[i]\mathbf{Y}[i] \tag{3.20}$$

$$\text{replace } \mathbf{w}_1[i+1] \text{ by } \mathbf{w}_1[i+1] - \left(\mathbf{w}_1^T[i+1]\mathbf{s}_1 - a\right)\mathbf{s}_1 \tag{3.21}$$

It is seen that the first step is an unconstrained MOE, while the second step is an error correcting procedure to ensure that the trajectory of $\mathbf{w}_1[i]$ always satisfy the constraint $\mathbf{w}_1^T[i]\mathbf{s}_1 = a \quad \forall i$.

A geometrical interpretation of this blindly constrained MOE algorithm is that it scales the size of the MOE cost level surface, until it touches the hyperplane represented by the specified constraints. Unlike the gradient projection in (3.7), the Frost's constraint projection in (3.17) is robust to accumulated finite precision errors. By increasing the constraint constant $a > 1$, more energy is put into the

[3] This constrained MOE detector is also independently proposed in [57] where an orthogonal filter decomposition is used.

recovery of the desired signal, at the expense of noise enhancement. In [36], an implicit constraint on the ℓ_2 norm of the filter coefficients (i.e., $\|\mathbf{w}_1[i]\|$) is used to obtain a compromise between MAI suppression and noise enhancement. In [57], it is shown that if any signature of the interfering users is known, additional linear constraints can be added to improve the convergence rate.

3.4.3 Blind CMA

Another approach to suppress MAI is to restore certain invariant property of the desired signal (e.g., CM, finite alphabet), as discussed in Section 2.5.8. The CM criterion has been chosen because of its reported robustness properties (e.g., [88, 100]) and its near convergence to the MMSE (Wiener) solution [64]. Analogous to the usage of temporal-based CMA in the single user channel equalisation to remove ISI [64], a CMA-based linear blind multiuser detector is proposed.

For linear filtering, the CM cost function in (2.45) can be written as

$$J_{CM}(\mathbf{w}_1) = E\left\{\left(\left(\mathbf{w}_1^T[i]\mathbf{Y}[i]\right)^2 - \xi\right)^2\right\}, \tag{3.22}$$

where ξ is the modulus radius. From (3.22), using a steepest gradient descent strategy, the CMA adaptation is given by [27, 56]

$$\begin{aligned}\mathbf{w}_1[i+1] &= \mathbf{w}_1[i] - \mu \cdot \frac{1}{4}\nabla_{\mathbf{w}_1[i]} J_{CM}(\mathbf{w}_1) \\ &= \mathbf{w}_1[i] - \mu \left(Z_1^2[i] - \xi\right) Z_1[i] \nabla_{\mathbf{w}_1[i]} Z_1[i] \\ &= \mathbf{w}_1[i] - \mu \left(Z_1^2[i] - \xi\right) Z_1[i]\mathbf{Y}[i], \end{aligned} \tag{3.23}$$

where $\nabla_{\mathbf{w}_1[i]} J_{CM}(\mathbf{w}_1)$ denotes the derivative of $J_{CM}(\mathbf{w}_1)$ with respect to $\mathbf{w}_1[i]$. The usage of the CMA in multiuser detection is viewed as a source separation problem, and is different from the temporal-based channel equalisation in a single-user case.

3.5 Steady State Behaviour

In this section, the steady state behaviours (i.e., stationary points) of the MOE and CMA detectors are examined and compared.

3.5.1 Lock and Capture Analysis of CMA

Following the same argument as in [101], the contribution of an individual user in the filter output $Z_1[i]$ can be represented in terms of the *user gain*, and is defined as

$$\mathbf{V}[i] \triangleq (\mathbf{SA})^T \mathbf{w}_1[i] = (v_1[i], \ldots, v_K[i])^T, \tag{3.24}$$

where $v_k[i]$ is the kth user gain at the ith bit iteration. Essentially, each user gain measures the amplitude of the linear filter with respect to individual user. Under a noiseless assumption, the stationary points of the CMA is expressed in terms of these user gains (see Appendix A for details). This is analogous to the single-user equalisation scenario for ISI channels, where the convergence analysis of the CMA is examined in the combined channel-equaliser space [64].

Substituting (A.1), (3.24) and (A.2) into (3.23), the CMA can be expressed in terms of the user gains, and is given by

$$\begin{aligned} \mathbf{V}[i+1] &= \mathbf{V}[i] - \mu (\mathbf{SA})^T \left(Z_1^2[i] - \xi\right) Z_1[i] \mathbf{Y}[i] \\ &= \mathbf{V}[i] - \mu (\mathbf{SA})^T \mathbf{SA} \cdot \frac{1}{4} \nabla_{\mathbf{V}} J_{CM}(\mathbf{V}) \\ &= \left(\mathbf{I}_K - \mu \widehat{\mathbf{R}} \mathbf{Q}[i]\right) \mathbf{V}[i], \end{aligned} \tag{3.25}$$

where $\nabla_{\mathbf{V}} J_{CM}(\mathbf{V})$ is given in (A.8), $\widehat{\mathbf{R}} \triangleq (\mathbf{SA})^T (\mathbf{SA})$ with the (i,j)-th element $\left(\widehat{\mathbf{R}}\right)_{i,j} = A_i A_j (\mathbf{R})_{i,j}$, and $\mathbf{Q}[i]$ is an $(K \times K)$ diagonal matrix with the (k,k)-th diagonal entry defined as the bracket term in (A.9)

$$(\mathbf{Q}[i])_{k,k} \triangleq 3 \sum_{j=1}^{K} v_j^2[i] - \xi - 2 v_k^2[i]. \tag{3.26}$$

Of the stable stationary points of CMA (i.e., local minima in (A.13)), the one that corresponds to the desired user $k = 1$ is given by

$$v_1[i] = \sqrt{\xi}, \text{ and } v_k[i] = 0 \quad \forall k \in \{2, \ldots, K\}, \tag{3.27}$$

and is referred to as the *lock convergence* (i.e., desired local minimum). It is seen that the lock convergence in (3.27) is equivalent to the decorrelator detector in

(3.16), and has the filter output $Z_1[i] = \mathbf{V}^T[i]\mathbf{b}[i] = \sqrt{\xi}b_1[i]$. However, since the CM criterion in (2.45) is a non-convex cost function, depending on its initialisation, the adaptation may converge to an incorrect local minimum. This situation of capturing an interfering user (i.e., other than the desired user $k = 1$) is referred to as the *capture convergence*, and is given by

$$|v_m| = \sqrt{\xi} \text{ for } m \neq 1, \text{ and } v_k = 0 \quad \forall k \neq m. \tag{3.28}$$

3.5.2 Capture Avoidance

In terms of multiuser detection, CMA is used to extract the desired signal and suppress MAI. That is, the goal of CMA here is to achieve the lock convergence in (3.27), and to avoid the capture convergence in (3.28). Thus, a proper initialisation of the linear filter $\mathbf{w}_1[i]$ is required. In the case of MF initialisation (i.e., $\mathbf{w}_1[0] = \mathbf{s}_1$), the corresponding user gains are given by

$$v_1[0] = A_1, \text{ and } v_k[0] = (\mathbf{R})_{1,k} A_k \quad \forall k \in \{2, \ldots, K\}. \tag{3.29}$$

The filter trajectory in terms of $\mathbf{V}$ that passes through the critical value v_c in (A.14), lies on the transition boundary between regions of the lock and capture convergence. That is, the lock convergence occurs if the filter initialisation lies within the lock region, and initialisation within capture region gives the capture convergence. In [27, 101], this lock-capture boundary is derived for $K = 2$ users by solving

$$\begin{aligned}
&(|v_1[0]| - v_c)\,|A_2^2 \left(2\,|v_1[0]|^2 + |v_2[0]|^2 - 1\right) v_2[0] \\
&\qquad + A_1 A_2 \rho \left(|v_1[0]|^2 + 2\,|v_2[0]|^2 - 1\right) v_1[0]| \\
&= (|v_2[0]| - v_c)\,|A_1^2 \left(|v_1[0]|^2 + 2\,|v_2[0]|^2 - 1\right) v_1[0] \\
&\qquad + A_1 A_2 \rho \left(2\,|v_1[0]|^2 + |v_2[0]|^2 - 1\right) v_2[0]|,
\end{aligned} \tag{3.30}$$

where $\rho \triangleq (\mathbf{R})_{1,2} = (\mathbf{R})_{2,1}$ is the non-zero signature cross-correlation between users $k = 1, 2$. Thus, the lock-capture boundary is dependent on the near far condition (i.e., ratio between A_1 and A_2) and the signature coupling (i.e., ρ). In [27, 101], using (3.30), lock-capture boundaries with different values of A_1, A_2 and ρ are plotted.

However, as the number of users, K, increases, the analytical expression of the exact lock-capture boundary becomes non-trivial. Fortunately, independent of the near far effect and the signature coupling, there exists a *positive lock region* where the lock convergence in (3.27) is almost surely to be achieved, and is generalised to any K users as [56, 101]

$$v_1[0] > v_c > |v_k[0]| \quad \forall k \in \{2, \ldots, K\}. \tag{3.31}$$

Conversely, there is also a *positive capture region* where the capture convergence in (3.28) is almost guaranteed, and is given as

$$|v_m| > v_c > |v_k[0]| \quad m \neq 1, \text{ and } \forall k \neq m. \tag{3.32}$$

Given an appropriate choice of ξ, v_c can be removed in (3.31), such that the necessary condition for the lock convergence becomes

$$v_1[0] > |v_k[0]| \quad \forall k \in \{2, \ldots, K\}. \tag{3.33}$$

As shown in Figure 3.2, for the $K = 2$ users case, the positive lock and capture regions are represented by different shaded areas, and the unshaded areas can be either lock or capture depending on the near far conditions and signature coupling as in (3.30). Also, the necessary lock condition in (3.33) is represented by the area below the diagonal $v_1[0] = |v_2[0]|$ which is lock-capture boundary for $A_1 = A_2$ and $\rho = 0$.

The direct approach is to avoid the erroneous capture convergence in (3.32), and to initialise within the positive lock region in (3.31). In this chapter, various capture avoidance methods have been proposed and are listed as follows.

- As shown in Figure 3.2, the received signal $\mathbf{Y}[i]$ is scaled by a factor ν such that the respective user gains are shifted from the "ultimate lock region" or fringes around the lock region into the positive lock region in (3.31) [56, 101]. The range of this input scaling factor ν is given by

$$\frac{v_c}{|v_1[0]|} < \nu < \frac{v_c}{|v_k[0]|} \quad k \in \{2, \ldots, K\}, \tag{3.34}$$

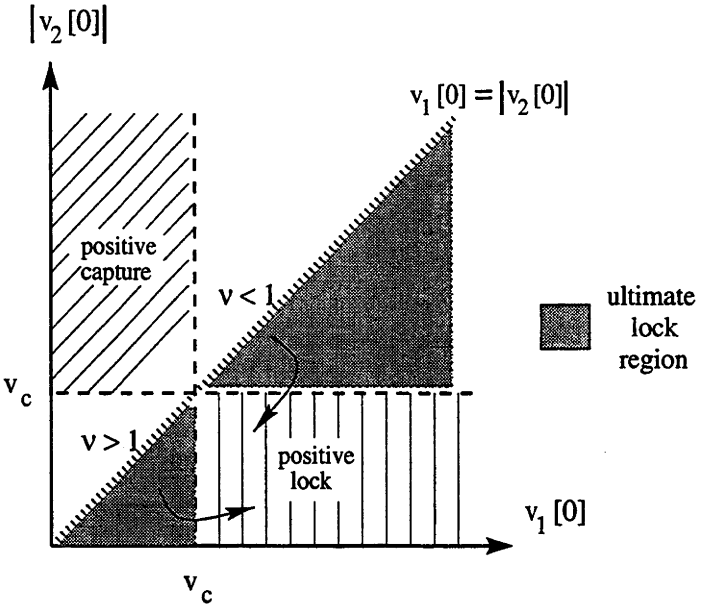

Figure 3.2: Capture avoidance of the CMA by scaling the received signal by ν.

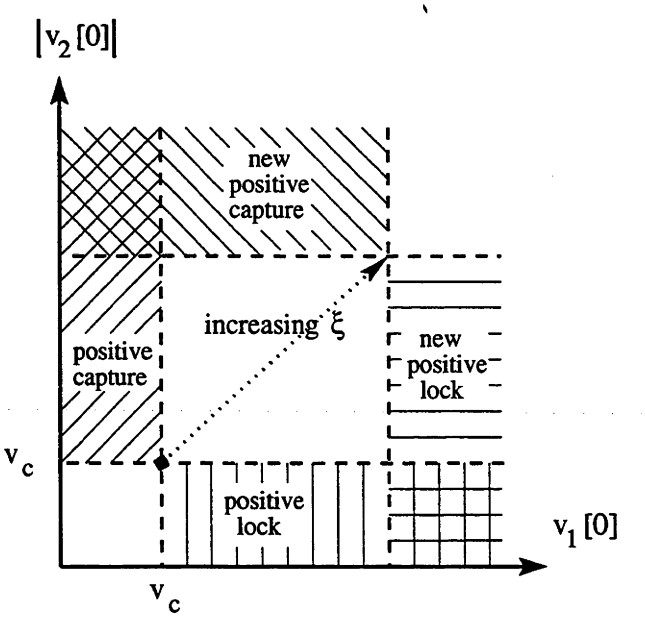

Figure 3.3: Capture avoidance of the CMA by increasing the modulus radius ξ.

where $\nu < 1$ if $|v_1[0]| > v_c$ (i.e., attenuation), and $\nu > 1$ if $|v_1[0]| < v_c$ (i.e., amplification).

This input scaling is only effective if (3.33) is satisfied. From (3.29), if all users are of equal power, (3.33) is always satisfied since $(\mathbf{R})_{1,k} \ll 1 \quad \forall k \in \{2, \ldots, K\}$. Unless in a severe near far environment or when there are excessive signature couplings, robust initialisation for the lock convergence can be achieved using the MF initialisation. Thus, in contrast to the CMA-based equaliser for the single user ISI channels, lock convergence initialisation for multiuser detection is more straightforward.

- As shown in Figure 3.3, by adjusting the modulus radius ξ, the locations of the positive lock and capture regions can be changed [56]. It is shown in [101] that if more users are present, v_c tends to approach zero and both the positive lock and capture regions become smaller. The resultant effect is that stronger users tend to get suppressed and weaker users dominated. For example, given a time varying user population, if the change in K is known, to facilitate the lock convergence initialisation, the respective v_c can be normalised to v_c of the $K = 2$ users case (i.e., $\sqrt{\xi}/2$) by multiplying ξ by $(3M - 2)/4$, where $2 \leq M \leq K$ in (A.14).

- As expected, the lock convergence initialisation is harder to achieve as more MAI is presented. One reason is that the signature coupling inevitably increases as $K \to N$. Following the same argument as in the RLS-based CMA [66], a decorrelated CMA is proposed in [27, 102] which eliminates the effect of signature coupling by pre-whitening the filter input. That is, in the CMA adaptation (3.23), the received signal $\mathbf{Y}[i]$ is first multiplied by a matrix inverse $\mathbf{R}_{\mathbf{yy}}^{-1}$. In [103], it is shown that the volumes of the CMA regions of convergence is proportional to its signal-space eigenvalues. A geometrical interpretation is that the pre-whitening has the effect of equating each user's region of convergence volume.

- In [73–75], a SOS-based constrained CMA is proposed that constraint the

CM criterion by a decorrelation constraint. Its cost function is given by

$$J_{CM-SOS} = \sum_{k=1}^{K} E\left\{(|Z_k[i]|^2 - \xi)^2\right\} + \alpha \sum_{k=1}^{K} \sum_{m=1, m\neq k}^{K} |E\{Z_k[i] Z_m^*[i]\}|^2, \tag{3.35}$$

where α is a real and positive constant. The selection of α should be large enough to prevent from converging to the same source, but small enough not to affect the convergence behaviour of the CMA. The second term in (3.35) represents the cross-correlations between different outputs, and is used to penalise the situation when two outputs extract the same user.

Another method to prevent different filters from converging to the same user is a subtraction-based CMA, proposed in [75, 76]. Similar to the MAI cancellation in Section 2.5.6, the idea is to remove the contributions of estimated user in the received signal $\mathbf{Y}[i]$, before feeding it into the filter.

Both the SOS-based constrained CMA and the subtracted-based CMA are most useful in a centralised setting where all users are required to be demodulated. However, they suffer from long delays (i.e., off-line adaptations) and the need to estimate the SOS constraints or the received amplitudes.

3.5.3 Global Convergence of MOE

As was done in deriving (3.25), the unconstrained MOE adaptation in (3.20) can be expressed in terms of the user gains. In a noiseless setting, substituting (A.1) and (3.24) in (3.20) yields

$$\begin{aligned} \mathbf{V}[i+1] &= \mathbf{V}[i] - \mu(\mathbf{SA})^T Z_1[i] \cdot \mathbf{Y}[i] \\ &= \mathbf{V}[i] - \mu(\mathbf{SA})^T \left(\mathbf{V}^T[i]\mathbf{b}[i]\right) \cdot \mathbf{SAb}[i] \\ &= \left(\mathbf{I}_K - \mu\widehat{\mathbf{R}}\right) \mathbf{V}[i], \end{aligned} \tag{3.36}$$

Since the MOE detector is globally convergent, its convergence analysis is simple and similar to that of the LMS algorithm. A detailed convergence analysis of the MOE adaptation in (3.7) can be found in [3] (e.g., its stability and steady state

excess MSE). In the case of constrained MOE detector in (3.17), the signal gain of the desired user is constrained as $v_1[i] = aA_1, \quad \forall i$.

3.6 Transient Behaviour

In this section, the transient behaviour (i.e., convergence rate) of the MOE and CMA detectors are examined and compared. The transient performance is studied through the convergence rate or the time constant[4] with respect to the user gain $\mathbf{V}[i]$ defined in (3.24). In mobile wireless communications, it is desirable to have robust transient behaviour under channel variations. For example, the rapidity at which the blind multiuser detector can react to a powering on of a strong interferer.

3.6.1 Convergence Rate of CMA

For trained LMS in (2.43), the convergence rate of $\mathbf{w}_1$ is dependent on the step size and the eigenvalues of the matrix which forms the kernel of the adaptation term [104]. This is possible because the underlying error surface is quadratic (i.e., same Hessian everywhere). However, the Hessian of the CMA in (A.10) is a function of the user gains themselves. Therefore, the convergence rate of CMA varies in different regions of the CM error surface in $\mathbf{V}[i]$ space. Following the argument in [4, 64], its convergence rate is examined in two settings: local and global behaviours as follows. The objective is to show that near lock convergence region, CMA converges faster than the LMS algorithm; but CMA can also converge slowly as its filter trajectory passes through some saddle regions.

1. **Local Behaviour** — local convergence rate near a local minimum. Assuming the filter is initialised inside the positive lock region in (3.31), the *asymptotic* convergence rate is derived in the vicinity of the lock convergence when the following condition is satisfied [105]

$$0 \leq |\epsilon_k[i]| \ll \sqrt{\xi} \quad \forall k \in \{1, \ldots, K\} \text{ and } \forall i, \tag{3.37}$$

[4] The time constant is defined as the number of bit iterations required for the user gain to decay to $(1/e)$ of its initial value [104].

where

$$\begin{aligned} \epsilon_1[i] &\triangleq v_1[i] - \sqrt{\xi}, \\ \epsilon_k[i] &\triangleq v_k[i] \quad \forall k \in \{2, \ldots, K\}. \end{aligned} \tag{3.38}$$

The *excess user gains* ϵ_k in (3.38) are used to measure the deviation from the lock convergence in (3.27).

First, the diagonal entries of $\mathbf{Q}[i]$ in (3.26) are expressed in terms of the excess user gains as follows

$$(\mathbf{Q}[i])_{k,k} = \begin{cases} 3\sum_{k=2}^{K} \epsilon_k^2[i] + (\sqrt{\xi} + \epsilon_1[i])^2 - \xi = 2\sqrt{\xi}\epsilon_1[i] & \text{if } k = 1, \\ 3\sum_{m=2, m\neq k}^{K} \epsilon_m^2[i] + 3(\sqrt{\xi} + \epsilon[i])^2 + \epsilon_k^2[i] - \xi \\ \quad = 2\xi + 6\sqrt{\xi}\epsilon_1[i] \quad \forall k \in \{2, \ldots, K\}. \end{cases} \tag{3.39}$$

It is assumed that the squared terms (i.e., ϵ_k^2 and $\epsilon_1\epsilon_k$) in (3.39) are negligible small under the condition in (3.37). Second, the adaptation of the kth user gains in (3.25) can be written as

$$v_k[i+1] = (1 - \mu A_k^2 (\mathbf{Q}[i])_{k,k}) v_k[i] - \mu A_k \sum_{m=1, m\neq k}^{K} A_m (\mathbf{R})_{m,k} (\mathbf{Q}[i])_{k,k} v_m[i]. \tag{3.40}$$

Third, substituting (3.39) into (3.40), the adaptation of the excess user gains for the desired user $k = 1$ is given by

$$\begin{aligned} \sqrt{\xi} + \epsilon_1[i+1] &= (1 - 2\mu A_1^2 \sqrt{\xi}\epsilon_1[i])(\sqrt{\xi} + \epsilon_1[i]) \\ &\quad -\mu A_1 \sum_{k=2}^{K} A_k (\mathbf{R})_{k,1} (2\xi + 6\sqrt{\xi}\epsilon_k[i])\epsilon_k[i] \\ \epsilon_1[i+1] &= (1 - 2\mu A_1^2 \xi)\epsilon_1[i] - 2\mu A_1 \xi \sum_{k=2}^{K} (\mathbf{R})_{k,1} \epsilon_k[i], \end{aligned} \tag{3.41}$$

and for the kth interfering user (where $k \in \{2, \ldots, K\}$)

$$\begin{aligned}\epsilon_k[i+1] &= \left(1 - \mu A_k^2 \left(2\xi + 6\sqrt{\xi}\epsilon_1[i]\right)\right)\epsilon_k[i] \\ &\quad -\mu A_1 A_k \left(\mathbf{R}\right)_{1,k} \left(2\sqrt{\xi}\epsilon_1[i]\right)\left(\sqrt{\xi} + \epsilon_1[i]\right) \\ &\quad -\mu A_k \sum_{m=2, m\neq k}^{K} A_m \left(\mathbf{R}\right)_{m,k} \left(2\xi + 6\sqrt{\xi}\epsilon_1[i]\right)\epsilon_m[i] \\ &= \left(1 - 2\mu A_k^2 \xi\right)\epsilon_k[i] - 2\mu A_1 A_k \xi \left(\mathbf{R}\right)_{1,k}\epsilon_1[i] \\ &\quad -2\mu A_k \xi \sum_{m=2, m\neq k}^{K} A_m \left(\mathbf{R}\right)_{m,k}\epsilon_m[i]. \end{aligned} \tag{3.42}$$

To further simplify (3.41) and (3.42), it is assumed that the terms involving $\left(\mathbf{R}\right)_{m,k}\epsilon_k \quad \forall m \neq k$ are negligible. Then, for the kth user, the adaptation of the excess user gain is given by

$$\epsilon_k[i+1] \simeq \left(1 - 2\mu A_k^2 \xi\right)\epsilon_k[i]. \tag{3.43}$$

For sufficiently small step size (i.e., $\mu \ll 1$), it follows that [104] the asymptotic time constant for $\epsilon_k[i]$ can be approximated as

$$\tau(\epsilon_k) \simeq \frac{1}{2\mu A_k^2 \xi}. \tag{3.44}$$

Analogous to the LMS result, the step size bound for stable local convergence is given by

$$0 < \mu < \min_{k\in\{1,\ldots,K\}} \frac{1}{A_k^2 \xi}. \tag{3.45}$$

Thus, at the vicinity of the lock convergence, the overall, local CMA convergence rate is twice that of the LMS. In [4, 106], for the case of fractionally spaced equaliser, a similar result has been derived by modelling the averaged CMA behaviour with ordinary differential equations. Furthermore, from (3.44), the local CMA convergence rate for each user is independent of other users' received amplitudes. This illustrates its robustness of local transient behaviour with respect to powering on of new interferers. Finally, similar to the constraint constant a in (3.14), the selection of the modulus radius ξ in the CMA is a tradeoff between achieving a faster local convergence and avoiding noise enhancement.

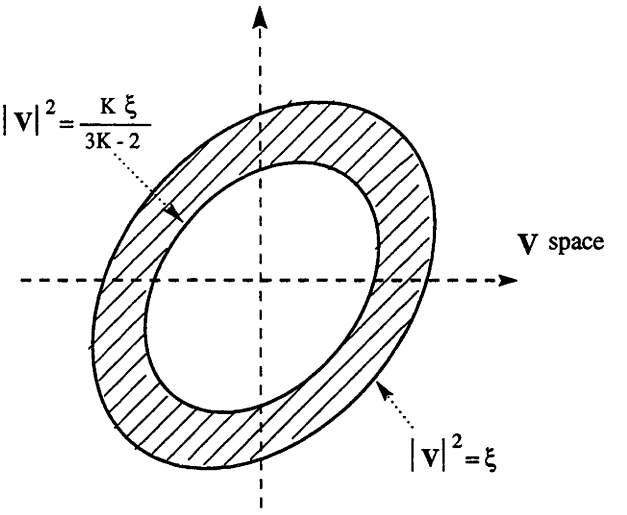

Figure 3.4: Region of annulus $\mathcal{S}$ that contains all CM local minima and saddle points [4].

2. **Global Behavior** — convergence rate far from a local minimum. Following the argument in [4, 106], the global convergence behavior of the CMA can be described with respect to the proximity of the filter trajectory to the region of annulus $\mathcal{S}$ in the $\mathbf{V}$ space. As shown in Figure 3.4, this region $\mathcal{S}$ contains all the local minima and the saddle points and is given by

$$\frac{K\xi}{3K-2} \leq \|\mathbf{V}\|^2 \leq \xi, \tag{3.46}$$

where the upper boundary represents the set of local minima in (A.13), and the lower boundary represents the lowest value[5] of $\|\mathbf{V}\|^2$ at the saddle point in (A.14).

From (A.2) and (A.8), the ℓ_2 norm of the mean gradient vector is given by

$$\|\nabla_{\mathbf{w}_1} J_{CM}(\mathbf{w}_1)\|^2 = \|\mathbf{SA} \cdot \nabla_{\mathbf{V}} J_{CM}(\mathbf{V})\|^2 = \|\mathbf{SA} \cdot \mathbf{QV}\|^2, \tag{3.47}$$

where $\mathbf{Q}$ is defined in (3.26). Thus, since $\|\nabla_{\mathbf{w}_1} J_{CM}(\mathbf{w}_1)\|^2$ is dependent on $\|\mathbf{V}\|^2$, the global convergence behaviour of the CMA can be approximately described by the following two stages [4, 106].

[5] The lowest value of $\|\mathbf{V}\|^2$ at a saddle point is when $v_c = \sqrt{\xi/(3K-2)}$ in (A.14).

(a) When $\|\mathbf{V}\|^2 \gg \xi$ (i.e., far away from $\mathcal{S}$), fast convergence towards the origin, until $\mathbf{V}[i]$ touches $\mathcal{S}$.

(b) When $0 < \|\mathbf{V}\|^2 \ll \xi$ (i.e., within $\mathcal{S}$), slower convergence to a local minimum.

Depending on the filter initialisation, as the trajectory of $\mathbf{V}[i]$ approaches $\mathcal{S}$, it will first converge to the nearest stationary point. Thus, the worst initialisation scenario is to initialise near some saddle points. This is because the trajectory can be temporally trapped[6] (i.e., where CMA converges slowly) within some saddle regions, before converging to the (desired) local minimum.

3.6.2 Convergence Rate of MOE

For simplicity, the convergence rate of the unconstrained MOE in (3.20) is examined first. In the same manner as the trained LMS, the time constant for the kth user gain in the unconstrained MOE adaptation in (3.20) is given by

$$\tau(v_k) = \frac{1}{\mu \left| \lambda_k \left(\widehat{\mathbf{R}} \right) \right|}, \tag{3.48}$$

where $\widehat{\mathbf{R}}$ is defined in (3.25), and $\lambda_k \left(\widehat{\mathbf{R}} \right)$ is the kth eigenvalue of $\widehat{\mathbf{R}}$. Comparing (3.44) and (3.48), it is observed that unlike the local CMA convergence, the convergence rate of the unconstrained MOE is a function of the received amplitudes and signature couplings. This implies that the transient behaviour of the MOE detector is more sensitive to the near far condition and its current traffic load.

Instead of using the user gains, the convergence rate is now derived in terms of the filter trajectory from its optimal solution. In [3], it is shown that the MOE with the orthogonal filter decomposition in (3.7) converges to the Wiener solution in (3.10) exponentially along N modes with parameter $1 - \mu\lambda_n \left(\mathbf{R}_{\mathbf{y}^\perp \mathbf{y}} \right)$, where $\mathbf{R}_{\mathbf{y}^\perp \mathbf{y}} \triangleq E\{\mathbf{Y}^\perp[i]\mathbf{Y}^T[i]\}$, and $\mathbf{Y}^\perp[i]$ is the component of $\mathbf{Y}[i]$ orthogonal to $\mathbf{s}_1$

[6] This problem becomes more apparent as the number of saddles increases (i.e., K increases) and the step size is sufficiently small.

(i.e., bracketed term in (3.7)), and is defined as

$$\mathbf{Y}^{\perp}[i] \triangleq \mathbf{P}_{\mathbf{s}_1}^{\perp}\mathbf{Y}[i] = \mathbf{Y}[i] - Z_{MF,1}[i]\mathbf{s}_1, \tag{3.49}$$

where $\mathbf{P}_{\mathbf{s}_1}^{\perp}$ is defined in (3.18). In the case of the MOE detector with Frost's constraint projection in (3.17), the deviation of the mean filter trajectory from the optimal constrained MOE solution $\mathbf{w}_{1,opt}$ in (3.15) is measured by

$$\mathbf{e}[i] \triangleq E\{\mathbf{w}_1[i]\} - \mathbf{w}_{1,opt}. \tag{3.50}$$

Following the derivation in [98]:

$$\mathbf{e}[i+1] = \left(\mathbf{I}_N - \mu\mathbf{P}_{\mathbf{s}_1}^{\perp}\mathbf{R}_{\mathbf{yy}}\right)\mathbf{e}[i]. \tag{3.51}$$

Since $\mathbf{P}_{\mathbf{s}_1}^{\perp}\mathbf{R}_{\mathbf{yy}} = \mathbf{R}_{\mathbf{y}^{\perp}\mathbf{y}}$, the convergence rates of the MOE detector in (3.7) and (3.17) are the same. For stability, the step sizes for both MOE detectors are bounded by [104]

$$0 < \mu < \min_{m\in\{1,\ldots,N\}} \frac{2}{\left|\lambda_m\left(\mathbf{R}_{\mathbf{y}^{\perp}\mathbf{y}}\right)\right|}. \tag{3.52}$$

In order to compare the convergence rate of the CMA in (3.23) and the MOE adaptation in (3.7) or (3.17), it is assumed that all the signature vectors are approximately orthogonal. Thus, the mth eigenvalue of $\mathbf{R}_{\mathbf{y}^{\perp}\mathbf{y}}$ can be approximated as [3]

$$\lambda_m\left(\mathbf{R}_{\mathbf{y}^{\perp}\mathbf{y}}\right) \simeq \begin{cases} 0 & m = 1, \\ A_k^2\left(1 - (\mathbf{R})_{1,k}^2\right) + \sigma_n^2 & m \in \{2,\ldots,K\}, \\ \sigma_n^2 & m \in \{K+1,\ldots,N\}. \end{cases} \tag{3.53}$$

Given that the system is noiseless, orthogonal and has equal-powered users, the eigenvalue with the maximum magnitude in (3.53) is equal to A_k^2. Under this setting, it is seen that the CMA with $\xi = 1$ converges locally twice as fast as the MOE adaptation in (3.7) or (3.17). Overall, in comparison with the MOE detector, the transient performance of the CMA is more robust to parameter variations, in the vicinity of the lock convergence.

3.7 Signature Mismatch Problem

To this point, the blind multiuser detection has assumed that the receiver has perfect knowledge of the desired user's signature waveform. However, in contrast to Section 3.2, each user's transmitted signature waveform $s_k(t)$ in (2.2) is subjected to some unknown channel induced distortion (e.g., multipath effect), and is different from the received signature waveform $f_k(t)$ in (2.16). This is referred to as the *signature mismatch problem.*

In this section, for any linear multiuser detector, the robustness issue against this signature mismatch is examined. Specifically, the constrained surplus energy approach in [3] is reviewed, and the effect of the constraint constant a in (3.14) is discussed. It is assumed that the received normalised signature of the desired user is given by

$$\hat{\mathbf{s}}_1 = \frac{\mathbf{s}_1 + \delta}{\|\mathbf{s}_1 + \delta\|}, \tag{3.54}$$

where δ represents the degree of mismatch.

3.7.1 Constrained Surplus Energy

Originally proposed in [3] and modified in [107], in order to make the linear detector robust against signature mismatch, the surplus energy $\chi = \|\mathbf{x}_1\|^2$ in (3.11), is bounded by $\chi_I \leq \chi < \chi_S$. The upper and lower bounds correspond to the minimum surplus energy necessary for the complete cancellation of the desired signal, and the complete removal of the MAI respectively. The condition $\chi_I < \chi_S$ assumes that the nominal signature $\mathbf{s}_1$ is closer to $\hat{\mathbf{s}}_1$, than to the MAI subspace, measured by ℓ_2 distance. In [16], it is shown that the presence of this surplus energy is equivalent to an additional amount of AWGN.

3.7.2 Selection of Linear Constraint

In a signature mismatch problem, it is most important to avoid the complete cancellation of the desired signal, which occurs when $\mathbf{w}_1^T[i]\hat{\mathbf{s}}_1 = 0$. As shown

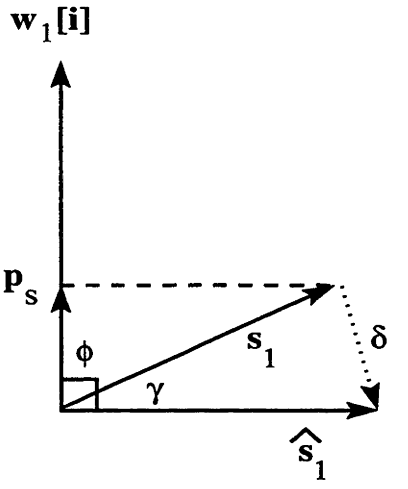

Figure 3.5: Filter constraint to avoid the complete desired signal cancellation.

in Figure 3.5, when $\mathbf{w}_1[i]$ and $\hat{\mathbf{s}}_1$ are orthogonal to each other, its geometrical relationship can be written as

$$\cos\phi[i] = \frac{\mathbf{w}_1^T[i]\mathbf{s}_1}{\|\mathbf{w}_1[i]\|} = \frac{\|\mathbf{p}_S\|}{\|\mathbf{s}_1\|}, \tag{3.55}$$

where $\mathbf{p}_S = \left(\mathbf{I}_N - \hat{\mathbf{s}}_1\hat{\mathbf{s}}_1^T\right)\mathbf{s}_1 = \mathbf{s}_1 - \hat{\mathbf{s}}_1\left(\hat{\mathbf{s}}_1^T\mathbf{s}_1\right)$ is the projection of $\mathbf{s}_1$ to the space orthogonal to that spanned by $\hat{\mathbf{s}}_1$.

The complete cancellation of the desired signal occurs if $\mathbf{w}_1[i]$ is a scaled version of $\mathbf{p}_S$. From (3.55), this occurs when the ℓ_2 norm of the linear filter becomes

$$\|\mathbf{w}_1[i]\|^2 = \frac{\left(\mathbf{w}_1^T[i]\mathbf{s}_1\right)^2}{\|\mathbf{p}_S\|^2} = \frac{a^2}{1-\cos^2\gamma}, \tag{3.56}$$

since $\|\mathbf{p}_S\|^2 = 1 - \left(\hat{\mathbf{s}}_1^T\mathbf{s}_1\right)^2 = 1 - \cos^2\gamma$, where γ is the angle between $\hat{\mathbf{s}}_1$ and $\mathbf{s}_1$. Hence, the ℓ_2 norm of the filter is "bounded away" from the origin such that $\|\mathbf{w}_1[i]\|^2 \in [a^2, \infty)$. Thus, to avoid the desired signal cancellation, the constraint $\|\mathbf{w}_1[i]\| < a \quad \forall i$, can be imposed. This means that the constraint a in (3.14) should be small enough to avoid signal cancellation, as well as to avoid noise enhancement.

3.8 Simulation Results

In this section, the simulation results are presented to demonstrate the performance of the proposed constrained MOE detector in (3.17) and the CMA detector in (3.23). Both detectors are compared with the conventional MF detector in (2.33) and the linear decorrelator in (3.16).

3.8.1 System Parameters

All simulations are based on a K-users uncoded, synchronous DS-CDMA system using a BPSK modulation scheme with binary PN spreading codes of length $N = 31$, and no multipath effect is considered. All multiuser detectors in this comparison have MF initialisations (i.e., $\mathbf{w}_1[0] = \mathbf{s}_1$) and the desired user is $k = 1$. It is assumed that all interfering users have the same received power. In order to illustrate a near far situation, the *Near-far ratio* (NFR) is used and is defined as

$$NFR[dB] \triangleq SNR(k = k')[dB] - SNR(k = 1)[dB] \quad \forall k' \in \{2, \ldots, K\}, \tag{3.57}$$

where $SNR(k) = A_k^2/(2\sigma_n^2)$ is the SNR of the kth user in decibel (dB).

The modulus radius for the CMA in (3.23) has been normalised as $\xi = A_1^2$, and the constraint constant in the MOE detector in (3.17) is set to $a = 1$. This is done to ensure that the desired user's gain of the CMA at the lock convergence is the same as that of the constrained MOE (i.e., $v_1[i \to \infty] = \sqrt{\xi} = aA_1$). The step sizes μ are chosen accordingly to ensure a stable convergence, and to provide a reasonable tradeoff between their convergence speed and steady state error variances: $\mu = 5 \cdot 10^{-6}$ for the CMA and $\mu = 10^{-4}$ for the constrained MOE.

3.8.2 Performance Measures

All performance measures are averaged over 100 Monto Carlo runs. The steady state behaviour is examined by the BER that is computed between $5 \cdot 10^3 - 10^4$ bit iterations. To compare the transient performance, a relevant measure is the

Signal-to-Interference Ratio (SIR) defined as

$$SIR[i] \triangleq \frac{A_1^2(\mathbf{w}_1^T[i]\mathbf{s}_1)^2}{\sigma_n^2\|\mathbf{w}_1[i]\|^2 + \sum_{k=2}^{K} A_k^2(\mathbf{w}_1^T[i]\mathbf{s}_k)^2} = \frac{v_1^2[i]}{\sigma_n^2\|\mathbf{w}_1[i]\|^2 + \sum_{k=2}^{K} v_k^2[i]}. \tag{3.58}$$

The SIR represents the output energy ratio of the desired signal, and the residual MAI with output noise. Analogous to the channel equalisation scenario, the "open-eye" condition is obtained when $SIR \gg 1$. In practice, after the initial blind adaptation attains a sufficiently high SIR, the adaptation is switched to the DD-LMS mode which delivers a lower excess MSE.

3.8.3 Discussion

For $SNR(k = 1) = 12dB$, the transient SIR performance is shown in Figure 3.6-3.8. Using Figure 3.6 as a reference with $NFR = 0dB$ and $K = 10$, the effect of near far condition is illustrated in Figure 3.7 with $NFR = 6dB$, and the effect of an increased user population is illustrated in Figure 3.8 with $K = 20$.

All three SIR plots have shown that both the constrained MOE and the CMA multiuser detectors converge to the decorrelator. Figure 3.6 shows that the CMA attains a higher SIR compared to that of the MOE case, as the CMA converges to a minimum norm solution [100]. It is seen that the convergence rate of the CMA is faster in Figure 3.6 compared to that of Figure 3.7 and Figure 3.8. As discussed in Section 3.6.1, with equal-powered users, the local convergence rate near the lock convergence is twice as fast as the MOE case. However, under severe near far condition, the CMA may be initialised far away from the lock convergence, and may first be hovering temporally around some saddle points. Similarly, with more users present, the number of saddle points increases, and it is now more likely to be attracted by a saddle point.

The steady state BERs are plotted in Figure 3.9- 3.11 with varying SNR of the desired user $k = 1$, varying the number of users, and varying NFR respectively. In Figure 3.9, it is shown that the BER performance for both the MOE and the CMA detectors outperform the MF significantly. Interestingly, at higher SNRs,

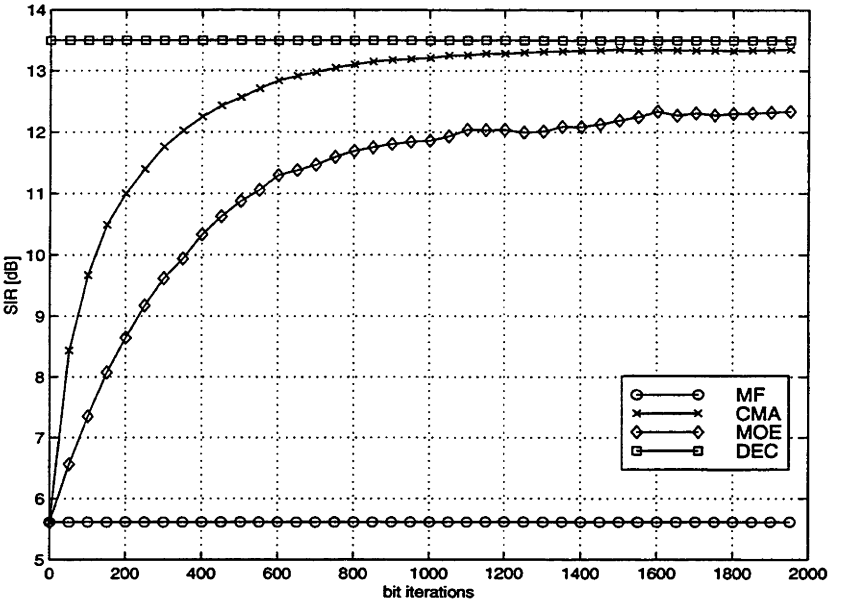

Figure 3.6: The transient SIR for different multiuser detectors: $K = 10$, $NFR = 0dB$, $SNR(k = 1) = 12dB$.

the BER of the MOE detector deviates increasingly from the decorrelator. In Figure 3.10, it is observed that the BER of the CMA is closer to the decorrelator than the MOE case, especially when there are fewer interferers present. As shown in Figure 3.11, under the near far effect, as expected, the MF gives the worst BER performance while the BER is unchanged in the decorrelator. However, the BER of the CMA seems to be more near far resistant than the MOE case. Also, under moderate near far conditions (e.g., $NFR \leq 3dB$), the BER of the CMA performs slightly better than that of the decorrelator detector. A possible explanation is that unlike the decorrelating approach, the CMA offers a tradeoff between suppressing MAI and minimising output noise.

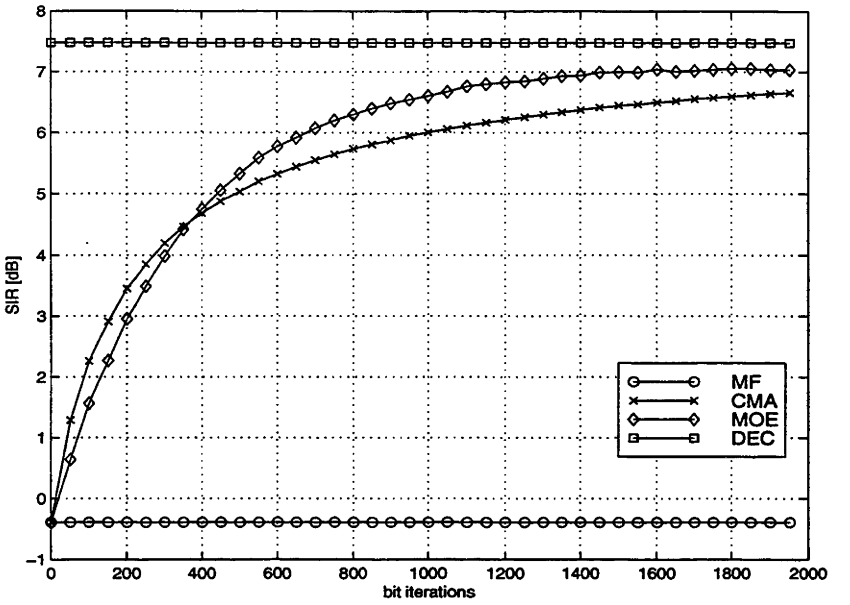

Figure 3.7: The transient SIR for different multiuser detectors with near far condition: $K = 10$, $NFR = 6dB$, $SNR(k = 1) = 12dB$.

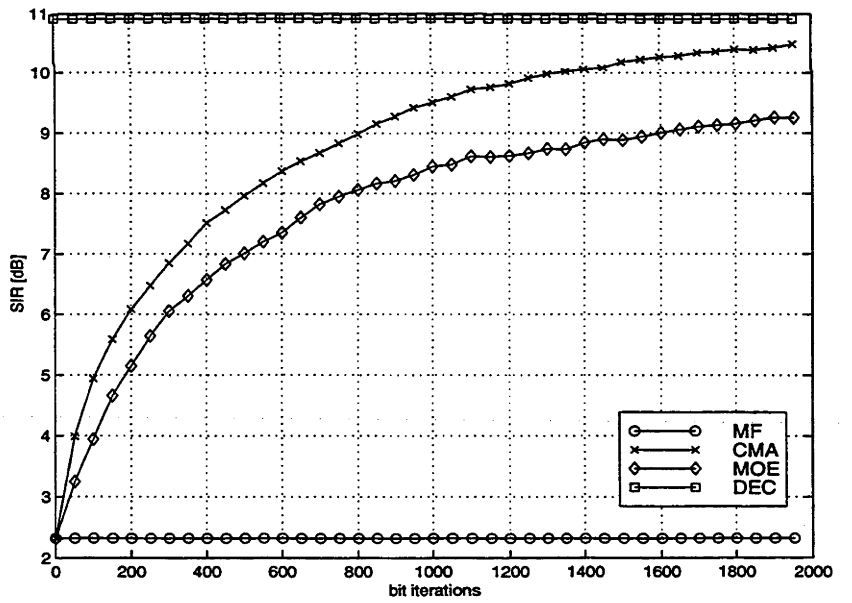

Figure 3.8: The transient SIR for different multiuser detectors with increased number of users: $K = 20$, $NFR = 0dB$, $SNR(k = 1) = 12dB$.

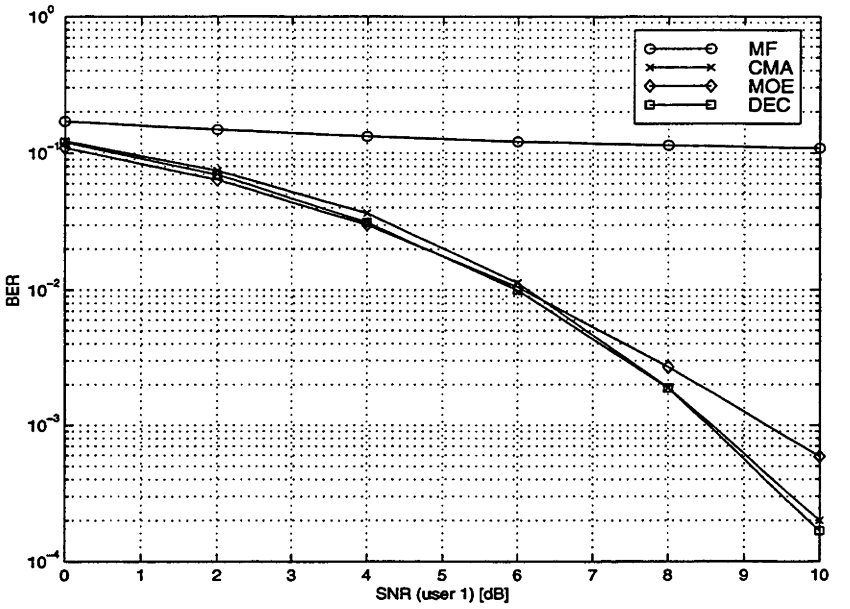

Figure 3.9: The steady state BER vs. $SNR(k=1)$ for different multiuser detectors: $K=10$ and $NFR=3dB$.

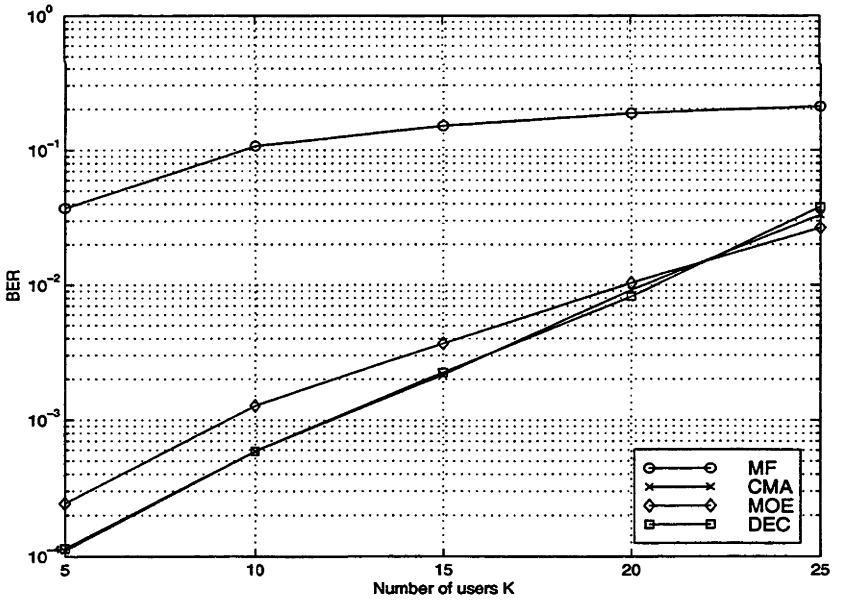

Figure 3.10: The steady state BER vs. K for different multiuser detectors: $SNR(k=1)=9dB$ and $NFR=3dB$.

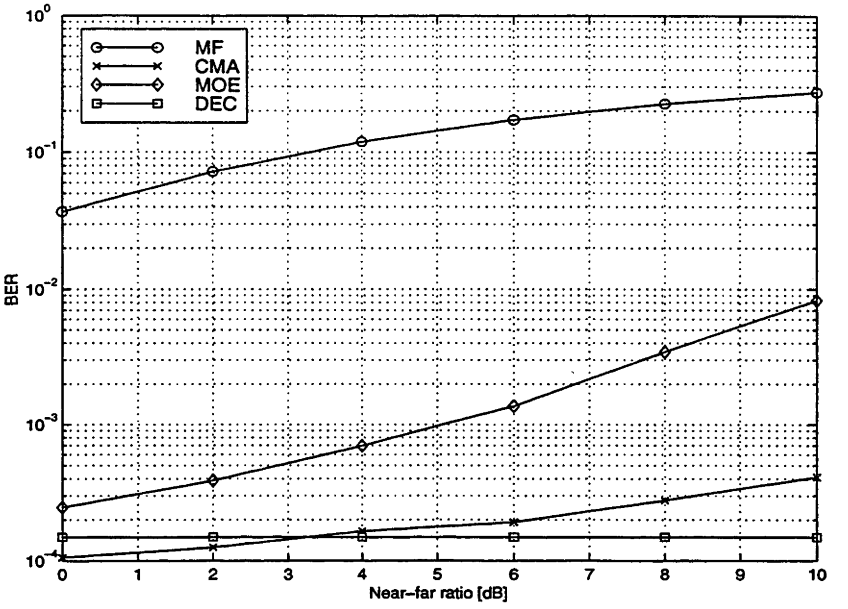

Figure 3.11: The steady state BER vs. NFR for different multiuser detectors: $K = 10$, $SNR(k = 1) = 10dB$.

3.9 Conclusions

In this chapter, two linear blind multiuser detectors have been proposed: a constrained MOE-based and a CMA-based detector. The CMA is shown to exhibit a lock convergence property which converges to a decorrelator receiver, under a noiseless assumption. Compared with the constrained MOE case, it is shown that if the CMA is initialised near the lock convergence, it has a faster local convergence rate and a slightly higher near far resistance. In contrast to the single user scenario, robust lock initialisation is possible, even under practical near far conditions (e.g., $NFR \leq 6dB$). For the constrained MOE detector, the constraint constant should be large enough to recover the desired signal, but small enough to avoid excessive noise enhancement and complete desired signal cancellation under signature mismatch.

Chapter 4

CMA-based RAKE-type Receiver

4.1 Chapter Outline

In this chapter, a new linear receiver structure for blind multiuser detection in DS-CDMA systems under a frequency selective multipath environment is proposed and analysed. The proposed receiver is designed to fully exploit the benefits of using multiple sensors by incorporating the time and space diversities in a joint fashion. It consists of a bank of linear filters that are blindly adapted by the CMA in a RAKE-type structure. The receiver uses a windowed sampling technique to remove ISI, and a set of projection matrices to decouple the ICI in terms of resolvable paths. Finally, similar to a conventional RAKE combiner, a linear diversity combiner is used to combine all filter outputs. In comparison with the conventional MF-based 2-D RAKE receiver in [28], it is shown that the proposed receiver is more robust to near far effect and can achieve superior BER performance with fewer number of sensors.

The rest of this chapter is organised as follows. Section 4.2 presents a literature review on multiuser detection under multipath effects. Section 4.3 explains the concept of space-time processing, and examines the 2-D RAKE receiver as a case study. Section 4.4 describes the system model. Section 4.5 presents the pro-

posed receiver. Section 4.6 presents the CMA-based blind adaptation of the filter bank. Section 4.7 contains its analysis in terms of the lock-capture convergence, initialisation, convergence rate and the effect of channel order mismatch. Section 4.8 gives a performance comparison based on simulation results. Section 4.9 contains the chapter's conclusions.

4.2 Literature Review

In this section, some previous works that deal with multipath induced distortions in the context of multiuser detection, are presented. Recall from Section 2.4.1 that in the presence of multipath induced distortions, apart from suppression of the MAI, the problem of multiuser detection is also concerned with the removal of the ICI and ISI.

As discussed in Section 3.7, even though the surplus energy can be constrained to make the MOE detector [3] more robust against the signature mismatch problem, a few attempts have been made to address explicitly the presence of the ICI and ISI. Exceptions are some recent works [58, 59] in which the MOE detector in [3] is extended to incorporate the multipath effect by addition of appropriate linear constraints. Furthermore, it has been shown [82] that the MOE approach suffers from a saturation effect in the steady state, which can cause the converged MOE detector to deviate significantly from the MMSE solution in (2.42).

To combat the signature mismatch problem, the direct approach is to estimate the received desired user's signature waveform itself (or the respective multipath channel). This implies a separate signature estimator before any multiuser detection can be applied. A number of signature estimators have been proposed in the literature, namely the training-based MMSE methods [104], the channel estimator based on Kalman filtering [108], and the blind subspace-based methods (e.g., [85]). Instead of direct estimation of received signature, both the MMSE (e.g., [2, 34]) and the subspace methods (e.g., [82, 84]) have also been modified as joint multiuser detection and equalisation. In the context of fractionally spaced equalisers, based on a multirate DS-CDMA system model, a linear SOS-based blind channel estimation method is proposed in [109].

Under the multipath fading conditions, various forms of optimum multiuser detectors in (2.36) have been developed (e.g., frequency-flat Rayleigh fading in [110], and frequency-flat/-selective Rician fading in [111]). In [112], it is shown that the optimum multiuser detector is highly sensitive to imperfect knowledge of channel parameters. This channel mismatch is modelled as some residual MAIs that increase as the near far effect increases. Recently, joint optimum multiuser detection and fading coefficients estimation has been developed [113] by using Kalman filtering.

4.3 Space-Time Processing

In this section, the use of space-time processing to combat multipath effect is discussed. First, to serve as background material, the concept of receiver diversity is introduced. Second, to illustrate the space-time processing for DS-CDMA system, the blind 2-D RAKE receiver in [28] is reviewed.

4.3.1 Concept of Receiver Diversity

A well-known method to mitigate the multipath fading is to exploit the temporal and spatial diversities of the receiver [10, 114, 115]. The generic concept of receiver diversity is that multiple copies of the received signal with independent fading statistics, can be selected or combined to improve the detection performance over that using any single copy. The diversity techniques vary in the manner by which different copies of the signal are obtained and how they are selected or combined eventually. A list of different diversity techniques is given as follows [30, 116]

- *Space diversity* — it uses two or more spatially separated antennas (e.g., the distance apart is typically on the order of tens of carrier wavelengths), to obtain sufficiently uncorrelated copies of the signal. The basic concept is that the received signals from all antennas would unlikely undergo deep fades simultaneously. Apart from using multiple antennas, a single reflector-type antenna (e.g., a parabolic dish) which receives multiple beams from different angles, can also induce space diversity.

- *Time diversity* — analogous to space diversity, it uses repeated transmissions that are sufficiently separated in time (e.g., time spacings exceeding the coherence time $(\Delta t)_c$ in Table 2.1). The best known usage of time diversity is the RAKE receiver [117] for detection of wideband signals such as the DS-CDMA system. Time diversity is also used in interleaving where the source bits are scrambled before channel coding, in order to protect against bursty errors.

- *Frequency diversity* — it transmits information on more than one carrier frequency (e.g., frequency spacings exceeding the coherence bandwidth $(\Delta f)_c$ in Table 2.1). As discussed in Section 1.1.4, frequency diversity is inherent in the DS-CDMA system, at the expense of larger bandwidth.

- *Polarisation diversity* — it allows two diversity branches by using co-located antennas that use two orthogonal polarisations (i.e., horizontal and vertical). This is most useful at the base station due to its fixed antenna orientation and limited antenna spacing.

4.3.2 2-D RAKE Receiver

Using a single antenna, the conventional 1-D RAKE[1] receiver exploits the temporal multipath structure of the received signal to enhance the detection performance. Originally proposed in [117], in a single-user scenario, the 1-D RAKE receiver uses a bank of correlators (or *fingers*) and combines their outputs based on some optimal criteria (e.g., selection diversity combining and maximal-ratio combining). Similar to the MF in (2.32), each correlator input is multiplied by a time-shifted version (i.e., path delays) of the transmitted signature waveform. The number of correlators represents the number of strongest and independent multipath signals to be resolved. From (2.9), in the case of the DS-CDMA system, since multipath components are resolved in chip intervals T_c, the maximum number of correlators required is L_1 for the desired user $k = 1$.

[1] The name RAKE is denoted for its rake-like collection of signal energies from independent multipaths [117].

The 1-D RAKE receiver has been extended to a 2-D RAKE receiver by using multiple sensors (i.e., antenna array) to resolve different multipath components both in the space and time domains [28, 83]. It consists of a bank of beamformers, one for each signal path, followed by the conventional, 1-D RAKE receiver. Beamforming is essentially a spatial filtering step that focuses the array's signal capturing capability in a particular direction or location. This means that the signals from a given spatial region are amplified while those from other regions are attenuated. The optimum beamformers (in the MMSE sense) is obtained by using a subspace-based approach that exploits the eigen-structure of the SOS of sensor outputs. Essentially, it is a bank of space-time MFs, one for each signal path, and its definition is given in Section 4.8.3. This 2-D RAKE receiver can be implemented blindly, and will form the basis for later comparison.

Although the 2-D RAKE receiver is the first to use space-time processing in DS-CDMA system, it has a number of practical deficiencies. These include:

- It assumes perfect knowledge of the time delays of all multipath components (i.e., $\tau_{k,l}$ in (2.7)). However, the multipath timing is difficult to estimate, especially in the presence of large user population [86].

- Beamformers are merely spatial filters, and do not automatically translate into spatial diversity. Furthermore, beamformers in the 2-D RAKE receiver use MFs which approximate MAI as AWGN (i.e., Gaussian approximation for MAI in the spatial domain). Thus, this beamforming approach is susceptible to near far effect, given non-orthogonal signature waveforms. Also, beamforming does not fully exploit the potential of multiple sensor. For example, two users whose angular separation is not resolvable by beamforming can still have their signals "separated" with joint space-time processing.

- It may have prohibitive computational complexity to perform the eigen-decomposition of large covariance matrices.

- As discussed in Section 2.4.4, these SOS-based methods are less suited to adaptation (i.e., off-line batch processing), since the covariance matrices are

required to be re-estimated whenever there are significant changes in the system parameters.

4.4 System Modelling

In this section, a signal model is developed for an uncoded K-users DS-CDMA system. Unlike Chapter 3, the system model used here accounts for the multipath induced distortion (i.e., ICI and ISI) and incorporates multiple sensors. In the receiver, let there be M sensors. The signal model is presented for the mth sensor where $m \in \{1, \ldots, M\}$, and is given in two parts: the frequency selective channels and the M-sensors receiver (see Section 2.3.2 for the transmitted signal model).

4.4.1 Channel Model

As discussed in Section 2.3.5, for the kth user, the frequency selective multipath channel is modelled as a LTI filter[2] $h_k(\tau)$ in (2.28), and this notation is extended for the case of multiple sensors as follows. For the mth sensor, the channel FIR between the kth user's transmitter to the mth sensor of the receiver is denoted as $h_k^m(\tau)$.

In this chapter, the following assumptions regarding $h_k^m(\tau)$ are made.

A1. For all users, and for all sensors, the multipath FIRs have the same number of resolvable paths L, such that

$$h_k^m(\tau) = 0, \quad \forall \tau > LT_c, \quad \forall k \in \{1, \ldots, K\}, \quad \text{and} \quad \forall m \in \{1, \ldots, M\}; \tag{4.1}$$

where $L_k = L \quad \forall k \in \{1, \ldots, K\}$ with L_k defined in (2.9). In modelling "real-life" multipath channels, this may require zero-padding of the shorter channels.

[2] The LTI assumption implies that the fading statistics are slow in comparison with the convergence speed of the receiver.

A2. In a typical frequency selective environment for low-rate DS-CDMA systems, the maximum multipath delay spread LT_c is small compared to one bit period $T_b = NT_c$ (i.e., $N \gg L$).

4.4.2 Received Signal Model

The received signal model in Section 2.3.4 is generalised to the case of multiple sensors. From (2.15), the received signal for the kth user and for the mth sensor can be written as the convolution

$$\begin{aligned} y_k^m(t) &= A_k x_k(t) * h_k^m(\tau = t) \\ &= A_k \sum_i b_k[i] f_k^m(t - iT_b), \end{aligned} \tag{4.2}$$

where A_k is the received amplitude, $b_k[i] \in \{\pm 1\}$ is the transmitted bit, and $x_k(t)$ is the transmitted signal of the kth user in (2.3),

$$f_k^m(t) = \sum_{n=1}^{N} c_k[n] g_k^m(t - nT_c), \tag{4.3}$$

is the received signature waveform (as in (2.16)), and

$$g_k^m(t) = \int_0^{LT_c} \psi(t - u) h_k^m(u) du, \tag{4.4}$$

is the composite FIR of the chip pulse $\psi(t)$ and the channel FIR $h_k^m(\tau)$.

For simplicity, a synchronous DS-CDMA system is assumed. From (4.2), for the mth sensor, the total received signal from all K users is given by

$$\begin{aligned} y^m(t) &= \sum_{k=1}^{K} y_k^m(t) + n^m(t) \\ &= \sum_{k=1}^{K} A_k \sum_i b_k[i] f_k^m(t - iT_b) + n^m(t), \end{aligned} \tag{4.5}$$

where $n^m(t)$ is the AWGN for the mth sensor with zero mean and power spectral density σ_n^2.

For simplicity, the subsequent development of the blind multiuser detector is presented in the theoretical context of the synchronous signal model in (4.5).

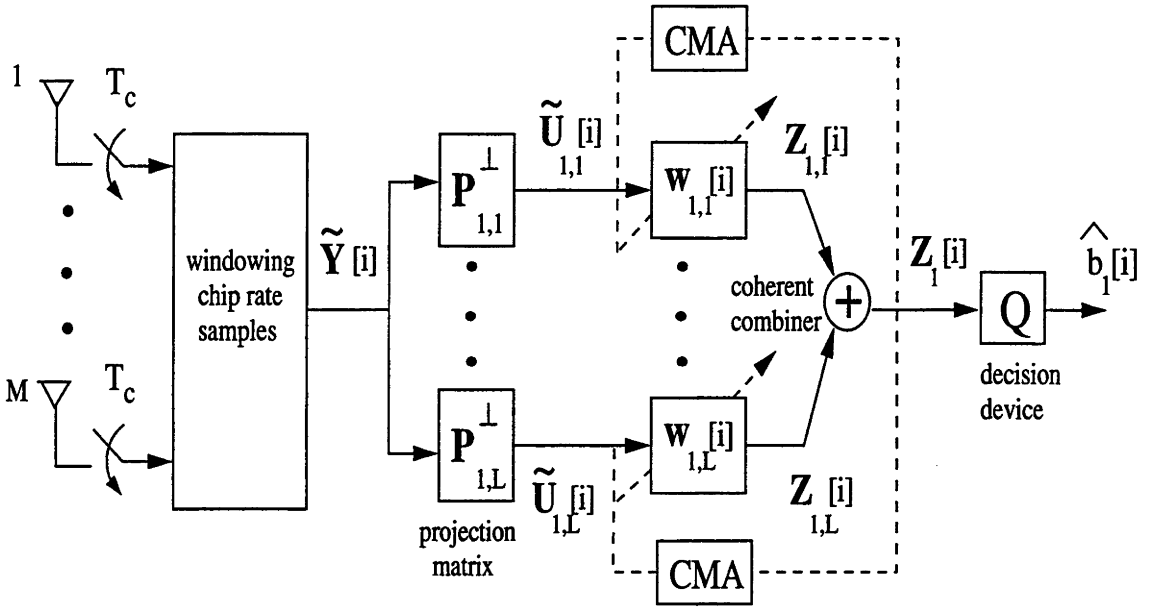

Figure 4.1: Structure of the proposed blind multiuser multiple sensor receiver.

However, as discussed in Section 2.5.2, an asynchronous K-users system can be modelled as an equivalent synchronous one with $2K-1$ users [34]. It is noted that the channel model in (4.1) admits a limited degree of asynchronicity or *quasi-synchronism*, as the relative timings of users τ_k in (2.18) can be absorbed into the definition of L_k in (2.9). This quasi-synchronism does not require the timing of the desired user τ to be estimated, as long as its uncertainty region is small enough, such that the assumption A2 in Section 4.4.1 $N \gg L$ holds.

4.5 Receiver Structure

As shown in Figure 4.1, the proposed linear receiver has four components: (i) windowed sampling — to remove ISI; (ii) projection matrix — to combat ICI; (iii) linear filtering — to suppress MAI; and (iv) a linear diversity combiner — RAKE-like combiner. In this section, first, the advantages of the proposed receiver are described. Then, the receiver structure in terms of (i), (ii) and (iv) are presented. The issue of the CMA-based filter adaptation in (iii) is discussed

in Section 4.6.

4.5.1 Benefits

This work aims to take the idea of the 2-D RAKE receiver [28] further, to develop a more practical and robust multiple sensor array receiver based on the multiuser detection principle. Its novelty is the simultaneous usage of diversity and linear multiuser detection. The main features of the proposed receiver are listed as follows

- Unlike the 2-D RAKE receiver, the proposed method exploits the time and space diversity in a joint fashion (i.e., without constraining them to be disjoint). This is possible since there is no difference in mathematical modelling whether the multipath signals arrive with different time delays or from different directions.

- Unlike some direction-finding-based beamforming techniques (e.g., MUSIC), no constraint is placed on the array structure, as long as the received signal from each sensor in (4.5) is independent from other sensors.

- Unlike the path-by-path beamforming-based approach used in the 2-D RAKE receiver, the composite channel FIR in (4.4) is used to avoid accurate estimation of individual path delays.

- Multiple sensors are used here for diversity, rather than beamforming.

4.5.2 Windowed Chip Rate Sampling

By applying chip rate sampling, a discrete time signal representation can be obtained. For the mth sensor, the chip sampled version of the composite channel in (4.4) is the L-length vector

$$\mathbf{g}_k^m = \left(g_{k,1}^m, \cdots, g_{k,L}^m\right)^T, \tag{4.6}$$

with the nth element given by

$$g_{k,n}^m = \int_0^{LT_c} \psi(nT_c - u) g_k^m(u) du. \tag{4.7}$$

Without loss of generality, all composite channel FIRs in (4.6) are normalised:

$$\|\mathbf{g}_k^m\| = 1 \quad \forall k \in \{1, \ldots, K\}, \text{ and } \forall m \in \{1, \ldots, M\}, \tag{4.8}$$

to give unity channel gains. From (4.3), the chip sampled received signature is the $(N + L - 1)$-length vector

$$\mathbf{f}_k^m = \left(f_{k,1}^m, \ldots, f_{k,N+L-1}^m\right)^T, \tag{4.9}$$

with the pth element given by

$$f_{k,p}^m = \sum_{n=1}^{N} c_k[n] g_{k,p-n}^m. \tag{4.10}$$

From (4.9), it is seen that the time support of the received signature waveform is bounded by $T_c(N + L - 1)$ which exceeds the bit duration $T_b = NT_c$. This gives rise to the ISI. However, since $N \gg L$ (assumption A2 in Section 4.4.1), the duration of this ISI is limited to a fraction of NT_c. As shown in Figure 4.2, to remove the contribution of the ISI in the received signal, a windowing procedure is applied, such that only its ISI-free portion (variables denoted by tilde) is used for further processing in the receiver [85]. These "ISI-free" received signature samples are defined as the $(N + L - 1)$-length subvector of (4.9)

$$\tilde{\mathbf{f}}_k^m \triangleq \left(f_{k,L}^m, \ldots, f_{k,N}^m\right)^T, \tag{4.11}$$

which can be written as

$$\tilde{\mathbf{f}}_k^m = \mathbf{C}_k \mathbf{g}_k^m, \tag{4.12}$$

where

$$\mathbf{C}_k \triangleq \begin{bmatrix} c_k[L] & c_k[L-1] & \cdots & c_k[1] \\ c_k[L+1] & c_k[L] & \cdots & c_k[2] \\ \vdots & \vdots & & \vdots \\ c_k[N] & c_k[N-1] & \cdots & c_k[N-L+1] \end{bmatrix} = \left(\mathbf{c}_{k,1}, \ldots, \mathbf{c}_{k,L}\right), \tag{4.13}$$

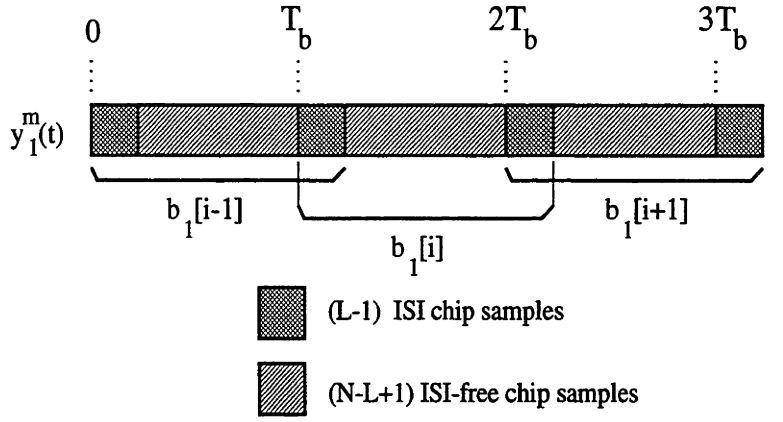

Figure 4.2: The ISI-free observation interval with the time window $T_c(N-L+1)$.

represents a $(N-L+1)\times L$ "windowed" convolution matrix with the lth column denoted as $\mathbf{c}_{k,l}$.

Finally, the ISI-free, discrete time total received signal corresponding to (4.5) can be written as the windowed one shot $(N+L-1)$-length vector

$$\tilde{\mathbf{Y}}^m[i] = \tilde{\mathcal{F}}^m\mathbf{A}\mathbf{b}[i] + \tilde{\mathbf{n}}^m[i] = (y^m[i,L],\ldots,y^m[i,N])^T, \tag{4.14}$$

where the nth element, from (2.31) is given by

$$y^m[i,n] \triangleq \frac{1}{T_c}\int_{iT_b+nT_c}^{iT_b+(n+1)T_c} y^m(t)dt, \tag{4.15}$$

and

$$\tilde{\mathcal{F}}^m \triangleq \left(\tilde{\mathbf{f}}_1^m,\ldots,\tilde{\mathbf{f}}_K^m\right), \tag{4.16}$$

is a $(N-L+1)\times K$ windowed matrix of received signature, $\mathbf{A}$ and $\mathbf{b}[i]$ are defined in (2.30), and $\tilde{\mathbf{n}}^m[i]$ is a $(N-L+1)$-length windowed noise vector of the mth sensor of the ith bit.

4.5.3 Generalisation to Multiple Sensors

From (4.14), the single sensor based windowed one shot samples can be generalised to the case of M sensors, by stacking together to form a $M(N-L+1)$-length

vector

$$\overbrace{\begin{bmatrix}\tilde{\mathbf{Y}}^1[i]\\ \vdots \\ \tilde{\mathbf{Y}}^M[i]\end{bmatrix}}^{\tilde{\mathbf{Y}}[i]} = \overbrace{\begin{bmatrix}\tilde{\mathcal{F}}^1\\ \vdots \\ \tilde{\mathcal{F}}^M\end{bmatrix}}^{\tilde{\mathcal{F}}} \mathbf{Ab}[i] + \begin{bmatrix}\tilde{\mathbf{n}}^1[i]\\ \vdots \\ \tilde{\mathbf{n}}^M[i]\end{bmatrix}. \tag{4.17}$$

It follows that $\tilde{\mathbf{Y}}[i]$ and $\tilde{\mathcal{F}}$ consist of the aggregation of $\tilde{\mathbf{Y}}^m[i]$ in (4.14) and $\tilde{\mathcal{F}}^m$ in (4.16) from all M sensors respectively. In (4.17), it is assumed that the signal delays between sensors are negligible.

From the viewpoint of the receiver, by organising the received chip samples as in (4.17), there is no distinction made between the contributions to the multipath signals form the space and time domains. Due to the added spatial diversity, this stacked received vector $\tilde{\mathbf{Y}}[i]$ offers an increased *effective spreading length* of $M(N-L+1)$, which is M times that of the single sensor case. It should be noted that temporal oversampling can also provide an identical framework as (4.17), albeit with reduced effective diversity [85].

4.5.4 Projection Matrix Processor

To separate the lth resolvable path from the others in the windowed received signal $\tilde{\mathbf{Y}}[i]$ in (4.17), each linear filter is preceded by an orthogonal projection matrix given by (see Figure 4.1)

$$\mathbf{P}_{1,l}^{\perp} = \begin{bmatrix}\mathcal{P}_{1,l} & & \mathbf{0}\\ & \ddots & \\ \mathbf{0} & & \mathcal{P}_{1,l}\end{bmatrix} \quad \text{where } l \in \{1,\ldots,L\}, \tag{4.18}$$

and

$$\mathcal{P}_{1,l} = \mathbf{I}_{N-L+1} - \mathbf{C}_{1,l}\mathbf{C}_{1,l}^{\dagger}, \tag{4.19}$$

$$\mathbf{C}_{1,l} \triangleq (\mathbf{c}_{1,1},\ldots,\mathbf{c}_{1,l-1},\ \mathbf{c}_{1,l+1},\ldots,\mathbf{c}_{1,L}), \tag{4.20}$$

with $\mathbf{C}_{1,l}^{\dagger}$ denotes the pseudo-inverse of $\mathbf{C}_{1,l}$, and $\mathbf{C}_{1,l}$ is a $(N-L+1\times(L-1))$ submatrix of $\mathbf{C}_k$ in (4.13) for the desired user $k=1$ without the lth column $\mathbf{c}_{1,l}$.

The lth projection matrix $\mathbf{P}_{1,l}^{\perp}$ in (4.18) is a block diagonal matrix with M blocks of $\mathcal{P}_{1,l}$ in (4.19). Using this projection matrix, the lth filter input is given by

$$\tilde{\mathbf{U}}_{1,l}[i] = \mathbf{P}_{1,l}^{\perp}\tilde{\mathbf{Y}}[i] = \left(\left(\tilde{\mathbf{U}}_{1,l}^{1}[i]\right)^{T}, \ldots, \left(\tilde{\mathbf{U}}_{1,l}^{M}[i]\right)^{T}\right)^{T}, \tag{4.21}$$

where from (4.18) and (4.21),

$$\tilde{\mathbf{U}}_{1,l}^{m}[i] = \mathcal{P}_{1,l}\tilde{\mathbf{Y}}^{m}[i]. \tag{4.22}$$

is the contribution from the mth sensor.

From (4.12), for each sensor, it is seen that the received signature matrix $\tilde{\mathcal{F}}^{m}$ in (4.17) shares the same set of windowed convolution matrices $\mathbf{C}_k \quad \forall k \in \{1, \ldots, K\}$, regardless of the multipath effect. Hence, given identical sensors, it is sufficient to consider the general case of $\tilde{\mathbf{U}}_{1,l}^{m}[i]$. Then, for each sensor, the projection matrix $\mathcal{P}_{1,l}$ maps its received signal $\tilde{\mathbf{Y}}^{m}[i]$ onto the subspace which is orthogonal to the one spanned by the columns of $\mathbf{C}_{1,l}$ in (4.20). For a noiseless scenario, it yields the following condition

$$\left(\mathbf{c}_{1,p}\right)^{T}\tilde{\mathbf{U}}_{1,l}^{m}[i] = 0 \quad \forall p \neq l, \forall m \in \{1, \ldots, M\}, \text{ and } \forall i. \tag{4.23}$$

The implication of (4.23) is that the subsequent filter adaptations are restricted to some constrained space, depending on $\mathbf{P}_{1,l}^{\perp}$ in (4.18). In terms of the ICI, the contributions of all resolvable paths except the lth one in $\tilde{\mathbf{U}}_{1,l}[i]$ are removed.

From (4.19), if $rank(\mathbf{C}_{1,l}) = L-1$, and $N \geq 2L-2$, its pseudo-inverse can be written as $\mathbf{C}_{1,l}^{\dagger} = \left(\mathbf{C}_{1,l}^{T}\mathbf{C}_{1,l}\right)^{-1}\mathbf{C}_{1,l}^{T}$. From a practical viewpoint, $\mathbf{C}_{1,l}^{\dagger}$ is computed via singular value decomposition of $\mathbf{C}_{1,l}$ [80], in order to minimise the numerical difficulties, when $\mathbf{C}_1$ in (4.13) is close to a rank deficient matrix. Also, as long as the channel order L does not increase, all projection matrices are only needed to calculate once (for the case of short codes).

4.5.5 Linear Diversity Combiner

The combined output from the bank of L linear filters is given by

$$Z_1[i] = \sum_{l=1}^{L} Z_{1,l}[i] = \sum_{l=1}^{L} \mathbf{w}_{1,l}^{T}[i]\tilde{\mathbf{U}}_{1,l}[i], \tag{4.24}$$

and $Z_{1,l}[i] = \mathbf{w}_{1,l}^T[i]\tilde{\mathbf{U}}_{1,l}[i]$ is the lth filter output, and $\mathbf{w}_{1,l}^T[i]$ is the lth linear filter denotes as a $M(N-L+1)$-length vector. In conventional RAKE receivers, individual filter outputs $Z_{1,l}[i]$ are weighted (e.g., maximal-ratio combining [30]), and then combined either coherently or incoherently before being fed into a decision device. In this work, for simplicity[3], it is assumed that coherent detection with equal gain diversity combining is used.

4.6 CMA-based Adaptation

This section presents the CMA-based adaptation of the bank of linear filters $\mathbf{w}_{1,l}[i]$, in part (iii) of the proposed receiver.

4.6.1 Objective

To emulate the multipath combining property of a RAKE receiver, the proposed receiver uses a bank of L linear filters $\mathbf{w}_{1,l}[i]$, one for each resolvable path. That is, L replicas of the transmitted signal are processed in an equivalent Lth-order diversity receiver. In contrast, the 2-D RAKE receiver [28] uses MFs and is designed primarily for orthogonal signals. Using this RAKE-type processing, our objective is to adapt $\mathbf{w}_{1,l}[i]$ blindly to suppress MAI, such that under multipath effect, the overall linear receiver should converge to the linear training-based MMSE receiver [2].

4.6.2 Algorithm

Since coherent combiner is used, for simplicity, all variables are assumed to be real for the rest of this chapter. Substituting (4.24) into (2.45), the CM cost function in this RAKE-type filtering can be expressed as

$$J_{CM,RAKE}(\mathbf{w}_{1,l}) = E\left\{\left(\left(\sum_{l=1}^{L}\mathbf{w}_{1,l}^T[i]\tilde{\mathbf{U}}_{1,l}[i]\right)^2 - \xi\right)^2\right\}. \tag{4.25}$$

[3] The knowledge of channel phase is not essential, since the CMA-based adaptation is phase-invariant. However, it would simplify the lock convergence initialisation, as discussed in Section 4.7.2.

Using the CM cost function in (4.25), analogous to (3.23), the CMA-based adaptation of the lth filter is given by

$$\begin{aligned}\mathbf{w}_{1,l}[i+1] &= \mathbf{w}_{1,l}[i] - \mu \cdot \frac{1}{4}\nabla_{\mathbf{w}_{1,l}[i]} J_{CM,RAKE}(\mathbf{w}_{1,l}) \\ &= \mathbf{w}_{1,l}[i] - \mu \left(Z_1^2[i] - \xi\right) Z_1[i] \nabla_{\mathbf{w}_{1,l}[i]} \left\{ \sum_{l=1}^{L} \mathbf{w}_{1,l}^T[i] \tilde{\mathbf{U}}_{1,l}[i] \right\} \\ &= \mathbf{w}_{1,l}[i] - \mu \left(Z_1^2[i] - \xi\right) Z_1[i] \tilde{\mathbf{U}}_{1,l}[i]. \end{aligned} \tag{4.26}$$

Thus, each filter adapts with the same combined output $Z_1[i]$ in (4.24), but has different input $\tilde{\mathbf{U}}_{1,l}[i]$. Recall from Section 4.5.5 that since a coherent combiner is used, all system parameters can be assumed to be real variables in (4.26). It should be noted that the CMA-based adaptation is insensitive to phase variation in $Z_1[i]$, but not so in $Z_{1,l}[i]$. The problem of phase recovery in the coherent combiner is decoupled from the suppression of the MAI and ICI, and is not considered in this work.

4.7 Analysis of CMA-based RAKE-type Receiver

In this section, the CMA-based blind receiver is examined in terms of its lock-capture analysis (i.e., steady state behaviour), initialisation, convergence rate (i.e., transient behaviour) and the channel order mismatch.

4.7.1 Lock and Capture Analysis

Let us recall from Section 3.5.1 that the steady state behaviour of the CMA can be characterised by its lock and capture convergence. Analogous to (3.24), each user's contribution in the combined filter output $Z_1[i]$ is represented as the user gain, and is defined as

$$\mathbf{V}_{RAKE}[i] \triangleq \sum_{l=1}^{L} \left(\mathbf{P}_{1,l}^{\perp} \tilde{\mathcal{F}} \mathbf{A}\right)^T \mathbf{w}_{1,l}[i] = \left(v_{1,RAKE}[i], \ldots, v_{K,RAKE}[i]\right)^T, \tag{4.27}$$

where $v_{k,RAKE}[i]$ is the kth user gain. Assuming the received signal is noiseless, combining (4.17), (4.21), (4.24) and (4.27), the combined filter output can be

written as

$$\begin{aligned} Z_1[i] &= \sum_{l=1}^{L} \mathbf{w}_{1,l}^T[i]\mathbf{P}_{1,l}^{\perp}\tilde{\mathbf{Y}}[i] \\ &= \sum_{l=1}^{L} \mathbf{w}_{1,l}^T[i]\mathbf{P}_{1,l}^{\perp}\tilde{\mathcal{F}}\mathbf{A}\mathbf{b}[i] \\ &= \mathbf{V}_{RAKE}^T\mathbf{b}. \end{aligned} \tag{4.28}$$

The analysis of the stationary points is similar to that of the single CMA in Appendix A. With the bit index i discarded temporally, using (4.17), (4.21) and (4.28), the adaptation term in (4.26) can be written as (similar to (A.2))

$$\begin{aligned} \frac{1}{4}\nabla_{\mathbf{w}_{1,l}} J_{CM,RAKE}(\mathbf{w}_{1,l}) &= E\left\{\left(Z_1^2-\xi\right) Z_1 \mathbf{P}_{1,l}^{\perp}\tilde{\mathbf{Y}}\right\} \\ &= \mathbf{P}_{1,l}^{\perp}\tilde{\mathcal{F}}\mathbf{A}\cdot E\left\{\left(\left(\mathbf{V}_{RAKE}^T\mathbf{b}\right)^2-\xi\right)\mathbf{V}_{RAKE}^T\mathbf{b}\cdot\mathbf{b}\right\} \\ &= \mathbf{P}_{1,l}^{\perp}\tilde{\mathcal{F}}\mathbf{A}\cdot\frac{1}{4}\nabla_{\mathbf{V}_{RAKE}} J_{CM}(\mathbf{V}_{RAKE}), \end{aligned} \tag{4.29}$$

where $\nabla_{\mathbf{V}_{RAKE}} J_{CM,RAKE}(\mathbf{V}_{RAKE})$ has the same form as $\nabla_{\mathbf{V}} J_{CM}(\mathbf{V})$ in (A.3), except that $\mathbf{V}$ is replaced by $\mathbf{V}_{RAKE}$. When $\nabla_{\mathbf{w}_{1,l}} J_{CM,RAKE} = \mathbf{0} \quad \forall l \in \{1,\ldots,L\}$, the CMA-based adaptation in (4.26) stops. From (4.29), there are two classes of stationary points:

Class 1 when $\nabla_{\mathbf{V}_{RAKE}} J_{CM,RAKE} = \mathbf{0}$, or

Class 2 when $\nabla_{\mathbf{V}_{RAKE}} J_{CM,RAKE} \in \mathit{Nullspace}\left(\mathbf{P}_{1,l}^{\perp}\tilde{\mathcal{F}}\right) \quad \forall l \in \{1,\ldots,L\}$, and $\nabla_{\mathbf{V}_{RAKE}} J_{CM,RAKE} \neq \mathbf{0}$,

where $\mathit{Nullspace}(\mathbf{X})$ is the *null-space* of $\mathbf{X}$ [80]. Class 1 is equivalent to those stationary points of an *unconstrained* CMA (i.e., without $\mathbf{P}_{1,l}^{\perp}$) in (A.12)-(A.14). Class 2 arises when $\nabla_{\mathbf{V}_{RAKE}} J_{CM}$ lies in some non-trivial nullspaces depending on $\mathbf{P}_{1,l}^{\perp}$. However, according to the definition of $\mathbf{P}_{1,l}^{\perp}$ in (4.18)-(4.20), it is deduced that there exists no subspace common to all nullspaces of $\mathbf{P}_{1,l}^{\perp}\tilde{\mathcal{F}}\mathbf{A} \quad \forall l \in \{1,\ldots,L\}$. Thus, Class 2 is empty, and the stationary points are solely contained in Class 1. Similar to (3.27), the desired local minimum in Class 1, or lock convergence is given by

$$v_{1,RAKE}[i] = \sqrt{\xi}, \text{ and } v_{k,RAKE}[i] = 0 \quad \forall k \in \{2,\ldots,K\}. \tag{4.30}$$

Thus, at the lock convergence, the overall linear operation is equivalent to the well-known decorrelator detector with a noiseless received signal. Other local minima are referred to as capture convergence, and have the same form of (3.28).

4.7.2 Robust Initialisation

As discussed in Section 3.5.2, the necessary condition to achieve the lock convergence in (4.30) is to initialise the user gains as

$$v_{1,RAKE}[0] > |v_{k,RAKE}[0]| \quad \forall k \in \{2,\ldots,K\}. \tag{4.31}$$

An example of a robust initialisation of the bank of L filters is given by

$$\mathbf{w}_{1,l}[0] = \overbrace{\left[\left(\mathcal{P}_{1,l}^{\dagger}\mathbf{c}_{1,l}\right)^{T},\ldots,\left(\mathcal{P}_{1,l}^{\dagger}\mathbf{c}_{1,l}\right)^{T}\right]^{T}}^{M \text{ blocks}} \quad \text{where } l \in \{1,\ldots,L\}. \tag{4.32}$$

From (4.12) and (4.27), the initial user gains of the kth user in (4.32) are given by

$$v_{k,RAKE}[0] = A_k \sum_{l=1}^{L}\sum_{m=1}^{M} \left(\mathcal{P}_{1,l}\mathbf{C}_k\mathbf{g}_k^m\right)^T \cdot \left(\mathcal{P}_{1,l}^{\dagger}\mathbf{c}_{1,l}\right) \tag{4.33}$$

In the case of the desired user $k = 1$, the initial user gain in (4.33) can be further simplified as

$$\begin{aligned} v_{1,RAKE}[0] &= A_1 \sum_{l=1}^{L}\sum_{m=1}^{M} g_{1,l}^m \left(\mathcal{P}_{1,l}\mathbf{c}_{1,l}\right)^T \cdot \left(\mathcal{P}_{1,l}^{\dagger}\mathbf{c}_{1,l}\right) \\ &= A_1 \left(\frac{N-L+1}{N}\right) \sum_{l=1}^{L}\sum_{m=1}^{M} g_{1,l}^m, \end{aligned} \tag{4.34}$$

since[4] $\|\mathbf{c}_{k,l}\|^2 = (N-L+1)/N$. Similarly, the initial user gain for the kth interfering user, where $k \in \{2,\ldots,K\}$, is given by

$$\begin{aligned} v_{k,RAKE}[0] &= A_k \sum_{l=1}^{L}\sum_{m=1}^{M} \left(\mathbf{g}_k^m\right)^T \mathbf{C}_k^T \mathbf{c}_{1,l} \\ &= A_k \sum_{l=1}^{L}\sum_{m=1}^{M} \left(\mathbf{c}_{k,l}^T\mathbf{c}_{1,l}\right) \cdot g_{k,l}^m. \end{aligned} \tag{4.35}$$

[4] In accordance with the normalised signature in (2.26), all spreading sequences have the form $c_k[n] \in \{\pm 1/\sqrt{N}\}$ $\forall k \in \{1,\ldots,N\}$ and $\forall n \in \{1,\ldots,N\}$.

From Section 4.5.5, follows that when a coherent combiner is used, it is sufficient to consider only the magnitude of the composite channel vector, $|\mathbf{g}_k^m|$ in (4.34) and (4.35). If all users are of equal power, the lock convergence condition in (4.31) is satisfied since $\left|\mathbf{c}_{k,l}^T \mathbf{c}_{1,l}\right| < (N-L+1)/N \quad \forall l \in \{1,\ldots,L\}$ and $\forall k \in \{2,\ldots,K\}$. Thus, similar to the unconstrained CMA, unless there are severe near far conditions and/or excessive signature coupling, lock convergence can be achieved with robust initialisation in (4.32). In pathological scenarios where the filter initialisations do not satisfy (4.31), various methods can be used to recover lock convergence, as discussed in Section 3.5.2.

4.7.3 Convergence Rate

Recall from Section 3.6.1, the transient behaviour of the CMA is difficult to predict, since its convergence rate varies in different regions described by user gains or $\mathbf{V}_{RAKE}$ space. The analysis of the CMA-based RAKE-type receiver is further complicated by the fact that the CMA-based adaptation now takes place in some constrained $\mathbf{V}_{RAKE}$ spaces due to the usage of the projection matrices $\mathbf{P}_{1,l}^{\perp}$.

In the absence of channel noise, the windowed received signal vector in (4.17) becomes $\tilde{\mathbf{Y}}[i] = \tilde{\mathcal{F}}\mathbf{A}\mathbf{b}[i]$. Then, the lth filter input in (4.21) and the combined filter output in (4.24) can be written respectively as

$$\begin{aligned} \tilde{\mathbf{U}}_{1,l}[i] &= \mathbf{P}_{1,l}^{\perp}\tilde{\mathcal{F}}\mathbf{A}\mathbf{b}[i] \\ Z_1[i] &= \sum_{l=1}^{L} \mathbf{w}_{1,l}^T[i]\mathbf{P}_{1,l}^{\perp}\tilde{\mathcal{F}}\mathbf{A}\mathbf{b}[i] = \mathbf{V}_{RAKE}^T[i]\mathbf{b}[i]. \end{aligned} \tag{4.36}$$

Analogous to (3.25), substituting (4.36) and (4.27) in (4.26), the CMA-based

adaptation can be expressed in terms of the user gains as follows

$$\begin{aligned}\mathbf{V}_{RAKE}[i+1] &= \mathbf{V}_{RAKE}[i] - \mu \sum_{l=1}^{L} \left(\mathbf{P}_{1,l}^{\perp}\tilde{\mathcal{F}}\mathbf{A}\right)^{T} \left(Z_1^2[i]-\xi\right) Z_1[i]\tilde{\mathbf{U}}_{1,l}[i] \\ &= \mathbf{V}_{RAKE}[i] - \mu \sum_{l=1}^{L} \left(\mathbf{P}_{1,l}^{\perp}\tilde{\mathcal{F}}\mathbf{A}\right)^{T} \left(\mathbf{P}_{1,l}^{\perp}\tilde{\mathcal{F}}\mathbf{A}\right) \cdot \\ &\qquad \left(\left(\mathbf{V}_{RAKE}^{T}[i]\mathbf{b}[i]\right)^2 - \xi\right) \mathbf{V}_{RAKE}^{T}[i]\mathbf{b}[i] \cdot \mathbf{b}[i] \\ &= \left(\mathbf{I}_K - \mu \sum_{l=1}^{L} \mathbf{R}_{1,l}\tilde{\mathbf{Q}}[i]\right) \mathbf{V}_{RAKE}[i], \end{aligned} \tag{4.37}$$

where, since $\mathbf{P}_{1,l}^{\perp}$ is both symmetric and *idempotent* (i.e., $\mathbf{P}_{1,l}^{\perp}\mathbf{P}_{1,l}^{\perp} = \mathbf{P}_{1,l}^{\perp}$),

$$\mathbf{R}_{1,l} \triangleq \left(\mathbf{P}_{1,l}^{\perp}\tilde{\mathcal{F}}\mathbf{A}\right)^{T} \left(\mathbf{P}_{1,l}^{\perp}\tilde{\mathcal{F}}\mathbf{A}\right) = \left(\tilde{\mathcal{F}}\mathbf{A}\right)^{T} \mathbf{P}_{1,l}^{\perp} \left(\tilde{\mathcal{F}}\mathbf{A}\right), \tag{4.38}$$

is the correlation matrix of the lth path, and $\tilde{\mathbf{Q}}[i]$ is a $(K \times K)$ diagonal matrix with diagonal entries have the same form ($v_k[i]$ replaces by $v_{k,RAKE}[i]$) in (3.26). From (4.37), in the same manner as the LMS algorithm, the convergence rate of the individual user gain in the lth filter is dependent on $\mathbf{R}_{1,l}$. This implies that some user gains from certain paths may converge faster than others, as determined by $\mathbf{P}_{1,l}^{\perp}$. As in the decorrelated CMA [27], the coupling effect due to $\mathbf{R}_{1,l}$ can be removed by pre-multiplying $\tilde{\mathbf{U}}_{1,l}[i]$ in (4.26) by $\mathbf{R}_{\mathbf{uu},1,l}^{-1}$, where $\mathbf{R}_{\mathbf{uu},1,l} \triangleq E\left\{\tilde{\mathbf{U}}_{1,l}[i]\tilde{\mathbf{U}}_{1,l}^{T}[i]\right\}$.

4.7.4 Channel Order Mismatch

In practice, the channel order L in (4.1) is effectively unknown. In the case of channel overmodelling (e.g., vanishing paths), the additional zeros induced in $\mathbf{g}_k^m$ (4.6) will not affect the lock condition in (4.31). Hence, L should be set to be the maximum channel order among all users, and all sensors. Following [88], the effect of channel undermodelling (e.g., new appearing paths) can be modelled as a perturbation in the kth user gain, and is denoted as $\Delta v_{k,RAKE}[i]$. Then, the lock condition in (4.31) can be modified as

$$v_{1,RAKE}[0] + \Delta v_{1,RAKE}[0] > \left|v_{k,RAKE}[0] + \Delta v_{k,RAKE}[0]\right| \quad \forall k \in \{2,\ldots,K\}. \tag{4.39}$$

Under severe channel undermodelling, due to the presence of $\Delta v_{k,RAKE}[0]$, the previously robust lock initialisation in (4.32) may be lost.

4.8 Simulation Results

This section presents simulation results to compare the performance of the proposed CMA-based RAKE-type receiver with other blind methods.

4.8.1 System Parameters

All simulations are based on a K-users, uncoded, synchronous DS-CDMA system using a BPSK modulation scheme. The spreading length is set to $N = 31$, and the number of sensors ranges from $M = 1$ to $M = 3$. The magnitudes of the multipath channel FIRs, $|\mathbf{g}_k^m|$ in (4.6) are independently, and randomly generated according to the Rayleigh distribution. In the same manner as Section 3.8.1, it is assumed that each interfering user has the same received power, and NFR [dB] in (3.57) is used to illustrate a near far condition. For simplicity, all system parameters are assumed to be real numbers (i.e., coherent combiner), and the filter initialisations are given in (4.32). For all simulations except Figure 4.5, $K = 10$, and $SNR(k = 1) = 12dB$. The step sizes μ for different blind methods are chosen to ensure a stable convergence: μ is set to be 10^{-4} for the MOE and $5 \cdot 10^{-7}$ for the CMA.

4.8.2 Performance Measures

Let us recall from Section 3.8.2 that the steady state and transient performances are examined in terms of the BER and the SIR [dB] respectively. In this framework, the SIR is re-defined as

$$SIR[i] \triangleq \frac{v_{1,RAKE}^2[i]}{\sum_{k=2}^{K} v_{k,RAKE}^2[i] + \sigma_n^2 \sum_{l=1}^{L} \|\mathbf{w}_{1,l}^T[i]\mathbf{P}_{1,l}^{\perp}\|^2}, \tag{4.40}$$

where $v_{k,RAKE}[i]$ is the kth user gain defined in (4.27), and σ_n^2 is the noise variance. Finally, in order to examine the effect of channel undermodelling on lock

convergence, the *probability of non-lock initialisation* is defined as the probability of filter initialisation outside the condition in (4.39). All BERs are computed between $2 \cdot 10^3$ to $4 \cdot 10^3$ bit iterations. Both the BER and the SIR are averaged over 100 Monte Carlo runs, and the probability of non-lock initialisation is averaged over 1000 runs.

4.8.3 Comparison to Other Multiuser Detectors

The proposed receiver is compared with both the single sensor based (Figures 4.3-4.5) and the multiple sensors based blind methods (Figure 4.6) as follows.

1. **Single sensor based blind methods (i.e., $M = 1$)**

   Comparisons are performed with the constrained MOE detector in (3.17), and the CMA detector in (3.23). The linear constraint of the MOE detector is set to $\mathbf{w}_1^T[i]\mathbf{c}_{1,1} = 1 \quad \forall i$, and the modulus radius in the CMA is normalised to $\xi = A_1^2$. Without RAKE-type processing (i.e., single-arm), their linear filters $\mathbf{w}_1[i]$ are $(N - L + 1)$-length vectors and are adapted based on the same windowed received signal vector $\tilde{\mathbf{Y}}^1[i]$ in (4.14).

   Three different cases are tested: the proposed constrained MOE detector in (3.20), and the CMA detector with/without signature mismatch in (3.23). For detectors with signature mismatch, both the MOE and the CMA detectors have filter initialisations $\mathbf{w}_1[0] = \mathbf{c}_{1,1}$. The case of no mismatch is included as a benchmark to illustrate when the received signature is known, and has filter initialisation $\mathbf{w}_1[0] = \tilde{\mathbf{f}}_1^1$, where $\tilde{\mathbf{f}}_k^m$ is defined in (4.11).

2. **Multiple sensors based 2-D RAKE receiver (i.e., $M > 1$)**

   In this framework, the received signal vectors in (4.14) and (4.17) are rearranged into a $M \times (N - L + 1)$ matrix as

   $$\tilde{\mathcal{Y}}[i] = \left(\tilde{\mathcal{Y}}_L[i], \ldots, \tilde{\mathcal{Y}}_N[i]\right), \tag{4.41}$$

   where

   $$\tilde{\mathcal{Y}}_p[i] \triangleq \left(y^1[i,p], \ldots, y^M[i,p]\right)^T, \quad \text{where } p \in \{L, \ldots, N\}, \tag{4.42}$$

and $y^m[i,p]$ is defined in (4.15). For the purpose of comparison, it is assumed that each individual path is equivalent to one resolvable path (i.e., each path delay is specified in integer multiples of chip intervals).

The multipath components are resolved separately in space and time by a bank of L space-time MFs (i.e., beamformers and correlators). In matrix notation, the combined output from the space-time MF bank is given by

$$Z_1[i] = \sum_{l=1}^{L} \mathbf{a}_{1,l}^T \mathbf{Z}_{1,l}[i], \tag{4.43}$$

where

$$\mathbf{Z}_{1,l}[i] = \tilde{\mathcal{Y}}[i]\mathbf{c}_{1,l}, \tag{4.44}$$

is the lth temporal MF output, and $\mathbf{a}_{1,l}$ is a M-length beamformer weight vector of the lth path. The optimal beamformer $\mathbf{a}_{1,l}$ in the MMSE sense is given by

$$\mathbf{a}_{1,l} = \zeta \mathbf{R}_{MAI,1,l}^{-1} \mathbf{g}_{1,l}, \tag{4.45}$$

where ζ is an arbitrary scalar, $\mathbf{g}_{k,l} \triangleq \left(g_{k,l}^1, \ldots, g_{k,l}^M\right)^T$ as the *array response vector* for the lth path from the kth user, with $g_{k,l}^m$ given in (4.7), and $\mathbf{R}_{MAI,1,l}$ is the interference-plus-noise correlation matrix defined in [28]. In [10], $\mathbf{R}_{MAI,k,l}$ is interpreted as the correlation of the antenna outpus with the lth path of user k subtracted out.

As explained in [28, 83], both $\mathbf{g}_{1,l}$ and $\mathbf{R}_{MAI,1,l}$ in (4.45) can be computed via principal component analysis as follows. Using (4.42) and (4.44), the auto-correlation matrices of the pre- and post-temporal MF signal vectors can be defined respectively as

$$\begin{aligned} \mathbf{R}_{PRE} &\triangleq E\left\{\tilde{\mathcal{Y}}_p[i]\tilde{\mathcal{Y}}_p^T[i]\right\} = A_k^2 \mathbf{g}_{k,l}\mathbf{g}_{k,l}^T + \mathbf{R}_{MAI,k,l} \\ \mathbf{R}_{POST,1,l} &\triangleq E\left\{\mathbf{Z}_{1,l}[i]\mathbf{Z}_{1,l}^T[i]\right\} = v^2 A_1^2 \mathbf{g}_{k,l}\mathbf{g}_{k,l}^T + v\mathbf{R}_{MAI,1,l}, \end{aligned} \tag{4.46}$$

where[5] $v = (N-L+1)$. From (4.46), $\mathbf{g}_{1,l}$ can be estimated as the generalised

[5] In order extract the desired signal in $\mathbf{Z}_{1,l}[i]$, $v^2 > v$ is required in $\mathbf{R}_{POST,1,l}$ in (4.46). Thus, the normalised signature in (2.26) can not be used, since $v = (N-L+1)/N < 1$; and $c_k[n] \in \{\pm 1\}$ is used instead with the amplitude A_k normalised accordingly. Also, since $(N-L+1)$ ISI-free chip samples are used in each temporal MF in (4.44), v is less than N.

principal eigenvector of the matrix pair $\mathbf{R}_{PRE}$ and $\mathbf{R}_{POST,1,l}$, and $\mathbf{R}_{MAI,1,l}$ is computed by

$$\mathbf{R}_{MAI,1,l} = \frac{1}{v^2 - v}\left(v^2\mathbf{R}_{PRE} - \mathbf{R}_{POST,1,l}\right). \tag{4.47}$$

In our simulation, to compute $\mathbf{R}_{MAI,1,l}$ in (4.47), 300 uncorrelated snapshots of $\tilde{\mathcal{Y}}_p[i]$ and $\mathbf{Z}_{1,l}[i]$ are used to estimate $\mathbf{P}_{PRE}$ and $\mathbf{P}_{POST,1,l}$ in (4.46) respectively. In accordance with (4.24), coherent combining with equal gain diversity is used in (4.43).

4.8.4 Discussion

Figure 4.3 shows the transient SIR performance with $K = 10$, $NFR = 3dB$, and $L = 3$ for the single sensor case. In the case of signature mismatch, it is seen that both the MOE and the CMA detectors are unable to converge to a satisfactory SIR, due to the presence of the ICI. It is of interest to note that with signature mismatch, the CMA gives a significant improvement over the MOE method. The proposed receiver outperforms the CMA detector without mismatch. This is because the proposed receiver offers diversity by combining all L filter outputs. Thus, it is more reliable than the single-arm CMA case, but at the expense of L times higher complexity.

The mechanism of this improved suppression of the MAI in the proposed over the single-arm CMA is explained as follows. The total output energy of the desired user (i.e., $|v_{1,RAKE}[i]|^2$) in the proposed receiver is L times that of the single-arm CMA, assuming identical convergence for each filter. This is due to the fact that the ICI in the lth filter input $\tilde{\mathbf{U}}_{1,l}$ in (4.21) only contains the contribution of received signal $\tilde{\mathbf{Y}}[i]$ from the lth resolvable path. However, the residual MAI in one filter output $Z_{1,l}[i]$ can partially cancel out those in other filter outputs. Thus, the output energy of each interfering user (i.e., $|v_{k,RAKE}[i]|^2$ where $k \in \{2, \ldots, K\}$) is less than L times that of the single-arm CMA.

Figure 4.4 shows the steady state BER performance of the single sensor based blind methods with $SNR(k = 1) = \{0, \ldots, 10\}dB$, and with other parameters the same as Figure 4.3. In the case of signature mismatch, the BERs of the

single-arm CMA and the MOE detector quickly flatten out and reach a very poor error floor. Again, the proposed receiver gives the best BER performance. The effect of increasing channel order L is illustrated in Figure 4.5 with $K = 5$ and $NFR = 3dB$. Again, the proposed receiver shows a significant BER improvement over other methods, but deteriorates gradually as more paths appear. For a higher channel order, there are the enhanced effect of non-vanishing step size and noise enhancement. Also, the assumption in Section 4.4.1 $N \gg L$, may no longer hold as the ISI becomes significant, and $\mathbf{C}_1$ in (4.13) becomes rank deficient.

For the multiple sensors case, Figure 4.6 shows the BER performance of the proposed receiver with $M = \{1, 2, 3\}$, and the 2-D RAKE receiver with $M = 3$ for different NFRs. It is seen that the proposed receiver is more near far resistant. A striking observation is that the performance of the 2-D RAKE receiver with three sensors is inferior to that of the proposed receiver with just one sensor. This result illustrates the inherent limitation of the beamforming approach (i.e., spatial MFs) for non-orthogonal signals. Also, the BER improves as more sensors are added. As discussed in Section 4.5.3, with M antennas, the effective spreading length as seen by the receiver is M times that of the single sensor case. However, the benefit of this added spatial diversity diminishes as M increases.

In Figure 4.7, the probability of the non-lock convergence initialisation is plotted using different NFRs and various actual channel order L_a. It is observed that for increasing channel undermodelling and near far effect, the previously robust lock initialisation may be lost. This is because that the user gains $\mathbf{V}_{RAKE}[i]$ in (4.27) is the summation of all contributions from each resolvable path. Thus, when there is significant channel undermodelling present, those user gains from the missing resolvable path may induce sufficient perturbation $\Delta v_{k,RAKE}[0]$ in (4.39) to give a non-lock convergence (i.e., trapped within some saddle regions or even capture convergence).

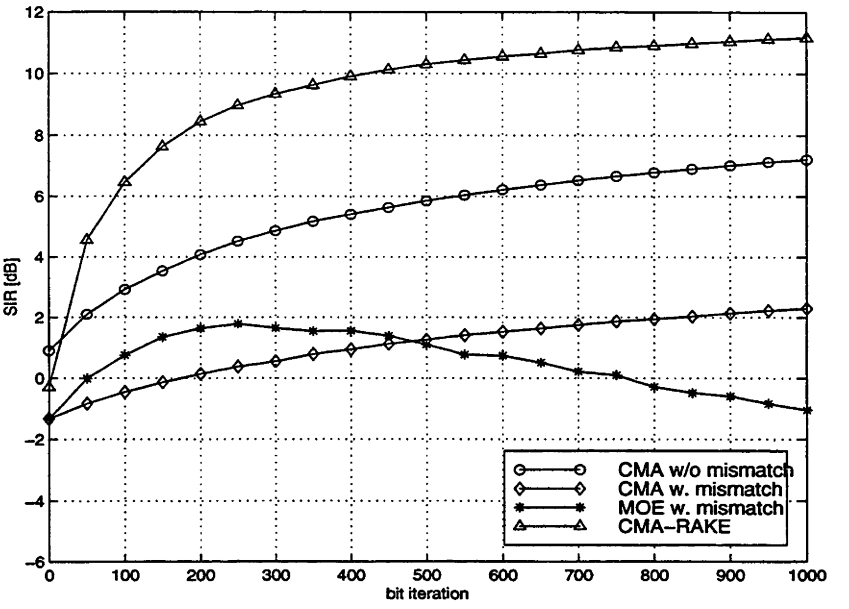

Figure 4.3: The transient SIR for single sensor based blind methods: $M = 1$, $N = 31$, $K = 10$, $SNR(k = 1) = 12dB$, $NFR = 3dB$, $L = 3$.

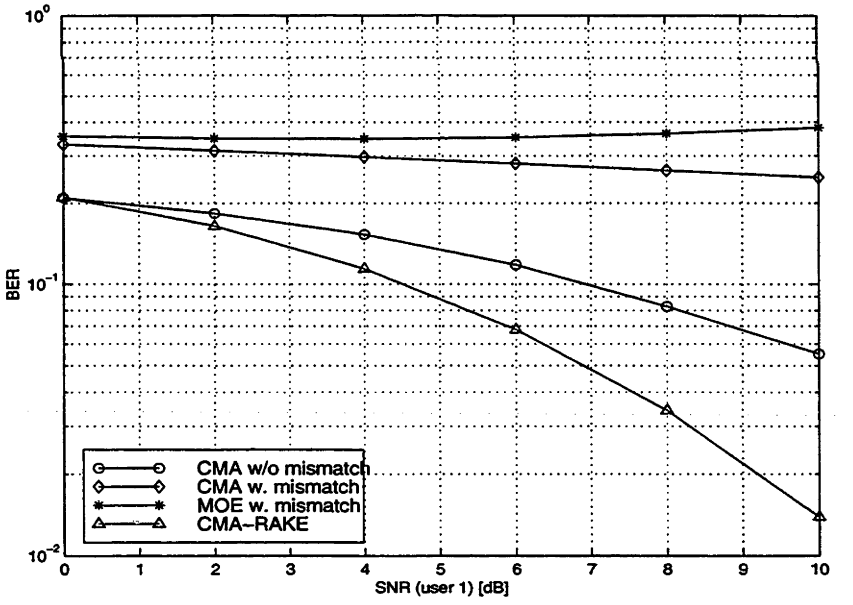

Figure 4.4: The steady state BER vs. $SNR(k = 1)$ for single sensor based blind methods: $M = 1$, $N = 31$, $K = 10$, $NFR = 3dB$, $L = 3$.

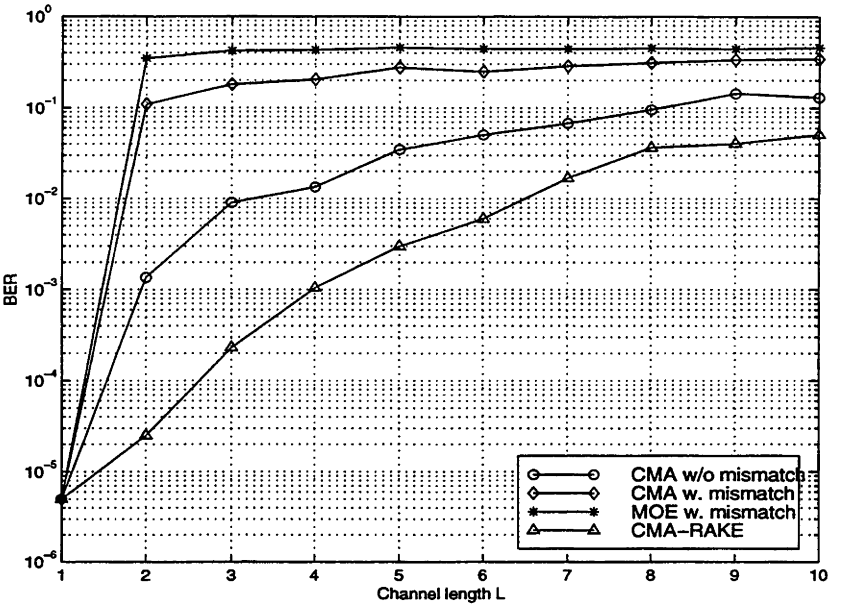

Figure 4.5: The steady state BER vs. channel order L for single sensor based blind methods: $M = 1$, $N = 31$, $K = 5$, $SNR(k = 1) = 12dB$, $NFR = 3dB$.

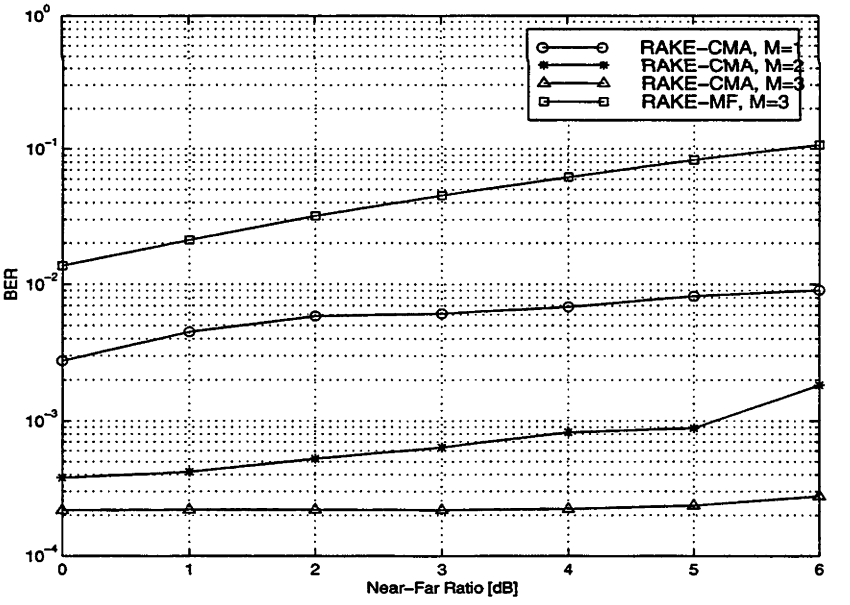

Figure 4.6: The steady state BER vs. NFR for multiple sensors based blind methods: $N = 31$, $K = 10$, $SNR(k = 1) = 12dB$, $M \in \{1, 2, 3\}$, $L = 3$.

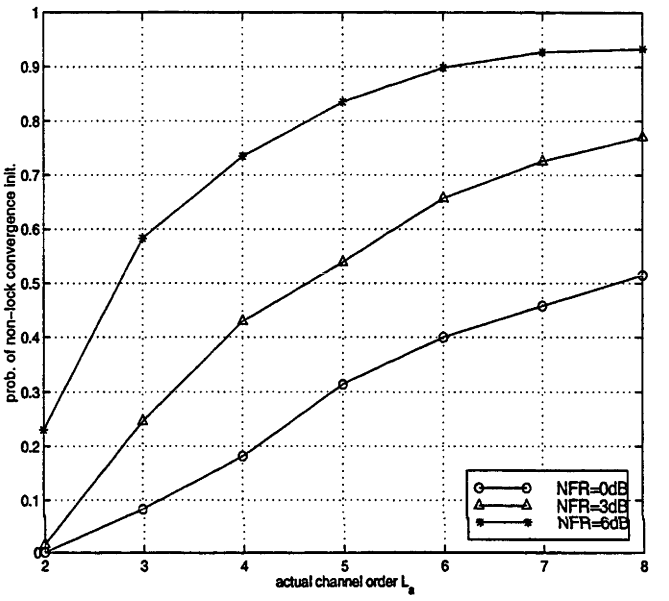

Figure 4.7: The probability of non-lock convergence initialisation vs. various actual channel orders L_a, for the single sensor based proposed receiver under channel undermodelling: $M = 1$, $N = 31$, $K = 10$, $SNR(k = 1) = 12dB$, $NFR \in \{0dB, 3dB, 6dB\}$, and modelled channel order is $L = 2$.

4.9 Conclusions

In this chapter, a new space-time, multiple sensor based receiver for blind linear multiuser detection in a low-rate DS-CDMA system under frequency selective multipath environment, is proposed. The receiver structure uses a bank of CMA-based linear filters in a RAKE-type processing, which is robust to non-orthogonal signals and multipath effect. In the same manner as the single-arm CMA, the overall linear operation converges to a decorrelator detector with a noiseless received signal. Robust initialisation can be achieved for lock convergence, but may be lost under severe channel undermodelling. In comparison with the conventional MF-based 2-D RAKE receiver, the proposed method offers superior BER performance (e.g., more near far resistant) with fewer number of sensors, permits adaptive implementation, and has less computational complexity.

Chapter 5

Constrained CMA-based Receiver

5.1 Chapter Outline

Similar to Chapter 4, this chapter is concerned with the same problem of blind linear multiuser detection under frequency selective multipath environment. But several assumptions used in Chapter 4, such as the knowledge of channel phase and synchronism, have been removed. A Multiple-Input Multiple-Output (MIMO) model has been derived as the DS-CDMA system under multipath effects. A linear blind receiver is proposed based on the inverse filtering approach. This approach uses orthogonal filter decomposition whereby a fixed filter component removes the ISI and ICI of the desired user, and an adaptive filter component is used solely to suppress MAI. Provided that the modulus radius is sufficiently small, the adaptive filter component is blindly adapted by CMA in a constrained space, such that the only stable stationary point is the desired lock convergence.

The rest of this chapter is organised as follows. Section 5.2 presents the MIMO model of the DS-CDMA system subject to multipath propagation. Section 5.3 explains the inverse filtering criterion in terms of the MIMO model. Section 5.4 presents the constrained CMA, and Section 5.5 examines its stationary points, stability and the choice of modulus radius. Section 5.6 compares the proposed

method with the constrained MOE and the MMSE detectors via simulation. Section 5.7 contains the chapter's conclusions.

5.2 System Model

In this section, a MIMO model is developed for an uncoded K-user DS-CDMA system under frequency selective multipath channels. In the same manner as Section 4.4, the MIMO model is derived using M sensors with $m \in \{1, \ldots, M\}$ denoting the sensor index.

5.2.1 Model Assumptions

Similar to the channel model in Section 4.4.1, the complex FIR describing the propagation from the kth user's transmitter to the mth sensor of the receiver is denoted as $h_k^m(\tau)$. In this chapter, the same assumptions A1 and A2 in Section 4.4.1 are used. However, the assumption A2 can be relaxed to as $N > L$ (instead of $N \gg L$), where L is the maximum number of resolvable path. Also, it is assumed that the relative delays between the received signal from different sensors are negligible. Finally, two assumptions that were used to simplify the analysis in Chapter 4, are not used in the derivation of the MIMO model. First, no knowledge of channel phase is required, as no coherent combiner is used. Second, asynchronism is considered in the MAI (i.e., each interfering user is asynchronous with respect to the desired user).

5.2.2 Received Signal Model

From (4.2), the received signal for the kth user of the mth sensor is given as

$$y_k^m(t) = A_k \sum_i b_k[i] f_k^m(t - iT_b),$$

where A_k, $b_k[i] \in \{\pm 1\}$, and $f_k^m(t)$ is the kth user's received amplitude, the ith transmitted bit and the received signature waveform given in (4.3), respectively.

Then, for the mth sensor, the total received signal from K users is generalised to an asynchronous case as

$$\begin{aligned} y^m(t) &= \sum_{k=1}^{K} y_k^m(t-\tau_k) + n^m(t) \\ &= \sum_{k=1}^{K} A_k \sum_i b_k[i] f_k^m(t - iT_b - \tau_k) + n^m(t), \end{aligned} \tag{5.1}$$

where $n^m(t)$ is the AWGN for the mth sensor with zero mean and power spectral density σ_n^2, and $\tau_k \in [0, T_b)$ is the kth user's timing delay. For simplicity, the desired user's delay estimate is assumed to be obtained prior to the detection stage, and the interfering users' timings are given in integer multiples of chip intervals as[1]

$$\tau_k = \eta_k T_c, \tag{5.2}$$

where $\eta_k \in \{0, \ldots, N-1\}$. Since the receiver is assumed to synchronise with the desired user, we can let $\tau_1 = \eta_1 = 0$.

Then, the discrete-time received signal of (5.1) is obtained as follows. By applying the chip MF filtering in (4.15), for the mth sensor, the nth chip sample of the ith bit internal of the received signal can be written as

$$y^m[i,n] \triangleq \frac{1}{T_c} \int_{iT_b+nT_c}^{iT_b+(n+1)T_c} y^m(t)dt.$$

For adaptation at bit rate (i.e., $1/T_b$), N chip samples are organised in the form of a N-length column vector as

$$\mathbf{Y}^m[i] = (y^m[i,1], \ldots, y^m[i,N])^T. \tag{5.3}$$

In the same manner as (4.17), in order to represent the received signal for the M sensors case, M vectors of (5.3) are stacked together to form a NM-length column vector as

$$\mathbf{Y}[i] = \sum_{k=1}^{K} \mathbf{Y}_k[i] + \mathbf{n}[i] = \left((\mathbf{Y}^m[i])^T, \ldots, (\mathbf{Y}^M[i])^T \right), \tag{5.4}$$

[1] In practice, interfering users do not synchronised themselves to chip intervals of each other. A more realistic expression for user's delay is given in (7.4).

where $\mathbf{Y}_k[i]$ is the received signal from the kth user, and $\mathbf{n}[i]$ is the NM-length column vector of noise samples.

Next, the discrete-time received signal in (5.4) is expressed as a MIMO model as follows. From (4.3), since each received signature waveform $f_k^m(t)$ has time support of $T_c(N-L+1)$, each bit $b_k[i]$ contributes to at most $(N+L-1)$ received chip samples. From the assumption $N > L$ in Section 5.2.1, since $N < N+L-1 < 2N$, the ISI contributes from at most two bits. Thus, the kth user's received signal can be written in terms of two consecutive bits as

$$\mathbf{Y}_k[i] = A_k \left(\mathbf{f}_{k,0} b_k[i] + \mathbf{f}_{k,-1} b_k[i-1]\right), \tag{5.5}$$

where

$$\begin{aligned} \mathbf{f}_{k,x} &= \mathcal{C}_{k,x}\mathcal{G}_k \quad \text{where } x \in \{0,-1\}, \\ \mathcal{G}_k &\triangleq \left((\mathbf{g}_k^1)^T, \ldots, (\mathbf{g}_k^M)^T\right)^T, \end{aligned} \tag{5.6}$$

and $\mathbf{g}_k^m$ is an L-length chip rate samples vector of the composite FIR $g_k^m(t)$ in (4.6). The $(MN \times ML)$ matrix $\mathcal{C}_{k,x}$ in (5.6) is a block diagonal matrix with each block diagonal term equal to an $(N \times L)$ matrix $\mathbf{C}_{k,x}(\eta_k)$ as follows

$$\mathcal{C}_{k,x} \triangleq \begin{bmatrix} \mathbf{C}_{k,x}(\eta_k) & & \mathbf{0} \\ & \ddots & \\ \mathbf{0} & & \mathbf{C}_{k,x}(\eta_k) \end{bmatrix} \quad \text{where } x \in \{0,-1\} \tag{5.7}$$

In the special case of synchronism (i.e., $\tau_k = \eta_k = 0$), $\mathbf{C}_{k,x}$ in (5.7) is defined as partial convolution matrix

$$\mathbf{C}_{k,0}(\eta_k = 0) \triangleq \begin{bmatrix} c_k[1] & 0 & \cdots & 0 \\ c_k[2] & c_k[1] & \ddots & \vdots \\ \vdots & \vdots & \ddots & \vdots \\ c_k[N] & c_k[N-1] & \cdots & c_k[N-L+1] \end{bmatrix} = \begin{bmatrix} \mathbf{c}_k^1 \\ \mathbf{c}_k^2 \\ \vdots \\ \mathbf{c}_k^N \end{bmatrix}, \tag{5.8}$$

$$\mathbf{C}_{k,-1}(\eta_k = 0) \triangleq \begin{bmatrix} 0 & c_k[N] & \cdots & \cdots & c_k[N-L+2] \\ 0 & 0 & c_k[N] & \cdots & c_k[N-L+3] \\ \vdots & \cdots & 0 & \ddots & \vdots \\ 0 & \cdots & \cdots & 0 & c_k[N] \\ & & \mathbf{0}_{k,-1} & & \end{bmatrix} = \begin{bmatrix} \mathbf{c}_k^{N+1} \\ \mathbf{c}_k^{N+2} \\ \vdots \\ \mathbf{c}_k^{N+L-1} \\ \mathbf{0}_{k,-1} \end{bmatrix}, \tag{5.9}$$

with $\mathbf{c}_k^n$ as the corresponding non-zero L-length row vector where $n \in \{1, \ldots, N-L+1\}$, and $\mathbf{0}_{k,-1}$ is a $(N-L+1-\eta_k \times L)$ zero matrix. Using the notation $\mathbf{c}_k^n$, the definition of $\mathbf{C}_{k,0}$ and $\mathbf{C}_{k,-1}$ in (5.8) and (5.9), respectively, can be generalised to the case of asynchronism as

$$\mathbf{C}_{k,0}(\eta_k) \triangleq \begin{bmatrix} \mathbf{0}_{k,0} \\ \mathbf{c}_k^1 \\ \vdots \\ \mathbf{c}_k^{N-\eta_k} \end{bmatrix} \quad \text{and} \quad \mathbf{C}_{k,-1}(\eta_k) \triangleq \begin{bmatrix} \mathbf{c}_k^{N+1-\eta_k} \\ \vdots \\ \mathbf{c}_k^{N+L-1} \\ \mathbf{0}_{k,-1} \end{bmatrix}, \tag{5.10}$$

where $\mathbf{0}_{k,0}$ is a $(\eta_k \times L)$ zero matrix. Substituting (5.5) into (5.4), the received signal is given by

$$\mathbf{Y}[i] = \mathcal{F}\mathcal{A}\mathcal{B}[i] + \mathbf{n}[i], \tag{5.11}$$

where $\mathcal{A}$ is an $(2K \times 2K)$ block diagonal matrix with elements $(A_1, \ldots, A_K, A_1, \ldots, A_K)$,

$$\begin{aligned} \mathcal{F} &\triangleq (\mathbf{f}_{1,-1}, \ldots, \mathbf{f}_{K,-1}, \mathbf{f}_{1,0}, \ldots, \mathbf{f}_{K,0}), \quad \text{and} \\ \mathcal{B}[i] &\triangleq (b_1[i-1], \ldots, b_K[i-1], b_1[i], \ldots, b_K[i])^T. \end{aligned} \tag{5.12}$$

From (5.11), $\mathcal{F}$ is an $(NM \times 2K)$ signature matrix which can be viewed as a MIMO system with $2K$ independent inputs and NM outputs.

5.3 Inverse Filtering Criterion

From (3.1), using the MIMO model, the objective of linear multiuser detection is to find a NM-length vector of filter coefficients $\mathbf{w}_1[i]$, such that $\hat{b}_1[i]$ is a good estimate of $b_1[i]$:

$$\hat{b}_1[i] = sgn(Z_1[i]) = sgn(\mathbf{w}_1^T[i]\mathbf{Y}[i]),$$

where $\mathbf{Y}[i]$ is the received signal in (5.11) and $Z_1[i]$ is the filter output from the ith bit. In this section, in order to illustrate the concept of inverse filtering based on the MIMO model, the decorrelating detector and the MMSE detector are briefly discussed as examples.

5.3.1 Decorrelating Detector

In the absence of channel noise, the decorrelating detector, $\mathbf{w}_{1,DEC}$, satisfies

$$\mathbf{w}_{1,DEC}^T \mathcal{F}\mathcal{A} = \beta \cdot \mathbf{1}_{K+1}^T \quad \text{or} \quad \mathbf{w}_{1,DEC}^T \mathcal{F} = \frac{1}{A_1}\beta \cdot \mathbf{1}_{K+1}, \tag{5.13}$$

where $\mathbf{1}_{K+1} = (0, \ldots, 0, 1, 0, \ldots, 0)^T$ with 1's in the $(K+1)$-th position, and β is an arbitrary non-zero, multiplicative constant. In the MIMO model, the decorrelator detector extracts the desired bit $b_1[i]$ and nulls all other $(2K-1)$ bits in $\mathcal{B}[i]$ in (5.12). A sufficient condition to guarantee the existence of decorrelating solution in (5.13) is that $\mathcal{F}$ is right-invertible [80] (i.e., full-column rank), or $MN \geq 2K$. This implies that more sensors are required, as the number of users increases (i.e., signature coupling increases). Solving (5.13), the decorrelating solution in the MIMO model is given by

$$\mathbf{w}_{1,DEC} = \beta \cdot \frac{1}{A_1} \left(\mathcal{F}\mathcal{F}^T\right)^{-1} \mathcal{F}\, \mathbf{1}_{K+1} = \beta \cdot \frac{1}{A_1} \left(\mathcal{F}\mathcal{F}^T\right)^{-1} \mathbf{f}_{1,0}. \tag{5.14}$$

5.3.2 MMSE Detector

From (2.42), by minimising $E\{|Z_1[i] - \hat{b}_1[i]|^2\}$, the MMSE detector is given as

$$\begin{aligned} \mathbf{w}_{1,MMSE} &= \left(E\left\{\mathbf{Y}[i]\mathbf{Y}^T[i]\right\}\right)^{-1} \cdot E\left\{\hat{b}_1[i]\mathbf{Y}[i]\right\} \\ &= \left(\mathcal{F}\mathcal{A}^2\mathcal{F}^T + \sigma_n^2 \mathbf{I}_{NM}\right)^{-1} \cdot \mathcal{F}\mathcal{A}\,\mathbf{1}_{K+1} \\ &= A_1 \left(\mathcal{F}\mathcal{A}^2\mathcal{F}^T + \sigma_n^2 \mathbf{I}_{NM}\right)^{-1} \cdot \mathbf{f}_{1,0}. \end{aligned} \tag{5.15}$$

Comparing (5.15) with (5.14), for the noiseless case, it is observed that the MMSE detector has the same form as the decorrelator detector.

5.4 Constrained CMA Approach

From (5.13), it is shown that given sufficient spatio-temporal diversity (i.e., $NM \geq 2K$), linear multiuser detection can extract the desired bit reliably. However, if CMA is used for its blind adaptation, the linear filter can converge to any of the $2K$ inputs. In the same manner as the MOE detector subject to multipath

constraints in [58], constrained inverse filtering criterion is used to ensure that the blind receiver selects the correct input (i.e., $b_1[i]$). This constrained inverse filtering is implemented by a constrained CMA, and is presented in this section.

5.4.1 Constrained Parameterisation

The underlying concept of the constrained inverse filtering is to guarantee the recovery of the desired bit $b_1[i]$, by setting the $(K+1)$-th component of $\mathbf{w}_1^T\mathcal{F}\mathcal{A}$ to be non-zero (i.e., $\mathbf{w}_1[i]^T\mathbf{f}_{1,0} \neq 0 \quad \forall i$). In the same manner as the canonical filter representation in (3.2), the linear filter can be decomposed into two orthogonal components as

$$\mathbf{w}_1[i] = \left(\widehat{\mathcal{C}}_1^{\dagger}\right)^T \mathbf{w}_{1,0} + \mathcal{P}_1^{\perp}\mathbf{w}_1^{\perp}[i], \tag{5.16}$$

where $\mathbf{w}_{1,0}$ is a fixed $M(2L-1)$-length column vector, $\mathbf{w}_1^{\perp}[i]$ is a NM-length column vector as the adaptive filter component, and $\widehat{\mathcal{C}}_1$ is an $(NM \times M(2L-1))$ block diagonal matrix with each block diagonal term equal to an $(N \times 2L-1)$ matrix $\widehat{\mathbf{C}}_1$ defined as

$$\widehat{\mathbf{C}}_1 \triangleq \left(\mathbf{C}_{1,0}(\eta_1 = 0),\ \widehat{\mathbf{C}}_{1,-1}(\eta_1 = 0)\right), \tag{5.17}$$

where $\mathbf{C}_{1,0}(\eta_1 = 0)$ is given in (5.10), and $\widehat{\mathbf{C}}_{1,-1}(\eta_1 = 0)$ has the same form as $\mathbf{C}_{1,-1}(\eta_1 = 0)$ with the first column removed. The projection matrix $\mathcal{P}_1^{\perp}$ in (5.16) is an $(NM \times NM)$ block diagonal matrix, with each block diagonal term equal to an $(N \times N)$ matrix $\mathbf{P}_1^{\perp}$, and is defined as

$$\mathbf{P}_1^{\perp} \triangleq \mathbf{I}_{NM} - \widehat{\mathbf{C}}_1\widehat{\mathbf{C}}_1^{\dagger}. \tag{5.18}$$

The projection matrix $\mathcal{P}_1^{\perp}$ ensures that the first and second terms in (5.16) are orthogonal to each other.

The constrained parameterisation in (5.16) is justified as follows. From (5.5) and (5.17), for the mth sensor, it can be shown that the contribution of received signal from the desired user $k=1$ can be written as

$$\mathbf{Y}_1^m[i] = A_1\widehat{\mathbf{C}}_1 \begin{bmatrix} b_1[i]\mathbf{g}_1^m \\ b_1[i-1]\hat{\mathbf{g}}_1^m \end{bmatrix}, \tag{5.19}$$

where $\mathbf{g}_1^m$ is given in (4.6), and $\hat{\mathbf{g}}_1^m$ is similar to $\mathbf{g}_1^m$, except with its first component removed. Thus, the contribution of the desired user can be generalised to the case of M sensors as

$$\mathbf{Y}_1[i] = \begin{bmatrix} \mathbf{Y}_1^m[i] \\ \vdots \\ \mathbf{Y}_1^M[i] \end{bmatrix} = A_1 \widehat{\mathcal{C}}_1 \begin{bmatrix} b_1[i]\mathbf{g}_1^1 \\ b_1[i-1]\hat{\mathbf{g}}_1^1 \\ \vdots \\ b_1[i]\mathbf{g}_1^M \\ b_1[i-1]\hat{\mathbf{g}}_1^M \end{bmatrix}. \tag{5.20}$$

From the definition of the projection matrix in (5.18), it is seen that $\mathbf{w}_1^{\perp}[i]$ in (5.16) is used to suppress MAI only. This is because the adaptation of $\mathbf{w}_1^{\perp}[i]$ is restricted in the constrained space which is orthogonal to $\mathbf{Y}_1[i]$. Thus, the contribution of desired user in the filter output $Z_1[i]$ is solely dependent on the fixed filter component $\mathbf{w}_{1,0}$, and is constrained to be non-zero as

$$\mathbf{w}_1^T[i]\mathbf{Y}_1[i] = \mathbf{w}_{1,0}^T \widehat{\mathcal{C}}_1^{\dagger} \mathbf{Y}_1[i] = \beta \cdot b_1[i]. \tag{5.21}$$

The constraint condition in (5.21) implies that the choice of $\mathbf{w}_{1,0}$ is crucial in the removal of the multipath induced ISI and ICI in $\mathbf{Y}_1[i]$. To facilitate the separation of ISI and ICI in $Z_1[i]$, $\mathbf{w}_{1,0}$ is decomposed as

$$\mathbf{w}_{1,0} = \left(\mathbf{w}_{1,1,ICI}^T,\ \mathbf{w}_{1,1,ISI}^T, \cdots, \mathbf{w}_{1,M,ICI}^T,\ \mathbf{w}_{1,M,ISI}^T\right)^T, \tag{5.22}$$

where $\mathbf{w}_{1,m,ICI}$ and $\mathbf{w}_{1,m,ISI}$ are the L-length and $(L-1)$-length column vectors respectively, and $m \in \{1, \ldots, M\}$. Combining (5.20) and (5.22), we have

$$\mathbf{w}_1^T[i]\mathbf{Y}_1[i] = A_1 \sum_{m=1}^{M} \left(b_1[i]\mathbf{w}_{1,m,ICI}^T \mathbf{g}_1^m + b_1[i-1]\mathbf{w}_{1,m,ISI}^T \hat{\mathbf{g}}_1^m\right). \tag{5.23}$$

From (5.23), it is observed that to remove ISI, $\mathbf{w}_{1,m,ISI} = \mathbf{0} \quad \forall m \in \{1, \ldots, M\}$. Also, in order to avoid desired signal cancellation due to presence of ICI, $\mathbf{w}_{1,m,ICI}$ is required to satisfy[2]

$$\sum_{m=1}^{M} \mathbf{w}_{1,m,ICI}^T \mathbf{g}_1^m \neq 0. \tag{5.24}$$

[2] This is in accordance with the constraint condition in (5.21).

Without prior knowledge of the composite channel FIR $\mathbf{g}_1^m$, one simple way to satisfy (5.24) is

$$\mathbf{w}_{1,n,ICI} = \beta \cdot \mathbf{1}_j, \quad \text{and} \quad \mathbf{w}_{1,m,ICI} = \mathbf{0} \quad \forall m \neq n; \tag{5.25}$$

where $j \in \{1, \ldots, L\}$ and $n \in \{1, \ldots, M\}$ are arbitrary indices. Hence, the signal cancellation problem is avoided by forcing the response of all copies of $b_1[i]$ but one, equal to zero.

5.4.2 Constrained CMA Adaptation

In this work, the CM cost function is used as the inverse filtering criterion[3]. Unlike the RAKE-type processing in Chapter 4, no knowledge of channel phase is required, since diversity combining is not used here. From (2.45), the cost function is given by

$$J_{CM}(\mathbf{w}_1) = E\left\{\left(|Z_1[i]|^2 - \xi\right)^2\right\},$$

where the modulus radius ξ is a positive constant. Since the CM criterion is phase invariant, the filter output $Z_1[i]$ is subject to an arbitrary phase rotation, as denoted by β in (5.21). Based on the orthogonal filter decomposition in (5.16), the constrained CMA is given by[4]

$$\begin{aligned} \mathbf{w}_1^{\perp}[i+1] &= \mathbf{w}_1^{\perp}[i] - \mu \cdot \frac{1}{4}\nabla_{\mathbf{w}_1^{\perp}[i]} J_{CM}(\mathbf{w}_1) \\ &= \mathbf{w}_1^{\perp}[i] - \mu \left(|Z_1[i]|^2 - \xi\right) Z_1[i] \nabla_{\mathbf{w}_1^{\perp}[i]} |Z_1[i]| \\ &= \mathbf{w}_1^{\perp}[i] - \mu \left(|Z_1[i]|^2 - \xi\right) Z_1[i] \mathcal{P}_1^{\perp} \mathbf{Y}^*[i]. \end{aligned} \tag{5.26}$$

5.5 Convergence Analysis

In this section, convergence analysis of the constrained CMA in (5.26) is presented under a noiseless signal assumption. First, the two classes of stationary points

[3] Minimisation of any cost function that involves only the filter output $Z_1[i]$ can be used as inverse filtering criterion. [4] Some linearly constrained CMAs similar to (5.26) have been proposed independently, for blind multiuser detection in [70, 118, 119], with or without multipath structure.

are derived. Second, the stability of the stationary points in the first class is examined. Third, the significance of stationary points in the second class is discussed.

5.5.1 Stationary Points

Analogous to (3.24), user gains are used to characterise the system response in the MIMO model and are defined as

$$\mathbf{V}_{IO}[i] \triangleq (\mathcal{F}\mathcal{A})^T \mathbf{w}_1[i] = (v_{1,IO}[i], \ldots, v_{2K,IO}[i])^T; \tag{5.27}$$

so that $Z_1[i] = \mathbf{V}_{IO}^T[i]\mathcal{B}[i]$ in the absence of noise. Substituting (5.16) into (5.27), the user gains can be written as

$$\mathbf{V}_{IO}[i] = (\mathcal{F}\mathcal{A})^T \left(\widehat{\mathcal{C}}_1^{\dagger}\right)^T \mathbf{w}_{1,0} + \mathcal{A}\mathcal{F}^T\mathcal{P}_1^{\perp}\mathbf{w}_1^{\perp}[i]. \tag{5.28}$$

Next, the stationary points of the constrained CMA is examined in terms of a sub-vector of $\mathbf{V}_{IO}[i]$ which is defined as

$$\widehat{\mathbf{V}}_{IO}[i] \triangleq (\mathbf{v}_{2,IO}[i], \ldots, \mathbf{v}_{K,IO}[i], \mathbf{v}_{K+2,IO}[i], \ldots, \mathbf{v}_{2K,IO}[i])^T. \tag{5.29}$$

The reason to use these $(2K-2)$ user gains in $\widehat{\mathbf{V}}_{IO}[i]$ is explained as follows. From (5.6) and (5.18), it can be shown that

$$\mathcal{P}_1^{\perp}\mathbf{f}_{1,0} = \mathcal{P}_1^{\perp}\mathbf{f}_{1,-1} = \mathbf{0}. \tag{5.30}$$

Hence, $v_{1,IO}[i]$ and $\mathbf{v}_{K+1,IO}[i]$ are independent of the second term in (5.28) which involves $\mathbf{w}_1^{\perp}[i]$. If $\mathbf{w}_{1,0}$ is set according to (5.25), these two user gains are constrained as

$$\begin{aligned} v_{1,IO}[i] &= A_1\mathbf{f}_{1,-1}^T \left(\widehat{\mathcal{C}}_1^{\dagger}\right)^T \mathbf{w}_{1,0} = \alpha \quad \forall i, \quad \text{and} \\ v_{K+1,IO}[i] &= A_1\mathbf{f}_{1,0}^T \left(\widehat{\mathcal{C}}_1^{\dagger}\right)^T \mathbf{w}_{1,0} = 0 \quad \forall i, \end{aligned} \tag{5.31}$$

where $\alpha = A_1\beta g_{1,j}^n$, and $g_{1,j}^n$ is the jth component of $\mathbf{g}_1^n$.

For notational convenience, the bit index i is removed. In the same manner as (4.29), the stationary points of the constrained CMA occur when

$$\nabla_{\mathbf{w}_1^{\perp}} J_{CM}(\mathbf{w}_1) = \mathcal{P}_1^{\perp}\mathcal{F}\mathcal{A} \cdot \nabla_{\mathbf{V}_{IO}} J_{CM}(\mathbf{V}_{IO}) = \mathbf{0}, \tag{5.32}$$

where $\nabla_{\mathbf{V}_{IO}} J_{CM}(\mathbf{V}_{IO})$ is similar to (A.8) in Appendix A, and is expressed as

$$\nabla_{\mathbf{V}_{IO}} J_{CM}(\mathbf{V}_{IO}) = \left[\left(3\|\mathbf{V}_{IO}\|^2 - \xi\right)\mathbf{I}_{2K} - 2\,diag\left(\mathbf{V}_{IO}\mathbf{V}_{IO}^T\right)\right]\cdot\mathbf{V}_{IO}. \tag{5.33}$$

Since $v_{1,IO}$ and $v_{K+1,IO}$ are constrained as in (5.31), the condition of stationary points in (5.32) can be modified as

$$\nabla_{\mathbf{w}_1^\perp} J_{CM}(\mathbf{w}_1) = \mathcal{P}_1^\perp \widehat{\mathcal{F}}\widehat{\mathcal{A}}\cdot\nabla_{\widehat{\mathbf{V}}_{IO}} J_{CM}(\widehat{\mathbf{V}}_{IO}) = \mathbf{0}, \tag{5.34}$$

where $\widehat{\mathcal{F}} \triangleq (\mathbf{f}_{2,-1},\ldots,\mathbf{f}_{K,-1},\ \mathbf{f}_{2,0},\ldots,\mathbf{f}_{K,0})$, $\widehat{\mathcal{A}}$ is an $(2K-2\times 2K-2)$ diagonal matrix with elements $(A_2,\ldots,A_K,\ A_2,\ldots,A_K)$, and

$$\nabla_{\widehat{\mathbf{V}}_{IO}} J_{CM}(\widehat{\mathbf{V}}_{IO}) = \left[\left(3\left(|\alpha|^2 + \|\widehat{\mathbf{V}}_{IO}\|^2\right) - \xi\right)\mathbf{I}_{2K} - 2\,diag\left(\widehat{\mathbf{V}}_{IO}\widehat{\mathbf{V}}_{IO}^T\right)\right]\cdot\widehat{\mathbf{V}}_{IO}. \tag{5.35}$$

In the same manner as Section 4.7.1, the stationary points in (5.34) can classified into two classes:

Class 1 these stationary points correspond to that of the *unconstrained* CMA (i.e., without $\mathcal{P}_1^\perp$), and satisfy $\nabla_{\widehat{\mathbf{V}}_{IO}} J_{CM}(\widehat{\mathbf{V}}_{IO}) = \mathbf{0}$:

1. $\widehat{\mathbf{V}}_{IO} = \mathbf{0}$, the desired solution (i.e., complete removal of all MAI),
2. analogous to (A.14), these stationary points occur when $\widehat{\mathbf{V}}_{IO}$ has M non-zero components of equal magnitude:

$$|v_{k,IO}| = \sqrt{\frac{\xi - 3\alpha^2}{3M-2}}, \tag{5.36}$$

where $M \in \{1,\ldots,2K-2\}$ and $k \in \{2,\ldots,K,K+2,\ldots,2K\}$. They exist only when $\alpha^2 < \xi/3$.

Class 2 Due to the usage of projection matrix $\mathcal{P}_1^\perp$, a new class of stationary points occur when

$$\nabla_{\widehat{\mathbf{V}}_{IO}} J_{CM}(\widehat{\mathbf{V}}_{IO}) \in Nullspace\left(\mathcal{P}_1^\perp\widehat{\mathcal{F}}\right),\ \text{and}\ \nabla_{\widehat{\mathbf{V}}_{IO}} J_{CM}(\widehat{\mathbf{V}}_{IO}) \neq \mathbf{0}. \tag{5.37}$$

It is seen that the stationary point in Class 1.1 is analogous to the lock convergence (i.e., desired local minimum) in (3.27). From (5.36), it is observed that if the output power of the desired user is large enough, or $\alpha^2 \geq \xi/3$, the stationary points in Class 1.2 can be removed. To prevent the existence of these stationary points, one can set $\xi = 0$, however, this may result in a slower convergence rate than the case of $\xi > 0$.

5.5.2 Stability of Class 1

The stability of the stationary points of in Class 1 is examined by the sign-definiteness of the corresponding Hessian matrix [120]. In the absence of noise, from (5.32)) and (5.34)), the Hessian matrix is given as

$$\begin{aligned} \nabla^2_{\mathbf{w}_1^\perp} J_{CM}(\mathbf{w}_1) &= \mathcal{P}_1^\perp \mathcal{F}\mathcal{A} \cdot \nabla^2_{\mathbf{V}_{IO}} J_{CM}(\mathbf{V}_{IO}) \cdot \left(\mathcal{P}_1^\perp \mathcal{F}\mathcal{A}\right)^T \\ &= \mathcal{P}_1^\perp \widehat{\mathcal{F}}\widehat{\mathcal{A}} \cdot \nabla^2_{\widehat{\mathbf{V}}_{IO}} J_{CM}(\widehat{\mathbf{V}}_{IO}) \cdot \left(\mathcal{P}_1^\perp \widehat{\mathcal{F}}\widehat{\mathcal{A}}\right)^T, \end{aligned} \tag{5.38}$$

where from (A.11), the unconstrained and constrained Hessians are given respectively as

$$\begin{aligned} \frac{1}{4}\nabla^2_{\mathbf{V}_{IO}} J_{CM}(\mathbf{V}_{IO}) &= \left(3\|\mathbf{V}_{IO}\|^2 - \xi\right)\mathbf{I}_{2K} + 2\mathbf{V}_{IO}\mathbf{V}_{IO}^T - 2\,diag\left(\mathbf{V}_{IO}\mathbf{V}_{IO}^T\right), \\ \frac{1}{4}\nabla^2_{\widehat{\mathbf{V}}_{IO}} J_{CM}(\widehat{\mathbf{V}}_{IO}) &= \left(3\left(\alpha^2 + \|\widehat{\mathbf{V}}_{IO}\|^2\right) - \xi\right)\mathbf{I}_{2K-2} + 2\widehat{\mathbf{V}}_{IO}\widehat{\mathbf{V}}_{IO}^T \\ &\qquad -2\,diag\left(\widehat{\mathbf{V}}_{IO}\widehat{\mathbf{V}}_{IO}^T\right). \end{aligned} \tag{5.39}$$

From (5.39), it is observed that at $\widehat{\mathbf{V}}_{IO} = \mathbf{0}$, $\nabla^2_{\widehat{\mathbf{V}}_{IO}} J_{CM}(\widehat{\mathbf{V}}_{IO}) = 4\left(3\alpha^2 - \xi\right)\mathbf{I}_{2K-2}$ which is positive definite for $\alpha^2 > \xi/3$. Hence, when $\alpha^2 > \xi/3$, the stationary point in Class 1.1 is stable (i.e., local minimum).

Recall that the stationary points in Class 1.2 exist only under the condition $\alpha^2 < \xi/3$. Substituting (5.36) into (5.39), the first term of $\frac{1}{4}\nabla^2_{\widehat{\mathbf{V}}_{IO}} J_{CM}(\widehat{\mathbf{V}}_{IO})$ can be simplified as

$$\begin{aligned} \left(3\left(\alpha^2 + \|\widehat{\mathbf{V}}_{IO}\|^2\right) - \xi\right)\mathbf{I}_{2K-2} &= \left(3\left(\alpha^2 + \frac{M\left(\xi - 3\alpha^2\right)}{3M-2}\right) - \xi\right)\mathbf{I}_{2K-2} \\ &= \left(\frac{2\xi - 6\alpha^2}{3M-2}\right)\mathbf{I}_{2K-2}. \end{aligned} \tag{5.40}$$

From (5.39) and (5.40), it is observed that if $M = 1$, $\frac{1}{4}\nabla^2_{\widehat{\mathbf{V}}_{IO}} J_{CM}(\widehat{\mathbf{V}}_{IO}) = (2\xi - 6\alpha^2)\,\mathbf{I}_{2K-2}$ which is definite positive for $\xi > 3\alpha^2$. Thus, when $\xi > 3\alpha^2$, this undesired solution exists and is stable. If $M > 1$, as in the CMA-based blind equaliser [121], the Hessian is non-sign-definite, and hence stationary points are unstable (i.e., saddle points).

Since $\alpha^2 > \xi/3$ is the stability condition for Class 1 (1), it is deduced that the same condition can be used to suppress the stationary points in Class 1 (2), regardless of their stabilities. Then, if $\alpha^2 > \xi/3$, the only stationary point in Class 1 is the desired solution $\widehat{\mathbf{V}} = \mathbf{0}$. Hence, the choice of the modulus radius[5] ξ is important to ensure $\xi < 3\alpha^2$. If $\xi = 0$, the subsequent CM criterion becomes $E\{|Z_1[i]|^4\}$, which is a squared version of the MOE criterion in (2.44). Furthermore, unlike the unconstrained CMA, the constrained CMA can ensure that capture convergence (i.e., convergence to other user sources other than $b_1[i]$) is avoided.

5.5.3 Stationary Points in Class 2

In Class 2, the stationary points are undesired solutions. From (5.34), it is observed that if $rank\left(\mathcal{P}_1^{\perp}\widehat{\mathcal{F}}\right) = 2K - 2$ (i.e., full column rank), this matrix is right-invertible and Class 2 is empty. In order to suppress the hidden stationary points in Class 2, the full column rank condition of $\mathcal{P}_1^{\perp}\widehat{\mathcal{F}}$ is derived as follows. From (5.18), the rank of $\mathcal{P}_1^{\perp}$ is given as

$$\begin{aligned} rank\left(\mathcal{P}_1^{\perp}\right) &= NM - \dim\left(Nullspace\left(\mathcal{P}_1^{\perp}\right)\right) \\ &= NM - M(2L-1) \\ &= M(N-2L+1), \end{aligned} \tag{5.41}$$

where "dim" denotes dimension. Thus, since

$$\begin{aligned} rank\left(\mathcal{P}_1^{\perp}\widehat{\mathcal{F}}\right) &= \min\left(rank\left(\mathcal{P}_1^{\perp}\right), rank\left(\widehat{\mathcal{F}}\right)\right) \\ &= \min\left(M(N-2L+1), 2K-2\right), \end{aligned} \tag{5.42}$$

[5] In the unconstrained CMA, the modulus radius is only served as a scaling factor on the user gains.

then, $\mathcal{P}_1^{\perp}\widehat{\mathcal{F}}$ is full column rank if

$$M\,(N-2L+1) \geq 2K-2. \tag{5.43}$$

If the received signatures of all interfering users have sufficiently low cross-correlations with various shifted versions of desired user's spreading codes (i.e., columns of $\mathbf{C}_{1,0}(\eta_1 = 0)$ and $\mathbf{C}_{1,-1}(\eta_1 = 0)$ in (5.10)), then $\mathcal{P}_1^{\perp}\widehat{\mathcal{F}} \simeq \widehat{\mathcal{F}}$. In practice, unless the multipath vectors $\mathcal{G}_k$ in (5.6) reduce the dimension of signature subspace, $\widehat{\mathcal{F}}$ is most likely to be full column rank. Thus, in this case, Class 2 is empty. However, as the number of users K and the number of resolvable paths L increases, the cross-correlations between the signatures increase, and $\mathcal{P}_1^{\perp}\widehat{\mathcal{F}}$ may become rank deficient. As shown in Figure 5.1, this loss of full column rank condition occurs for large user populations and/or under severe multipath conditions. It is important that the full column rank condition in (5.43) is satisfied. This is done to ensure that Class 2 is empty, and the filter adaptation will always converge to lock convergence in Class 1, if $\xi < 3\alpha^2$.

5.6 Simulation Results

In this section, simulation results are presented to demonstrate the performance of the proposed multiuser receiver based on the constrained CMA.

5.6.1 Other multiuser detectors

The proposed method is compared with two multiuser detectors that are briefly described as follows

1. **Constrained MOE blind multiuser detector**

   In our comparison, the orthogonal filter decomposition in (5.16) is used. From the MOE cost function in (2.44), the filter adaptation is given by [58]

$$\mathbf{w}_1^{\perp}[i+1] = \mathbf{w}_1^{\perp}[i] - \mu Z_1[i]\mathcal{P}_1^{\perp}\mathbf{Y}^*[i]. \tag{5.44}$$

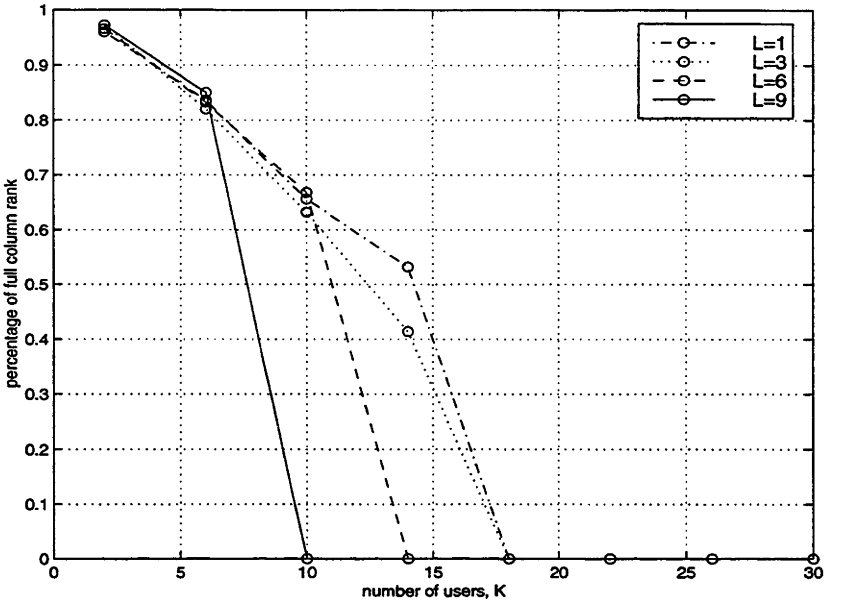

(a) $M = 1$

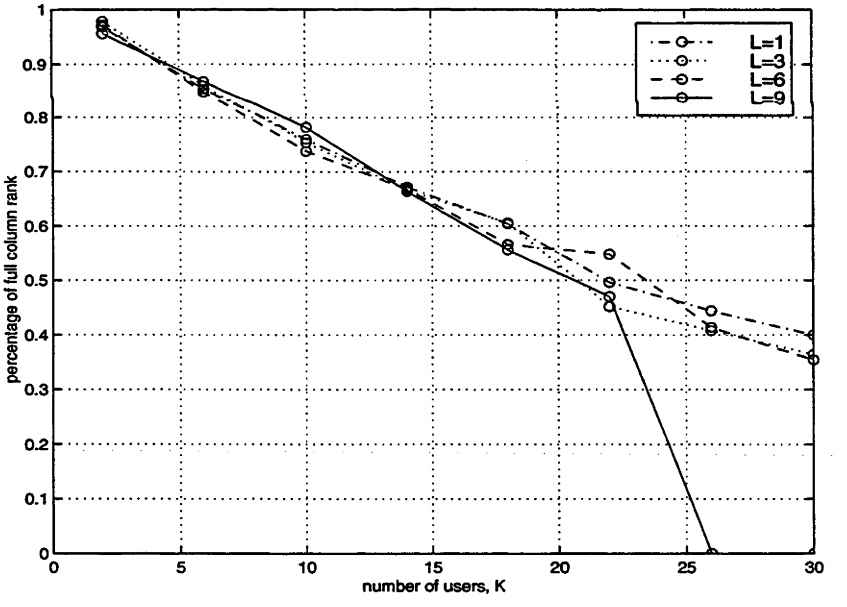

(b) $M = 3$

Figure 5.1: Percentage of $rank\left(\mathcal{P}_1^{\perp}\widehat{\mathcal{F}}\right) = 2K - 2$ vs. number of users K, using 500 Monte Carlo runs with $N = 31$, $M \in \{1,3\}$ and $L \in \{1,3,6,9\}$.

2. **Training-based MMSE multiuser detector**

   In the same manner as (2.43), the MMSE-LMS adaptation is given by [2, 34]

$$\mathbf{w}_1[i+1] = \mathbf{w}_1[i] - \mu \left(Z_1[i] - \alpha \hat{b}_1[i] \right) \mathbf{Y}^*[i], \tag{5.45}$$

   where α is given in (5.31), and $\hat{b}_1[i] = b[i] \quad \forall i$ (i.e., correct training bits are received).

For filter initialisations, to satisfy (5.25), both the constrained CMA and constrained MOE methods have $\mathbf{w}_{1,0} = \left(\beta, \overbrace{0, \ldots, 0}^{M(2L-1)-1} \right)^T$ with $\beta = 2$, and $\mathbf{w}_1^{\perp}[0] = \mathbf{0}$. In the case of the MMSE detector, the filter is initialised as the conventional MF: $\mathbf{w}_1[0] = \left(\mathbf{s}_1^T, \ldots, \mathbf{s}_1^T\right)^T$, where $\mathbf{s}_1 = (c_1[1], \ldots, c_1[N])^T$.

5.6.2 System Parameters and Performance Measure

All simulations are based on a 10-users, uncoded, asynchronous DS-CDMA system with a BPSK modulation scheme. The spreading length is set to $N = 31$. For simplicity, the desired user's timing is assumed to be known (i.e., $\tau_1 = 0$), and the timings of interfering users[6] τ_k where $k \in \{2, \ldots, 10\}$, are generated randomly and independently in the interval $[0, T_b)$. The SNRs of all interfering users are fixed and equal to $SNR(k) = 15dB \quad k \in \{2, \ldots, K\}$, and NFR [dB] in (3.57) is used to illustrate some near far conditions. The step sizes μ for all three methods are chosen to ensure a stable convergence. With the exception of Figure 5.4, the modulus radius of the constrained CMA is set to be $\xi = 1$.

For performance measure, in the same manner as (3.58), the SIR [dB] is used to illustrate its transient behaviour and is given as

$$SIR[i] = \frac{|v_{K+1,IO}[i]|^2}{\sum_{k=2,k\neq K+1}^{2K} |v_{k,IO}[i]|^2 + \sigma_n^2 \|\mathbf{w}_1[i]\|^2}, \tag{5.46}$$

where $v_{k,IO}[i]$ is defined in (5.27). All SIRs are averaged over 100 Monte Carlo runs.

[6] Unlike (5.2), fractional chip delay is considered in the timings of interfering users.

5.6.3 Discussion

As shown in Figure 5.2, with $M = 1$, the SIRs of the constrained CMA and constrained MOE detector are almost the same. This is because under a noiseless assumption, both constrained inverse filtering methods converge to the decorrelating detector. From Figure 5.2 (b) and (c) respectively, it is shown that both constrained inverse filtering methods are robust to the effect of increasing number of resolvable paths L and NFR. However, it is observed that both methods suffer from a saturation effect which results in a significant gap away from the MMSE detector. In particular, this performance gap widens as L increases. A possible explanation is offered in [58, 122] that since optimisation takes place in a constrained space, the corresponding filter trajectory is not guaranteed to coincide with the global MMSE solution. Also, from the filter initialisation in (5.25), the nulling of ICI implies that the constrained inverse filtering method does not exploit all the energy of the received signal, and results in sub-optimal performance.

Figure 5.3 shows the SIR performance for $M = 2$ sensors. Comparing Figure 5.2 (b) with 5.3, all detectors are shown to have improved SIR performance. Finally to illustrate the importance of the modulus radius in the constrained CMA with $M = 1$, SIRs are plotted for various ξ in Figure 5.4. It is observed that the constrained CMA is unable to converge to the desired solution, if ξ is too large. This verified the claim in Section 5.5.2 that ξ should be small enough (i.e., $\xi < 3\alpha^2$) to suppress the stationary points in Class 1.2.

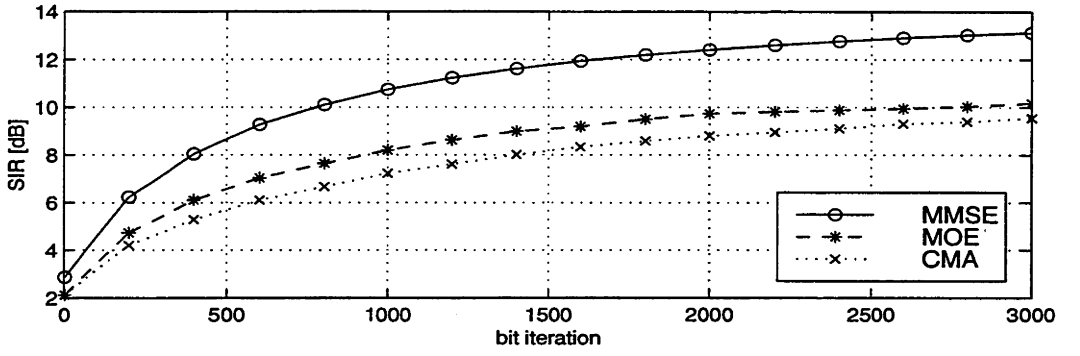

(a) $L = 3$ and $NFR = 0dB$

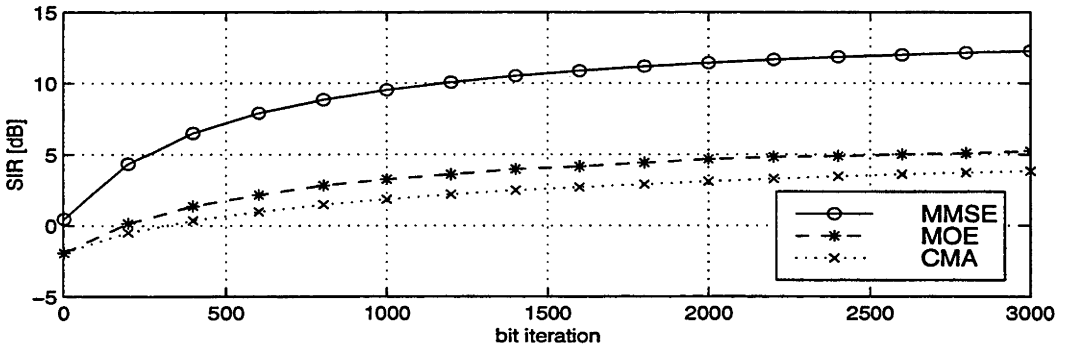

(b) $L = 6$ and $NFR = 0dB$

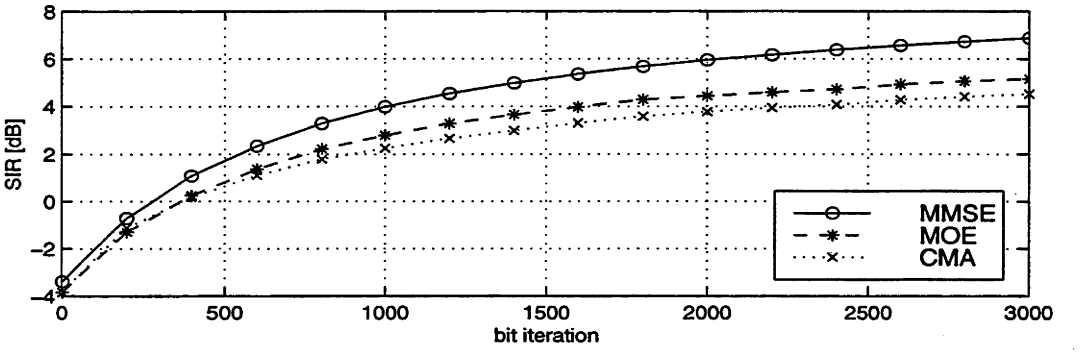

(c) $L = 3$ and $NFR = 6dB$

Figure 5.2: The transient SIR [dB] performance of the constrained CMA, constrained MOE and MMSE detectors: $N = 31$, $M = 1$, $K = 10$ and $SNR(k) = 15dB \quad \forall k \in \{2, \ldots, 10\}$.

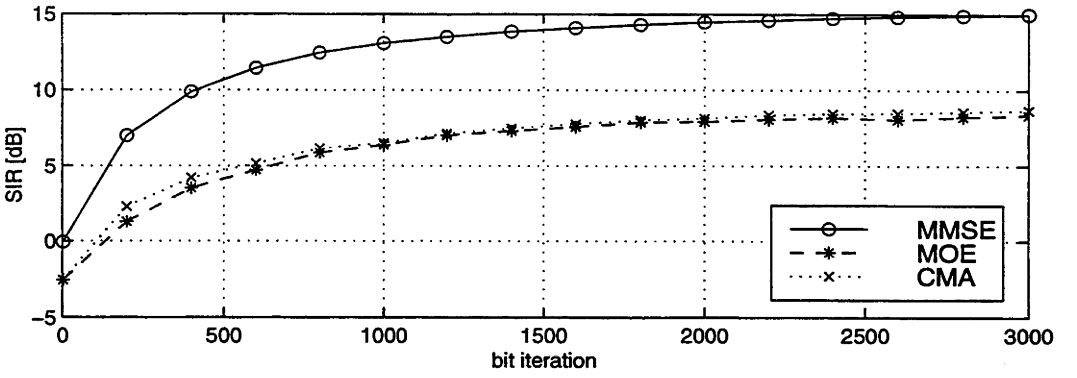

Figure 5.3: The transient SIR [dB] performance of the constrained CMA, constrained MOE and MMSE detectors with $M = 2$ sensors: $N = 31$, $K = 10$, $L = 6$, and $SNR = 15dB$ for all users.

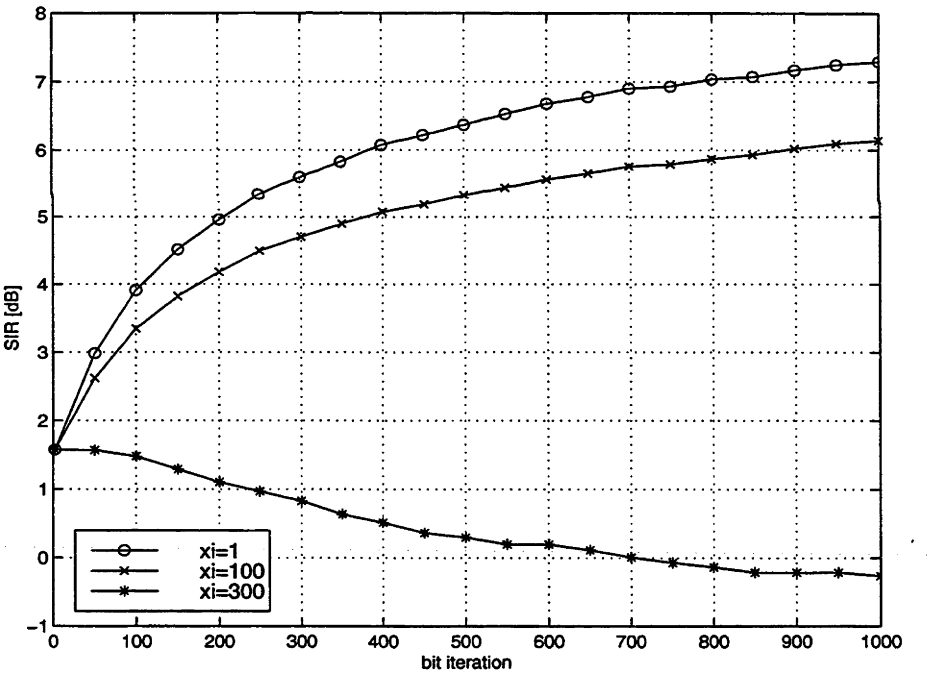

Figure 5.4: The transient SIR [dB] performance of the constrained CMA detector with various modulus radius ξ: $N = 31$, $K = 10$, $M = 1$, and $SNR = 15dB$ for all users.

5.7 Conclusions

In this chapter, based on the constrained inverse filtering concept, a blind linear multiuser detector based on the constrained CMA, is proposed. Using an orthogonal filter decomposition, the multipath induced ICI and ISI are removed such that the CMA-based adaptation is solely used to suppress MAI. It is shown that unlike the unconstrained CMA, lock convergence is ensured in the constrained CMA. However, a new class of hidden stationary points arise, which can be suppressed if certain rank condition in the MIMO model is satisfied. Also, in order to prevent the filter adaptation from being trapped in some saddle regions, the modulus radius should be sufficiently small. Finally, especially in severe multipath propagation conditions, it is observed that the constrained filtering approach suffers from a performance gap between the converged blind detector and the training-based MMSE detector.

Chapter 6

Effect of Arrival of Additional Users

6.1 Chapter Outline

In this chapter, the effect of arrival of additional users to the CMA-based and the MOE-based multiuser detectors are examined, and compared with the training-based MMSE detector, in terms of their transient performance (e.g., SIR and MSE). This chapter is organised as follows. Section 6.2 gives the motivation of investigating the effect of arrivals of new interferers. Section 6.3 lists past works that were done on multiuser detection with a dynamic user population. Section 6.4 describes the signal model, and the analytical approach that models the perturbation caused by the sudden birth of interferers. Section 6.5 examines this perturbation in terms of the corresponding deformations of cost error surfaces under a noiseless setting. Section 6.6 contains the simulations of the transient performances of the CMA, the MOE and the MMSE detectors with sudden inclusions of new users. Section 6.7 gives the chapter's conclusions.

6.2 Motivation

The main focus of analysis of multiuser detection has been the steady state performance. For example, as described in Section 2.5.5, sub-optimal, near far resistant, linear multiuser detectors (e.g., the decorrelator) have been developed to relax the power control requirement in the conventional MF detector. In the context of cellular system, it is of considerable interest to study the robustness of multiuser detectors with the random arrival and departure of inter-cell or intra-cell users. This is because in practice, users activate and terminate their access at random times.

As the number of users K changes, the MAI level varies which can compromise the (non-) adaptability of the multiuser detectors. To illustrate the effect of a time-varying user population, the following two multiuser detectors are discussed as case studies.

1. **Linear Decorrelator** — whenever K changes, this detector (2.37) requires re-computation of the signature cross-correlation matrix $\mathbf{R}$. Thus, the decorrelator is ill-suited to adaptation in a time-varying user population.

2. **Subspace-based** — although this method is analytically tractable, it relies on the estimation of signal subspace by choosing the K largest eigenvalues of $\mathbf{R}_{\mathbf{yy}}$ (i.e., the rank of the signal subspace). Typically, the number of active users can be estimated adaptively using information theoretic criteria such as *Akaike information criterion* or *minimum description length* [123]. Also, as with all SOS-based methods, during the estimation of $\mathbf{R}_{\mathbf{yy}}$, all system parameters are assumed to be constant. Thus, the batch form of the subspace-based multiuser detector is non-adaptive to K, since $\mathbf{R}_{\mathbf{yy}}$ is required to be re-estimated whenever K changes.

6.3 Literature Review

In this section, a literature review is presented in the context of multiuser detection under a dynamic user population. Because real-life systems are too complex

to model exactly, the arrival and departure of users can be modelled by different stochastic processes under different assumptions [1]. Two popular traffic models are Poisson and binomial models which are special cases of the Markov chain model. The traffic load is typically measured in Erlangs per cell (defined in Section 1.1.2).

The following multiuser detectors contain simulation results of multiuser detection under changes in K.

- *LMS-MMSE detector with decision feedback* — the effect of the sudden birth and death of users on the transient MSE performance is examined in [46]. As expected, if some users terminate their access, it will cause a gradual improvement of the transient MSE. The powering-on of some strong interferers can cause a sudden drop in detection performance for all users.

- *Various adaptive detectors* — the average SIR and BER are plotted as a function of traffic loads for different linear adaptive multiuser detectors (e.g., LMS-MMSE, RLS-MMSE and subspace-based) in [124]. A multiple cell system model is used with Poisson arrival process. It is shown that in comparison to the conventional MF approach, all adaptive methods can support much higher traffic loads under moderate power controls. However, unless a training sequence is re-transmitted occasionally, their performances in the DD mode can deteriorate quickly at high traffic loads.

- *Subspace-based detectors* — it is shown [82] that using a subspace tracking algorithm, the subspace-based multiuser detector can outperforms the RLS-based MOE detector in [55] with lesser complexity. Also, it can adapt rapidly to the random (dis-)appearance of interferers.

- *Provision for new users* — by constraining the spreading codes to be used by the active users, an adaptive decorrelator is developed in [42] that can blindly determine the spreading code of a new user. In practice, multiuser detectors do not know when there is presence of new users. In [125], ML tests are developed to estimate the number of active users present in the system.

A literature survey has revealed that for multiuser detection, most research on the effect of channel dynamics target at the effect of multipath fading. Robustness issues with respect to the effect of a dynamic user population have largely been neglected in the literature.

6.4 System Modelling

In this section, the signal model and the analytical approach used to model the perturbation caused by arrival of new interferers are presented. It is assumed that the nominal number of users at steady state is K_m. The aim is to examine the perturbation caused by a sudden inclusion of $(K_p - K_m)$ users (i.e., $K_p > K_m$). To account for the presence of new users, variables with subscript m denotes modelled contributions from K_m users, while subscript p denotes perturbation from $(K_p - K_m)$ users.

6.4.1 Signal Model

Assume no signature mismatch (i.e., no multipath effect), the synchronous DS-CDMA system model in (2.30) is used as the received signal model. For the ith bit, the N chip samples of received signal can be written as

$$\mathbf{Y}[i] = \mathbf{SAb}[i] + \mathbf{n}[i] = (y[i,1], \ldots, y[i,N])^T,$$

where $\mathbf{A}$ is an $(K_p \times K_p)$ diagonal matrix composed of A_k, $\mathbf{b}[i] = (b_1[i], \ldots, b_{K_p}[i])^T$ is an K_p-length column vector of the ith bit of each user, and $\mathbf{n}[i]$ is an N-length vector of noise samples. Specifically, to account for the presence of new users, the $(N \times K_p)$ signature matrix is partitioned into the modelled and perturbation terms as follows

$$\mathbf{S} = \mathbf{S}_m + \mathbf{S}_p = (\mathbf{s}_1, \ldots, \mathbf{s}_{K_p}), \tag{6.1}$$

where

$$\mathbf{S}_m \triangleq \left(\mathrm{s}_1, \ldots, \mathrm{s}_{K_m} \overbrace{0,\ 0 \ldots, 0}^{K_p - K_m} \right),$$

$$\mathbf{S}_p \triangleq \left(\overbrace{0,\ 0 \ldots, 0}^{K_m}\ \mathrm{s}_{K_m+1}, \ldots, \mathrm{s}_{K_p} \right). \tag{6.2}$$

6.4.2 Robustness in terms of User Gains

As defined in (3.24), the user's contribution in the filter output $Z_1[i]$ is measured by its user gain $\mathbf{V}[i]$. In the same manner as (6.1), the user gain can be partitioned in the modelled term $\mathbf{V}_m[i]$ and the perturbation term $\mathbf{V}_p[i]$ as follows

$$\begin{aligned} \mathbf{V}[i] &= (\mathbf{SA})^T \mathbf{w}_1[i] \\ &= \left(v_1[i], \ldots, v_{K_p}[i]\right)^T \\ &= \mathbf{V}_m[i] + \mathbf{V}_p[i], \end{aligned} \tag{6.3}$$

where

$$\begin{aligned} \mathbf{V}_m[i] &= (\mathbf{S}_m\mathbf{A})^T \mathbf{w}_1[i] \\ &= \left(v_1[i], \ldots, v_{K_m}[i], \overbrace{0,\ 0, \ldots, 0}^{K_p - K_m} \right)^T, \\ &\triangleq \left(\gamma_1[i], \ldots, \gamma_{K_p}[i]\right)^T, \\ \mathbf{V}_p[i] &= (\mathbf{S}_p\mathbf{A})^T \mathbf{w}_1[i] \\ &= \left(\overbrace{0,\ 0, \ldots, 0}^{K_m},\ v_{K_m+1}[i], \ldots, v_{K_p}[i] \right)^T \\ &\triangleq \left(\epsilon_1[i], \ldots, \epsilon_{K_p}[i]\right)^T, \end{aligned} \tag{6.4}$$

with γ_k and ϵ_k are the kth modelled and perturbation user gain respectively. From (6.3) and (6.4), it is seen that

$$\begin{aligned} v_k[i] &= \gamma_k[i] + \epsilon_k[i], \quad \text{where } k \in \{1, \ldots, K_p\}, \\ \gamma_k[i] &= 0 \quad \forall k \in \{K_m + 1, \ldots, K_p\}, \quad \text{and} \\ \epsilon_k[i] &= 0 \quad \forall k \in \{1, \ldots, K_m\}. \end{aligned} \tag{6.5}$$

When the number of users is K_m (i.e., no arrival of additional users), $\mathbf{V}_p[i] = \mathbf{0}$. Under a noiseless setting, the steady state solution of the MOE, the CMA and the MMSE detectors all approach the decorrelator detector. Thus, the residual user gains of the interfering users $v_k[i]$ or $\gamma_k[i]$ $\forall k \in \{2, \ldots, K_m\}$ represent the deviations of a given linear multiuser detector from the decorrelating solution.

6.5 Change in the CM, MSE and MOE Costs

To examine the robustness of the CMA, the MOE and the MMSE detectors with respect to the arrival of $(K_p - K_m)$ users, their cost functions are expressed in terms of the partitioned user gains $\mathbf{V}_m[i]$ and $\mathbf{V}_p[i]$ in (6.3). It is assumed that a decorrelating solution can be achieved for the existing K_m users. Then, the effect of perturbation due to new users is represented by the error surface deformation due to $\mathbf{V}_p[i]$. This is analogous to the algebraic approach in [88] that analyses the robustness of the fractionally spaced CMA to channel undermodelling. Also, the perturbation on the corresponding derivative of cost function with respect to individual user gain is examined. For notational convenience, the bit index i is suppressed.

6.5.1 CM Cost

Substituting (3.24) into (2.45), the CM cost function can be written as a function of user gains $\mathbf{V}$ as

$$\begin{aligned} J_{CM} &= E\left\{\left(\left(\mathbf{V}^T\mathbf{b}\right)^2 - \xi\right)^2\right\} \\ &= E\left\{\left(\mathbf{V}^T\mathbf{b}\right)^4\right\} - 2\xi \cdot E\left\{\left(\mathbf{V}^T\mathbf{b}\right)^2\right\} + \xi^2. \end{aligned} \tag{6.6}$$

In the same manner as the temporal based CMA in [126], given that each user uses a BPSK, zero-mean, equiprobable and independent source, the expectation terms in (6.6) can be written as

$$E\left\{\left(\mathbf{V}^T\mathbf{b}\right)^2\right\} = \sum_{k=1}^{K_p}\sum_{l=1}^{K_p} v_k v_l E\{b_k b_l\} = \sum_{k=1}^{K_p} v_k^2, \tag{6.7}$$

and

$$E\left\{\left(\mathbf{V}^T\mathbf{b}\right)^4\right\} = \sum_{k=1}^{K_p}\sum_{l=1}^{K_p}\sum_{m=1}^{K_p}\sum_{n=1}^{K_p} v_k v_l v_m v_n E\left\{b_k b_l b_m b_n\right\}. \tag{6.8}$$

From Appendix A, using (A.5), the non-zero terms in (6.8) can be collected as

$$E\left\{\left(\mathbf{V}^T\mathbf{b}\right)^4\right\} = 3\sum_{k=1}^{K_p}\sum_{l=1}^{K_p} v_k^2 v_l^2 + \sum_{k=1}^{K_p} v_k^4. \tag{6.9}$$

Substituting (6.5) into (6.7) and (6.9), the expectation terms in (6.6) can be expressed in terms of γ_k and ϵ_k as

$$\begin{aligned} E\left\{\left(\mathbf{V}^T\mathbf{b}\right)^2\right\} &= \sum_{k=1}^{K_m}\gamma_k^2 + \sum_{k=K_m+1}^{K_p}\epsilon_k^2 \\ E\left\{\left(\mathbf{V}^T\mathbf{b}\right)^4\right\} &= 3\left(\sum_{k=1}^{K_m}\sum_{\substack{l=1\\ l\neq k}}^{K_m}\gamma_k^2\gamma_l^2 + \sum_{k=K_m+1}^{K_p}\sum_{\substack{l=K_m+1\\ l\neq k}}^{K_p}\epsilon_k^2\epsilon_l^2 + 2\sum_{k=1}^{K_m}\sum_{l=K_m+1}^{K_p}\gamma_k^2\epsilon_l^2\right) \\ &\quad + \sum_{k=1}^{K_m}\gamma_k^4 + \sum_{K_m+1}^{K_p}\epsilon_k^4 \end{aligned} \tag{6.10}$$

Substituting (6.10) into (6.6) and collecting terms involving ϵ_k, the perturbation in the CM cost function due to arrival of new users is given by

$$\Delta J_{CM} = -2\xi\sum_{k=K_m+1}^{K_p}\epsilon_k^2 + \sum_{k=K_m+1}^{K_p}\epsilon_k^4 + 3\sum_{k=K_m+1}^{K_p}\sum_{\substack{l=K_m+1\\ l\neq k}}^{K_p}\epsilon_k^2\epsilon_l^2 + 6\sum_{k=1}^{K_m}\sum_{l=K_m+1}^{K_p}\gamma_k^2\epsilon_l^2. \tag{6.11}$$

If the perturbation user gain ϵ_k is small enough, the higher order terms of ϵ_k^4 and $\epsilon_k^2\epsilon_l^2$ in (6.11) can be neglected. Furthermore, it is assumed that the inclusion of interferers occur when the CMA detector is in the vicinity of lock convergence in

(3.27). Then the CM cost perturbation in (6.11) can be approximated as

$$\begin{aligned}\Delta J_{CM} &\simeq -2\xi \sum_{k=K_m+1}^{K_p} \epsilon_k^2 + 6 \sum_{k=1}^{K_m} \sum_{l=K_m+1}^{K_p} \gamma_k^2 \epsilon_l^2 \\ &= -2\xi \sum_{k=K_m+1}^{K_p} \epsilon_k^2 + 6\xi \sum_{k=K_m+1}^{K_p} \epsilon_k^2 \\ &= 4\xi \sum_{k=K_m+1}^{K_p} \epsilon_k^2. \end{aligned} \tag{6.12}$$

From (A.9), the derivative of J_{CM} with respect to v_k is given by

$$\frac{1}{4}\nabla_{v_k} J_{CM} = \left[3 \sum_{i=1}^{K_m} \gamma_i + 3 \sum_{j=K_m+1}^{K_p} \epsilon_j - \xi - 2v_k^2 \right] v_k \quad \text{where } k \in \{1, \ldots, K_p\}. \tag{6.13}$$

In the same manner as (6.12), near lock convergence, (6.13) can be written as

$$\begin{aligned}\frac{1}{4}\nabla_{v_k} J_{CM} &= \left[2\xi + 3 \sum_{j=K_m+1}^{K_p} \epsilon_j - 2v_k^2 \right] v_k \\ &= \begin{cases} 3\sqrt{\xi} \sum_{j=K_m+1}^{K_p} \epsilon_j^2 & \text{if } k = 1, \\ 0 & \text{if } k \in \{2, \ldots, K_m\}, \\ \left[2\xi + 3 \sum_{j=K_m+1}^{K_p} \epsilon_j^2 - 2\epsilon_k^2 \right] \epsilon_k & \\ \quad \simeq 2\xi\epsilon_k & \text{if } k \in \{K_m+1, \ldots, K_p\}, \end{cases} \end{aligned} \tag{6.14}$$

where the higher order terms of $\epsilon_k \epsilon_j^2$ are neglected. The CM cost perturbation and its derivative in (6.12) and (6.14) are to be used for comparison with other cost functions in Section 6.5.4.

6.5.2 MSE Cost

In the same manner as deriving (6.6), in terms of user gains $\mathbf{V}$, the MSE criterion in (2.41) is given by

$$\begin{aligned} J_{MSE} &= E\left\{ \left(\mathbf{V}^T \mathbf{b} - \hat{b}_1 \right)^2 \right\} \\ &= E\left\{ \left(\mathbf{V}^T \mathbf{b} \right)^2 \right\} - 2E\left\{ \hat{b}_1 \mathbf{V}^T \mathbf{b} \right\} + 1. \end{aligned} \tag{6.15}$$

Since each user source is independent in bit sense (i.e., $E\{b_k b_l\} = 0 \quad \forall k \neq l$), the second expectation term in (6.15) can be simplified as

$$\hat{b}_1 \mathbf{V}^T \mathbf{b} = \hat{b}_1 \left(\sum_{k=2}^{K_m} \gamma_k b_k + \sum_{k=K_m+1}^{K_p} \epsilon_k b_k \right) + \hat{b}_1 \gamma_1 b_1 = \gamma_1, \tag{6.16}$$

where the training-based bit estimate $\hat{b}_1$ is assumed to be correct. Substituting (6.5), (6.7) and (6.16) into (6.15), J_{CM} can be expressed in terms of γ_k and ϵ_k as

$$J_{MSE} = 1 + \sum_{k=1}^{K_m} \gamma_k^2 + \sum_{k=K_m+1}^{K_p} \epsilon_k^2 - 2\gamma_1. \tag{6.17}$$

Thus, the change in the MSE cost function due to arrival of new interferers is

$$\Delta J_{MSE} = \sum_{K_m+1}^{K_p} \epsilon_k^2. \tag{6.18}$$

Also, the derivative of J_{MSE} with respect to v_k is given by

$$\frac{1}{2} \nabla_{v_k} J_{MSE} = \begin{cases} v_k - 1 = \gamma_1 - 1 = 0 & \text{if } k = 1, \\ v_k = \gamma_k & \text{if } k \in \{2, \ldots, K_m\}, \\ v_k = \epsilon_k & \text{if } k \in \{K_m + 1, \ldots, K_p\}. \end{cases} \tag{6.19}$$

This is in a form that is suitable for later comparison in Section 6.5.4.

6.5.3 MOE Cost

From (2.44), in terms of γ_k and ϵ_k, the MOE cost function is given by

$$J_{MOE} = E\left\{ \left(\mathbf{V}^T \mathbf{b} \right)^2 \right\} = \sum_{k=1}^{K_m} \gamma_k^2 + \sum_{k=K_m+1}^{K_p} \epsilon_k^2. \tag{6.20}$$

Then, the change in the MOE cost due to new users is

$$\Delta J_{MOE} = \sum_{k+K_m+1}^{K_p} \epsilon_k^2. \tag{6.21}$$

Also, the derivative of J_{MOE} with respect to v_k is given by

$$\frac{1}{2} \nabla_{v_k} J_{MOE} = v_k = \begin{cases} \gamma_k & \text{if } k \in \{1, \ldots, K_m\}, \\ \epsilon_k & \text{if } k \in \{K_m + 1, \ldots, K_p\}. \end{cases} \tag{6.22}$$

If the constrained MOE algorithm in (3.17) is used, $\frac{1}{2}\nabla_{v_1} J_{MOE} = 0$, since the desired user's gain is constrained as $v_1 = aA_1$, with a as the constraint constant in (3.14).

6.5.4 Comparison of CM, MSE and MOE costs

From (6.18) and (6.21), it is observed that the deformations of MSE and MOE error surface due to new interferers, are the same. Also, from (6.19) and (6.22), if a decorrelating solution has been obtained for the existing K_m users, the derivatives of the MSE and constrained MOE cost functions are the same. This follows the fact that the MOE and MSE cost functions are related by an energy constant, as given in (3.9).

Comparing the CM and MSE cost perturbations, from (6.12) and (6.18), it is seen[1] that $\Delta J_{CM} \simeq 4\xi \cdot \Delta J_{MSE}$. In the case of the CMA, from (6.14), the adaptation of the desired user's gain v_1 and user gains of new interferers v_k, where $k \in \{K_m + 1, \ldots, K_p\}$, are dependent on the modulus radius ξ. Thus, the choice of ξ should be small enough such that for a small perturbation due to arrival of new users, the lock convergence of the CMA stays in a tight neighbourhood of the MMSE minimum. Finally, if the existing number of users K_m is large, the interfering users' gains $\gamma_k \quad k \in \{2, \ldots, K_m\}$ in the last term of (6.12) may become significant. Hence, the robustness of the CMA to new users decreases as K_m approaches the spreading length N.

6.6 Simulation Results

In this section, simulation results are presented to show the transient performance of the constrained MOE and the CMA multiuser detectors in (3.17) and (3.23), respectively. They are compared with the training-based LMS-MMSE detector in (2.43) and the conventional MF detector in (2.32). The simulations are performed to verify the analysis of deformation of cost functions in Section 6.5.

[1] The same result was obtained in [88] for the CMA-based fractionally-spaced equaliser under channel undermodelling and equaliser truncation.

6.6.1 System Parameters and Performance Measures

Both system parameters and performance measures are the same as Section 3.8.1 and 3.8.2. The DS-CDMA system considered, has uncoded, synchronous users with BPSK modulation and $N = 31$. Let the desired user be $k = 1$, and all multiuser detectors have MF initialisation (i.e., $\mathbf{w}_1[0] = \mathbf{s}_1$). The step size is $\mu = 10^{-4}$ for the constrained MOE and LMS-MMSE algorithms, and $\mu = 5 \cdot 10^{-6}$ for the CMA[2]. Both the modulus radius of the CMA ξ, and the constraint constant a of the constrained MOE are normalised as $\xi = A_1^2$ and $a = 1$.

As defined in (3.58), the SIR is used to measure its transient performance. To illustrate the arrival of new users, the system starts with 5 users, and another $(K_p - K_m) = 5$ users are added every 5000 bits to a maximum of 20 users. The near far effect is set to $NFR = 6dB$. Also, for each detector, the MSE is computed and is normalised with respect to the MSE cost function (i.e., $\gamma_1[i \to \infty] = 1$) in (2.41). A total of 100 independent Monte Carlo runs are used to compute the SIR and normalised MSE plots.

6.6.2 Discussion

As shown in Figure 6.1, all three adaptive algorithms have the same initial drop of the SIR, whenever there is addition of new interferers. As supported in [55], it is observed that the steady state MOE solution suffers from a saturation effect that causes the converged MOE detector to deviate significantly from the training-based MMSE detector. Also, as more users are added, the transient SIR of the CMA becomes slower to recover. This can be explained by the larger deformation in the CM error surface for larger K_m, as observed in (6.11). As expected, the conventional MF deteriorates gives the worst SIR performance, and is not robust at all to the presence of new users. As shown in Figure 6.2, it is seen that the normalised MSEs of the constrained MOE and the CMA detectors both approach that of the MMSE case. Thus, for small perturbations, the lock convergence of the CMA stays in the neighbourhood of the MMSE minimum.

[2] The step sizes μ for these detectors are chosen to be small enough to ensure convergent stability for large user population.

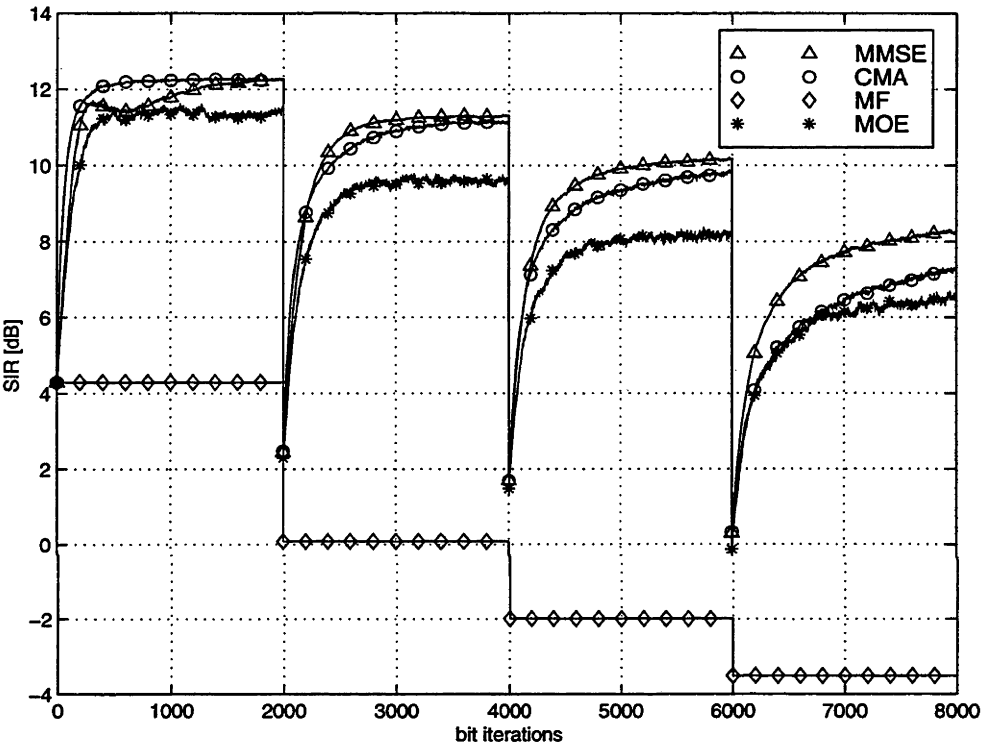

Figure 6.1: The transient SIR performance of the training-based MMSE, the CMA, the constrained MOE and the MF detectors, when there are sudden arrivals of 5 new users every 5000 bits: $NFR = 6dB$ and $SNR(k = 1) = 10dB$.

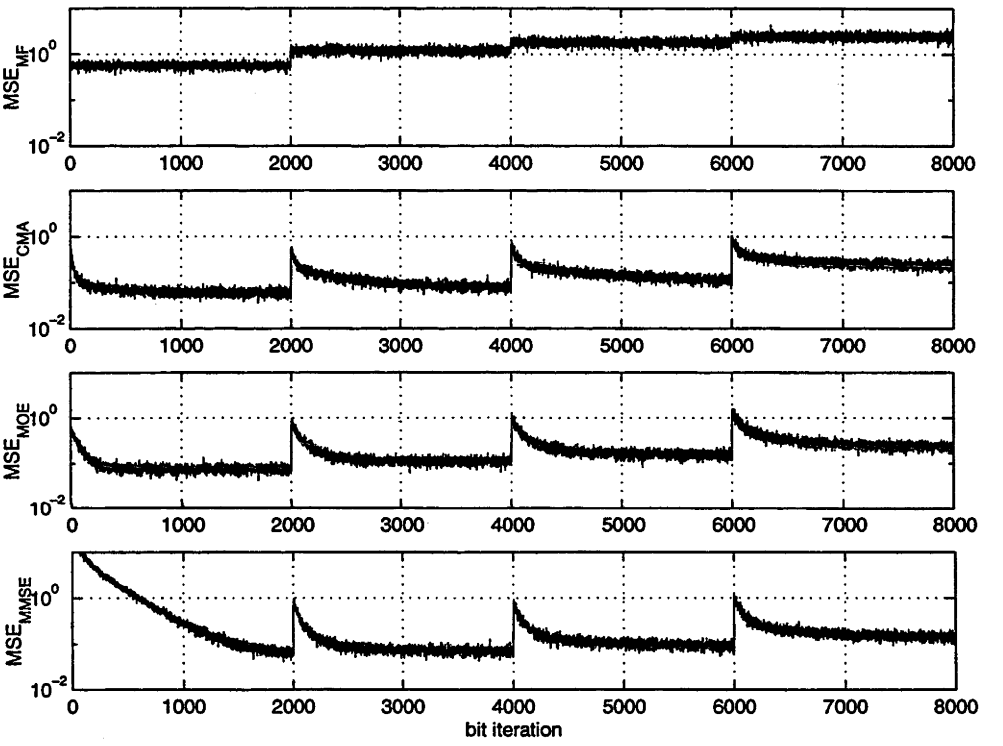

Figure 6.2: The transient normalised MSE performance of Figure 6.1.

6.7 Conclusions

In this chapter, the effect of arrival of additional users to the CMA, MOE and MMSE multiuser detectors are examined in terms of its perturbation on their cost functions and derivatives. It is shown that for small perturbation, provided that the modulus radius is not excessively large, the lock convergence of the CMA stays in the neighbourhood of the MMSE minimum. Although the perturbation in the MOE cost function is the same as the MMSE, the MOE detector attains a lower steady state SIR performance compared to the CMA. Also, the CMA detector becomes less robust, as the previous existing number of users increases. However, since the change in the cost functions and their derivatives concern mainly with the initial drop in the SIR performance, further insight into their tracking capabilities for a time-varying user population is required.

Chapter 7

Constrained CMA-based Code Acquisition Scheme

7.1 Chapter Outline

Previous chapters have assumed that the knowledge of the desired user's time delay. However, in DS-CDMA systems, code synchronisation must take place before any multiuser detection. As the initial synchronisation stage, a code acquisition scheme is used to estimate the relative timing phase of the desired transmission in chip intervals. The uncertainty of the required delay is initially discretised in chip intervals, which are associated with a number of hypotheses. In this chapter, a blind code acquisition scheme using an adaptive linear filtering based on a constrained CMA, is proposed to choose the best delay in chip intervals.

This chapter is organised as follows. Section 7.2 gives the background of the code acquisition problem. Section 7.3 describes the discrete-time received signal model and its equivalent synchronous model. Section 7.4 gives a review of various code acquisition methods in the literature. Section 7.5 presents the proposed constrained CMA-based acquisition scheme. Section 7.6 gives the simulation results which compare the proposed method with the conventional sliding correlator, the subspace-based and the MOE-based methods. Finally, Section 7.7 contains the chapter's conclusions.

7.2 Background

In any CDMA system, code synchronisation is a critical issue, since it must be done before any multiuser detection can be applied. Code synchronisation can be divided into two parts: code acquisition and tracking. Code acquisition is the initial coarse estimation of the relative timing phase of the desired transmission, usually within one chip interval. As the delay offset between the actual and estimated timing is within the pull-in range of the tracking loop, tracking is initiated for finer adjustment of the delay estimate. Tracking is used to minimise the delay offset error, and to compensate for the changes caused by channel variations (e.g., Doppler effect) and clock instabilities [127].

As discussed in Section 2.5.3, the conventional MF approach assumes perfect knowledge of the timing and the usage of quasi-orthogonal modulation. However, it is emphasised that orthogonal signature waveforms in the synchronous system do not translate their orthogonalities in the asynchronous case. Thus, under the assumption of synchronised users, bounds derived for MFs will always give over-optimistic results [17].

It has been shown that in the presence of MAI, the acquisition problem can significantly reduce the system capacity, especially when the timing uncertainties are large [6]. This so-called *acquisition-limited capacity* [128] is lower, but more realistic than the one deriving using the BER or SNR criteria with perfect synchronism assumed. For simplicity, in this chapter, it is assumed that there is no frequency uncertainty in the code acquisition problem[1]. Then, the acquisition problem is to estimate the relative delay of the desired user in the time domain. Since short codes are used, the delay uncertainty region is bounded within one symbol period, and is discretised into chip intervals. There is a hypothesis for every chip delay. The aim is to choose the best hypothesis based on some *decision variables* that should give the correct chip timing estimate. In a blind setting, the code acquisition is carried out where neither training nor the knowledge of all signature waveforms of interfering users are available.

[1] The delay uncertainty is in time and frequency, when there is oscillator drift and/or Doppler offset.

7.3 System Modelling

In this section, the system model of an uncoded K-users asynchronous DS-CDMA system is presented. In particular, the equivalent synchronous discrete-time model is considered.

7.3.1 Discrete-Time Received Signal Model

The following assumptions are made that lead to a simplified system model:

A1. A heuristic approach is taken whereby the carrier synchronisation is done prior to the code acquisition stage. For simplicity, it is assumed that there is no frequency uncertainty due to Doppler offset and/or oscillator drift; thus, all system parameters are real variables.

A2. This work does not consider the scenario of signature mismatch. That is, there is no modelling errors in the received signature waveforms (e.g., due to multipath effects).

A3. For simplicity, it is assumed that all time delays remain fixed during the acquisition process.

A4. The case of underloaded system is considered (i.e., number of users is less than the spreading length $K < N$).

From (2.18), the total received signal in an asynchronous DS-CDMA system is given by

$$y(t) = \sum_{k=1}^{K} A_k \sum_{i} b_k[i] s_k(t - iT_b - \tau_k) + n(t), \tag{7.1}$$

where $\tau_k \in [0, T_b)$, A_k, $b_k[i] \in \{\pm 1\}$ and $s_k(t)$ are the relative time delay, received amplitude, the ith transmitted bit and signature waveform of the kth user respectively, and $n(t)$ is the AWGN. In the acquisition scheme, since the adaptive filtering is used with a symbol-by-symbol processing, the length of observation

interval is set to one bit T_b long. Thus, for chip-rate sampling, the discrete-time received signal vector of the ith bit contains N chip samples, and is given by

$$\mathbf{Y}[i] = \sum_{k=1}^{K} \mathbf{Y}_k[i] = (y[i,1], \ldots, y[i,N])^T, \tag{7.2}$$

where $y[i,n]$ is given in (2.31), and $\mathbf{Y}_k[i]$ is the contribution from the kth user. It should be noted that the results presented in this chapter can be easily extended[2] to the longer observation interval of $2T_b$ as in [6].

7.3.2 Equivalent Synchronous Model

In order to separate the ISI (i.e., contribution from the adjacent bits) from the desired transmission, as discussed in Section 2.5.2, the K-users asynchronous system can be transformed to an equivalent synchronous system with $2K$ independent users [6, 84]. In the remainder of this section, this transformation is applied to the received signal in (7.2). First, the left and right partitions of the spreading sequence of the kth user in (2.2) are defined respectively as

$$\begin{aligned} \mathbf{c}_{n,L}(x) &\triangleq \left[c_k[N-n+1] \ldots c_k[N] \overbrace{0 \ldots 0}^{N-n} \right]^T, \\ \mathbf{c}_{n,R}(n) &\triangleq \left[\overbrace{0 \ldots 0}^{n} \, c_k[1] \ldots c_k[N-n] \right]^T, \end{aligned} \tag{7.3}$$

where $c_k[n]$ is the nth spreading code of the kth user, and $n \in \{0, \ldots, N-1\}$. Then, the time delay of the kth user can be expressed in terms of its integral and fractional chip duration as

$$\tau_k = (\eta_k + \delta_k) T_c, \tag{7.4}$$

where $\eta_k \in \{0, \ldots, N-1\}$ is an integer, and $\delta_k \in [0, 1)$ is a fractional real number.

Since the exact chip timings of different users are unknown, the integration interval of the chip MF in (2.31) is chosen arbitrarily. This implies that the

[2] In [6], an $2T_b$-long observation interval is used to ensure that one complete bit of the desired transmission is encompassed.

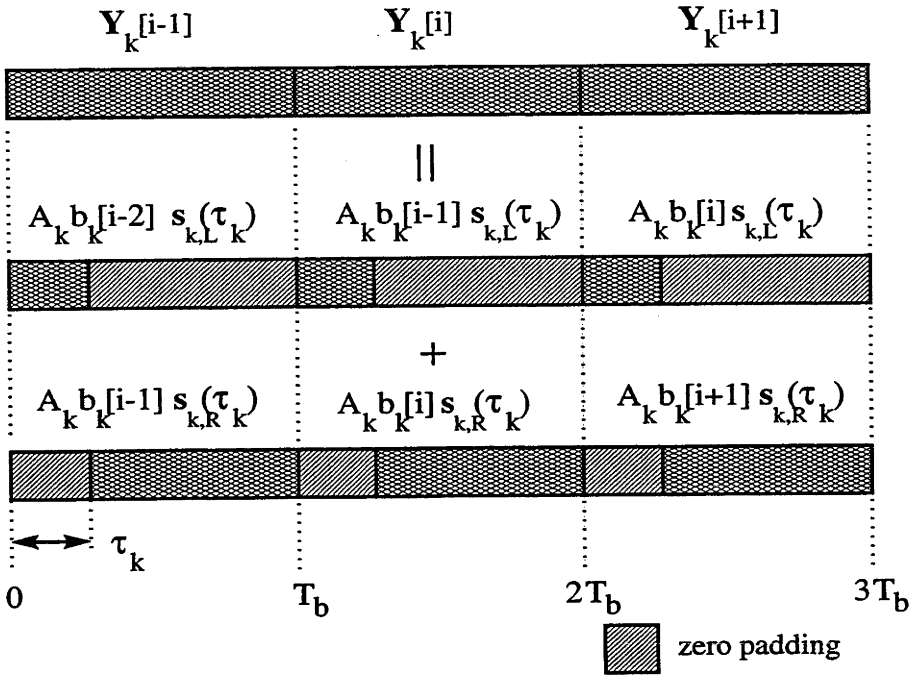

Figure 7.1: Left and right partitions of the discrete-time signature of the kth user, in an one-shot signal model [5, 6].

system is chip-asynchronous, where each chip sample in $\mathbf{Y}_k[i]$ in (7.2) consists of contributions from two adjacent chips, depending on the fractional chip delay δ_k in (7.4). The corresponding left and right partitions of the discrete-time signature of the kth user can be expressed as convex combinations of two adjacent chips, and are given respectively by

$$\begin{aligned} \mathbf{s}_{k,L}(\tau_k) &= (1-\delta_k)\mathbf{c}_{k,L}(\eta_k) + \delta_k \mathbf{c}_{k,L}(\eta_k+1), \\ \mathbf{s}_{k,R}(\tau_k) &= (1-\delta_k)\mathbf{c}_{k,R}(\eta_k) + \delta_k \mathbf{c}_{k,R}(\eta_k+1). \end{aligned} \tag{7.5}$$

Using (7.5), the contribution of the received signal vector from the kth user can be written as[3]

$$\mathbf{Y}_k[i] = A_k \left(b_k[i-1]\mathbf{s}_{k,L}(\tau_k) + b_k[i]\mathbf{s}_{k,R}(\tau_k) \right). \tag{7.6}$$

[3] Since $\tau_k \in [0, T_b)$ is assumed in this chapter, the ISI in the received signal $\mathbf{Y}_k[i]$ in (7.6) is of the previous bit $b_k[i-1]$. However, a more general description is to use $\tau_k \in (\frac{-1}{2}T_b, \frac{1}{2}T_b)$ which would involve either $b_k[i-1]$ and $b_k[i+1]$ as the ISI.

Three consecutive bits of $\mathbf{Y}_k[i]$ in (7.6) is illustrated in Figure 7.1 which shows the received signal as the sum of signals from the left and right partitions of the kth signature. Substituting (7.6) into (7.2), the received signal vector of the ith bit has the same one-shot form as (5.11), and is given by

$$\mathbf{Y}[i] = \mathbf{S}(\boldsymbol{\tau})\mathcal{A}\mathcal{B}[i] + \mathbf{n}[i], \tag{7.7}$$

where $\mathbf{n}[i]$ is an N-length noise vector, $\mathcal{A}$ is an $(2K \times 2K)$ diagonal matrix with diagonal entries $(A_1, \ldots, A_K, A_1, \ldots, A_K)$, and

$$\begin{aligned} \boldsymbol{\tau} &\triangleq (\tau_1, \ldots, \tau_K) \\ \mathcal{B}[i] &\triangleq (b_1[i-1], \ldots, b_K[i-1], b_1[i], \ldots, b_K[i])^T \\ \mathbf{S}(\boldsymbol{\tau}) &\triangleq (\mathbf{s}_{1,L}(\tau_1), \ldots, \mathbf{s}_{K,L}(\tau_K), \mathbf{s}_{1,R}(\tau_1), \ldots, \mathbf{s}_{K,R}(\tau_K)) . \end{aligned} \tag{7.8}$$

From (7.7), it is observed that apart from the presence of MAI, the received vector is contaminated with ISI due to contribution from the desired user's previous bit (i.e., $A_1 b_1[i-1]\mathbf{s}_{1,L}(\tau_1)$).

7.4 Literature Review

In this section, different methods of code acquisition for DS-CDMA system in the literature are reviewed and described as follows.

- *ML-based methods* — in the same manner as the optimal MLSE multiuser detection in (2.36), delay estimates for all users are found by maximising the log-likelihood function for all possible data sequences. It involves solving a multi-dimensional optimisation problem that is mixed with both continuous and discrete parameters. In the absence of multipath fading and carrier phase offset, the ML estimator can be generalised as [86]

$$\begin{bmatrix} \hat{\mathcal{B}}_{ML} \\ \hat{\boldsymbol{\tau}}_{ML} \\ \hat{\mathcal{A}}_{ML} \end{bmatrix} = \arg \min_{\mathcal{B},\boldsymbol{\tau},\mathcal{A}} \sum_{i=1}^{Q} \|\mathbf{Y}[i] - \mathbf{S}(\boldsymbol{\tau})\mathcal{A}\mathcal{B}[i]\|^2 , \tag{7.9}$$

where Q is the length of received block in bits per user, and $\hat{\mathcal{B}}_{ML} = \left(\hat{\mathcal{B}}^T[1], \ldots, \hat{\mathcal{B}}^T[Q]\right)^T$, $\hat{\tau}_{ML}$ and $\hat{\mathcal{A}}_{ML}$ are the ML estimates of the transmitted bits, time delays and received amplitudes, respectively. This ML approach gives an optimal acquisition performance (e.g., near far resistant) at the expense of prohibitive computation complexity.

Various modified ML method have also been developed. In [86,129], a blind, approximate ML delay estimator using a variable type projection algorithm, is proposed. However, since its cost function is highly nonlinear with many local minima, it is sensitive to correct initialisation. In [130], a ML parameter estimation method is developed, by decomposing the multiuser estimation problem into a series of single-user problems. However, it relies on an all-one training sequence. In [131], a large sample ML timing estimator is derived by modelling the training sequence as the desired signal, and MAI as some independent coloured Gaussian noise. Other joint signal detection and parameter estimation methods include the extended Kalman Filter [132], the EM (estimation/maxisation) algorithm [133], and a recursive estimator using a reduced tree structure [134].

- *Correlation techniques* — similar to the MF detector, this is the conventional acquisition scheme whereby the received signal is correlated with the time delayed versions of the desired user's signature waveform [135]. It can be implemented as serial-search (i.e., *sliding correlator*) or parallel-search scheme, with tradeoff in acquisition time and computational complexity. The delay estimate is the one which gives the maximum correlation.

  The correlation techniques are based on the concept that each signature waveform consists of PN spreading codes which all have triangular autocorrelations. However, all disturbance sources in the correlator's output, namely contributions from MAI, AWGN and partial correlation of the same signature, are treated as independent Gaussian random variables. Thus, despite its simple implementation, the correlator is only optimal in a single-user scenario, or the case with orthogonal signatures. In multiuser environment, the correlation techniques fail especially under near far conditions.

- *Sequential estimation* — unlike the correlation techniques with fixed *dwell time* (i.e., time interval allocated to each hypothesis decision), a sequential search gathers information from past hypothesis decisions to improve current decisions [136]. In the same manner as the decision feedback detector, due to the problem of error propagation, its merits decrease with decreasing SNR or with an increasing number of users.

- *Adaptive Filtering* — this method replaces the MF with adaptive linear filtering. In [137], code acquisition based on a MMSE-based adaptive filtering is proposed. However, it requires that all training sequence be all-ones, and thus can not be used to acquire more than one user at a time. In [53], this all-ones restriction can be removed, by using its periodic training sequence as a signature.

- *SOS-based methods* — these include the subspace-based channel estimation [82, 84, 86] and the MOE-based methods [6, 58]. The SOS-based methods can be implemented blindly and are near far resistant. However, they require the estimation of the correlation matrices of the received signals $\mathbf{R}_{\mathbf{yy}}$ in (7.34). As discussed in Section 2.4.4, since $\mathbf{R}_{\mathbf{yy}}$ are sensitive to variations in the system parameters, these SOS-based methods are non-adaptive with respect to channel dynamics. In particular, the MOE-based method is sensitive to the estimated noise variance (i.e., $\hat{\sigma}_n^2$ in (7.33)).

7.5 CMA-based Code Acquisition Scheme

In this section, the proposed code acquisition scheme is presented. First, the acquisition problem is formulated as finding the best chip delay hypothesis. Second, to obtain the decision variable for testing hypotheses, constrained CMA based adaptive filtering is presented. Third, the convergence behaviour of this constrained CMA is examined. It is shown that the desired local minimum (i.e., lock convergence) will always occur for the correct hypothesis, while filter trajectories from all incorrect hypotheses are most likely to be trapped within some saddle regions, given sufficiently small step sizes. Finally, it is shown that the

correct hypothesis is the one gives the closest decorrelating solution. In a blind setting, since a decision variable based on this decorrelation criterion can not be implemented, an alternative decision variable based on an average output energy criterion is proposed.

7.5.1 Problem statement of Code Acquisition

The problem of code acquisition is concerned with the estimation of the chip timing delay[4] of the desired user $k = 1$, η_1 in (7.4). Since η_1 is an integer bounded between 0 and $N-1$, the nth hypothesised chip delays is defined as $\eta_1(n) \triangleq nT_c$, where $n \in \{0, \ldots, N-1\}$ is the hypothesis index. The acquisition problem is to test each hypothesised delay $\eta_1(n)$ independently, and then select the one which corresponds to the correct chip timing. In this chapter, this hypothesis testing is done by maximising some decision variables $\Lambda(n)$. Then, the chip timing estimate is computed as

$$\hat{\eta}_1 = \arg \max_{n \in \{0,\ldots,N-1\}} \Lambda(n). \tag{7.10}$$

7.5.2 Filter Adaptation

As in [137], linear adaptive filtering is used to obtain the decision variable $\Lambda(n)$ in (7.10). Next, for each hypothesised delay, the respective filter is blindly adapted based on the constrained CMA and is explained as follows. For the nth hypothesis, the filter output at the ith bit iteration is given by

$$Z_{1,n}[i] = \mathbf{w}_{1,n}^T[i]\mathbf{Y}[i], \tag{7.11}$$

where $\mathbf{w}_{1,n}[i]$ is an N-length vector of corresponding filter coefficients. In the same manner as (2.45), the CM criterion of the nth delay hypothesis is given by

$$J_{CM,n}(\mathbf{w}_{1,n}) = E\left\{(Z_{1,n}^2[i] - \xi)^2\right\}, \tag{7.12}$$

[4] The fine tuning of the fractional chip delay δ_1 in (7.4) is usually performed by a code tracking loop. However, both acquisition and tracking can be performed with the same proposed method.

Using the canonical linear multiuser detector in (3.2), all filters are decomposed into two orthogonal components via some projection matrices $\mathbf{P}_{1,n}^{\perp}$ as

$$\mathbf{w}_{1,n}[i] = \mathbf{c}_{1,n} + \mathbf{P}_{1,n}^{\perp}\mathbf{w}_{1,n}^{\perp}[i], \tag{7.13}$$

where $\mathbf{w}_{1,n}^{\perp}[i]$ and $\mathbf{c}_{1,n} \triangleq \mathbf{c}_{1,L}(n) + \mathbf{c}_{1,R}(n)$ are the adaptive and fixed components respectively, and the projection matrix of the nth hypothesis is defined as

$$\begin{aligned} \mathbf{P}_{1}^{\perp}(n) &\triangleq \mathbf{I}_N - \mathbf{s}_{1,n}\mathbf{s}_{1,n}^{\dagger}, \quad \text{and} \\ \mathbf{s}_{1,n} &= (\mathbf{c}_{1,L}(n),\ \mathbf{c}_{1,R}(n)). \end{aligned} \tag{7.14}$$

Since $\mathbf{P}_{1,n}^{\perp}\mathbf{c}_{1,n} = \mathbf{0} \quad \forall n \in \{0,\ldots,N-1\}$, the first and second terms of (7.13) are orthogonal to each other. Also, since $rank(\mathbf{s}_{1,n}) = 2 \quad \forall n \in \{0,\ldots,N-1\}$ (i.e., always full column rank), its pseudo-inverse can be written as $\mathbf{s}_{1,n}^{\dagger} = \left(\mathbf{s}_{1,n}^{T}\mathbf{s}_{1,n}\right)^{-1}\mathbf{s}_{1,n}$. Also, all projection matrices are only needed to be computed once at initialisation.

The usage of the projection matrices is to restrict the filter adaptation in a constrained space, which satisfy the following conditions:

$$\begin{aligned} \mathbf{w}_{1,n}^{T}[i]\mathbf{c}_{1,L}(n) &= \frac{n}{N}, \quad \text{and} \\ \mathbf{w}_{1,n}^{T}[i]\mathbf{c}_{1,R}(n) &= \frac{N-n}{N}, \quad \forall i, \end{aligned} \tag{7.15}$$

where all the signature vectors are normalised according to (2.26). Since the only adaptive term is $\mathbf{w}_{1,n}^{\perp}[i]$, from (7.11) and (7.12), in the same manner as (5.26), the constrained CMA-based adaptation is given by

$$\begin{aligned} \mathbf{w}_{1,n}^{\perp}[i+1] &= \mathbf{w}_{1,n}^{\perp}[i] - \mu \cdot \frac{1}{4}\nabla_{\mathbf{w}_{1,n}^{\perp}[i]}J_{CM}(\mathbf{w}_{1,n}) \\ &= \mathbf{w}_{1,n}^{\perp}[i] - \mu\left(Z_{1,n}^{2}[i] - \xi\right)Z_{1,n}[i]\nabla_{\mathbf{w}_{1,n}^{\perp}[i]}Z_{1,n}[i] \\ &= \mathbf{w}_{1,n}^{\perp}[i] - \mu\left(Z_{1,n}^{2}[i] - \xi\right)Z_{1,n}[i]\mathbf{P}_{1,n}^{\perp}\mathbf{Y}[i]. \end{aligned} \tag{7.16}$$

From (7.16), it is observed that there are N independent, parallel constrained CMAs that adapt from the same received signal vector $\mathbf{Y}[i]$, but projected on a different constrained space by $\mathbf{P}_{1,n}^{\perp}$. The filter initialisations are equivalent to that of the conventional sliding correlators [135]. That is, for the nth delay

hypothesis, the filter is initialised as the shifted version of the desired user's spreading sequence as follows

$$\mathbf{w}_{1,n}[0] = \mathbf{c}_{1,n}, \quad \text{where } n \in \{0, \ldots, N-1\}. \tag{7.17}$$

7.5.3 Convergence Analysis of Constrained CMA

Using the equivalent $2K$-users synchronous system model in Section 7.3.2, in the same manner as (3.24), the contribution of individual user in the filter output can be represented as user gains which are defined as

$$\mathbf{V}_n[i] \triangleq (\mathbf{S}(\tau)\mathcal{A})^T \mathbf{w}_{1,n}[i] = (v_{1,n}[i], \ldots, v_{2K,n}[i])^T. \tag{7.18}$$

In a noiseless setting with the bit index i temporally suppressed, from (7.7) and (7.18), the filter output of the nth hypothesis can be written as

$$Z_{1,n} = \mathbf{w}_{1,n}^T \mathbf{S}(\tau)\mathcal{A}\mathcal{B} = \mathbf{V}_n^T \mathcal{B}. \tag{7.19}$$

In the same manner as (4.29), from (7.7) and (7.19), the adaptation term of the constrained CMA in (7.16) is given by

$$\begin{aligned} \frac{1}{4}\nabla_{\mathbf{w}_{1,n}^{\perp}} J_{CM}(\mathbf{w}_{1,n}) &= E\left\{\left(Z_{1,n}^2 - \xi\right) Z_{1,n} \mathbf{P}_{1,n}^{\perp} \mathbf{Y}\right\} \\ &= \mathbf{P}_{1,n}^{\perp} \mathbf{S}(\tau)\mathcal{A} \cdot E\left\{\left(\left(\mathbf{V}_n^T \mathcal{B}\right)^2 - \xi\right) \mathbf{V}_n^T \mathcal{B} \cdot \mathcal{B}\right\} \\ &= \mathbf{P}_{1,n}^{\perp} \mathbf{S}(\tau)\mathcal{A} \cdot \frac{1}{4}\nabla_{\mathbf{V}_n} J_{CM,n}(\mathbf{V}_n), \end{aligned} \tag{7.20}$$

where $\nabla_{\mathbf{V}_n} J_{CM,n}(\mathbf{V}_n)$ has the same form as $\nabla_{\mathbf{V}} J_{CM}(\mathbf{V})$ in (A.3), except with $\mathbf{V}$ replaces by $\mathbf{V}_n$. From (7.20), when $\nabla_{\mathbf{w}_{1,n}^{\perp}} J_{CM}(\mathbf{w}_{1,n}) = \mathbf{0}$, there are two classes of stationary points for the constrained CMA in (7.16):

Class 1 when $\nabla_{\mathbf{V}_n} J_{CM,n} = \mathbf{0}$, or

Class 2 when $\nabla_{\mathbf{V}_n} J_{CM,n} \in \mathit{Nullspace}\left(\mathbf{P}_{1,n}^{\perp}\mathbf{S}(\tau)\right)$, and $\nabla_{\mathbf{V}_n} J_{CM,n} \neq \mathbf{0}$.

Class 1 corresponds to those stationary points of an *unconstrained* CMA (i.e., without $\mathbf{P}_{1,n}^{\perp}$ in (7.16)) in (A.12)-(A.14); while Class 2 arises when $\nabla_{\mathbf{V}_n} J_{CM}$ lies in some non-trivial nullspaces depending on $\mathbf{P}_{1,n}^{\perp}$. In the synchronous scenario,

it has been shown in Section 3.5.1 that the unconstrained CMA exhibits an important property of lock convergence (i.e., desired local minimum within Class 1), which is equivalent to a decorrelating solution under a noiseless setting. In an asynchronous system, depending on the desired user's delay τ_1, the lock convergence can be defined in terms of user gains as follows

$$v_{k,n} = 0 \;\; \forall k \neq \{1, K+1\}, \;\; \text{and}$$
$$\begin{cases} |v_{1,n}| \gg 0 \;\text{and}\; v_{K+1,n} = 0; & \text{if } \tau_1 \simeq T_b \\ |v_{K+1,n}| \gg 0 \;\text{and}\; v_{1,n} = 0; & \text{if } \tau_1 \simeq 0 \\ |v_{1,n}|, |v_{K+1,n}| \gg 0; & \text{if } 0 \ll \tau_1 \ll T_b. \end{cases} \tag{7.21}$$

When $0 \ll \tau_1 \ll T_b$, it is noted that the lock convergence in (7.21) is classified as an unstable saddle point in (A.14) for the unconstrained CMA. However, since both $v_{1,n}$ and $v_{K+1,n}$ are user gains correspond to the same desired user $k = 1$, this particular saddle point of the unconstrained CMA, can be classified as the desired local minimum (i.e., lock convergence) in the constrained CMA case.

The stationary points of the constrained CMA in (7.16) is evaluated below for both correct and incorrect hypotheses. We do not intended to give exhaustive mathematical details, but to give some insights for a better understanding of its convergence behaviour.

1. **Correct hypothesis (i.e., $n = \eta_1$)**

   For simplicity, it is assumed temporally that the desired user $k = 1$ has no fractional chip delay (i.e., $\delta_1 = 0$ in (7.4)). Then its left and right partitions of the signature vector in (7.5) become $\mathbf{s}_{1,x}(\tau_1 = \eta_1) = \mathbf{c}_{1,x}(\eta_1)$, where $x = [L, R]$. Then, the constraints in (7.15) can be expressed in terms of user gains as

$$\begin{aligned} v_{1,n=\eta_1} &= A_1 \mathbf{c}_{1,L}(\tau_1 = \eta_1)^T \mathbf{w}_{1,n=\eta_1} = A_1 \frac{\eta_1}{N}, \\ v_{K+1,n=\eta_1} &= A_1 \mathbf{c}_{1,R}(\tau_1 = \eta_1)^T \mathbf{w}_{1,n=\eta_1} = A_1 \frac{N - \eta_1}{N}. \end{aligned} \tag{7.22}$$

   Due to the two constrained user gains in (7.22), it is observed that the only possible stationary points in Class 1 are of the lock convergence in

(7.21). The hidden stationary points in Class 2 are introduced in exchange for this lock convergence advantage. Furthermore, since the first and the $(K+1)$th columns of $\mathbf{P}^{\perp}_{1,n=\eta_1}\mathbf{S}(\boldsymbol{\tau})\mathcal{A}$ are zero vectors, it is sufficient to consider the adaptation of the remaining $(2K-2)$ user gains $v_{k,n=\eta_1})\ \ \forall k \in \{2,\ldots,K,K+2,\ldots,2K\}$ of the constrained CMA which are equivalent to that of the unconstrained CMA. This is because that as discussed in Section 5.5.1, if the first and $(K+1)$th columns of $\mathbf{P}^{\perp}_{1,n=\eta_1}\mathbf{S}(\boldsymbol{\tau})\mathcal{A}$ are removed, the resultant matrix is generally right-invertible. Hence, for the case of correct hypothesis, it is sufficient to consider the stationary points in Class 1 only.

2. **Incorrect hypothesis (i.e., $\forall n \neq \eta_1$)**

For the case of incorrect hypothesis, it is difficult to predict exactly the value of converged user gains. In order to avoid dealing with the hidden stationary points in Class 2, the following conditions are imposed such that $\mathbf{P}^{\perp}_{1,n\neq\eta_1}\mathbf{S}(\boldsymbol{\tau})\mathcal{A}$ is right-invertible (i.e., full column rank):

$$\begin{aligned} \text{rank}(\mathbf{S}(\boldsymbol{\tau})) &= 2K, \\ \text{and rank}(\mathbf{P}^{\perp}_{1,n\neq\eta_1}) &\geq \text{rank}(\mathbf{S}(\boldsymbol{\tau}))\ \ \forall n \neq \eta_1. \end{aligned} \tag{7.23}$$

In general, it can be assumed that $\mathbf{S}(\boldsymbol{\tau})$ is of full column rank[5]. From the definition of the projection matrix in (7.14), $\text{rank}(\mathbf{P}^{\perp}_{1,n\neq\eta_1}) = N-2$. Hence, from (7.23) if $N-2 \geq 2K$, the stationary points of the constrained CMA can be represented solely by that of the unconstrained CMA (i.e., Class 1). Intuition also comes from [126] where it is illustrated that stationary points within Class 2 are most likely to be unstable.

In the unconstrained CMA case, different initialisations will lead to different local minima or temporally trapped within some saddle regions [64]. The necessary condition for lock convergence in (3.33) can be generalised to that of the kth local minimum (i.e., capture of the kth user in (A.13)) as

[5] It should be noted that due to the usage of the equivalent $2K$-users synchronous model, $\mathbf{S}(\boldsymbol{\tau})$ may be close to rank deficient when $\tau_k \simeq 0$ for some users.

follows [101]

$$|v_{k,n\neq\eta_1}[0]| > |v_{m,n\neq\eta_1}[0]| \quad \forall k \neq m, \tag{7.24}$$

where, from (7.17) and (7.18), the kth initial user gain is given by

$$v_{k,n}[0] = \begin{cases} A_k \mathbf{s}_{k,L}^T(\tau_k)\mathbf{c}_{1,n} & \forall k \in \{1,\ldots,K\}, \\ A_{k-K}\mathbf{s}_{k-K,R}^T(\tau_{k-K})\mathbf{c}_{1,n} & \forall k \in \{K+1,\ldots,2K\}. \end{cases} \tag{7.25}$$

In the case of incorrect hypotheses, it can be generally assumed that the cross-correlations between any shifts of desired spreading sequence and every signature waveform (i.e., $\mathbf{s}_{k,x}^T(\tau_k)\mathbf{c}_{1,n}$ where $x = [L, R]$) are sufficiently low [6] and approximately equal. Thus, the inequality in (7.24) is unlikely to be satisfied. Instead, given suitably small step sizes, the trajectories of filters are most likely to be trapped within various saddle regions in (A.14)[6]. This phenomenon is to be verified via simulations in Section 7.6.

7.5.4 Two Decision Variables: Decorrelation and Average Output Energy Criteria

Since the lock convergence in (7.24) always occurs for the correct hypothesis, the correct delay hypothesis is the one which gives the closest decorrelating solution. Then, this decorrelation criterion can be directly translated[7] into the decision variable in (7.10) as

$$\Lambda(n) = v_{1,n}^2[i_s] + v_{K+1,n}^2[i_s], \tag{7.26}$$

where all filters are assumed to attain steady state at the i_sth bit iteration. However, the decision variable in (7.26) is not applicable in a blind setting. This is because computing $v_{1,n}[i]$ and $v_{K+1,n}[i]$ require the knowledge of desired user's delay τ_1.

In the same manner as [6] whereby a larger output energy is expected for better hypotheses, an alternative decision variable can be used to replace (7.26)

[6] Naturally, the saddle point for lock convergence in (7.21) is excluded. [7] An equivalent decorrelation based hypothesis test to (7.26) is: $\hat{\eta}_1 = \arg\min \sum_{k=2,k\neq K+1}^{2K} v_{k,n}^2[i_s]$.

and is based on average output energy

$$\Lambda(n) = E\{Z_{1,n}^2[i_s]\}. \tag{7.27}$$

Next, the mechanism behind the output energy based decision variable in (7.27) is discussed. Under a noiseless setting, for white, zero-mean, binary user sources [126], the average output energy can be expressed as

$$E\{Z_{1,n}^2[i_s]\} = \|\mathbf{V}_n\|^2. \tag{7.28}$$

We then evaluate (7.28) for both the correct and incorrect hypotheses as follows.

1. **Correct hypothesis (i.e., $n = \eta_1$)**

   Since the lock convergence in (7.21) always occurs for the correct hypothesis, using the constrained user gains in (7.22), the corresponding output energy energy can be approximated under the assumption $\delta_1 = 0$ as

$$\begin{aligned} \|\mathbf{V}_{n=\eta_1}[i_s]\|^2 &= v_{1,n=\eta_1}^2[i_s] + v_{K+1,n=\eta_1}^2[i_s] \\ &\simeq A_1^2\left(\frac{N^2 - 2N\eta_1 + 2\eta_1^2}{N^2}\right). \end{aligned} \tag{7.29}$$

   Furthermore, it can be easily shown that (7.29) is lower bounded by

$$\min_{\eta_1 \in \{0,\ldots,N-1\}} \|\mathbf{V}_{\eta_1}[i_s]\|^2 = |\mathbf{V}_{\eta_1=N/2}[i_s]\|^2 = A_1^2/2. \tag{7.30}$$

2. **Incorrect hypothesis (i.e., $\forall n \neq \eta_1$)**

   In the same manner as (3.46), since the stationary points of incorrect hypotheses are those of the unconstrained CMA, the output energies of local minima and saddle points are bounded by

$$\frac{K\xi}{3K-2} \leq \|\mathbf{V}_{n\neq\eta_1}[i_s]\|^2 \leq \xi. \tag{7.31}$$

   Thus, it is seen that even if local minima do occur (i.e., upper bound in (7.31)), as long as $\xi < A_1^2/2$, the decision variables based on the average output energy in (7.27) will have $\Lambda(n = \eta_1) > \Lambda(n \neq \eta_1)$.

Overall, the proposed blind constrained CMA-based code acquisition scheme is summarised by the following steps:

Step 1 Initialise all N filters $\mathbf{w}_{1,n}[0]$ as in (7.17) and compute the projection matrix $\mathbf{P}_{1,n}^{\perp}$ in (7.14).

Step 2 Each filter is adapted independently as in (7.16).

Step 3 At the i_s bit iteration (i.e., steady state), the chip timing estimate $\hat{\eta}_1$ is obtained as:
$\hat{\eta}_1 = \arg\max_c \sum_{i=i_s}^{Q_{CMA}+i_s-1} Z^2(i,c)$, where Q_{CMA} is the number of bits to compute the averaged output energy in (7.27).

7.6 Simulation Results

In this section, two set of simulation results are presented. The first set (Figure 7.2 and 7.3) is to demonstrate the convergence behaviour of the constrained CMA-based acquisition scheme. The second set (Figure 7.4 to 7.7) is to compare the proposed method with three other blind acquisition schemes that are briefly described in Section 7.6.1.

7.6.1 Other Acquisition Methods

1. **Sliding correlator**

   This is the straight serial-search implementation of the correlation techniques [135]. Analogous to the MF, the received signal is correlated with some shifted versions of the spreading code of the desired user as follows

$$\hat{\eta}_1 = \arg \max_{n\in\{0,\ldots,N-1\}} \left(\sum_{i=1}^{Q_{MF}} (\mathbf{Y}[i]\mathbf{c}_{1,n})^2 \right), \tag{7.32}$$

   where Q_{MF} is the length of the averaging window.

2. **MOE-based timing estimator**

For our purpose of comparison, the MOE-based acquisition algorithm in [6] is modified to a shorter observation of one symbol duration or N number of chip delay hypotheses. The least squares implementation[8] of the MOE-based acquisition algorithm is summarised in the following steps

(a) Compute the linear filter for the nth hypothesis as follows

$$\mathbf{w}_{1,n} = \left(\widehat{\mathbf{R}}_{\mathbf{yy}} + \hat{\sigma}_n^2 \mathbf{I}_N\right)^{-1} \mathbf{c}_{1,n} \quad \text{where } n \in \{0, \ldots, N-1\}, \tag{7.33}$$

where is the sample cross-correlation matrix of the received signal is defined as

$$\widehat{\mathbf{R}}_{\mathbf{yy}} = \sum_{i=1}^{Q_R} \mathbf{Y}[i]\mathbf{Y}^T[i], \tag{7.34}$$

with Q_R as the averaging window length, and $\hat{\sigma}_n^2$ is the *fictitious* noise variance that is used to constrain the filter energy $\|\mathbf{w}_{1,n}\|^2$. It is assumed that the same $\hat{\sigma}_n^2$ is used to find the MOE solutions in (7.33) for all N hypotheses. A practical choice of $\hat{\sigma}_n^2$ is to scale it according to the net power of the received signal as $\hat{\sigma}_n^2 = \varpi \cdot trace(\widehat{\mathbf{R}}_{\mathbf{yy}})$, where ϖ is the scaling factor. The MOE-based method is sensitive to the choice of ϖ, and unfortunately, the method to choose ϖ automatically is fairly complex [6]. For simplicity[9], we set $\hat{\sigma}_n^2 = 0$.

(b) Normalise all N filters to satisfy the constraint $\mathbf{w}_{1,n}^T \mathbf{c}_{1,n} = 1 \ \forall n \in \{0, \ldots, N-1\}$ as follows

$$\mathbf{w}_{1,n} = \frac{\mathbf{w}_{1,n}}{\mathbf{w}_{1,n}^T \mathbf{c}_{1,n}}. \tag{7.35}$$

(c) Select the best hypothesis with the largest average output energy

$$\hat{\eta}_1 = \arg \max_{n \in \{0,\ldots,N-1\}} \left(\sum_{i=Q_R+1}^{Q_R+Q_{MOE}} (\mathbf{w}_{1,n}\mathbf{Y}[i])^2 \right), \tag{7.36}$$

where Q_{MOE} is the length of averaging window (analogous to Q_{CMA} in Section 7.5.4).

[8] In [6], it is stated that only the least squares MOE-based acquisition scheme is feasible, since acquisition with its adaptive implementation (e.g., LMS) would be unreliable. [9] It is shown [6] via simulation that $\varpi = 10^{-4}$ is small enough to permit suppression of strong MAI for typical SNR values.

3. **Subspace-based timing estimator**

The well known MUSIC algorithm [84, 86] is a geometric solution to minimise the ℓ_2 norm of the projection of the desired user's signature vector into the estimated noise subspace. The MUSIC chip timing estimate is given by

$$\hat{\eta}_1 = \arg \min_{n \in \{0,\ldots,N-1\}} \left(\|\mathbf{c}_{1,L}^T(n)\widehat{\mathbf{E}}_N\|^2 + \|\mathbf{c}_{1,R}^T(n)\widehat{\mathbf{E}}_N\|^2 \right), \tag{7.37}$$

where $\widehat{\mathbf{E}}_N$ is the estimated noise subspace whose columns are the eigenvectors corresponding to the $(N - 2K)$ smallest eigenvalues of $\widehat{\mathbf{R}}_{\mathbf{yy}}$.

7.6.2 Simulation Parameters and Performance Measure

All simulations are based on an uncoded, asynchronous K-users DS-CDMA system with a BPSK modulation, and binary PN spreading sequence of length $N = 31$. All time delays τ_k are generated randomly and independently in the interval $[0, T_b)$ and are assumed to be fixed during the acquisition period. To illustrate a near-far situation, the Near-Far Ratio (NFR) [dB] in (3.57) is used. For all simulations, $SNR(k) = 15dB \quad \forall k \in \{2, \ldots, K\}$. For the proposed method, the modulus radius is set at $\xi = 1$ with step size $\mu = 10^{-6}$. To compute the chip timing estimate, all the averaging windows are set to be of the same length, $Q_{CMA} = Q_R = Q_{MOE} = Q_{MF} = 100$. It is assumed that the constrained CMA reaches the steady state at the $i_s = 500$th bit iteration.

For a code acquisition process, the critical performance measure is the probability of acquisition P_{ACQ} (i.e., probability of obtaining correct chip timing estimate or $|\tau_1 - \hat{\eta}_1 T_c| < T_c$), or the required acquisition time T_{ACQ}. To enable a rapid initial link setup and smooth handoffs in a mobile environment, we need to maximise P_{ACQ} with a minimal T_{ACQ}. From [128], the acquisition-limited capacity is defined in terms of these two performance measures as follows

$$\begin{aligned} C_{ACQ} &= \min(C_1, C_2) \\ C_1 &= \arg\max_K (T_{ACQ}(K) \leq T_0), \\ C_2 &= \arg\max_K \left(P_{ACQ}(K) \geq \widehat{P}_{ACQ} \right), \end{aligned} \tag{7.38}$$

where C_1 and C_2 correspond to the maximum number of users for a specified stopping time T_0 and acquisition probability benchmarks $\widehat{P}_{ACQ}$, respectively. In our comparison, we use C_2 in (7.38) as the acquisition-limited capacity, assuming there is no limit placed on the acquisition time. All plots are averaged over 100 Monte Carlo runs. Each Monte Carlo run represents a particular realization of the noise, data and signature sequences

7.6.3 Discussion

1. **Convergence Behaviour**

   Figures 7.2 and 7.3 show the magnitude of converged user gains $|v_{k,n}[i_s]|$ along the entire range of the delay hypothesis $n \in \{0, \ldots, N-1\}$ and user index $k \in \{1, \ldots, 2K\}$ using the equivalent $2K$-users synchronous model in Section 7.3.2. The desired user's delay is set to be $\tau_1 = 0$ for Figure 7.2 and $\tau_1 = N/2$ for Figure 7.3. Thus, the correct hypotheses are $n = 0$ and $n = \{15,\ 16\}$ for Figure 7.2 and 7.3, respectively. In particular, from (7.30), it is observed that Figure 7.3 represents the worst case scenario when the output energy of the correct hypothesis is minimal.

   From both Figure 7.2 and 7.3, it is observed that the user gains that have the largest magnitude are those of the desired user at the correct hypothesis (i.e., $v_{1,n=\eta_1}[i_s]$ and $v_{K+1,n=\eta_1}[i_s]$). This verified the convergence behaviour of the constrained CMA, as discussed in Section 7.5.3. That is, the lock convergence is the only feasible stationary point for the correct hypothesis; and all incorrect hypotheses are trapped within some saddle regions. From subplots b in Figures 7.2 and 7.3, it is seen that the magnitude of this desired user's gains are reduced under near far effect. Also from subplots c in Figures 7.2 and 7.3 where 10 more users are added, there is no significant change in the convergence behaviour of constrained CMA.

2. **Acquisition Performance**

   Figures 7.4 to 7.7 demonstrate the acquisition performance of the proposed method in comparison with the sliding correlator, the MOE-based and the

MUSIC methods, as described in Section 7.6.1. The probability of acquisition P_{ACQ} is plotted with different NFR and K. For a 10-users system, Figure 7.4 shows that the proposed method is near far resistant up to $NFR \simeq 3dB$. The MUSIC method is most near far resistant, since its chip timing estimate is independent of the changes in the MAI level. Also, since the MOE-based solution is an approximated form (depending on the choice of $\hat{\sigma}_n^2$ in (7.33)) of the well-known decorrelator, the MOE-based method has a high near far resistance [6]. Finally, the acquisition performance of the sliding correlator deteriorates the fastest for increasing NFR values.

In Figure 7.5, it is shown that the near-far resistance of the proposed method can be enhanced by scaling the filter initialisation in (7.17) by β as $\mathbf{w}_{1,n}[0] = \beta\,\mathbf{c}_{1,n}$, and the orthogonal filter decomposition in (7.13) becomes $\mathbf{w}_{1,n}[i] = \beta\mathbf{c}_{1,n} + \mathbf{P}_{1,n}^{\perp}\mathbf{w}_{1,n}^{\perp}[i]$. The intuition comes from the fact that the desired user's gains at the correct hypothesis $v_{1,n=\eta_1}[i]$ and $v_{K+1,n=\eta_1}[i]$ are explicitly constrained as their initial values. Hence, for higher values of β, the margin between the output energies of the correct and incorrect hypotheses in (7.30) and (7.31) can be widened to compensate for the near far effect. However, since all other initial user gains are also scaled to higher values, a slower convergence may result.

The acquisition-limited capacity C_2 in (7.38) is illustrated in Figure 7.6 and 7.7 for the case of equal-power users and $NFR = 3dB$, respectively. For the MUSIC method, since the subspace partition is only analytical tractable [84, 86] under the assumption $N > 2K$, it does not function[10] if $K > 15$. The sliding correlator has the lowest C_2, especially under near far condition in Figure 7.7. For both Figure 7.6 and 7.7, it is observed that the C_2 of the proposed method is slightly less than that of the MOE-based case. Also, in the same manner as the MOE-based method, the acquisition performance of the proposed method deteriorates gradually as more active users are presented. This supports the claim in (7.23) that the stationary points of the constrained CMA for the incorrect hypotheses can no longer

[10] If $K \geq N/2$, the noise subspace may have zero rank, and a common practice is to include weaker users within the noise subspace.

be represented solely by that of the unconstrained CMA case (i.e., Class 1) if $N - 2 < 2K$.

7.7 Conclusions

A new blind code acquisition scheme for DS-CDMA system based on a linearly constrained CMA has been proposed. This method exploits its lock convergence behaviour such that the correct delay hypothesis is the one which gives the maximum average output energy. For a small user population K, such that $N - 2 < 2K$, the acquisition performance of the proposed method approaches that of the subspace-based and the MOE-based methods. Also, it has a higher acquisition limited capacity than the conventional sliding correlator method. It is shown that the proposed method is robust to some near far conditions (e.g., 2 to $3dB$). However, its near far resistance can be enhanced by appropriate scaling of the constraints involved. It is concluded that although the proposed method has a lower acquisition performance than the SOS-based methods under severe near far conditions and/or large user populations, it offers adaptability to changes in system parameters.

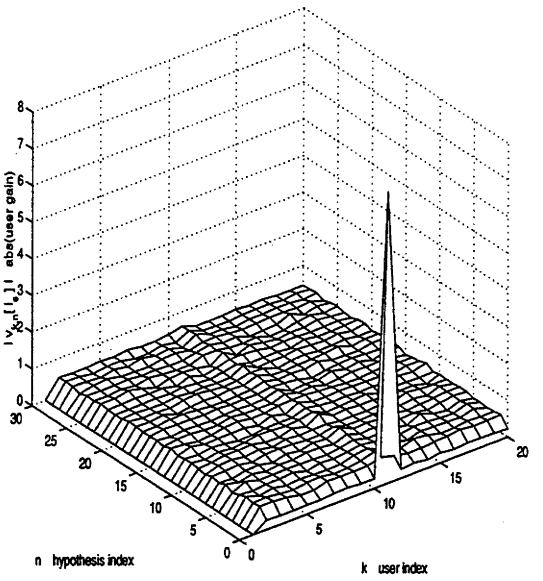

(a) $K = 10$ and equal-power users

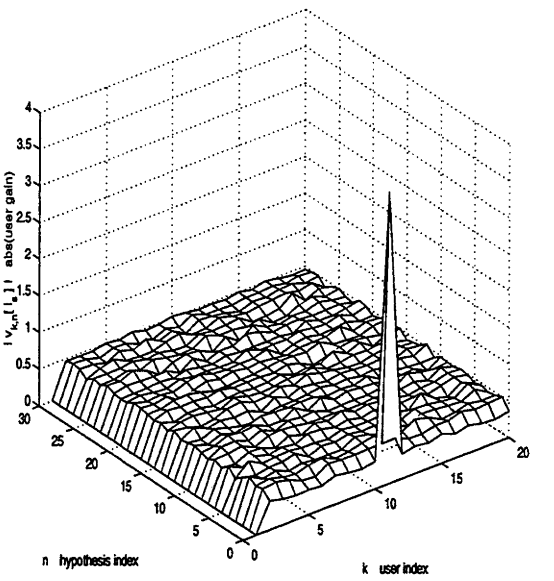

(b) $K = 10$ and $NFR = 6dB$

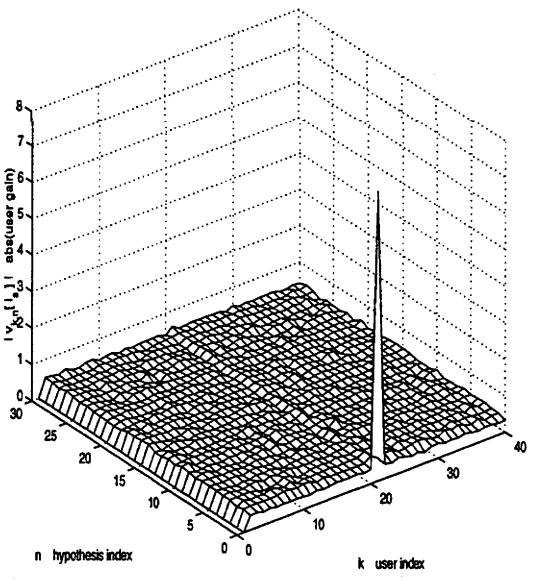

(c) $K = 20$ and equal-power users

Figure 7.2: Magnitude of converged user gains $|v_{k,n}[i_s]|$ vs. delay hypotheses n and user indices k using the equivalent $2K$-user synchronous model: $N = 31$, $\tau_1 = 0$, $i_s = 500$, and $SNR(k) = 15dB \quad \forall k \in \{2, \ldots, K\}$.

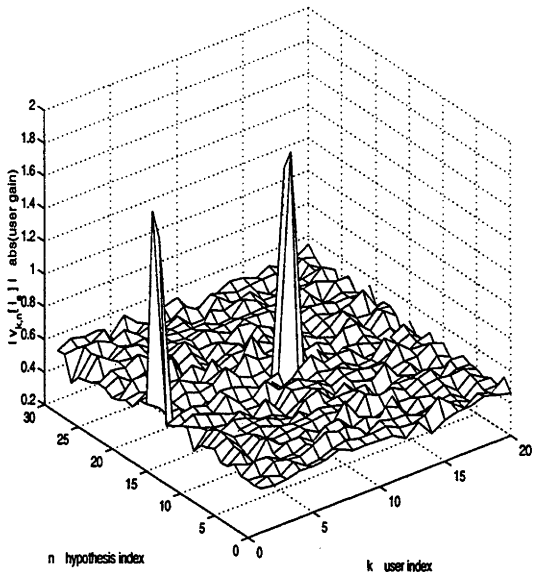

(a) $K = 10$ and equal-power users

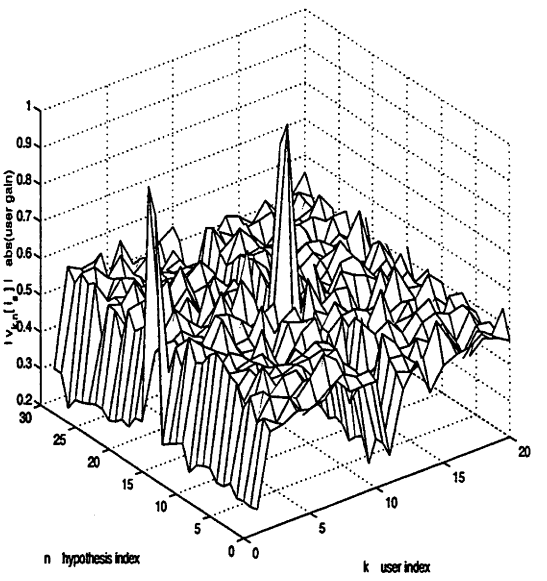

(b) $K = 10$ and $NFR = 6dB$

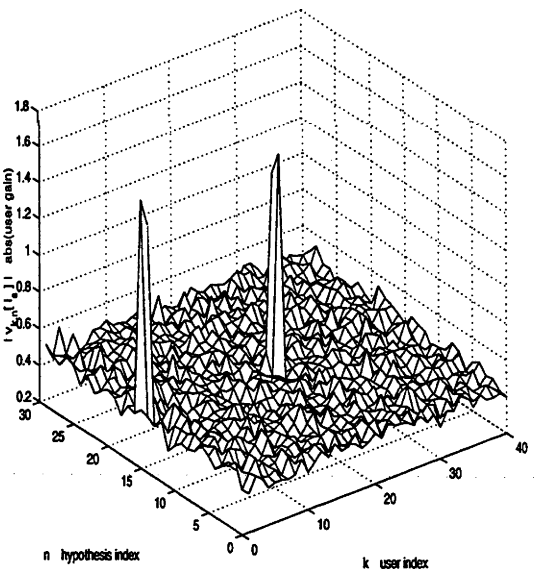

(c) $K = 20$ and equal-power users

Figure 7.3: Magnitude of converged user gains $|v_{k,n}[i_s]|$ vs. delay hypotheses n and user indices k using the equivalent $2K$-user synchronous model: $N = 31$, $\tau_1 = N/2$, $i_s = 500$, and $SNR(k) = 15dB \quad \forall k \in \{2, \ldots, K\}$.

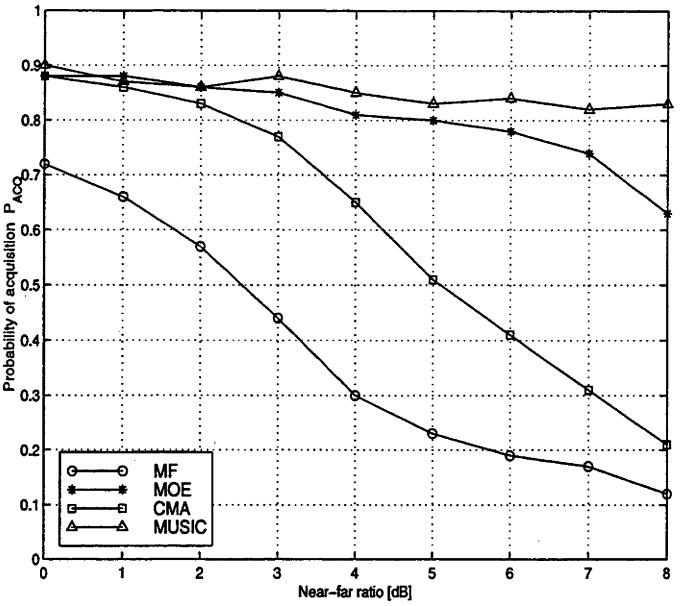

Figure 7.4: Probability of acquisition vs. NFR: $N = 31$, $K = 10$, and $SNR(k) = 15dB \quad \forall k \in \{2, \ldots, 10\}$.

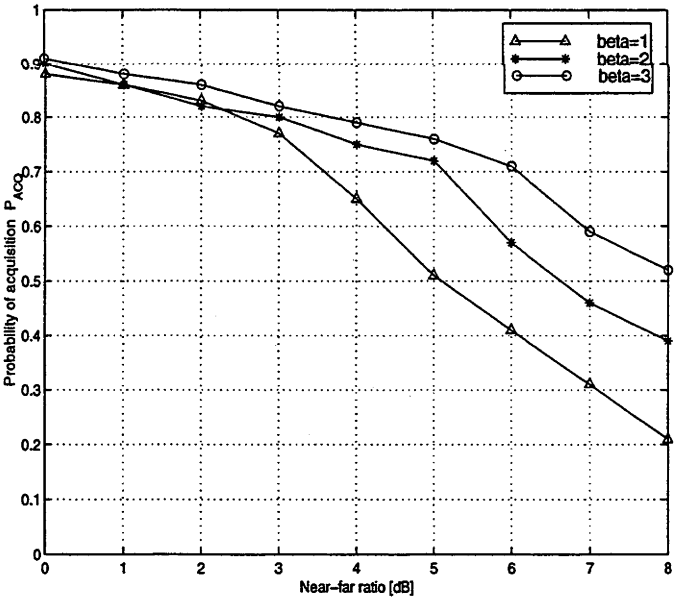

Figure 7.5: Probability of acquisition vs. NFR for the proposed method with various filter scaling β: $N = 31$, $K = 10$, and $SNR(k) = 15dB \quad \forall k \in \{2, \ldots, 10\}$.

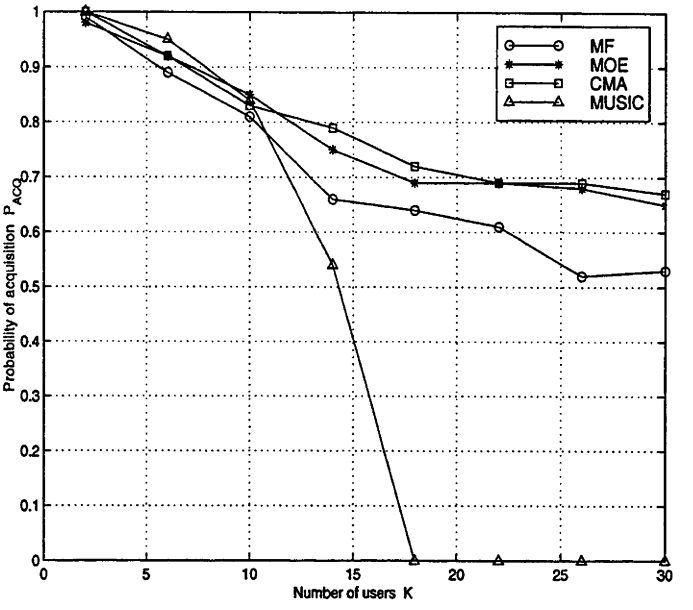

Figure 7.6: Probability of acquisition vs. K: $N = 31$, $SNR(k) = 15dB \quad \forall k \in \{2, \ldots, K\}$, and equal-power users

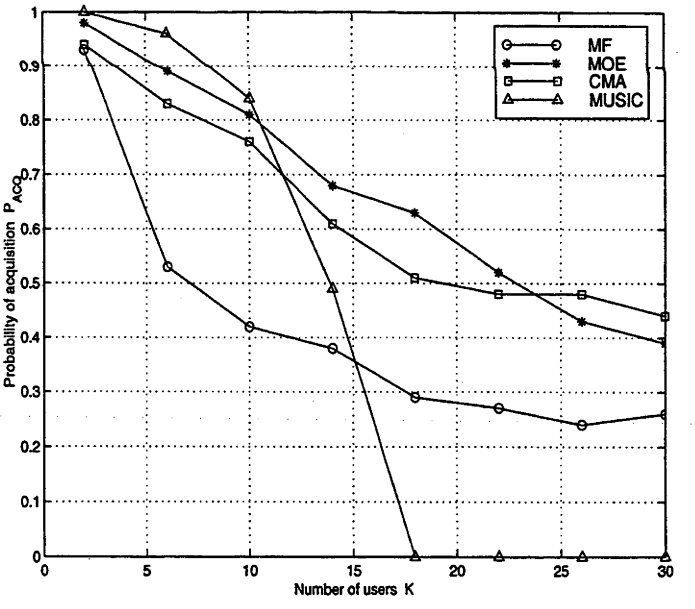

Figure 7.7: Probability of acquisition vs. K: $N = 31$, $SNR(k) = 15dB \quad \forall k \in \{2, \ldots, K\}$, and $NFR = 3dB$.

Chapter 8

Conclusions and Future Research Directions

This final chapter presents the conclusions of this thesis and a number of possible research extensions.

8.1 Conclusions

A main incentive for the proposed implementation of CDMA networks as the next generation PCS, is its potential capacity improvement over the traditional TDMA and FDMA. In the case of DS-CDMA system using non-orthogonal signature waveforms, multiuser detection is required to suppress the MAI, in order to detect the signal of interest most reliably. The multiuser detection is further complicated by other factors, such as near far conditions, asynchronism between users and multipath fading. In the last decade, the literature has seen many forms of multiuser detectors, from optimal MLSE detector to sub-optimal linear/non-linear detector. Recently, some blind multiuser detectors have been proposed which remove the need for training, and only the knowledge of transmitted signature of the user of interest is required. The objective of this thesis was to derive new blind methods for linear multiuser detection, and to compare them with existing methods which have exhibited limitations. In particular, much emphasis

has been placed on the usage of the CMA-based adaptation, due to its reported robustness properties and ready adaptability to channel dynamics.

In Chapter 3, the problem of linear multiuser detection was considered without multipath effect and asynchronism. Despite its global convergence behaviour and LMS-like complexity, it is revealed that the popular MOE blind detector suffers from several weaknesses. In an attempt to alleviate this weaknesses, two blind detectors, one based on a constrained MOE algorithm and one based on the CMA, were proposed and their steady state and transient behaviours were analysed. The proposed constrained MOE detector turns out to be a generalisation of the original MOE detector. Also, the choice of constraint involves tradeoffs in the recovery of the desired signal, robustness against signal cancellation in the presence of signal mismatch, and minimising noise enhancement. Also, it is shown that the CMA detector exhibits a desirable property of lock convergence which nulls all interfering users, in the absence of channel noise. Unlike the usage of the CMA in single-user channel equalisation, robust initialisation for lock convergence can be achieved, under practical near far conditions. Comparing the CMA and the constrained MOE detectors, it is concluded that the CMA has a faster local convergence rate and is slightly more near far resistant.

In Chapter 4 and 5, the blind multiuser detection problem is extended to consider the presence of multipath effect and the usage of multiple sensors. Low-rate DS-CDMA system is considered under frequency selective channels. Two blind methods, one using a CMA-based RAKE-type filtering and another using a constrained CMA-based filtering, are proposed in Chapter 4 and 5, respectively.

In Chapter 4, it is revealed that the conventional MF-based 2-D RAKE receiver is essentially a bank of space-time MFs, one for each signal path, and suffers the near far problem. Unlike the MF-based 2-D RAKE receiver, the proposed receiver structure fully exploits the benefits of multiple sensors. As long as channel undermodelling is minimised, robust initialisation for lock convergence is possible. Simulations have shown that the proposed method offers superior BER performance compared to the MF-based 2-D RAKE receiver, with fewer number of sensors. This work illustrates the inherent deficiencies of using MF-based beamforming in multiuser detection, and the benefits of joint space-time diversity

processing.

In Chapter 5, a blind detector is derived based on the constrained inverse filtering concept. The underlying concept is to adapt CMA to suppress MAI, within some constrained spaces that have multipath induced ISI and ICI removed. The main result is that given the modulus radius is sufficiently small and a certain rank condition is satisfied, the only stable stationary point is the lock convergence. In comparison with the proposed RAKE-type receiver in Chapter 4, it does not have any initialisation problem and has less complexity. However, it suffers some performance loss, since not all energy of the received signal is utilised.

In Chapter 6, the effect of arrival of additional interferers to the CMA, constrained MOE and the training-based MMSE detectors are examined in terms of perturbations to their respective cost functions and derivatives. This analysis has shown that for small perturbations, the robustness of CMA to new users decreases as the modulus radius increases and as the existing user population increases. This work suggests that the modulus radius should be large enough to maintain a fast convergence rate, and small enough to retain its robustness property. However, the robustness of the constrained MOE detector is same as the MMSE case.

In Chapter 7, the problem of blind acquisition of the timing delay of the desired user is considered, in integer multiples of chip intervals. The constrained CMA in Chapter 5 is modified to blindly adapt each linear filter associated with its hypothesised delay. The underlying concept is that lock convergence should only occur for the correct hypothesised delay. Simulations have shown that under moderate user populations and near far conditions, its acquisition performance is similar to various SOS-based acquisition methods. However, unlike the SOS-based methods, the proposed method offers an adaptive implementation with respect to changes in system parameters.

8.2 Future Research Directions

Although this thesis has proposed several forms of blind linear multiuser detectors using various CMA-based adaptations, many of the results can be extended. A

number of future research directions are listed as follows.

- For a more realistic modelling, the acquisition-limited capacity in (7.38) should be considered along with imperfect power control and multipath fading. Furthermore, in the presence of fast fading or time varying time delay, it is of interest to investigate the tracking performance of CMA.

- Instead of having separate algorithms for code acquisition and multiuser detection, constrained CMAs in Chapter 5 and 7 can be combined to jointly perform these two operations. More importantly, the constrained CMA-based code acquisition scheme in Chapter 7 does not consider the multipath effect which should be included in future work.

- As illustrated in Chapter 5 and 7, since constrained inverse filtering method does not fully exploit the signal energy, its steady state performance can deviate from the MMSE detector significantly. As shown in [122], improved performance can be obtained by determining the optimal constraints that can maximise the signal energy under various multipath conditions. However, since no information of multipath channels is available, an interesting problem would be to blindly choose the optimal constraints that would match to respective channels.

- In Chapter 4, the initialisation issue for the CMA-based RAKE-type detector is only examined for the case of coherent diversity combiner. However, if phase information is not available, output signals from certain paths may partially cancel out each other and lock convergence can no longer be ensured. In future work, various methods of capture avoidance of CMA, as discussed in Section 3.5.2, should be further investigated. Also, the possible loss of lock convergence under severe channel undermodelling remains an open problem.

- In future work, a more realistic system model would be to relax those assumptions that are listed in Section 2.3.5. For example, in the case of users moving at vehicular speed, the Doppler effect should be introduced, and the multipath channels can no longer be modelled as LTI filters.

Appendix A

Stationary Points of CMA

As in most studies of single user blind equalization algorithms (e.g., [88]), the analysis for the locations of stationary points of CMA is done under the assumption that the received signal is noiseless. In DS-CDMA systems whose performance is MAI-limited, the assumption that noise is negligible compared to the MAI will be plausible for practical SNR values (e.g., SNR >8dB). As shown in [100], in the presence of additive channel noise, the CMA is expected to perform a smoothing effect on the noise-free CM cost function. This smoothing effect sets a constraint on the output noise and forces the filter $\mathbf{w}_1$ towards the minimal norm solution. That is, the CMA offers a tradeoff between achieving a decorrelating solution and avoiding noise enhancement.

Since the aim here is to categorize all stationary points of the CMA, for notational convenience, the index for the bit iteration (i.e., i) is to be temporally discarded. In a noiseless setting, since the synchronous received vector in (2.30) becomes $\mathbf{Y} = \mathbf{SAb}$, the linear filter output in (3.1) can be written as

$$Z_1 = \mathbf{w}_1^T\mathbf{Y} = \mathbf{w}_1^T\mathbf{SAb} = \mathbf{V}^T\mathbf{b}, \tag{A.1}$$

where $\mathbf{V}$ is the user gains defined in (3.24). Substituting (A.1) in (3.23), the

adaptation term in the CMA can be expressed as follows [101]

$$\begin{aligned}\frac{1}{4}\nabla_{\mathbf{w}_1} J_{CM}(\mathbf{w}_1) &= E\left\{\left(Z_1^2-\xi\right) Z_1 \mathbf{Y}\right\} \\ &= \mathbf{SA}\cdot E\left\{\left(\left(\mathbf{V}^T\mathbf{b}\right)^2-\xi\right)\mathbf{V}^T\mathbf{b}\cdot\mathbf{b}\right\} \\ &= \mathbf{SA}\cdot\frac{1}{4}\nabla_{\mathbf{V}} J_{CM}(\mathbf{V}). \end{aligned} \tag{A.2}$$

In (A.2), the derivative term $\frac{1}{4}\nabla_{\mathbf{V}} J_{CM}(\mathbf{V})$ can be simplified as follows

$$\begin{aligned}\frac{1}{4}\nabla_{\mathbf{V}} J_{CM}(\mathbf{V}) &= E\left\{\left(\left(\mathbf{V}^T\mathbf{b}\right)^2\xi\right)\mathbf{b}\mathbf{b}^T\right\}\cdot\mathbf{V} \\ &= \left[E\left\{\left(\mathbf{V}^T\mathbf{b}\right)^2\mathbf{b}\mathbf{b}^T\right\}-\xi E\left\{\mathbf{b}\mathbf{b}^T\right\}\right]\cdot\mathbf{V} \end{aligned} \tag{A.3}$$

In deriving (A.3), it is assumed that $(Z_1^2-\xi)\mathbf{b}\mathbf{b}^T$ is uncorrelated with $\mathbf{V}$. This assumption is generally plausible, if the step size μ is sufficiently small [101].

The two expectation terms in (A.3) are $(K\times K)$ matrices and are further simplified as follows. First, since independent user sources are assumed, $E\{\mathbf{b}\mathbf{b}^T\} = \mathbf{I}_K$. Second, the other term can be written as

$$\begin{aligned}E\left\{\left(\mathbf{V}^T\mathbf{b}\right)^2\mathbf{b}\mathbf{b}^T\right\} &= E\left\{\sum_{i=1}^{K} v_i b_i \sum_{j=1}^{K} v_j b_j \mathbf{b}\mathbf{b}^T\right\} \\ &= \sum_{i=1}^{K}\sum_{j=1}^{K} v_i v_j E\left\{b_i b_j \mathbf{b}\mathbf{b}^T\right\}. \end{aligned} \tag{A.4}$$

The (m,l)-th component of the matrix in (A.4) is equal to $\sum_{i=1}^{K}\sum_{j=1}^{K} v_i v_j E\{b_i b_j b_m b_l\}$. It can be easily shown that since $E\{b_i\} = 0 \quad \forall i \in \{1,\ldots,K\}$, and $E\{b_i b_j\} = 0 \quad \forall i \neq j$, the terms which contribute to the non-zero (m,l)-th component are

$$\begin{aligned} E\left\{b_i^4\right\} &= 1 \qquad \text{if } i=j=m=l, \\ E\left\{b_i^2 b_m^2\right\} &= 1 \qquad \text{if } i=j\neq m=l, \\ E\left\{b_i^2 b_j^2\right\} &= 1 \qquad \text{if } i=m\neq j=l, \\ E\left\{b_i^2 b_m^2\right\} &= 1 \qquad \text{if } i=l\neq j=m. \end{aligned} \tag{A.5}$$

From (A.5), the corresponding (m,l)-th component of $E\left\{\left(\mathbf{V}^T\mathbf{b}\right)^2\mathbf{b}\mathbf{b}^T\right\}$ is given

by

$$\begin{cases} \sum_{k=1}^{K} v_k & \text{if } m = l, \\ 2v_m v_l & \text{if } m \neq l. \end{cases} \tag{A.6}$$

In matrix notation, (A.4) can be written as

$$E\left\{\left(\mathbf{V}^T\mathbf{b}\right)^2 \mathbf{b}\mathbf{b}^T\right\} = \mathbf{V}^T\mathbf{V}\mathbf{I}_K + 2\left(\mathbf{V}\mathbf{V}^T - diag\left(\mathbf{V}\mathbf{V}^T\right)\right), \tag{A.7}$$

where $diag(\mathbf{X})$ is defined as the matrix extracted from $\mathbf{X}$, with the same diagonal entries and 0 elsewhere.

Substituting (A.7) into (A.3) yields

$$\begin{aligned} \frac{1}{4}\nabla_{\mathbf{V}} J_{CM}(\mathbf{V}) &= \left[\mathbf{V}^T\mathbf{V}\mathbf{I}_K + 2\mathbf{V}\mathbf{V}^T - 2\,diag\left(\mathbf{V}\mathbf{V}^T\right) - \xi\mathbf{I}_K\right]\mathbf{V} \\ &= \left[\left(\mathbf{V}^T\mathbf{V} - \xi\right)\mathbf{I}_K + 2\mathbf{V}\mathbf{V}^T - 2\,diag\left(\mathbf{V}\mathbf{V}^T\right)\right]\mathbf{V} \\ &= \left[\left(3\mathbf{V}^T\mathbf{V} - \xi\right)\mathbf{I}_K - 2\,diag\left(\mathbf{V}\mathbf{V}^T\right)\right]\mathbf{V} \\ &= \frac{1}{4}\cdot\left(\nabla_{v_1} J_{CM}(\mathbf{V}), \ldots, \nabla_{v_K} J_{CM}(\mathbf{V})\right)^T, \end{aligned} \tag{A.8}$$

where $\nabla_{v_k} J_{CM}(\mathbf{V})$ is the kth component of $\nabla_{\mathbf{V}} J_{CM}(\mathbf{V})$.

The CMA-based adaptation in (3.23) stops when $\nabla_{\mathbf{w}_1} J_{CM}(\mathbf{w}_1) = 0$. Given that all users' signatures are linearly independent, $\mathbf{SA}$ is full column rank and right-invertible. Therefore, there is an one-to-one mapping between the stationary points of $\mathbf{w}_1$ at $\nabla_{\mathbf{w}_1} J_{CM}(\mathbf{w}_1) = \mathbf{0}$, and those of $\mathbf{V}$ at $\nabla_{\mathbf{V}} J_{CM}(\mathbf{V}) = \mathbf{0}$. From (A.8), the stationary points at $\nabla_{\mathbf{V}} J_{CM}(\mathbf{V}) = \mathbf{0}$ is when

$$\frac{1}{4}\nabla_{v_k} J_{CM}(\mathbf{V}) = \left[3\sum_{j=1}^{K} v_j^2 - \xi - 2v_k^2\right] v_k = 0 \quad \forall k \in \{1, \ldots, K\}. \tag{A.9}$$

From (A.2), the expression for the Hessian with respect to $\mathbf{w}_1$ is given by

$$\begin{aligned} \frac{1}{4}\nabla^2_{\mathbf{w}_1} J_{CM}(\mathbf{w}_1) &= \mathbf{SA}\cdot\left(\nabla_{\mathbf{w}_1} E\left\{\left(Z_1^2 - \xi\right) Z_1\mathbf{b}\right\}\right)^T \\ &= \mathbf{SA}\cdot E\left\{\left(Z_1^2 - \xi\right)\mathbf{b}\left(\nabla_{\mathbf{w}_1} Z_1\right)^T + 2Z_1^2\mathbf{b}\left(\nabla_{\mathbf{w}_1} Z_1\right)^T\right\} \\ &= \mathbf{SA}\cdot E\left\{\left(3Z_1^2 - \xi\right)\mathbf{b}\mathbf{Y}^T\right\} \\ &= \mathbf{SA}\cdot E\left\{\left(3\left(\mathbf{V}^T\mathbf{b}\right)^2 - \xi\right)\mathbf{b}\mathbf{b}^T\right\}\cdot(\mathbf{SA})^T \\ &= \mathbf{SA}\cdot\frac{1}{4}\nabla^2_{\mathbf{V}} J_{CM}(\mathbf{V})\cdot\mathbf{A}\mathbf{S}^T. \end{aligned} \tag{A.10}$$

Using (A.7), the Hessian with respect to $\mathbf{V}$ in (A.10) is given by

$$\begin{aligned}\frac{1}{4}\nabla^2_{\mathbf{V}} J_{CM}(\mathbf{V}) &= 3E\left\{\left(\mathbf{V}^T\mathbf{b}\right)^2 \mathbf{b}\mathbf{b}^T\right\} - \xi\mathbf{I}_K \\ &= 3\left(\mathbf{V}^T\mathbf{V}\mathbf{I}_K + 2\mathbf{V}\mathbf{V}^T - 2\,diag\left(\mathbf{V}\mathbf{V}^T\right)\right) - \xi\mathbf{I}_K \\ &= \left(3\mathbf{V}^T\mathbf{V} - \xi\right)\mathbf{I}_K + 2\mathbf{V}\mathbf{V}^T - 2\,diag\left(\mathbf{V}\mathbf{V}^T\right). \qquad \text{(A.11)}\end{aligned}$$

The stability of these stationary points [120] can be determined by the sign-definiteness of the Hessian matrix $\nabla^2_{\mathbf{V}} J_{CM}(\mathbf{V})$ in (A.11). Overall, there are three types of stationary points, and are categorized as follows.

1. **Local maximum** — (i.e., $\nabla^2_{\mathbf{V}} J_{CM}(\mathbf{V})$ is negative definite) when $\mathbf{V} = \mathbf{0}$ giving a trivial solution.

$$v_k = 0 \quad \forall k \in \{1, \ldots, K\}. \qquad \text{(A.12)}$$

2. **Local minima** — (i.e., $\nabla^2_{\mathbf{V}} J_{CM}(\mathbf{V})$ is positive definite) when one user's signal is extracted and all other $(K-1)$ users are nulled.

$$|v_k| = \sqrt{\xi}, \text{ and } v_{k'} = 0 \quad \forall k' \neq k. \qquad \text{(A.13)}$$

3. **Saddle points** — (i.e., $\nabla^2_{\mathbf{V}} J_{CM}(\mathbf{V})$ is indefinite) when M users are simultaneously captured and their user gains are equal to some critical value v_c, and all other $(K-M)$ users are nulled.

$$|v_k| = v_c = \sqrt{\frac{\xi}{3M-2}} \quad \forall k \in \mathcal{M} \text{ and } v_{k'} = 0 \quad \forall k \notin \mathcal{M}, \qquad \text{(A.14)}$$

where $\mathcal{M}$ is the set of user indices corresponds to M $(2 \leq M \leq K)$ non-zero components of $\mathbf{V}$.

Bibliography

[1] R.Prasad, Ed., *CDMA for Wireless Personal Communications*, Artech House, Inc., Boston, 1996.

[2] P.B.Rapajic and B.S.Vucetic, "Adaptive Receiver Structures for Asynchronous CDMA Systems," *IEEE J. Selected Areas Commun.*, vol. 12, no. 4, pp. 685–697, May 1994.

[3] M.L.Honig, U.Madhow and S.Verdú, "Blind Adaptive Multiuser Detection," *IEEE Trans. Inform. Theory*, vol. 41, no. 4, pp. 944–960, July 1995.

[4] C.R.Johnson, Jr., P.Schniter, I.Fijalkow, L.Tong, J.D.Behm, M.G.Larimore, D.R.Brown, R.A.Casas, T.J.Endres, S.Lambotharan, A.Touzni, H.H.Zeng, M.Green, and J.R.Treichler, *"The Core of FSE-CMA Behavior Theory" in (S.Haykin, Ed.,) Unsupervised Adaptive Learning*, Wiley, N.Y., to appear, 1999.

[5] S.Verdú, *"Recent Progress in multiuser detection" in (N.Abramson, Ed.,) Multiple Access Communications: Foundations for Emerging Technologies*, IEEE Press, N.Y., 1993.

[6] U.Madhow, "Blind Adaptive Interference Suppression for the Near-Far Resistant Acquisition and Demodulation of Direct-Sequence CDMA Signals," *IEEE Trans. Signal Processing*, vol. 45, no. 1, pp. 124–136, Jan. 1997.

[7] W.C.Y.Lee, Ed., *Mobile Cellular Telecommunications: Analog and Digital Systems*, McGraw-Hill Inc., New York, second edition, 1995.

[8] D.J.Goodman, Ed., *Wireless Personal Communications*, Addison-Wesley, Massachusetts, 1997.

[9] ITU-R — TG 8/1, "IMT-2000 or FPLMTS," in *ITU brochure on IMT-2000 from its official web pages (***www.itu.int/imt-2000***)*, Sept. 1998.

[10] A.J.Paulraj and C.B.Papadias, "Space-Time Processing for Wireless Communications," *IEEE Signal Processing Magazine*, vol. 14, no. 6, pp. 49–83, Nov. 1997.

[11] N.Abramson, "Multiple Access in Wireless Digital Networks," *Proc. of IEEE*, vol. 82, no. 9, pp. 1360–1370, Sept. 1994.

[12] N.Abramson, "Development of the ALOHANET," *IEEE Trans. Inform. Theory*, vol. 31, pp. 119–123, Mar. 1985.

[13] J.C.Liberti, Ed., *Spatial Processing for High Tier Wireless Systems*, Bellcore Pub. IM-558, Sept. 1996.

[14] S.Moshavi, "Multi-User Detection for DS-CDMA Communications," *IEEE Commun. Magazine*, vol. 34, no. 10, pp. 124–136, Oct. 1996.

[15] A.H.M.Ross, Ed., *Welcome to the World of CDMA*, Offical web-page of CDMA Development Group (http://www.cdg.org), 1996.

[16] S.Verdú, Ed., *Multiuser Detection*, Cambridge University Press, Cambridge, U.K., 1998.

[17] A.J.Viterbi, Ed., *Principles of Spread Spectrum Multiple Access Communications*, Addison-Wesley, Reading, M.A., 1995.

[18] TIA/EIA/IS-95, "Mobile Station - Base Station Compatibility Standard for Dual-Mode Wideband Spread Spectrum Cellular System," in *Telecommunications Industry Association (TIA)*, July 1993.

[19] K.S.Gilhousen, I.Jacobs, R.Padovani, A.J.Viterbi, L.Weaver and C.Wheatley, "On the capacity of a cellular CDMA system," *IEEE Trans. Veh. Tech.*, vol. 40, pp. 303–311, May 1991.

[20] S.Vembu and A.J.Viterbi, "Two Different Philosophies in CDMA - A Comparison," in *Proc. IEEE Veh. Tech. Conf.*, Apr. 1996, pp. 869–873.

[21] A.J.Viterbi, "Wireless Digital Communication: A View Based on Three Lessons Learned," *IEEE Commun. Magazine*, pp. 33–36, Sept. 1991.

[22] C.E.Shannon, "A Mathematical Theory of Communication," *Bell Sys. Tech. J.*, vol. 27, pp. (379–423, 623–656), July and Oct. 1948.

[23] S.Verdú, Ed., *"Demodulation in the Presence of Multiuser Interference: Progress and Misconceptions", in Chapter 2, (D.Docampo, A.Figueiras-Vidla and F.Perez-Gonzalez, Ed.,) Intelligent Methods in Signal Processing and Communications*, Birkhauser, Boston, 1997.

[24] A.J.Viterbi, "Very low rate convolutional codes for maximum theoretical performance of spread-spectrum multiple-access channels," *IEEE J. Selected Areas Commun.*, vol. 8, no. 4, pp. 641–649, May 1990.

[25] D.V.Sarwate and M.B.Pursley, "Crosscorrelation Properties of Pseudorandom and Related Sequence," *IEEE J. Selected Areas Commun.*, vol. 68, no. 5, pp. 593–619, May 1980.

[26] M.Varanasi and B.Aazhang, "Multistage detection in asynchronous code-division multiple-access communications," *IEEE Trans. Commun.*, vol. 38, pp. 509–519, Apr. 1990.

[27] W.Lee, B.R.Vojcic and R.L.Pickholtz, "Constant Modulus Algorithm for Blind Multiuser Detection," in *Proc. IEEE Int. Symp. on Spread Spectrum Tech. and Applications*, Mainz, Germany, Sept. 1996, pp. 1262–1266.

[28] A.F.Naguib, *Adaptive Antennas for CDMA Wireless Networks*, Ph.D. thesis, Stanford University, 1996.

[29] G.Turin, "Introduction to spread-spectrum antimultipath techniques and their application to urban digital radio," *Proc. of IEEE*, vol. 68, pp. 328–353, Mar. 1980.

[30] J.G.Proakis, Ed., *Digital Communications*, McGraw-Hill, N.Y., third edition, 1995.

[31] Jr. G.B.Thomas and R.L.Finney, Eds., *Calculus and Analytic Geometry*, Addison-Wesley, Reading, M.A., 1988.

[32] R.Casas, Z.Ding, R.A.Kennedy, C.R.Johnson, Jr., and R.Malamut, "Blind Adaptation of Decision Feedback Equalizers Based on the Constant Modulus Algorithm," in *Proc. of 29th Asilomar Conf. on Signals, Systems and Computers*, Pacific Grove, CA, Oct. 1995.

[33] A.Duel-Hallen, J.Holtzman, and Z.Zvonar, "Multi-user detection for cdma systems," *IEEE Personal Commun.*, vol. 2, no. 2, pp. 46–58, Apr. 1995.

[34] U.Madhow and M.L.Honig, "MMSE Interference Suppression for Direct Sequence Spread-Spectrum CDMA," *IEEE Trans. Commun.*, vol. 42, no. 12, pp. 3178–3188, Dec. 1994.

[35] S.Verdú, "Adaptive multiuser detection," in *Proc. IEEE Int. Symp. on Spread Spectrum Tech. and Applications*, Oulu, Finland, July 1994, pp. 43–50.

[36] D.A.Pados and S.B.Batalama, "Low-Complexity Blind Detection of DS/CDMA Systems," *IEEE Trans. Commun.*, vol. 45, no. 12, pp. 1586–1594, Dec. 1997.

[37] J.D.Laster and J.H.Reed, "Interference rejection in digital wireless communications," *IEEE Signal Processing Magazine*, vol. 14, no. 3, pp. 37–62, May 1997.

[38] S.Verdú, "Minimum probability of error for Asynchronous Gaussian multiple-access channels," *IEEE Trans. Inform. Theory*, vol. 32, pp. 85–96, Jan. 1986.

[39] R.Lupas and S.Verdú, "Linear multiuser detectors for synchronous code-division multiple-access channels," *IEEE Trans. Inform. Theory*, vol. 35, pp. 123–136, Jan. 1989.

[40] Z.Xie, R.T.Short, and C.K.Rushforth, "A Family of Suboptimum Detectors for Coherent Multi-User Communications," *IEEE J. Selected Areas Commun.*, vol. 8, no. 4, pp. 683–690, May 1990.

[41] D.S.Chen and S.Roy, "An Adaptive Multiuser Receiver for CDMA Systems," *IEEE J. Selected Areas Commun.*, vol. 12, no. 5, pp. 808–816, June 1994.

[42] U.Mitra and H.V.Poor, "Analysis of an Adaptive Decorrelating Detector for Synchronous CDMA Channels," *IEEE Trans. Commun.*, vol. 44, no. 2, pp. 257–268, Feb. 1996.

[43] M.L.Honig and D.G.Messerschmitt, Ed., *Adaptive Filters: Structure, Algorithms and Applications*, Kluwer, Boston, MA, 1984.

[44] D.Jitsukawa and R.Kohno, "Adaptive multi-user equalizer using multi-dimensional lattice filters for ds-cdma," *IEICE Trans. Fundamentals*, vol. E79-A, no. 9, pp. 1464–1470, Sept. 1996.

[45] A.Duel-Hallen, "Decorrelating decision-feedback multiuser detector for synchronous code-division multiple-access channel," *IEEE Trans. Commun.*, vol. 41, no. 2, pp. 285–290, Feb. 1993.

[46] M.Abdulrahman, A.Sheikh, and D.Falconer, "Decision feedback equalization for cdma in indoor wireless communications," *IEEE J. Selected Areas Commun.*, vol. 12, no. 5, pp. 698–706, May 1994.

[47] P.Patel and J.Holtzman, "Performance Comparison of a DS/CDMA System using a Successive Interference Cancellation (IC) Scheme and a Parallel IC Scheme under Fading," in *Proc. IEEE Int. Conf. on Commun.*, New Orleans, LA, May 1994, pp. 510–515.

[48] B.Aazhang, B.-P.Paris, and G.C.Orsak, "Neural networks for multiuser detection in code-division multiple-access communications," *IEEE Trans. Commun.*, vol. 40, no. 7, pp. 1212–1222, July 1992.

[49] K.B.Lee, "Orthogonalization based adaptive interference suppression for direct-sequence code-division multiple-access systems," *IEEE Trans. Commun.*, vol. 44, no. 9, pp. 1082–1085, Sept. 1996.

[50] V.Aue and J.H.Reed, "An interference robust CDMA demodulator that uses spectral correlation properties," in *Proc. IEEE Veh. Tech. Conf.*, 1994, pp. 563–567.

[51] E.G.Ström and S.L.Miller, "Optimum complexity reduction of minimum mean sqaure error ds-cdma receivers," in *Proc. IEEE Veh. Tech. Conf.*, 1994, pp. 568–572.

[52] C-C.Yeh, J.R.Barry, and R.R.Lopes, "Approximate Minimum Bit-Error Rate Multiuser Detection," in *Proc. IEEE Global Telecommun. Conf.*, Sydney, Australia, 1998.

[53] U.Madhow, "MMSE Interference Suppression for Timing Acquisition and Demodulation in Direct-Sequence CDMA Systems," *IEEE Trans. Commun.*, vol. 46, no. 8, pp. 1065–1075, Aug. 1998.

[54] Z.Zvonar and D.Brady, "Adaptive Multiuser Receiver for Fading CDMA Channels with Severe ISI," in *Proc. of Conf. on Inf. Sc. & System*, Baltimore, Maryland, Mar. 1993.

[55] H.V.Poor and X.Wang, "Code-aided interference suppression for ds/cdma communications - part ii: Parallel blind adaptive implementations," *IEEE Trans. Commun.*, vol. 45, no. 9, pp. 1112–1122, Sept. 1997.

[56] P.K.P.Cheung and R.A.Kennedy, "Improved Blind Adaptive Detection for Synchronous Multiuser CDMA Systems," in *Proc. IEEE Workshop on Signal Processing Adv. in Wireless Commun.*, Paris, France, Apr. 1997, pp. 249–252.

[57] J.B.Schodorf and D.B.Williams, "A Constrained Optimization Approach to Multiuser Detection," *IEEE Trans. Signal Processing*, vol. 45, no. 1, pp. 258–262, Jan. 1997.

[58] M.K.Tsatsanis, "Inverse Filtering Criteria for CDMA Systems," *IEEE Trans. Signal Processing*, vol. 45, no. 1, pp. 102–112, Jan. 1997.

[59] J.Shen and Z.Ding, "Blind Adaptive Multiuser CDMA Detection Based on a Linear Projection Constraint," in *Proc. IEEE Workshop on Signal Processing Adv. in Wireless Commun.*, Paris, France, Apr. 1997, pp. 261–264.

[60] R.De Gaudenzi, F.Giannetti, and M.Luise, "Design of a Low-Complexity Adaptive Interference-Mitigating Detector for DS/SS Receivers in CDMA Radio Networks," *IEEE Trans. Commun.*, vol. 46, no. 1, pp. 125–134, Jan. 1998.

[61] J.R.Treichler and B.G.Agee, "A new approach to multipath correction of constant modulus signals," *IEEE Trans. Acoust. Speech, Signal Processing*, vol. ASSP-31, no. 2, pp. 459–472, Apr. 1983.

[62] D.N.Godard, "Self-Recovering Equalization and Carrier Tracking in Two-Dimensional Data Communication Systems," *IEEE Trans. Commun.*, vol. 28, no. 11, pp. 1867–1875, Nov. 1980.

[63] J.J.Shynk, A.V.Kerrthi, and A.Mathur, "Steady-state analysis of the multistage constant modulus array," *IEEE Trans. Signal Processing*, vol. 44, no. 4, pp. 948–962, Apr. 1996.

[64] C.R.Johnson, Jr., P.Schniter, T.J.Endres, J.Behm, R.A.Casas, D.R.Brown, and C.Berg, "Blind Equalization using the Constant Modulus criterion: A review," *Proc. of IEEE — Special Issue on Blind Identification and Estimation*, Oct. 1998.

[65] Z.Ding, R.A.Kennedy, B.D.O.Anderson, and C.R.Johnson, Jr., "Ill-convergence of godard blind equalizers in data communications," *IEEE Trans. Commun.*, vol. 39, no. 9, pp. 1313–1328, Sept. 1991.

[66] B.G.Agee, "The least-sqaures CMA: A new techniques for rapid correction of constant modulus signals," in *Proc. IEEE Int. Conf. Acoust., Speech, Signal Processing*, Tokyo, Japan, 1986, pp. 953–956.

[67] C.B.Papadias and D.T.M.Slock, "Normalized Sliding Window Constant Modulus and Decision-Directed Algorithms: A Link Between Blind Equalization and Classical Adaptive Filtering," *IEEE Trans. Signal Processing*, vol. 45, no. 1, pp. 231–235, Jan. 1997.

[68] P.Schniter and C.R.Johnson, Jr., "Dithered Signed-Error CMA: The Complex-Valued Case," in *Asilomar Conf. on Signals, Systems and Computers*, Pacific Grove, CA, Nov. 1998.

[69] L.M.Garth, "Dynamic Convergence Analysis of the Multi-Modulus Blind Equalization Algorithm," in *Proc. IEEE Global Telecommun. Conf. - Commun. Theory Mini Conf.*, Sydney, Australia, 1998, pp. 71–75.

[70] J.Míguez and L.Castedo, "A Linearly Constrained Constant Modulus Approach to Blind Adaptive Multiuser Interference Suppression," *IEEE Commun. Lett.*, vol. 2, no. 8, pp. 217–219, Aug. 1998.

[71] N.Zečević and J.H.Reed, "Blind Adaptation Algorithms for Direct-Sequence Spread Spectrum CDMA Single-User Detection," in *Proc. IEEE Veh. Tech. Conf.*, 1997, pp. 2133–2137.

[72] R.E.Kamel and Y.Bar-Ness, "Anchored Blind Equalization Using the Constant Modulus Algorithm," *IEEE Trans. Circuits and Systems-II: Analog and Digital Signal Processing*, vol. 44, no. 5, pp. 397–403, May 1997.

[73] C.B.Papadias and A.J.Paulraj, "A Constant Modulus Algorithm for Multiuser Signal Separation in Presence of Delay Spread Using Antenna Arrays," *IEEE Signal Processing Lett.*, vol. 4, no. 6, pp. 178–181, June 1997.

[74] L.Castedo, C.J.Escudero and A.Dapena, "A Blind Signal Separation Method for Multiuser Communications," *IEEE Trans. Signal Processing*, vol. 45, no. 5, pp. 1343–1348, May 1997.

[75] A.Touzni and I.Fijalkow, "Blind adaptive equalization and simultaneous separation of convolutive mixtures," in *Proc. of International DSP conf.*, July 1997.

[76] J.K.Tugnait, "Blind spatio-temporal equalization and impulse response estimation for MIMO channels using a Godard cost function," *IEEE Trans. Signal Processing*, vol. 45, no. 1, pp. 268–271, Jan. 1997.

[77] Z.Rong, P.Petrus, T.S.Rappaport, and J.H.Reed, "Despread-Respread Multi-Target Constant Modulus Array for CDMA Systems," *IEEE Commun. Lett.*, vol. 1, no. 4, pp. 114–116, July 1997.

[78] A-J.van der Veen and A.J.Paulraj, "An Analytical Constant Modulus Algorithm," *IEEE Trans. Signal Processing*, vol. 44, no. 5, pp. 1136–1155, May 1996.

[79] L.Tong, G.Xu, and T.Kailath, "Blind Identification and Equalisation Based on Second-order Statistics: A Time Domain Approach," *IEEE Trans. Inform. Theory*, vol. 40, no. 2, pp. 340–349, Mar. 1994.

[80] G.H.Golub and C.F.Van Loan, Eds., *Matrix Computations*, Johns Hopkins University Press, Baltimore, third edition, 1996.

[81] E.Moulines, P.Duhamel, J.Cardoso, and S.Mayrargue, "Subspace Methods for Blind Identification of Multichannel FIR Filters," *IEEE Trans. Signal Processing*, vol. 43, no. 2, pp. 516–525, Feb. 1995.

[82] H.V.Poor and X.Wang, "Blind Multiuser Detection: A Subspace Approach," *IEEE Trans. Inform. Theory*, vol. 44, no. 2, pp. 677–690, Mar. 1998.

[83] H.Liu and M.D.Zoltowski, "Blind Equalization in Antenna Array CDMA Systems," *IEEE Trans. Signal Processing*, vol. 45, no. 1, pp. 161–172, Jan. 1997.

[84] S.E.Bensley and B.Aazhang, "Subspace-based channel estimation for code-division multiple-access communication systems," *IEEE Trans. Commun.*, vol. 44, no. 8, pp. 1009–1020, Aug. 1996.

[85] H.Liu and G.Xu, "A Subspace Method for Signature Waveform Estimation in Synchronous CDMA Systems," *IEEE Trans. Commun.*, vol. 44, no. 10, pp. 1346–1354, Oct. 1996.

[86] E.G.Ström, S.Parkvall, S.L.Miller, and B.E.Ottersten, "Propagation Delay Estimation in Asynchronous Direct-Sequence Code-Division Multiple Access Systems," *IEEE Trans. Commun.*, vol. 44, no. 1, pp. 84–93, Jan. 1996.

[87] M.K.Tsatsanis and G.B.Giannakis, "Transmitter Induced Cyclostationarity for Blind Channel Equalization," *IEEE Trans. Signal Processing*, vol. 45, no. 7, pp. 1785–1794, July 1997.

[88] T.J.Endres, *Equalizing with Fractionally-Spaced Constant Modulus and Second-Order-Statistics Blind Receivers*, Ph.D. thesis, Cornell University, 1997.

[89] D.Slock, "Blind joint equalization of multiple synchronous mobile users using oversampling and/or multiple antennas," in *Proc. of 28th Asilomar Conf. Signals, Systems and Computers*, Oct. 1994, pp. 1154–1158.

[90] D.Yellin and E.Weinstein, "Multichannel signal separation: methods and analysis," *IEEE Trans. Signal Processing*, vol. 44, no. 1, pp. 106–118, Jan. 1996.

[91] C.Antón-Haro, Jośe A.R.Fonollosa, and J.R.Fonollosa, "Blind Multiuser Detection using Hidden Markov Models Theory," in *Proc. IEEE Int. Symp. on Spread Spectrum Tech. and Applications*, Mainz, Germany, Sept. 1996, pp. 1248–1252.

[92] S.Talwar, M.Viberg and A.Paulraj, "Blind estimation of multiple co-channel digital signals using an antenna array," *IEEE Signal Processing Lett.*, vol. 1, no. 2, pp. 29–31, Feb. 1994.

[93] A-J.van der Veen, S.Talwar, and A.J.Paulraj, "Blind estimation of multiple digital signals transmitted over FIR channels," *IEEE Signal Processing Lett.*, vol. 2, no. 5, pp. 99–102, May 1995.

[94] B.P.Paris, "Asymptotic Properties of Self-Adaptive Maximum-Likelihood Sequence Estimation," in *Proc. 27th Annual Conf. Inf. Sc. & Systems*, Baltimore, 1993, pp. 161–166.

[95] D.L.Donoho, Ed., *"On minimum entropy deconvolution" in (D.F.Findley, Ed.,) Applied Time Series Analysis II*, Academic Press, New York, 1981.

[96] H.Oda and Y.Sato, "A Method of Multidimensional Blind Equalization," in *Proc. IEEE Int. Symp. on Inf. Theory*, San Antonio, TX, Jan. 1993, p. 327.

[97] P.Schniter and C.R.Johnson, Jr., "Minimum-Entropy Blind Acquisition/Equalization for Uplink DS-CDMA," in *the 36th Allerton Conf. on Commun., Control, and Computing*, Monticello, IL, Sept. 1998.

[98] O.L.Frost,III, "An Algorithm for Linearly Constrained Adaptive Array Processing," *Proc. of IEEE*, vol. 60, no. 8, pp. 926–935, Aug. 1972.

[99] D.G.Luenberger, Ed., *Optimization by Vector Space Methods*, Wiley, New York, 1969.

[100] I.Fijalkow, A.Touzni and J.R.Treichler, "Fractionally-spaced equalization using CMA: Robustness to channel noise and lack of disparity," *IEEE Trans. Signal Processing*, vol. 45, pp. 56–66, Jan. 1997.

[101] J.R.Treichler and M.G.Larimore, "The Tone Capture Properties of CMA-Based Interference Suppressors," *IEEE Trans. Acoust. Speech, Signal Processing*, vol. ASSP-33, no. 4, pp. 946–958, Aug. 1985.

[102] R.Gooch and J.Lundell, "The CM array: An adaptive beamformer for constant modulus signals," in *Proc. IEEE Int. Conf. Acoust., Speech, Signal Processing*, Tokyo, Japan, Sept. 1986, pp. 2523–2526.

[103] W.Chung, M.Gu, C.R.Johnson, Jr., and L.Tong, "Characterization of the regions of convergence of CMA adaptive blind fractionally spaced equalizers," in *Proc. Asilomar Conf. on Signals, Systems and Computers*, Pacific Grove, CA, Nov. 1998.

[104] S.Haykin, Ed., *Adaptive Filter Theory*, Prentice Hall, New Jersey, third edition, 1996.

[105] J.R.Treichler and M.G.Larimore, "Convergence rates for CMA with sinusoidal inputs," in *Proc. IEEE Int. Conf. Acoust., Speech, Signal Processing*, Tampa, USA, Mar. 1985, pp. 1157–1160.

[106] A.Touzni and I.Fijalkow, "Does fractionally-spaced CMA converge faster than LMS?," in *Proc. European Signal Processing Conf.*, Trieste, Italy, Sept. 1996, pp. 1227–1230.

[107] J.B.Schodorf and D.B.Williams, "Array Processing Techniques for Multiuser Detection," *IEEE Trans. Commun.*, vol. 45, no. 11, pp. 1375–1378, Nov. 1997.

[108] M.Stojanovic and Z.Zvonar, "Performance of linear multiuser detectors in time-varying multipath fading channels," in *Proc. Fifth Commun. Theory Mini-Conf.*, London, U.K., 1996, pp. 163–167.

[109] M.K.Tsatsanis and G.B.Giannakis, "Blind Estimation of Direct Sequence Spread Spectrum Signals in Multipath," *IEEE Trans. Signal Processing*, vol. 45, no. 5, pp. 1241–1252, May 1997.

[110] Z.Zvonar and D.Brady, "Multiuser detection in single-path fading channels," *IEEE Trans. Commun.*, vol. 42, no. 2, pp. 1729–1739, Feb. 1994.

[111] M.Varanasi and S.Vasudevan, "Multiuser detectors for synchronous CDMA communications over non-selective Rician fading channels," *IEEE Trans. Commun.*, vol. 42, no. 2/3/4, pp. 711–722, Feb./Mar./Apr. 1994.

[112] S.D.Gray, M.Kocic, and D.Brady, "Multiuser Detection in Mismatched Multiple-Access Channels," *IEEE Trans. Commun.*, vol. 43, no. 12, pp. 3080–3089, Dec. 1995.

[113] X.Wang and H.V.Poor, "Adaptive joint multiuser detection and channel estimation for multipath fading cdma channels," *Wireless Networks*, to appear 1998.

[114] J.S.Thompson, P.M.Grant, and B.Mulgrew, "Smart Antenna Arrays for CDMA Systems," *IEEE Personal Commun.*, pp. 16–25, Oct. 1996.

[115] S.Y.Miller and S.C.Schwartz, "Integrated Spatial-Temporal Detectors for Asynchronous Gaussian Multiple-Access Channels," *IEEE Trans. Commun.*, vol. 43, no. 2/3/4, pp. 396–411, Feb./Mar./Apr. 1995.

[116] G.C.Hess, Ed., *Land-Mobile Radio System Engineering*, Artech House Inc., New York, 1993.

[117] R.Price and P.E.Green, "A communication technique for multipath channels," *Proc. IRE*, vol. 46, pp. 555–570, Mar. 1958.

[118] N.R.Mangalvedhe and J.H.Reed, "Blind CMA Interference Rejection in Multipath Channels," in *Proc. IEEE Veh. Tech. Conf.*, 1997, pp. 21–25.

[119] N.Zečević and J.H.Reed, "Blind Adaptation Algorithms for Direct-Sequence Spread-Spectrum CDMA Single-User Detection," in *Proc. IEEE Veh. Tech. Conf.*, 1997, pp. 2133–2137.

[120] J.P.LeBlanc, I.Fijalkow and C.R.Johnson, Jr., "CMA Fractionally Spaced Equalizers: Stationary Points and Stability Under IID and Temporally Correlated Sources," *Int. J. Adapt. Control Signal Processing*, vol. 12, pp. 135–155, Jan. 1998.

[121] I.Fijalkow, C.E.Manlove, and C.R.Johnson, Jr., "Adaptive Fractionally Spaced Blind CMA Equalization: Excess MSE," *IEEE Trans. Signal Processing*, vol. 46, pp. 227–231, Jan. 1998.

[122] M.K.Tsatsanis and Z.Xu, "Performance Analysis of Minimum Variance CDMA Receivers," *IEEE Trans. Signal Processing*, vol. 46, no. 11, pp. 3014–2022, Nov. 1998.

[123] M.Wax and T.Kailath, "Detection of signals by information theoretic criteria," *IEEE Trans. Acoust. Speech, Signal Processing*, vol. ASSP-33, pp. 387–392, Apr. 1995.

[124] M.L.Honig, "Performance of Adaptive Interference Suppression For DS-CDMA with a Time-Varying User Population," in *Proc. IEEE Int. Symp. on Spread Spectrum Tech. and Applications*, Mainz, Germany, Sept. 1996, pp. 267–271.

[125] K.W.Halford and M.Brandt-Pearce, "New-User Identification in a CDMA System," *IEEE Trans. Commun.*, vol. 46, no. 1, pp. 144–155, Jan. 1998.

[126] C.R.Johnson, Jr., and B.D.O.Anderson, "Godard Blind Equalizer Error Surface Characteristics: white, Zero-Mean, Binary Source Case," *Int. J. Adapt. Control Signal Processing*, vol. 9, pp. 301–324, 1995.

[127] M.G.El-Tarhuni and A.U.H.Sheikh, "Performance Analysis for an Adaptive Filter Code-Tracking Technique in Direct-Sequence Spread-Spectrum Systems," *IEEE Trans. Commun.*, vol. 46, no. 8, pp. 1058–1064, Aug. 1998.

[128] G.E.Corazza and V.Degli-Esposti, "Acquisition-based Capacity estimates for CDMA with Imperfect Power Control," in *Proc. IEEE Int. Symp. on Spread Spectrum Tech. and Applications*, Oulu, Finland, July 1994, pp. 325–329.

[129] J.Lilleberg, E.Nieminen and M.Latva-aho, "Blind Iterative Multiuser Delay Estimator for CDMA," in *Proc. IEEE Personal, Indoor, Mobile Radio Conf.*, Taipei, Taiwan, May 1996, pp. 565–568.

[130] S.E.Bensley and B.Aazhang, "Maximum likelihood synchronization of a single user for code division multiple access communication systems," *IEEE Trans. Commun.*, vol. 46, no. 3, pp. 392–399, Mar. 1998.

[131] D.Zheng, J.Li, S.L.Miller, and E.G.Ström, "An Efficient Code-Timing Estimator for DS-CDMA Signals," *IEEE Trans. Signal Processing*, vol. 45, no. 1, pp. 82–89, Jan. 1997.

[132] R.A.Iltis and L.Mailaender, "An adaptive multiuser detector with joint amplitude and delay estimation," *IEEE J. Selected Areas Commun.*, vol. 12, no. 5, pp. 774–785, June 1994.

[133] H.V.Poor, *"On parameter estimation in DS/SSMA formats" in Advances in Communications and Signal Processing*, Springer-Verlag, N.Y., 1989.

[134] Z.Xie, C.K.Rushforth, R.T.Short, and T.K.Moon, "Joint signal detection and parameter estimatino in multiuser communications," *IEEE Trans. Commun.*, vol. 41, no. 8, pp. 1208–1216, Aug. 1993.

[135] A.Polydoros and C.L.Weber, "A Unified Approach to Serial Search Spread Spectrum Code Acquisition - Part I General Theory," *IEEE Trans. Commun.*, vol. 32, no. 5, pp. 542–549, May 1984.

[136] R.B.Ward and K.P.Yiu, "Acquisition of pseudonoise signals by recursion-aided sequential estimation," *IEEE Trans. Commun.*, vol. 25, pp. 784–794, Aug. 1977.

[137] R.F.Smith and S.L.Miller, "Coarse acquisition performance of the minimum mean-squared error receiver," in *Proc. IEEE Milcom.*, 1995, pp. 1186–1189.